Factors influencing mixing and mass transfer in the small intestine

A thesis presented in partial fulfilment of the

requirements for the degree of Doctor of Philosophy in Digestive Biomechanics

(Physical Process of Digestion)

at Massey University, Turitea,

New Zealand.

Ian Lim Yuen Feung

2015

Abstract

This work sought to determine the factors influencing mixing and mass transfer in the small intestine. Specifically, the work was focussed on the gut periphery (i.e. perivillous region) of the terminal ileum in the brushtail possum (*Trichusurus vulpecula*). The salient questions to answer were;

1. What are the microrheological properties and disposition of mucus in the perivillous space?
2. What are the disposition and movements of the mucosa and the associated villi during postprandial gut motility patterns of pendular contractions?
3. Are villi rigid structures during physiological levels of lumen flow?

The following three main experimental works of this thesis were all conducted using live gut wall samples maintained *ex vivo*. In addition, computational models were developed incorporating the novel findings detailed in this thesis to assist in visualizing mixing and mass transfer in the perivillous space.

1. The properties of the perivillous fluid environment were assessed by multiple-particle-tracking of the Brownian motion of fluorescent microbeads on gut samples.
2. The movements and disposition of the mucosal surface and associated villi during pendular contractions were observed for whole lengths of everted gut samples.
3. Flow velocities in the perivillous space of gut samples were determined by microparticle-image-velocimetery of microbeads. The movement of villi in response to physiological levels of lumen flow were quantified by image analysis.

The following are the main findings and implications of the work.

1. The perivillous fluid environment consisted of discrete viscoelastic bodies dispersed within a watery Newtonian phase. Such characteristics of the fluid environment were thought to be conducive for mixing and mass transfer, and likened to the processes of gel filtration.
2. Gut pendular contractions generated transient mucosal microfolds, which resulted in the formation of periodic congregation and separation of villous tips. Such a mechanism was predicted (using computational simulations) to augment mixing and mass transfer of nutrients at the gut periphery.
3. Villi were rigid structures, which were more prone to pivot than to bend, while intervillous fluid was predicted to be quasi-static during physiological levels of lumen flow. Such a feature of villi supports a perivillous mixing and mass transfer mechanism driven by mucosal microfolding

In conclusion, mixing and mass transfer in the perivillous space are governed by more complex dynamics than previously assumed and by factors previously unknown.

Table of contents

List of Figures

List of Tables

List of Videos Referenced Throughout this Thesis

Preface

This thesis is written according to the regulations stipulated in the latest version of the Handbook for Doctoral Study, published by the Doctoral Research Committee in January 2011 (GRS version 7).

All animal works were carried out in strict accordance with the 'New Zealand Code of Practice for the Care and Use of Animals for Scientific Purposes'. The procedures carried in this thesis were also approved by the Massey University Animal Ethics Committee (MUAEC approval no. 10/31, 11/45 and 12/77).

The thesis format complies with the format of a thesis based on publications, as described on page 63-64 under the section 'Submission of a thesis based on publications'. My journal articles have been reproduced in this thesis in its entirety at the relevant chapters and are interspersed in between introductory and additional material that were not included in the articles. At each chapter that contains a publication, a 'DRC 16 – Statement of contribution to doctoral thesis containing publications' is attached as a page just before the sections of the journal article.

Below, details of the journal articles that have been published and the chapter of which it may be found are listed in the order they would appear in my thesis.

Chapter 3:

Yuen Feung Lim, Martin A. K. Williams, Roger G. Lentle, Patrick W. M. Janssen, Bradley Mansel, Stephen Keen, and Paul Chambers (2013). An exploration of the microrheological environment around the distal ileal villi and proximal colonic mucosa of the possum (*Trichosurus vulpecula*).

Published in: **Journal of the Royal Society Interface 10(81):** 20121008

Chapter 5:

Roger G. Lentle, Patrick W. M. Janssen, Clement de Loubens, Yuen Feung Lim, Corrin Hulls, Paul Chambers (2013). Mucosal microfolds augment mixing at the wall of the distal ileum of the brushtail possum.

Published in: **Neurogastroenterology and Motility 25(11):** 881-e700

Chapter 6:

Yuen Feung Lim, Roger G. Lentle, Patrick W. M. Janssen, Martin A. K. Williams, Clement de Loubens, Bradley Mansel, and Paul Chambers (2014). Determination of villous rigidity and intervillous flow in the distal ileum of the brushtail possum (*Trichosurus vulpecula*).

Published in: **Plos One 9(6):** e100140

Acknowledgements

To God be the glory, great things He has done.

First of all, I thank God for the privilege of being given the opportunity to explore His design in His creation of the small intestine. Thank you for carrying me this far in the journey and for the way ahead. Thank you Jing Xiu, my wife and love of my life for your love, support, encouragement and great cooking to sustain me especially during the home straight of this leg of my journey. I also want to thank you, mum and dad for your love, inspiration and encouragement along the way.

I would like to thank all of my supervisors for putting up with me, freely provided me with access to your time, expertise and support. First of all, thank you Roger for your steadfastness in your desire to see me grow to be a better researcher. Regardless of how I felt at that point in time when the pressure was on, I know you had my best interest in mind. Thank you Pat for keeping me grounded in my engineering roots as I 'traversed distally' into the exciting but many times more unpredictable realm of gastrointestinal biology. I appreciate you hearing me out on my many 'navel gazing' moments especially nearer to the end and for the fine craftsmanship of the experimental apparatus that made my work possible. Finally, Bill, thank you for letting me use your precious equipment, for sparing me the time of your 'underlings' and for being a third voice for opinions that has been really useful to me. I appreciate the different (i.e. more 'chilled out') style of supervision from you that can be a real 'pressure release valve'.

At this space, though you were not my formal supervisor, I just want to thank you Clement for your patience in helping me further develop my computational modelling skills and for bearing with me during times when our conversation gets *perdue dans la traduction*. Also Richard Love for your help looking through few chapters and for

advice with MatLab in the absence of Clement. I too want to acknowledge John Bronlund my masters supervisor who found and suggested the PhD to me in addition to the help you provided with MatLab to get me started early in my work.

I also want to thank Dick and Mary Earle for their generousity in providing the scholarship administered by the Riddet Institute that enabled me to do the PhD. I too appreciate the Riddet Institute for their work in facilitating comraderie amongst all their PhD students in diverse disciplines through the various student symposiums, trips and activities organized – it has been fun and enlightening to be involved in something larger than my little 'PhD world' whilst being involved with the CoRE Future Foods programme.

Thank you as well to all those who have assisted me in my work either in the experimental preparations, during the experiments or post experiments as well as 'outside' advice for my PhD work; Paul Chambers, Gordon Reynolds, Byron McKillop, William Thielicke, Shampa De, Fran Wolber, Marlena Kruger, Chua Wei-Hang, Kevin Pedley, John Pedley, Corrin Hulls, Stephen Keen and Brad Mansel. I would also like to give a special mention to the latter three guys who were willing to drag themselves out of bed to help with experiments in the early hours of the morning and for allowing me to contact you 'after hours'.

To my fellow 'comrade-in-arms' of Ivana, Yen and Corrin under the 'bearded one', thank you for your support, friendship and to share the load of high expectations. In addition, to the crew who regularly hangs out for a cuppa in the tearoom of the 'secret third floor' that I never knew existed until commencing my PhD – thank you for all the yummy food that you feed to a 'starving grad student' and for the conversations as well

xxx

as laughter that helps place the challenging aspects of the PhD into a different perspective.

A big ‘shout-out’ also to my ‘office-mates’ (i.e. Team TWO-THREE-EIGHT) past and present: Sandra, Teresa, Oni, Soffa, Jeremy, Elham, Hayley, Chalida, Haoran, Sina and others. Thank you for the conversations, fun, laughter, parties and craziness shared with people who walk and know the journey towards the PhD that can many times be lonely.

Last but certainly in no way least, thank you also to friends not mentioned, mentors and other family for your encouragements, prayers and support of me in this time. Among them, a special mention is to be made of Yuen Leung, Yuen Xin, Janeen, Teng Yang, Mark G, Michael Loh, Kellis, Dawn, Srikanth, Horng Yuan, DJ, Julian, Natalia, Neil, Shoichi and Thomas. Finally, I also would like to thank Paul Stock and Terry McGrath for their help in proof-reading my various chapters.

Glossary

Postprandial period – The period following the consumption of a meal a.k.a. the fed state

Interdigestive period – The period that commences after and precludes the postprandial period a.k.a. the fasting/intercibal period

Unstirred water layer – Commonly abbreviated as the 'UWL'. Initially thought to be an actual diffusion barrier of unstirred fluid overlying the intestinal mucosa that acts as a barrier to mass transfer

Perivillous region – The region encompassing the intervillous space as well as the region directly above villi up to a distance of no more than a length of a villous from the villous tips

Small intestinal villi – Small, often finger-like projections that protrude from the epithelial lining of the intestinal wall. Its outer surfaces are composed of a variety of epithelial cells of which absorptive enterocytes are the pre-dominant type

Mucus islands – Mucin secreted by goblet cells into the extracellular regions that is undergoing swelling by hydration

Mass transfer – Net movement of mass from one location to another. It usually refers to movement by diffusive (i.e. the diffusion of solute within the bulk phase) and/or advective (i.e. mass movement of the bulk phase with contained solute) mass transfer.

Copyright and permissions

Permissions to reproduce the figures from other authors/publishers and material from my published journal articles have either been obtained or are in the process of hearing back from the relevant authorities at the time of submission of this thesis.

Chapter One - Introduction

Initial studies on the mass transfer of gut lumen contents prior to absorption detected a delay of the absorption of solutes from the lumen as compared with direct absorption at the mucosal surface (Amidon et al. 1980; Anderson et al. 1988). This delay was initially thought to be the result of a diffusion barrier composed of an equivalent layer of unstirred water layer (UWL) thickness (Westergaard and Dietschy 1974; Levitt et al. 1992) at the gut periphery regions. However, the quantification of the resistance to mass transfer by the calculation in an UWL value proved to be misleading. This was due to the large variability of calculated barrier thickness depending on the mixing conditions of luminal fluid (Pappenheimer 2001b), type of solute (Read et al. 1977; Levitt et al. 1984) and perfusion rates (Winne 1978; Johnson and Amidon 1988) used.

Further, early work (Westergaard and Dietschy 1974; Wilson and Dietschy 1974; Read et al. 1977) that may be considered foundational to the formation of the hypothesis of a UWL in the small intestine has since been challenged (Levitt et al. 1987), especially on their usage of the osmotic transient technique to measure the UWL – a technique previously used to measure the UWL in the gallbladder (Diamond 1966). Levitt et al. (1987) argued that the observation of an UWL adjacent to the intestinal mucosa may actually have been a result of an artefact generated by the *in vitro* techniques used and of the assumption that the contents of the gut lumen centre were well-mixed (i.e. turbulence being generated). Conversely, the flow of luminal contents in the small intestine was observed to approach that of laminar flow (Levitt et al. 1987; Levitt et al. 1988; Levitt et al. 1990). In addition, the technique used, especially by Westergaard and Dietschy (1974), involved the dipping of a flattened sheet of gut in a beaker of well-mixed fluid (an *in vitro* technique). Such conditions would be vastly different to that

generated during the flow of luminal contents through an intact gut during the postprandial period.

The current understanding of mass transfer is that it is governed by a combination of effects rather than a quantifiable thickness of a diffusion barrier (Lentle and Janssen 2011). Some main factors that may affect mixing and mass transfer include; disposition and properties of a supposed continuous layer of mucus (Smithson et al. 1981), the influence of small intestinal wall 'architecture' e.g. the presence of villi (Ryu and Grim 1982) as well as the mixing and dispersion of luminal contents engendered by postprandial motility (Lentle et al. 2012).

An understanding of the mechanisms of mixing and mass transfer of the gut contents particularly in the perivillous region is important as this process is a requisite before absorption (of e.g. nutrients) can take place through enterocytes (i.e. absorptive cells) situated on intestinal villi. Hence, the purpose of this thesis is to determine the impact of these factors on mixing and mass transfer of nutrients and pharmaceuticals in the perivillous region, which would further contribute to the current knowledge of the physical processes of digestion.

To be able to develop drugs that have increased efficacy or to better understand the effects of different food formulations on satiety and nutrient absorption, an increased understanding of the barriers or 'delay' to mass transfer is paramount. In addition to the experimental work conducted, computational simulations have also been developed that incorporated the contemporary experimental findings in order to better understand mixing and mass transfer in the perivillous region.

For you created my inmost being;
you knit me together in my mother's womb.

I praise you because I am fearfully and wonderfully
made;
your works are wonderful,
I know that full well.

Psalms 139:13-14

Chapter Two -

Literature review

2.1. Foreword

The principal objective of this thesis is to determine the influence and contribution of postprandial gut motilities, small intestinal villi and secreted mucus in the small intestine to the mass transfer of nutrients and other substances in the perivillous space. Mass transfer to regions adjacent to the mucosal surface is necessary to allow absorption at the mucosal surface to take place. This review is to set the stage of this thesis, summarizing previous relevant work that has a bearing on the objective, most (if not all) of which will be from studies conducted on mammals. The following sections provide an overview of what is currently known about the three aforementioned factors, each of which will also be considered in the context of their contributions to mass transfer.

2.2. Small intestinal motility

Small intestinal motility could influence mixing and mass transfer in the small intestine as it provides the driving force to transport and disperse (radially or axially) luminal contents. Gut motility patterns vary in their time interval of activity, grouping of contractile events as well as the extent of the migration of contractile activity and may be broadly classified into two main categories; fasting (i.e. fasting or interdigestive) and postprandial (i.e. fed) periods (Husebye 1999). The following sub-sections will highlight the main small intestinal motility patterns and periods, followed by a discussion on their potential contribution to mixing and mass transfer.

2.2.1. Migrating motor complex (MMC)

The migrating motor complex (MMC) is a sequence of gut contractile events that is a feature of the interdigestive period (Sarna 1985; Husebye 1999) and is typically classified into three phases (I to III) with phase III the most distinctive and easily recognizable phase (Kellow et al. 1986; Ehrlein et al. 1987). Phase I is generally observed as a period of quiescence with relatively infrequent contractile activity of the gut (i.e. less than three pressure waves every ten minutes) (Hellström et al. 1991). This is followed by phase II, which is typically observed as a period of irregular contractile activity with limited transport of luminal contents occurring (Sarna 1985). Subsequently, phase III commences and is observed as a period featuring regular bands of peristaltic pressure waves that migrate aborally (away from the mouth) (Husebye 1999). These peristaltic pressure waves typically arise from the ligament of Treitz and terminate anywhere between the midpoint of the small intestine and the terminal ileum. The velocity of migration is thought to be around 5 to 10 cm min^{-1}, a rate that decreases aborally until its lowest point in the ileum with rates between 0.5 and 1 cm min^{-1} (Kellow et al. 1986).

The average recurrence of phase III MMC has been observed to be at intervals of 2 to 3 hours although the interval for a single cycle of MMC may vary by an additional 3 to 4 hours for a given individual (Husebye 1999). The main function of MMCs are thought to be the removal of meal remnants and intestinal secretions as well as preventing backflow in the small intestine (Sarna 1985; Ehrlein et al. 1987).

Substantially more details on the attributes of MMC (but not relevant to the scope of this survey) can be found in these references - Sarna (1985), Ehrlein et al. (1987) and Lentle and Janssen (2011).

2.2.2. Peristalsis

Peristalsis is a gut motility pattern observed during *in vivo* conditions that is known to transport luminal contents in the aboral direction involving either partial or total occlusion of the small intestinal lumen (Huizinga and Lammers 2009). While terms such as 'peristaltic waves' or 'peristaltic contractions' all typically refers to peristalsis (Huizinga and Lammers 2009), caution is required when interpreting and comparing results that are derived from *ex vivo* preparations in the same way as those derived from *in vivo* preparations (Lentle and Janssen 2011). Peristaltic-like motility patterns observed from *ex vivo* preparations are typically known as the peristaltic reflex (Huizinga and Lammers 2009; Lentle and Janssen 2011) and were first observed by Baylis and Starling (1899). Given the scarcity of observations that are derived from *in vivo* experiments, descriptions and discussions about the peristaltic contractions in this survey will be necessarily limited to *ex vivo* observations of the peristaltic reflex unless stated otherwise.

The visual parameters of the peristaltic reflex has been documented by Schulze-Delrieu (1999) using *ex vivo* preparations of the guinea pig ileum and can be seen in Figure 2-1. A peristaltic contraction may be viewed as being composed of an occluded section (of varying degree and length) flanked by an upstream and downstream shoulder. The gut wall occlusion has been reported to be caused by indentations on the gut wall mostly on the antimesenteric side. The downstream shoulder (i.e. leading slope) typically migrates at a different rate to the upstream shoulder (i.e. trailing slope) resulting in the variation of the length of the occluded section (Schulze-Delrieu 1999). This pattern of contractile activity suggests that peristalsis is a result of the concerted action of longitudinal and circular muscles.

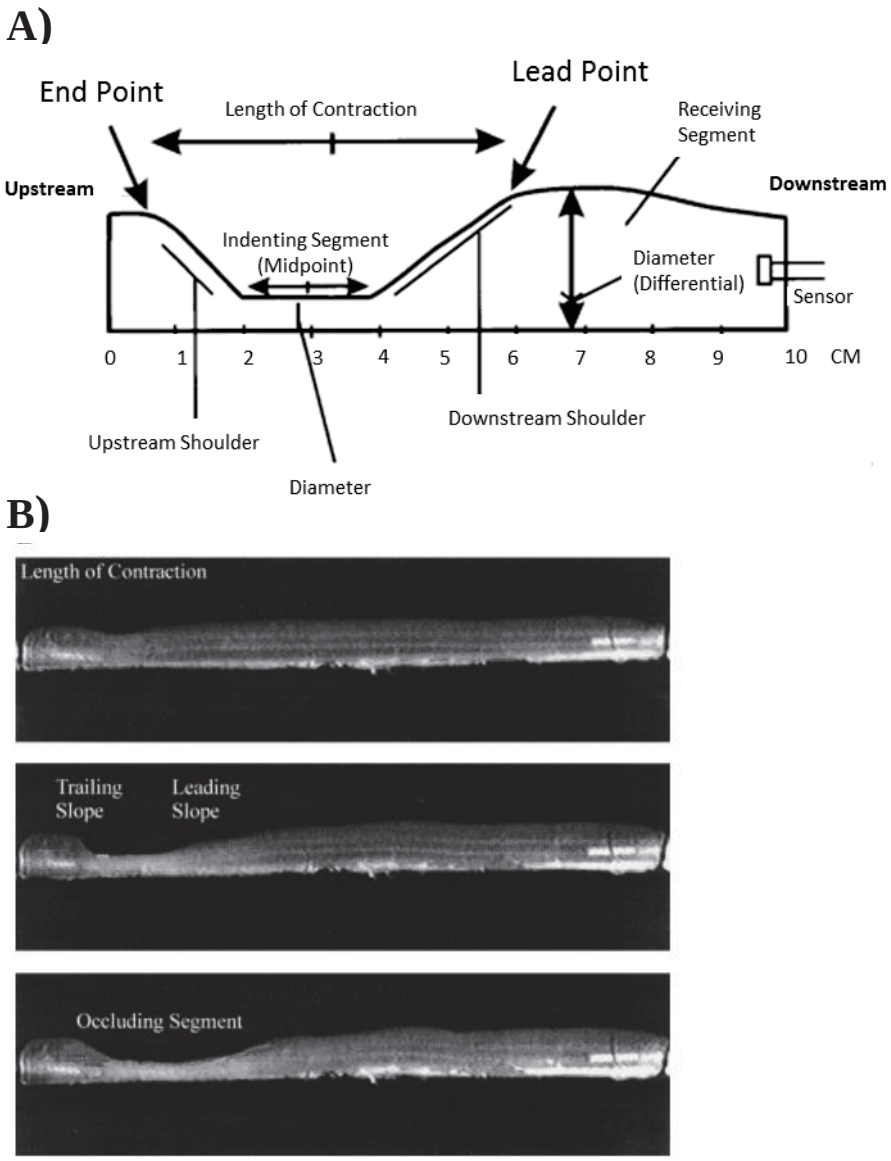

Figure 2-1: Observations of the peristaltic reflex on an *ex vivo* preparation of a 10 cm segment of guinea pig ileum following the injection of a 0.8 ml bolus. A) Morphology of the peristaltic reflex. The occlusion is caused mostly by an indentation on the antimesenteric wall. B) A series of images 1 s apart, of the peristaltic reflex are shown. In the top image, an indentation develops on the antimesenteric border of the gut. In the middle image, the indentation deepens forming a short and steep trailing slope and a longer and shallow leading slope. In the bottom image, the indentation deepens increasing the length of the occluded section until both the slopes were nearly symmetrical with one another (adapted from Schulze-Delrieu 1999).

2.2.2.1. Promotion of mass transfer

The mechanism of digestion in the small intestine has been likened to a linked series of plug flow chemical reactors (Penry and Jumars 1987; Jumars 2000), with each notional reactor having homogenous properties. This conjecture assumes perfect mixing in the radial direction and none in the axial direction resulting in a first order profile reduction of concentration (e.g. solutes and other substances) with time. However, this assumption is not realistic given the influence of gut motility patterns such as peristalsis that was demonstrated to promote mixing and mass transfer in the axial direction in finite element mathematical simulations (Jeffrey et al. 2003), and was later validated by observations of dye dispersion studies within isolated segments of guinea pig small intestine (Schulze and Clark 2008). Moreover, it has also been demonstrated that peristalsis produces backflow of luminal contents (i.e. digesta) during a single peristaltic contraction (Schulze and Clark 2008), which would also likely result in a concentration profile that departs from the first order.

For mixing to occur during contractile activity, it has been assumed that some form of asymmetry of the movement of luminal contents would need to occur (Melville et al. 1975; Lentle et al. 2007). Asymmetry is needed to prevent vortical circulation from occurring (i.e. luminal contents displaced are returned to their original position) at the conclusion of a single contractile event. Recent work by Lentle and colleagues (2007) has postulated a possible mechanism whereby radial dispersion and mixing of luminal contents could be achieved by peristaltic contractions (Figure 2-2). This is based on the finding that the progression of peristalsis along the length of the gut is through a series of surges rather than a single sustained steadily progressing event (Lentle et al. 2007).

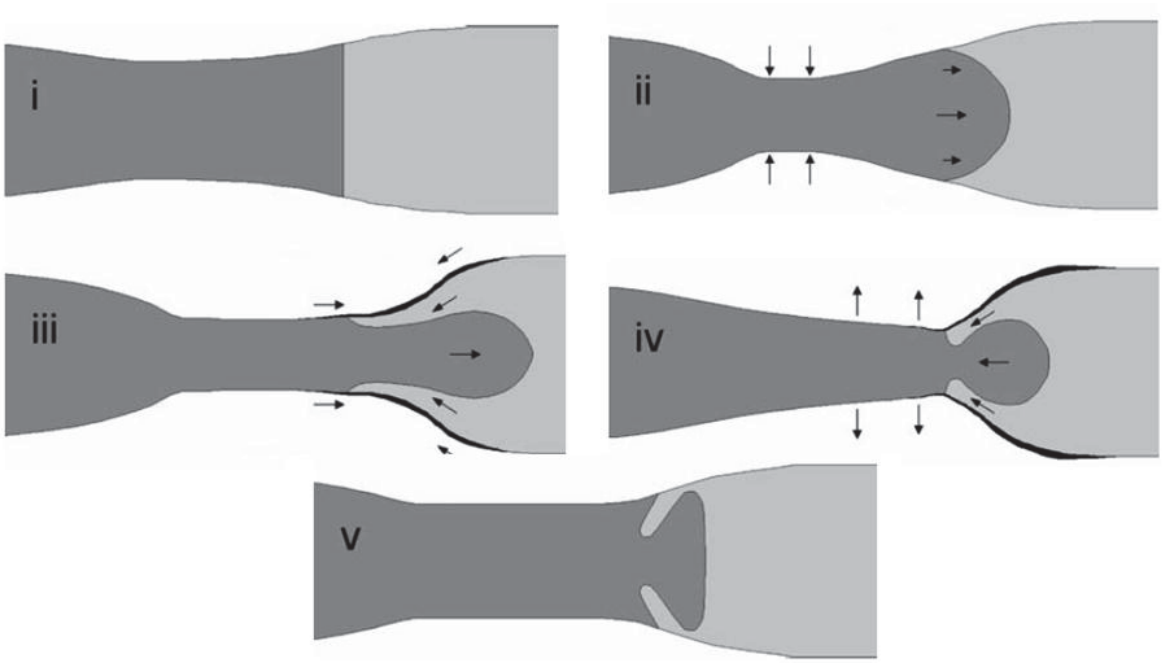

Figure 2-2: Suggested mechanism for mixing by peristaltic contractions. The locations of longitudinal contractions and timings of contractile sequences are shown by arrows. The suggested interior flow is a consequence of the following sequence: (i)–(ii) Circular contraction commences at the oral (left) end of the segment. (ii)–(iii) Circular contraction propagates aborally causing contents to be propelled aborally. Concerted longitudinal contraction commences at the aboral end. (iii)–(iv) Circular relaxation commences at the aboral end while longitudinal contraction continues. (iv)–(v) Return to starting position (i) with permanent displacement of contents in longitudinal and radial directions (adapted from Lentle et al. 2007)

Asymmetric mixing may be achieved by stochastic (i.e. random) variation of the successive surges of the peristaltic event – each successive peristaltic contraction being slightly different in form from the previous (e.g. differences in the profile of the gut section undergoing contractile activity and muscles involved in the contraction) (Lentle and Janssen 2011). Evidence for such a mechanism was observed in an earlier work by Schulze-Delrieu (1999) where the differences in the rate of migration of the leading and trailing shoulders of the occluded section of a peristaltic event have been documented. This may result in an axially asymmetric profile of the contraction (Lentle and Janssen 2011) and hence asymmetry of luminal contents movement as well as the formation of a

stochastic distribution of vortex sizes particularly in the region of the gut at the leading shoulder of the occluded section. A peristaltic event leading shoulder that is steeper would generate larger wall pressures and influence flow over a longer length of gut as compared to a flatter gradient of the shoulder (Jeffrey et al. 2003). In depth spatiotemporal analysis of the peristaltic reflex conducted by Lentle and colleagues (2007) provided further experimental evidence for asymmetric mixing by such a mechanism (Figure 2-3). Variations in the profile of the front of the contracted section (lighter shade) of the gut seen on the D-maps (left image of Figure 2-3) published by Lentle et al. (2007) is evidence for the stochasticity of successive peristaltic surges – the fronts of the contracted section of successive peristaltic contractions were observed to vary in its length and form (e.g., some having finger-shaped ends while others tapered to form a pointed end).

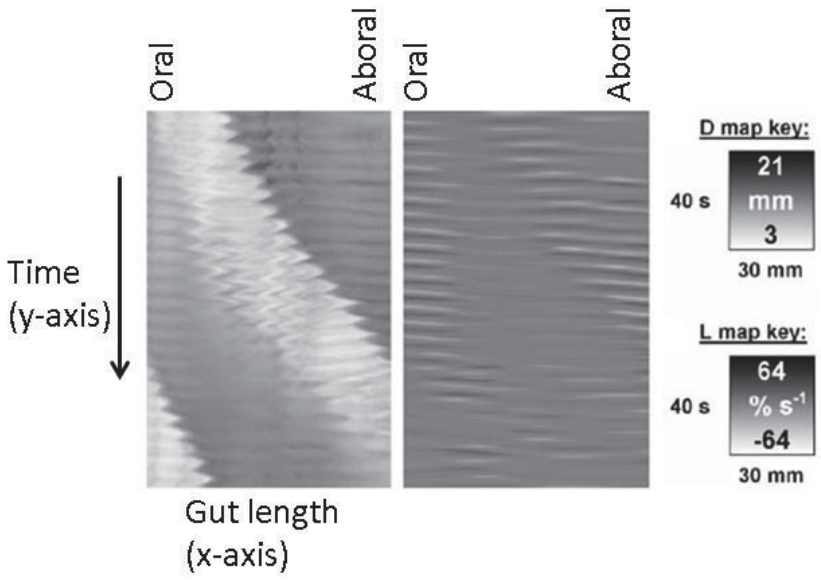

Figure 2-3: A pair of spatiotemporal maps obtained from a segment of possum ileum undergoing peristaltic contractions. The long axis of the gut segment was represented in the x-direction of the map while each successive scans of the contracting gut segment were stacked along the y-direction of the map. The image on the left is a 'Diameter' or D map with the intensity of each pixel along the x-axis representing the diameter of the gut segment at that point. A lighter shade corresponds to a smaller gut diameter (i.e. occlusion) while a darker shade corresponds to a larger diameter (i.e. distension). The image on the right is a 'Longitudinal' or L map with the intensity of each pixel along the x-axis representing the strain rate at a given point on the gut segment. A lighter shade corresponds to a negative strain rate or a longitudinal muscle contraction while a darker shade corresponds to a positive strain rate or a longitudinal muscle relaxation. These maps are also evidence that peristaltic contractions required the concerted action of circular and longitudinal muscles contractile activity (adapted from Lentle et al. 2007).

In addition, asymmetry may be further promoted by the varying speeds of the contractile activity of longitudinal and circular muscles of the gut wall at both oral and aboral ends during the propagation of the contracted section of the gut (Lentle et al. 2007). Such an effect would be increasingly pronounced as the indentations of the gut wall approach complete occlusion over long stretches of the small intestine (Weinberg et al. 1971). Finite element mathematical modelling has also suggested that vortical flow may be introduced by the release of sufficiently high pressures within the occluded section of the peristaltic event (Jeffrey et al. 2003).

Overall, it is noteworthy that all mechanisms postulated above of mixing and mass transfer of luminal contents by peristaltic contractile activity assumes laminar flow conditions. Such conditions may be especially found in the distal small intestine where dry matter content of digesta is thought to increase (McDonald et al. 2001) resulting in luminal contents that are of high viscosity and/or approach pseudoplasticity (Lentle et al. 2005).

Especially in the terminal ileum, another way peristalsis may augment mixing and mass transfer of luminal contents to be absorbed is through a potential 'intestinal stomach' effect (Lentle and Janssen 2011). Solid (Khosla et al. 1989) and liquid (Spiller et al. 1987) phases of luminal contents have been found to accumulate in the terminal ileum due to the ileocaecal valve acting as a gateway regulating onflow of luminal contents to the colon through temporal variation of tone and contractile activity of the valve (Hammer et al. 1993). For the 'intestinal stomach' effect to promote mixing and mass transfer of accumulated luminal contents, a sequential ante- and retrograde peristalsis (i.e. back peristalsis, which would facilitate backflow of luminal contents) mechanism would need to be observed in the distal ileum. While retrograde peristaltic events have been observed in the terminal ileum, these events were typically observed to be of a lesser magnitude and frequency as compared to antegrade peristalsis (Shiina et al. 2005). In addition, observations of clustered antegrade peristaltic events (Ehrlein et al. 1987) bringing luminal contents to the closed ileocaecal valve may intensify mixing especially during backflow and facilitate the 'intestinal stomach' effect to a lesser extent. Overall, it remains to be seen if peristaltic contractions do indeed promote mixing and mass transfer of luminal contents especially *in vivo* and warrants further experimentation.

2.2.3. Segmentation

Segmentation is a gut motility pattern first described by (Cannon 1902) as ring-like constrictive rhythmic movement that may appear at multiple sites along the gut formed by the action of circular muscles (Saladin 2007). However, it has been postulated that longitudinal muscle contraction may also occur during, or even be the sole cause of segmentation (Cannon 1902; Gwynne et al. 2004). For segmentation to be caused by longitudinal muscle contractions, the dilation of a section of gut may be caused by the action of longitudinal muscles on adjacent constricted sections pulling in both the oral and aboral directions.

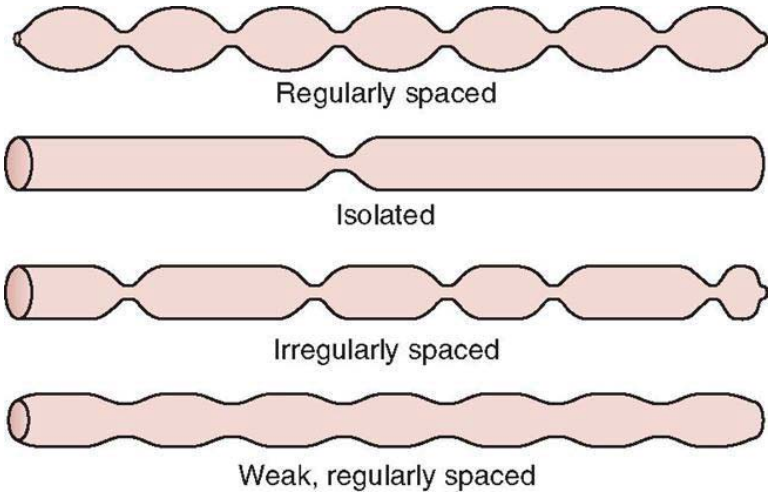

Figure 2-4: Segmentative gut motility pattern. There are four types of segmentative activity that have been recorded in medical textbooks (adapted from Hall and Guyton 2000).

There are four types of segmentation that have been recorded so far (Hall and Guyton 2000); regularly spaced, isolated, irregularly spaced, and weak regularly spaced segmentative activity (Figure 2-4). The radially oriented constrictions could appear at a fixed site (Thuneberg and Peters 2001) or propagate over short (2-3 mm) or longer distances (Grivel and Ruckebusch 1972; Gwynne et al. 2004). An example of the

frequency of segmentative contractions was 35 to 40 cpm of the proximal small intestine of mice (Thuneberg and Peters 2001).

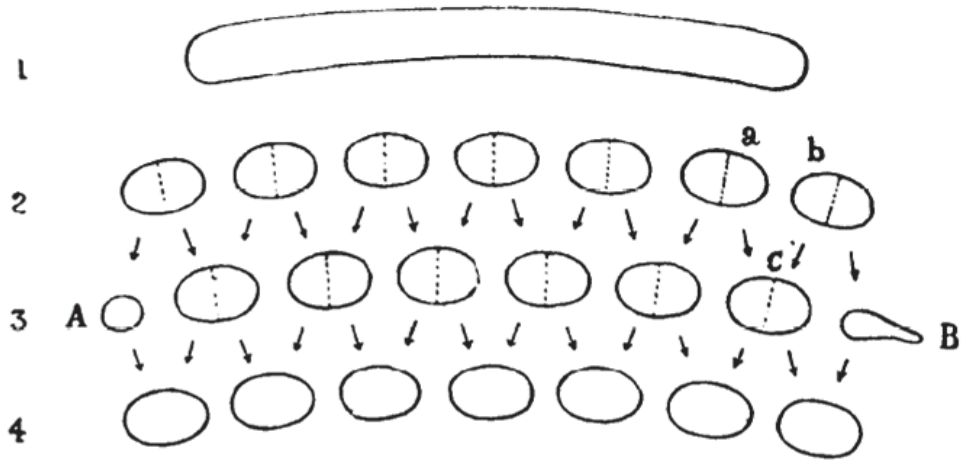

Figure 2-5: The first published illustration of a possible mechanism of mixing by segmentation. Lines 1, 2, 3 and 4 indicate the sequence of appearances in the loop. The dotted lines mark the sections of division. The arrows show the relation of the particles to the segments they subsequently form (reproduced from Cannon 1902).

The mechanics of Cannon's segmentative motility patterns is illustrated in Figure 2-5 showing the way in which regularly spaced-type segmentation divides and re-divides luminal contents (e.g. digesta) with each successive contraction. While such motility patterns has been observed previously during *in vivo* preparations, to date, there have been no studies that have observed similar patterns of rhythmic segmentation in *ex vivo* preparations. While 'short lengths' of constricted gut sections that propagated were observed during *in vitro* studies conducted by Gwynne et al. (2004) and were presumed to be similar to segmentative motility patterns, these constrictions were only present after the addition of a nutrient solution, which was diluted with ethanol. Hence, it is possible that the segmentative motility patterns observed by Gwynne et al. (2004) may not be the effect of a fed-state (i.e. the presence of nutrients) but were a response to the irritative effects of ethanol.

A recent study (Lentle et al. 2012) conducted on the duodenum of guinea pigs using *ex vivo* preparations demonstrated the occurrence of non-propagating circular muscle (i.e. segmentative) contractions that was thought to be similar to a form of segmentation. However, these contractions occurred as isolated events and were in no way distributed over time and over the gut segment as those observed during *in vivo* studies (Figure 2-6).

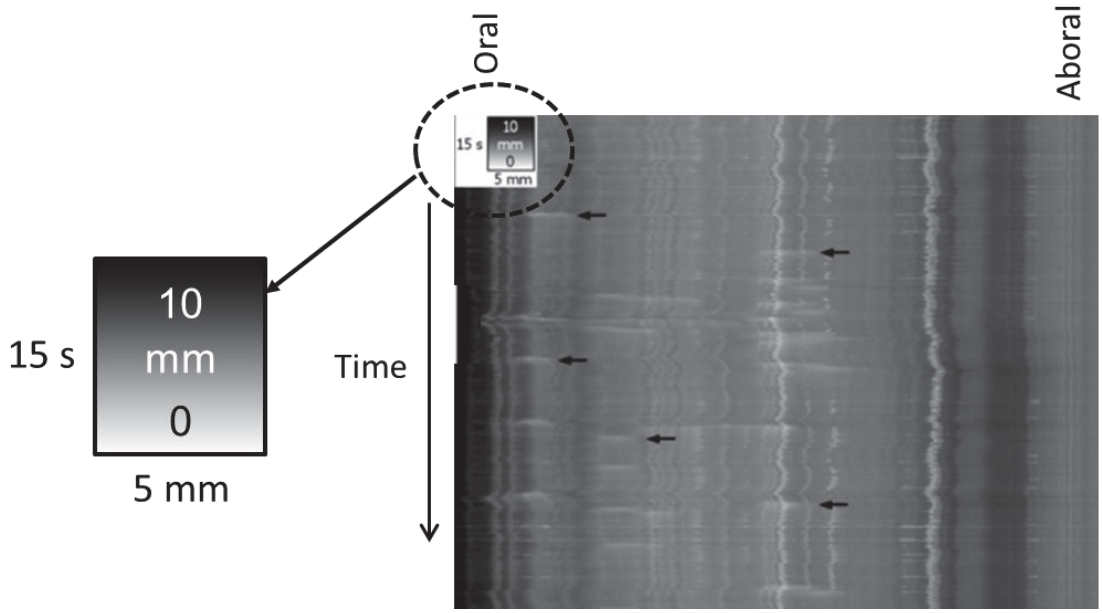

Figure 2-6: Diameter 'D' map of the occurrence of non-propagating circular muscle contractions on a guinea pig duodenum (adapted from Lentle et al. 2012). Explanations on the way to read the map have been outlined in Figure 2-3. While the map shows stationary circular muscle contractions recurring at sites along the duodenum that may be associated with segmentation (black arrows), the distribution of these contractions along the length of the gut segment or in time were dissimilar to those described by Cannon (1902). A magnification of the map scale is provided.

It is noteworthy that in addition to the postulated mixing capability of segmentative gut motility patterns, segmentation may also act as a 'duodenal brake' at the proximal end of the small intestine. Periodic non-propagating segmentative contractions in adjacent sections may restrict the rate of onflow of acidic gastric contents into the duodenum (Rao et al. 1996). In this way, the low pH of luminal contents in the proximal duodenum

could be neutralized over time by mixing with intestinal secretions before it progresses to more distal sites.

2.2.3.1. Promotion of mass transfer

Assuming that segmentative motility patterns occur only by circular muscle contractions without any additional influence of concurrent longitudinal muscle contractions or vice versa, it is unlikely that any asymmetric vortexes could form that may augment mixing and mass transfer (Lentle and Janssen 2011). Such an event was observed during mathematical modelling of segmentative contractile activity in the gut where simulated particles in luminal content were not advected beyond their starting position at the end of a contraction cycle (de Loubens et al. 2013).

Conversely, assuming that the velocity of flow into the relaxed sections of gut generated by segmentative activity wall constrictions are of a sufficiently high level, mixing and mass transfer may occur from two situations. Firstly, it may be that under certain conditions the local flow velocity generated by segmentative contractions is sufficiently high as to induce local turbulence and hence local mixing (Dimotakis 2000). Secondly, assuming also that segmentation manifests as multiple regularly spaced constrictions as observed by Cannon (1902) (Figure 2-5), mixing and mass transfer in a relaxed section of gut in between two constricted sections may occur. If both constricted sections adjacent to a relaxed section contracted at similar times with similar velocities and also were of sufficient proximity that their generated vortexes were to overlap, this may generate local asymmetry of flow and therefore mixing (Lentle and Janssen 2011). Such mixing mechanisms also assumed that viscosity of luminal contents is low. However, there is currently little evidence to suggest that such ideal environments and conditions exist during *in vivo* segmentation.

It is more likely that segmentation is effective in the promotion of mixing and mass transfer under certain diet conditions and not in others. A diet in which segmentation was thought to be effective was that in herbivores (e.g. guinea pigs) whose diet have a higher solid volume ratio (Thuneberg and Peters 2001; de Loubens et al. 2013). Under such conditions, luminal contents would exhibit weak gel-like properties (Lentle et al. 2005) ideal to promote the irreversibility of flow (i.e. luminal contents are mixed). Irreversibility of flow may occur during segmentative contraction as the liquid phase may be expressed from digesta to the gut periphery and subsequent incomplete re-expansion of digesta due to incomplete recovery of the liquid phase (de Loubens et al. 2013).

2.2.4. Pendular activity

Pendular activity (i.e. contraction) motility patterns of the small intestine was first described by Baylis and Starling (1899) as akin to the movement of a pendulum due to the observed 'side to side' movement of a section of gut wall that did not propagate and could be easily detected by the naked eye. Pendular activity has also been described as 'sleeve contractions' (Christensen 1984) due to observations of the gut section undergoing pendular contraction being drawn over adjacent sections in a 'sleeve-like' manner (Krishnan 1932). Pendular activity is thought to occur by the alternation of relaxation and contraction in longitudinal muscles (Thuneberg and Peters 2001) and associated small passive dilatations of circular muscle (Krishnan 1932). An example of the frequency of pendular contractions was 34 to 38 cpm of the proximal small intestine of rats (Lentle et al. 2012).

2.2.4.1. Promotion of mass transfer

Initial reports on the effect of pendular activity on the movement of luminal contents in the small intestine have suggested that such gut motility patterns could generate vortexes and hence augment mixing and mass transfer in all regions of the gut lumen (Christensen 1984, Melville et al. 1975). However, a recently developed Lattice Boltzmann computational model predicted that pendular activity does not result in such straightforward and efficient models of mass transfer. Pendular activity was not able to generate sufficient radial velocity to facilitate the movement of lumen contents from the lumen centre to the gut periphery for absorption especially only after a single contraction (de Loubens et al. 2013). It is more likely that inter-mixing of luminal contents would occur by the deformation of the boundary of adjacent and unique elements (within lumen contents) thus resulting in an increase of the interface area between the elements. However, such a model of mixing and mass transfer would be predominantly valid only for luminal contents located at the gut periphery (de Loubens et al. 2013).

In addition, the generation of asymmetric mixing by such a motility pattern would also lead to the enhancement of mixing and mass transfer in the small intestine (Lentle and Janssen 2011) especially at the gut periphery. Asymmetric mixing may be generated during pendular activity by three possible causes: uneven distribution of contractile activity over the radius of the gut wall causing visible local indentations on the antimesenteric side of the gut (Thuneberg and Peters 2001), the inconsistency of the contractions of longitudinal muscle that may vary in their origin and direction of propagation (Stevens et al. 2000; Lammers 2005) as well as differences in amplitude and phase angle of each successive pendular contraction (Lentle et al. 2012).

2.2.5. The postprandial period

The time interval from the time of the intake of food until the return of phase III of MMC (see sub-section 2.2.1), is known as the postprandial period (Husebye 1999). While some gut motility patterns observed during the MMC cycle of the interdigestive period were similar to those observed during the postprandial period, those observed during the postprandial period were not as active. For example, peristaltic contractions during the postprandial period were marked by a reduction of half (on average) the propagation length of that observed during the MMC (Sarna et al. 1989).

It has been long presumed that peristaltic contraction was one of the main motility patterns of the postprandial period that drives mixing and mass transfer of luminal contents (Saladin 2007). However, a number of studies report that peristalsis observed during the postprandial period were not as vigorous (Sarna 1985; Schemann and Ehrlein 1986). Conversely, the predominant small intestinal motility patterns of the postprandial period such as segmentation and pendular activity (Thuneberg and Peters 2001, Lentle and Janssen 2011) have so far been conspicuously ignored in studies of their effect on mixing and mass transfer.

It is likely that both motility patterns (segmentation and pendular activity) are both not prominent at the same time for a given type of animal with a particular diet. For example, as was detailed previously (sub-section 2.2.3.1), segmentation may be suitable for augmenting mixing and mass transfer in an herbivore. Under these conditions (i.e. digestion in a herbivore) the expression of the liquid-phase from digesta may also increase slip at the wall (Barnes et al. 1989). As such, for reasons that make segmentation effective (of the specific rheological conditions of the herbivore's digesta), are the reasons why pendular activity may not be as effective. The increase of

slip at the wall of the gut may impair the transmission of shear from the wall to luminal contents and hence render pendular activity less effective in promoting mixing and mass transfer in the herbivore gut (de Loubens et al. 2013). The findings that lower frequencies of pendular activity were observed in herbivores (e.g. guinea pig) while higher frequencies were observed in omnivores (e.g. rat) supports such a hypothesis (Lentle et al. 2012).

2.2.6. Compartmental organization of mixing and mass transfer in the lumen.

It has been typically assumed that mass transfer of nutrients and pharmaceuticals to regions adjacent to the enterocytes for absorption can be accounted for in a single step. Computational models that have been used in industry such as advanced compartmental absorption and transit (ACAT) models (e.g., TNO Gastro-Intestinal Model built by TNO Nutrition and Food Research based in the Netherlands and GastroPLUS^{TM} built by Simulations Incorporated based in the USA) used to assess drug pharmacokinetics and pharmacodynamics, have mostly been developed using such simplifications. However, it is conceivable that mixing and mass transfer of luminal contents in the gut lumen may well approximate a two-step (i.e. two-compartment) process. Initial work that suggested such organization of gut lumen mass transfer was that of Melville et al. (1975). They postulated that gut motility patterns such as pendular contractions may play an important role to displace nutrients and other substances from the lumen centre to the gut periphery.

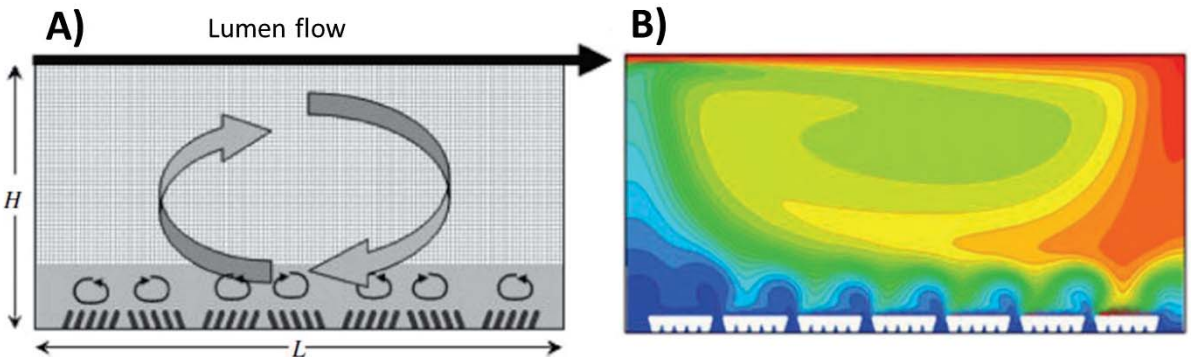

Figure 2-7: Multiscale numerical model of mass transfer in the gut developed by Wang et al. (2010). A) The model of half the diameter of the small intestine (H) and a given segment of length (L) was developed to study macro-micro-scale interactions with lumen flow in the gut lumen and groupings of villi at the lower surface. B) One of their findings is that the outer macro scale eddy (generated by propulsive gut motility patterns such as peristalsis) augments the mass transfer of lumen contents between the outer macro compartment of the lumen centre and the second micro compartment at the gut periphery (adapted from Wang et al. 2010).

More recent research has postulated a similar model of mixing and mass transfer (Wang et al. 2010) (Figure 2-7). In computational simulations, the authors indicated that fluid containing high concentrations of solutes in the macro compartment in the lumen centre would be exchanged with fluid of low solute concentration at the second micro compartment at the gut periphery. The exchange was thought to be facilitated by the formation of an outer macro scale eddy generated by propulsive gut motility (e.g. peristalsis) causing aboral lumen flow, which transmitted shear through the gut lumen Figure 2-7A. In addition, this model also predicted that a separate mixing mechanism of the pendular movements of villi augmented mass transfer in the micro compartments (i.e. perivillous region) and contributed to micro-macro compartmental exchange (Wang et al. 2010).

2.2.7. Concluding remarks on the effects of small intestinal motility patterns

This section highlighted the various types of postprandial motility patterns and periods as well as their potential contributions to mass transfer in the perivillous space. Overall,

there are still gaps in current knowledge of how mixing actually occurs in the *in vivo* gut from an 'insiders' perspective (i.e. understanding gut mixing functions from inside a live gut).

More work is needed on gut motility patterns such as pendular activity and segmentation given that they are likely to be more prominent while peristalsis is less so during the postprandial period. In addition, most of the observations of the mechanisms of mixing and mass transfer attributed to postprandial gut motilities noted in the section have been inferred from external observations of the function of the small intestine (i.e. the 'black box' effect). Hence more studies are needed to determine the effects and mechanisms of segmentation and pendular activity especially experimental observations conducted under conditions that are more reflective of *in vivo* digestion.

Computational modelling studies that were purportedly built on pre-existing knowledge of the mechanisms of gut function have also been highlighted in this survey. From a survey of those studies, it is clear that there is a need for the development of models that better reflect physiological conditions and parameters as well as being incorporated with up to date information that has been outlined in this section and those to come.

2.3. Small intestinal villi

One of the main features of the gut wall architecture is the presence of villi. For this reason, a survey of literature of the current knowledge available on the external and internal structure of villi, its motility, known functions, and possible contribution by villi to mixing and mass transfer in the small intestine will be explored in this chapter.

Much of the works are based upon histological formalin fixed small intestinal samples unless stated otherwise. As such, caution is required before the generalisation of the information presented to inform the knowledge of conditions that would be encountered by digesta *in vivo*. Further, it is known that histological fixing of gut samples can permanently alter the mucosal surface and associated villi (Lentle et al. 1997).

2.3.1. Morphology of villi

Overall, villous morphology and numbers vary over a wide spectrum across different sites within the small intestine of humans and animals.

2.3.1.1. Shape

Scanning election microscopic observations of the chicken duodenal mucosal surface showed villi that were flattened and plate like (Yamauchi and Isshiki 1991). Endoscopic observations in the duodenum of humans appears to support the reported shape of duodenal villi showing a predominance of flattened finger shaped villi (Cammarota et al. 2004). Fresh biopsy intestinal samples viewed under the microscope show that in the jejunum of humans, finger shaped villi were interspersed with flattened leaf shaped villi. In the ileum there was a greater number of rounder finger shaped villi observed than in the jejunum (Holmes et al. 1961). Although the authors use differing terms (e.g. flattened paddle, plate-like or leaf-shape) to describe their observations, it seems that the

observed villi in the proximal small intestine were all similarly shaped as shown in Figure 2-8 presenting the villi observed in the various studies mentioned above.

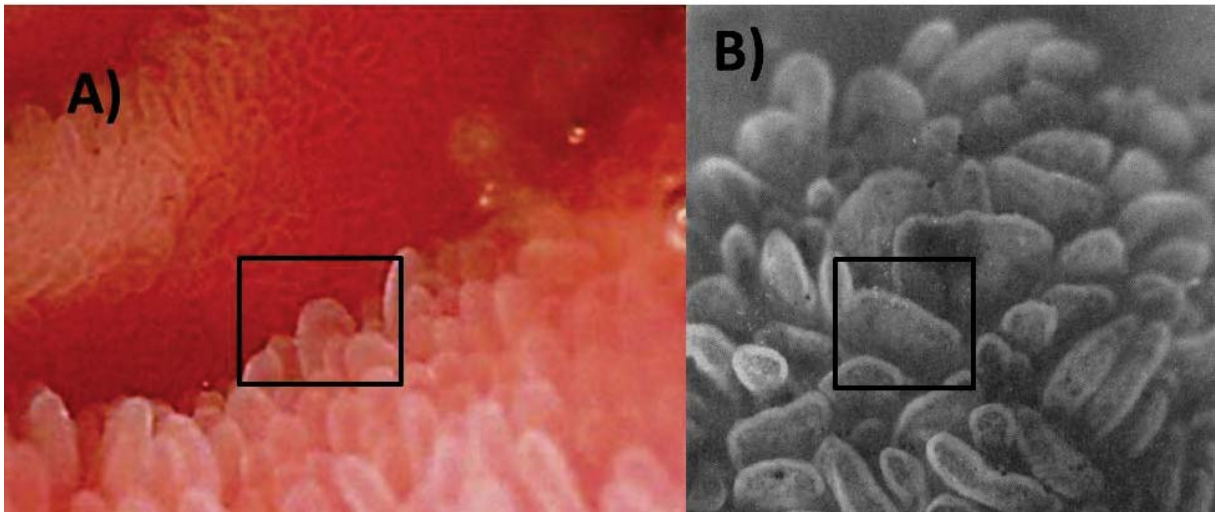

Figure 2-8: Reproduced images of duodenal villi from endoscopy A) (Cammarota et al. 2004) and B) microscopy of fresh biopsy samples of jejunal villi (Holmes et al. 1964). Though different names were used to describe the shape (flattened finger or plate like), they appear to have a similar flattened 'paddle-like' shape as seen in the squares on the images.

Therefore, on the reports of these studies, it is possible that the shape of villi from proximal to more distal sections of the small intestine is distributed in the following manner: a predominance of flattened 'paddle-like' shape in the duodenum, a mix of flattened 'paddle-like' shaped villi and rounder finger shaped villi in the jejunum and a predominance of the rounder finger shaped villi in the ileum. The latter being demonstrated in Figure 2-9A and B, which shows a predominance of rounder finger shaped villi on fresh biopsied ileal samples of humans (Holmes et al. 1961) and histologically fixed distal ilea of small mammals (Barry Jr 1976; Koopman et al. 1987).

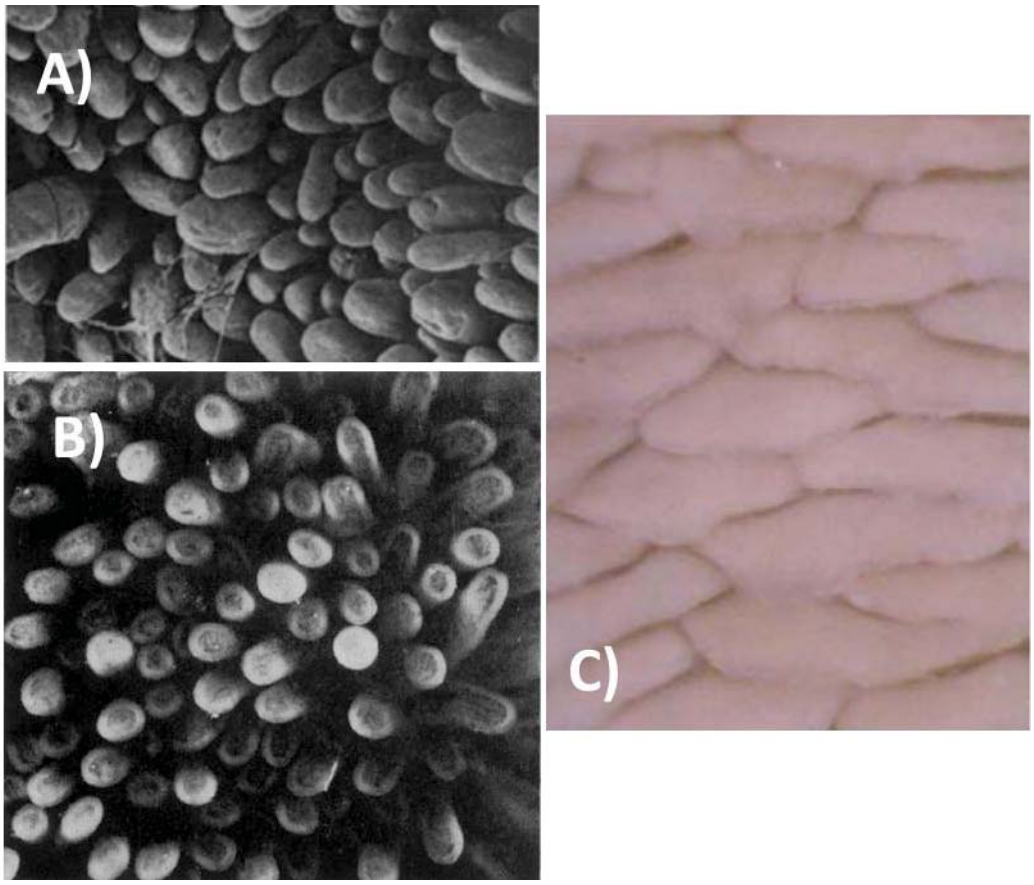

Figure 2-9: Images of ileal villi published in A) Koopman et al. (1987), B) Holmes et al. (1965) and C) Hosoyamada and Sakai (2005). The ileal samples of Holmes et al. (1965) were fresh biopsy samples while the rest were histologically fixed samples.

However, other observations of the ileal villi in the rat small intestine show ridge-like villi with villous widths that were almost the same as their lengths (Yamauchi and Isshiki 1991; Hosoyamada and Sakai 2005, Figure 2-9C). These ridge-like villi may be an artefact of histological procedures (e.g., the application of formalin to the sample that may have permanently altered the landscape of the mucosal surface and associated villi) (Lentle et al. 1997). Alternatively, the appearance of ridge shaped villi may also have been due to the diet of the rats prior to harvesting of their intestine (Takano 1964). In addition, it was observed that fresh biopsied intestinal samples appear to have larger gaps in between villi (i.e. intervillous spaces) as compared to histologically processed samples (Figure 2-9B and C).

2.3.1.2. Dimensions

Table 2-1 and Table 2-2 present the length and width of villi for a selection of mammals. There appears to be a general trend for villous lengths and widths to decrease in the aboral direction. The range of duodenal, jejunal and ileal villous lengths across all animals compared were 380-840 µm, 360-780 µm and 210-550 µm respectively.The range of duodenal, jejunal and ileal villous widths across all animals compared were 110-600 µm, 80-550 µm and 95-470 µm respectively.

Length (µm)	Duodenum	Jejunum	Ileum	References
Dogs	650-810	580-670	460-550	Kuzmuk et al. (2005)
Rats	450-590	420-570	250-375	Daniel et al. (1989)
Pigs	380-430	360-400	275-310	Davidson et al. (1977)
Shrew	440-810	390-610	210-410	Barry (1976)
Bats	500-840	450-780	260-420	Barry (1976)

Table 2-1: Villous lengths for a selection of small mammals. There appears to be a general trend for villous lengths to decrease in the aboral direction. The lengths are in the lower end of that reported in humans. The figures also indicate that an increase of body mass does not necessarily result in a proportionate increase in villi lengths.

Width (µm)	Duodenum	Jejunum	Ileum	References
Dogs	165-185	185-220	170-190	Kuzmuk et al. (2005)
Rats	500-600	185-215	95-115	Southon et al. (1989), Levitt et al. (1996), Menge et al. (1975)
Pigs	140-170	110-170	110-160	Jin et al. (1994)
Shrew	110-170	80-140	100-290	Barry (1976)
Bats	300-600	310-550	230-470	Barry (1976)

Table 2-2: Villous widths for a selection of small mammals**.** There appears to be a general trend for villous widths to decrease in the aboral direction.

The range of villi lengths were at the lower end of that reported in humans of 400-1000 μm (Ham 1969; Weinstein et al. 1969; Troeger et al. 2007). The tables also indicate that an increase of body mass does not result in a proportionate increase in villi lengths given that the villous lengths of the rat were either longer or of the same length as those of a pig. It should also be noted that all data presented were from findings of histological studies (e.g., hematoxin & eosin or formalin-fixed samples). Such data of the small intestine may not be truly reflective of actual dimensions *in vivo* but given the scarcity of results available from fresh intestinal samples, these results are the best estimates available of villous dimensions.

2.3.1.3. Density

Villous density of formalin-fixed intestinal samples of various small of mammals ranged from 5 to 40 villi per mm^2 of gut mucosa (Barry Jr 1976; Carr and Toner 1984; Dressman and Yamada 1991). The villous densities on exteriorized loops of dog small intestine (*in vivo* observations) were 18-20 villi per mm^2 (Womack et al. 1987). This example shows that villous densities on fresh gut samples of dogs at least were within the range of those observed for a range of formalin fixed gut samples of mammals.

However, as noted earlier, caution is required before accepting the results that were from samples that have been histologically fixed. The discrepancy between histological and of living samples is highlighted in the following: the villous density of rat small intestine on formalin fixed samples was lower (65 per mm^2) (Kararli 1995) than that from examinations of *ex vivo* gut samples (80 to 90 villi per mm^2) (Nakajima et al. 2001). While this observation appears to contradict an earlier observation (see sub-section 2.3.1.1) that the effect of histological processing reduces the intervillous space size, the salient point is that the true effects of histological processing (of which there

are a variety of techniques) on intestinal samples are currently unknown. Thus there is a need to perform studies to formally characterize the effects of various types of histological processing techniques on intestinal samples.

2.3.2. Cellular composition of villi

The mucosa of the small intestinal lumen is an irregular surface as a result of villi and invaginations (small 'pockets' also known as crypts of Lieberkühn) that are lined by intestinal epithelial cells (Potten et al. 1997). It is currently believed that epithelial cell genesis occurs from within the crypts with most of the cells migrating upwards along villi as they mature (Gordon 1989). However, there is currently debate as to the exact location within the crypts that epithelial cell genesis occurs (Barker 2014). The cells undergo apoptosis (i.e. cell death) before being sloughed off at the villous tips into the intestinal lumen (Lee 1971). The morphology and function of the main types of epithelial cells that line the small intestinal mucosa are described below.

2.3.2.1. Morphology and function of intestinal epithelium cells

The four principal varieties of epithelial cells that line the intestinal mucosal are; absorptive enterocytes, goblet cells, paneth cells and enteroendocrine (EC) cells (descriptions are below). All cells are linked by intercellular tight junctions that bind the epithelial cells together by their lateral surfaces as well as generally preventing the breach of large substances and foreign particles across the epithelium (Trier and Madara 1994), although transport of molecules of water and sodium have been reported to occur across tight junctions (Ma and Anderson 2006). In addition, dendritic cell (DC) processes, which play a role in the intestinal lumen in detecting microorganisms in this region (Rescigno et al. 2001), were observed to extend across the epithelium into the lumen through the tight junctions.

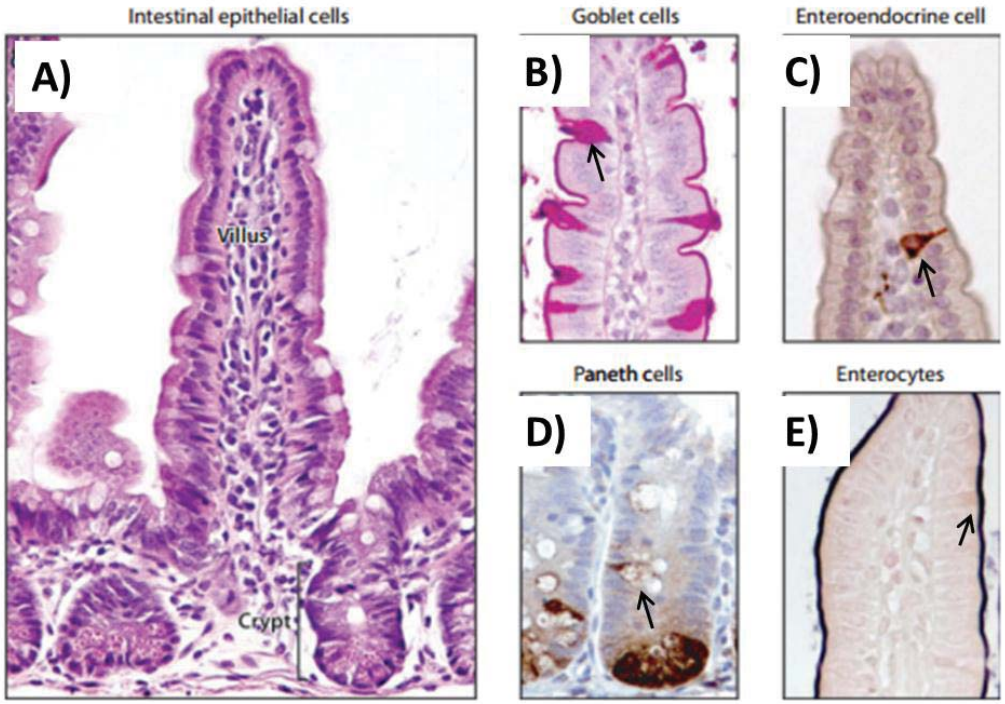

Figure 2-10: The intestinal epithelium and immuno-histochemical analysis of the four main cell types that are located on the epithelium. A) Haematoxylin and Eocin (H&E) stained gut mucosa shows the general morphology of the intestinal epithelium and its organization into crypts and villi. B) Periodic acid-Shiff (PAS) stain highlights goblet cells (e.g. indicated by the arrow), C) anti-synatophysin staining highlighting enteroendocrine cells (e.g. indicated by the arrow), D) lysozyme stain highlighting Paneth cells (e.g. indicated by the arrow) whilst the E) alkaline phosphatase stain highlights the enterocytes (e.g. indicated by the arrow) (Adapted from van der Flier and Clevers 2009).Absorptive enterocytes are columnar, highly polarized cells covered by closely packed micro-villi protruding out through the apical cell membrane forming a 'brush border' at the cell apical surface (Snoeck et al. 2005) (Figure 2-10A and E). The micro-villi begin to elongate out of the cell membrane as the absorptive enterocytes differentiate from stem cells in the crypts before achieving its normal size and density during cell maturity (Smith 1985). Absorptive enterocytes make up the majority of the cells found on the epithelial surface of the intestinal mucosa (up to 80%) (van der Flier and Clevers 2009). The initiation of solute absorption by the absorptive enterocytes occurs in the region of the apical cell surface known as the glycocalyx, which reportedly has a thickness of half a micron in the rabbit (Maury et al. 1995). The glycocalyx of this

cell is composed of secreted transmembrane mucins (for more detail and discussions see section 2.4) (Snoeck et al. 2005).

Goblet cells have an appearance of a wine goblet due to the distension of the upper two thirds of the cell as a result of mucin granule storage (Specian and Oliver 1991) (Figure 2-10B). This intestinal cell-type is known to be both a mucus and trefoil factor (proteins with a defensive function in the intestinal lumen) secreting cell (Trier and Madara 1994). Goblet cell mucus functions include the lubrication of the mucosa, as a protection barrier against mechanical and chemical damage and as a barrier against pathogenic invasions (van der Flier and Clevers 2009).

Enteroendocrine (EC) cells are columnar cells that are similar in structure to the absorptive enterocytes but are broader than the latter and possess a slender apex (Figure 2-10C). Unlike the absorptive enterocytes, they have sparse and irregular micro-villi (Sander et al. 2006). These cells in the gut are the largest population of hormone-producing cells, which serve to regulate gut function and are the chemo-receptors that sample lumen contents (Sternini et al. 2008). EC cells make up approximately 1% of the total population of cells located on the epithelial surface.

Paneth cells have a broad base and an increasingly narrower apex forming a truncated pyramid shape (Figure 2-10D). Some rudimentary micro-villi have been observed at the apex. Paneth cells are the main variety of the four principal differentiated cells that migrates towards and resides in the crypts of Lieberkühn and may extend up to halfway up the crypts (Trier and Madara 1994). Paneth cells have a defensive function in the gut through the secretion of peptides, defensins and other antimicrobial substances (Barker et al. 2008; van der Flier and Clevers 2009).

Other smaller populations of cells that line the small intestine mucosa include M-cells and 'brush' cells (Trier and Madara 1994). M-cells have similar attributes to absorptive enterocytes but do not have a brush border and glycocalyx. The apical surface of M-cell is covered in sparse microvilli or nanofolds that facilitate its putative function of foreign matter identification and activation of host immunity (Borchard 2009). M-cells were thought to originate from crypts that are adjacent to both villi and a Peyer's patch (i.e. aggregated lymphoid tissue tasked with the role of immune surveillance of the gut lumen environment). While the stem cells on the villus side of the crypts would differentiate into any one of the four principal epithelial cells, some of the stem cells on the Peyer's patch side of the crypts would differentiate into M-cells and migrate upwards to reside on the Peyer's patch (Corr et al. 2008). Brush cells are pear-shaped with a narrow apex and are also known as caveolated or tuft cells – are so-called due to the presence of long brush-like structures (thick micro-villi unlike those of the absorptive enterocytes) protruding from the apical surface. These cells may also play the role of a chemo-regulator (Pavelka and Roth 2010) by detecting and secreting electrolytes such as Na^+ and K^+ (Ogata 2006) as well as sensory receptors of gustatory perception in the small intestine (Gebhard and Gebert 1999).

2.3.3. Villous internal structure

The main villi stroma (i.e. the collective network of connective tissue of the villi internal structure) is composed of an upward projection of lamina propria (LP; connective tissue) (Palay and Karlin 1959), which progressively increases in density from the villous apex to the base (Hosoyamada and Sakai 2005). Within the villous LP is a central lacteal that is surrounded by a mesh of arteries (Jodal and Lundgren 1986; Hosoyamada and Sakai 2007). Blood vessels are aligned parallel to the lacteal and together with the villous central arteries, begin at the submucosal layer and extend into

the villous apex (DeSesso and Jacobson 2001; Hosoyamada and Sakai 2007) (Figure 2-11A). The lacteal, which extends to the level of mucosal crypts from the villous apex, joins to a musculated central lymphatic system connected to the intestinal mesenteries (Miller et al. 2010).

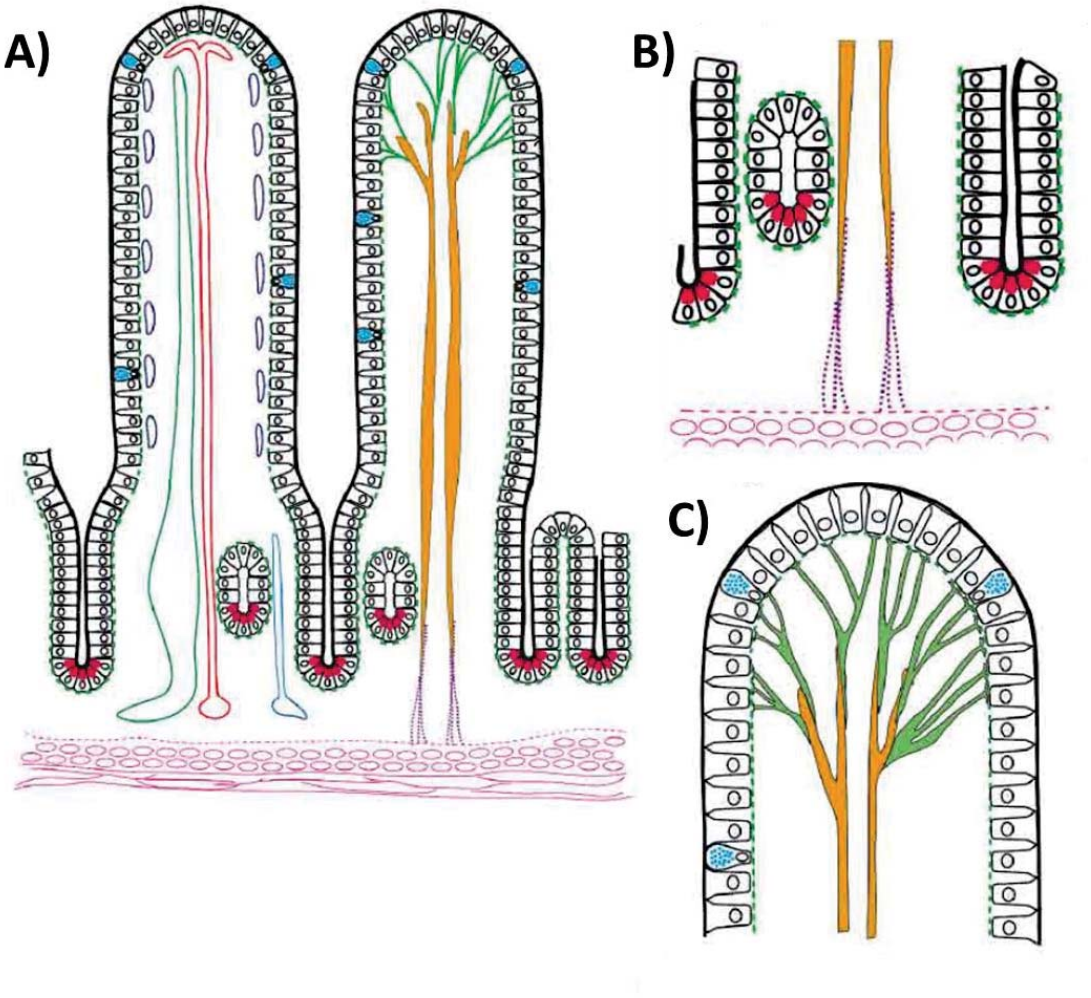

Figure 2-11: The structural organization of selected constituents of the villi stroma. A) In the villi on the left side, the ascending (red) and descending blood vessels (blue), arteries (purple) and lacteal (green) at the centre of the intravillous space are illustrated. On villi on the right side, villous smooth muscle (VSM) (orange), fibroblasts (green), in addition to smooth muscle in the underlying lamina propria (LP) are shown. B) The VSM are tapered and connected to microtendons of collagen fibrils at the lower part of pericryptal LP, which are anchored to the bottom surface of the underlying mucosa LP. C) VSMs are also connected to the basolateral surface of epithelial cells at the villous apex by fibroblasts (adapted from Hosoyamada and Sakai 2007).

Within the villous stroma LP, villous smooth muscle (VSM) fibres that are spindle shaped with tapered ends extend to the apex of villi (Güldner et al. 1972). VSM are aligned perpendicularly with respect to the underlying mucosa and are grouped in bundles of varying numbers and lengths with a progressive reduction of smooth muscle cells towards the villous apex (Güldner et al. 1972; Hosoyamada and Sakai 2007). The highest concentrations of VSM are observed adjacent to the arteries and lacteal at the centre of the villi (Güldner et al. 1972), where they appear to act as a centrally located 'backbone'. VSM are connected to the underlying mucosa LP (that is just above the muscularis mucosae) by collagen fibrils that are anchored to the bottom of the LP (Figure 2-11B). The collagen fibrils act to mechanically transfer any forces experienced by the VSM to the gut wall smooth muscle layer (Hosoyamada and Sakai 2007) – possibly to dissipate any shear forces experienced by the villous apical regions hence maintaining a rigid villous.

Cells with multi-branched projections known as fibroblasts that are regularly distributed throughout the villous stroma are also located within the villous LP network (Palay and Karlin 1959). The fibroblast processes usually branch out to approach and 'embrace' all of the other intravillous constituents (e.g. lacteal, arteries) and VSM bundles where some constituents may even be embraced by more than one fibroblast (Güldner et al. 1972). Fibroblasts also connect the VSM to the basolateral surface of apical epithelial cells overlying villi (Figure 2-11C).

2.3.4. Villous motility

The motility of villi in animals was first observed by Gruby and Delafond (1843) and the few studies done on villi motility in the ensuing 100 years describe similar villous motility patterns to those found initially (Hambleton 1914; King and Arnold 1922;

Carleton and Florey 1927). Villous motility patterns reported in literature may be broadly categorized as two types; villous waving and 'piston-like' (i.e. periodic retraction and subsequent extension) movements of villi (Hambleton 1914; King and Robinson 1945; Womack et al. 1987).

Villous motility was reported to be abolished by agonist substances such as atropine (Hambleton 1914) on the exteriorized loop of intestine from a living dog. In addition, villous motility is temperature dependent. Studies reported that villi from an exteriorized loop of small intestine of a living animal (i.e. *in vivo* preparations) have been found to be most active at physiological temperatures (37-38°C) (King and Robinson 1945, Womack et al. 1987) while Lee (1971) claimed that villi of *in vitro* gut samples would only begin to contract at temperatures below 28°C. However, contractile activity of villi at lower temperatures was also accompanied by shedding of the villus tissue from the villous tips (i.e. 'epithelial sloughing') and zero or negligible fluid transports occurring across the intestinal mucosa (Lee 1971).

A video-microscopy study of canine intestinal samples *in vivo* claimed that villous motility could be established as independent from gut contractions (e.g. peristalsis) (Womack et al. 1987). Despite this, there are no quantitative comparisons of villous motility and gut contraction frequency reported to date, especially during the postprandial period. Hence, it is unclear that genuine villous motility, as opposed to that induced by minor gut wall contractions (i.e. segmentation or pendular activity) has actually been observed. For example, it may be that 'waving' movements of villi could be attributed to pendular activity of the gut. Likewise, initial suggestions of the existence of the hormone villikinin that would act as a humoral promoter of villi motility (Kokas and Johnston 1965) has been questioned in more recent research (Womack et al. 1988a).

The intravillous structure of villi has been put forth as evidence for the existence of villous motility. For example, contractile activity of villous smooth muscle (VSM) bundles that are oriented along the longitudinal axis of villi within the villous stroma has been postulated as the cause of villous motility (Carleton and Florey 1927, Hosoyamada and Sakai 2005). However, there is currently no evidence of the contractility of VSM and it is likely that VSM instead confers rigidity to villi. For example, Hosoyamada and Sakai (2007) propose that the VSM plays a role as an intravillous scaffold that maintains the integrity of the shape of villi against the osmotic pressures of fluid being absorbed into villi.

Overall, even if genuine villous motility exists, there is currently no experimental evidence that villous motility has any contributions towards the enhancement of mixing and mass transfer in the perivillous space despite suggestions to the contrary by Strocchi and Levitt (1993). During *in vitro* experimentation of villous motility on the jejunum of dogs, it was observed that an increase in villous motility correlates with a *decrease* in the amount of fluid absorbed across the mucosal epithelium (Lee 1971). This suggests that villous motility is actually not favourable for absorption of nutrients and other substances. Evidence for initial suggestions that villous motility improves mass transfer (Mailman et al. 1990, Strocchi and Levitt 1993) has not been forthcoming to date.

Finally, it is also conspicuous that the last major body of work that directly assessed villous motility and its possible effects on luminal contents mass transfer were conducted more than 20 years ago (Womack et al. 1987; Womack et al. 1988a; Womack et al. 1988b; Mailman et al. 1990). While this could mean that the body of work available to date is conclusive evidence of the presence of villi motility, the discussions presented in this sub-section suggests otherwise. More experimental work is especially required to establish the existence of the motility of villi (whether

spontaneous or coordinated) as an event separate to *in situ* non-propagating radial and longitudinal contractions of gut wall.

2.3.5. Possible villous functions

Various functions of villi have been suggested from a survey of the literature, some are discussed in the following sub-sections:

2.3.5.1. Increased surface area for absorption

It has long been stated as 'fact' that the reason why the mucosal surface of the small intestine is convoluted to form evaginations known as villi was so that the available surface area for absorption (e.g. nutrients and other substances) was increased. Some authors estimate that small intestinal villi increase the surface area of the intestinal mucosa by a factor of 3 to 10 times depending on the species of animal (Wilson 1967; Pappenheimer 1998). Others have even suggested that the total area of small intestinal mucosa available for absorption of nutrients and other substances is equal to the area of a tennis court (Cairns 1970; Parekh et al. 2005) (= 260 m^2).

However, it is not clear that the entire surface of villi (i.e. all absorptive enterocytes) is capable of absorption functions. The suggestion that villi increase the total area for absorption hinges on the assumption that all absorptive enterocytes are equally capable of absorption of luminal contents. It has been suggested that only those enterocytes near the apex of a villous are mature enough to be capable of absorbing nutrients and other substances (Potten et al. 1997; Booth and Potten 2000). The observation that microvilli on enterocytes are still elongating while migrating up along villi appears supportive of this supposition (Smith et al. 1984). Other researchers using auto-radiographic imaging (Kinter and Wilson 1965; King et al. 1981), micro-puncture transport (Lee 1969),

genome expression analysis (Tümer et al. 2013) (Figure 2-12), and solute perfusion studies (Westergaard and Dietschy 1974; Ryu and Grim 1982; Levitt et al. 1990) have indicated similar conclusions.

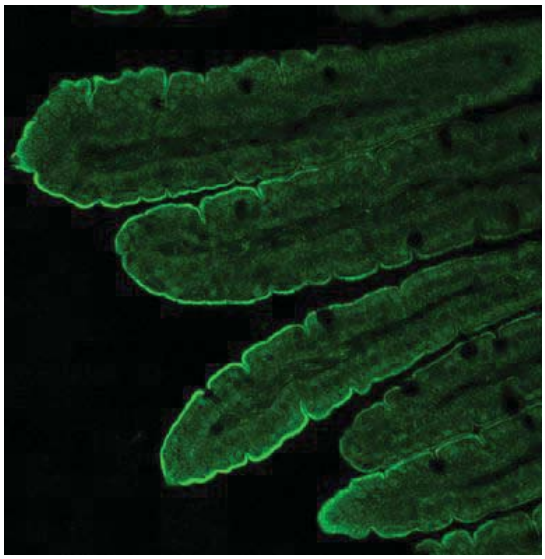

Figure 2-12: Expression of the B°AT1 amino acid transporter along the length of villi in the mouse small intestine. A clear gradient of protein expression from the villous apex to the base can be observed from the decreasing intensity of the green dye from the villous tips to the base (adapted from Tümer et al. 2013). This result is in support of the idea that not all of the villous surface area would play an absorptive role.

2.3.5.2. Micro-mixing system

It has been postulated that mixing and mass transfer of nutrients and other substances from the lumen centre to regions adjacent to enterocytes for absorption is facilitated by a degree of advective flow to displace fluid rather than being totally reliant on molecular diffusion (Levitt et al. 1984; Levitt et al. 1990; Strocchi and Levitt 1993). This suggestion is supported by the work of Anderson et al. (1988) who observed that anesthetized animals showed larger resistance to mass transfer in the small intestine as compared to conscious animals.

Based on these studies, it was thought that villous motility was able to augment mixing and mass transfer of luminal contents especially in the perivillous region. The ‘piston-

like' or 'waving' movements of villi (Hambleton 1914; King and Arnold 1922) were thought to be mixing mechanisms that could stir luminal contents thus augmenting mass transfer (Womack et al. 1987; Wang et al. 2010). Reports that human patients with coeliac disease (i.e. a condition characterized by villous atrophy) had a larger unstirred water layer value (an early measure of the extent of resistance to mass transfer) as compared with patients with a healthy gut (Read et al. 1977) have been used as evidence for such supposition (Wang et al. 2010).

However it may be fallacious to regard the findings of those studies as conclusive evidence of the impact of villous motility on mixing and mass transfer. The finding that anesthetized animals had higher levels of resistance to mass transfer of luminal contents may be due to the absence of gut contractile activity and not necessarily due to the motility (or otherwise) of villi, whilst the finding that the absence or lack of villi in coeliac disease patients contributes to reduced rates of mass transfer may instead be attributed to a reduction of enterocytes (prominently found on villi) available for absorption.

With new knowledge being gained of postprandial gut contractions *in situ* in recent decades (Lentle and Janssen 2011), it may be revealed that villi do play a role in the mixing of perivillous luminal contents, albeit in a passive mixing system. Such a mechanism may be able to generate necessary asymmetric vortexes or local flow turbulence to augment mixing and mass transfer. The following are two possible mechanisms:

A) Assuming that villi were rigid structures that have little or negligible movements when in contact with lumen flow, a 'forest' of villi may augment mixing and mass transfer in the small intestine just as static micro-mixers are increasingly used in

chemical and allied industries for this function in micro-channels (Bertsch et al. 2001). Such mixers function on the basis of the mixer element (in the case of the small intestine, an array of rigid and relatively immobile villi) being able to split, rearrange and recombine the various elements of flow. Such mixing mechanisms have been reported to be effective in mixing fluids under laminar flow (i.e. of Reynolds numbers as low as 1 and no more than 100), conditions that are common in the field of microfluidics (Bertsch et al. 2001) and within the range expected of flow and mixing in the small intestine (Takahashi 2011; Love et al. 2013).

B) Under similar assumptions as mentioned in A), it is also likely that vortexes may form behind villi from lumen flow (e.g. flow that follows Poiseuille's law[1]) given that villi may typically be approximated as bluff bodies (i.e. an angular body rather than one aerodynamically shaped) (Buresti 2000). Indeed similar mixing mechanisms have been postulated by Takahashi (2011) who suggested that Karman vortexes (i.e. a pattern of swirling vortexes; Figure 2-13) could be formed behind villi that could augment mixing and mass transfer in the perivillous space. However, Karman vortexes may not form should the local Reynolds number be any less than 40 (Takahashi 2011).

[1] Poiseuille's flow, also known as pressure induced (i.e. steady viscous fluid) flow in an enclosed channel (e.g. pipe) and is a function of the viscosity of flow and the length as well as radius of the pipe. Flow is laminar and the axial velocity flow profile is typically recognized by a parabolic shape with the flow velocity fastest at the pipe centre and slowest at the pipe wall.

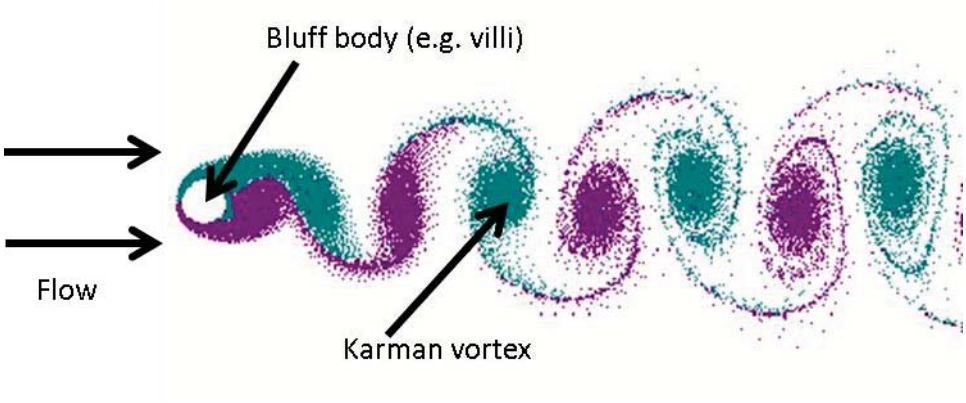

Figure 2-13: Assuming that villi are rigid structures and may be approximated as a bluff body, Karman vortexes may form behind villi. The flows routes on opposite sides of the bluff object are given different colours to better illustrate that the vortices are shedded from alternate sides of the object.

2.3.5.3. 'Cape Canaveral' for luminal hormones and enzymes

Micro-villi that make up the 'brush-border' of absorptive enterocytes located on villi contain bundles of actin filaments (Ubelmann et al. 2011). The actin filament's core is linked to the outer micro-villar plasma membrane by associated protein forming cross-bridges in a 'spoke-like' manner (Mooseker and Tilney 1975). The micro-villi are attached to the apical cytoskeleton of the enterocytes through the cores of the micro-villi descending through the apices of cells (Hull and Staehelin 1979). It was initially assumed thought that these 'brush-border' structures play an important role in nutrient absorption by further increasing the area available for nutrient absorption (Mooseker 1985; Daugherty and Mrsny 1999).

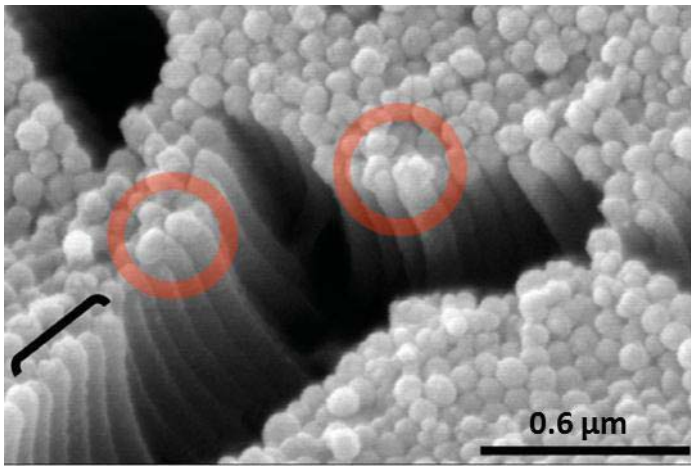

Figure 2-14: Electron microscope picture as evidence for the possible function of villi as 'launching pads' for hormones and enzymes via their micro-villi. The black bracket shows that some microvilli are of regular height and similarly sized tips. The red-circled areas show that other microvilli have irregular or enlarged tips that may indicate the budding of what could be micro-vesicles at the tips of the micro-villi (adapted from McConnell et al. 2009).

Very recent studies have shown strong evidence that micro-villi are 'launching pads' for vesicles (Figure 2-14) with contents that have vital roles for nutrient processing and for the protection against pathogenic invasions (McConnell et al. 2009; Shifrin et al. 2012). Extrusion of micro-vesicles from micro-villi is an active process that occurs by the contractions of actin-myosin fibres (McConnell and Tyska 2007) ejecting micro-vesicles into the intestinal lumen.

2.3.6. Concluding remarks on the influence of villi

In this sub-section, the structure and possible functions of villi have been outlined. Given their structure, villi may play a role in augmenting mixing and mass transfer of solutes in the perivillous space. Together with postprandial gut motility (as outlined in the previous section) a picture of mixing mechanisms, which may enhance mass transfer in the small intestine, has been presented. In the next section, information regarding the type of fluid environment that exists in the gut lumen will be presented. Thus the

literature regarding the context in which mixing and mass transfer in the gut lumen (especially in the perivillous region) occurs will be examined and discussed.

2.4. Mucus in the small intestine

Intestinal mucus was first postulated to be a contributor to the barrier (i.e. resistance) to mass transfer by Smithson et al. (1981). Such a suggestion is conceivable given that mucus is secreted into the lumen of the small intestine and would likely interface between digesta and the intestinal mucosa. As such, it is important to consider the properties, genesis, composition and organization of mucus especially in the context of the small intestine.

Mucus in the small intestine is typically observed as a slippery gel-like semi-permeable barrier that permits the transit of some forms of nutrients while hindering most bacteria and pathogens. Such properties of mucus were due to their attributes as a barrier against substances either by their size (see sub-section 2.4.7) or chemistry (see sub-section 2.4.6) (Cone 2009). Mucus is predominantly composed of water (approx. 95%) while the predominant constituent of the remaining ~5% is a glycoprotein known as mucin (Bell et al. 1984), which is a product of the Muc genes (see sub-section 2.4.1). Electrolytes (e.g. bicarbonate), traces of sloughed off epithelial cells and bacteria (e.g. lipids and proteins) as well as antimicrobial peptides, are among the substances that make up the remaining composition of secreted mucus (Allen et al. 1993; Corfield et al. 2001). The mucus observed in the small intestine is generally hydrated mucin (see sub-section 2.4.2.2) that is secreted from goblet cells (Corfield et al 2001). In addition, enterocytes also secrete mucin that forms the brush border glycocalyx, thought to be attached to a region around the apex of the enterocyte apical microvilli (Maury et al. 1995).

There are generally three distinct types of mucin in the gastrointestinal tract (GIT) (Strous and Dekker 1992; Atuma et al. 2001; Phillipson et al. 2008); A) Mucin that is

secreted but usually remains adhered to enterocytes, B) Mucin secreted by goblet cells, are highly viscid and may not be easily extracted or aspirated from the mucosal surface and C) Secreted mucin (by goblet cells) that forms a mobile and watery mucus that is located above and has similar characteristics as the prior type (mucin type B) of mucus. Assuming that mucus in the small intestine forms a contiguous layer (Allen et al. 1982; Neutra 1987) overlying villi, the thickness of both the adherent and mobile mucus layer have been quantified (Figure 2-15) by micropipette sampling of rat mucus *in vivo*. The adherent mucus layer was thickest in the stomach and colon while the mobile mucus layer was thickest in the distal ileum and proximal colon (Atuma et al. 2001). However, it should be noted that the calculations of the thickness of the adherent mucus by Atuma et al. (2001) did not take into account the thickness of the glycocalyx that has been reported to have a thickness of 400 to 500 nm (Frey et al. 1996). In addition, it is noted that the observation of two types of mucus by Atuma et al. (2001), a mobile and adherent layer in the small intestine has since been challenged (Johansson et al. 2011a). Johansson et al. (2011a) postulated that the mucus that could not be removed by Atuma et al. (2001), which was labelled as the small intestinal adherent layer may in fact have been mucus that could not be removed due to interferences by villi especially in the distal small intestine.

The thickness of the mucus layer over a range of animals was also quantified in a recent study using a cryosample staining method that did not discriminate between adherent or mobile mucus layers. The study found interspecies variation of mucus thickness across pigs, rats and rabbits, with the thickness of mucus disposition in the pig being the most similar to humans (Varum et al. 2012). The mucus thickness calculated by Varum et al. (2012) was 2-3 times less than estimations by Atuma et al. (2001). The discrepancy between the two reported thicknesses of the mucus layer may be due to the technique

used by Atuma et al. (2001), which may have sufficiently agitated the goblet cells of the gut mucosa to secrete more mucins than they would under normal conditions.

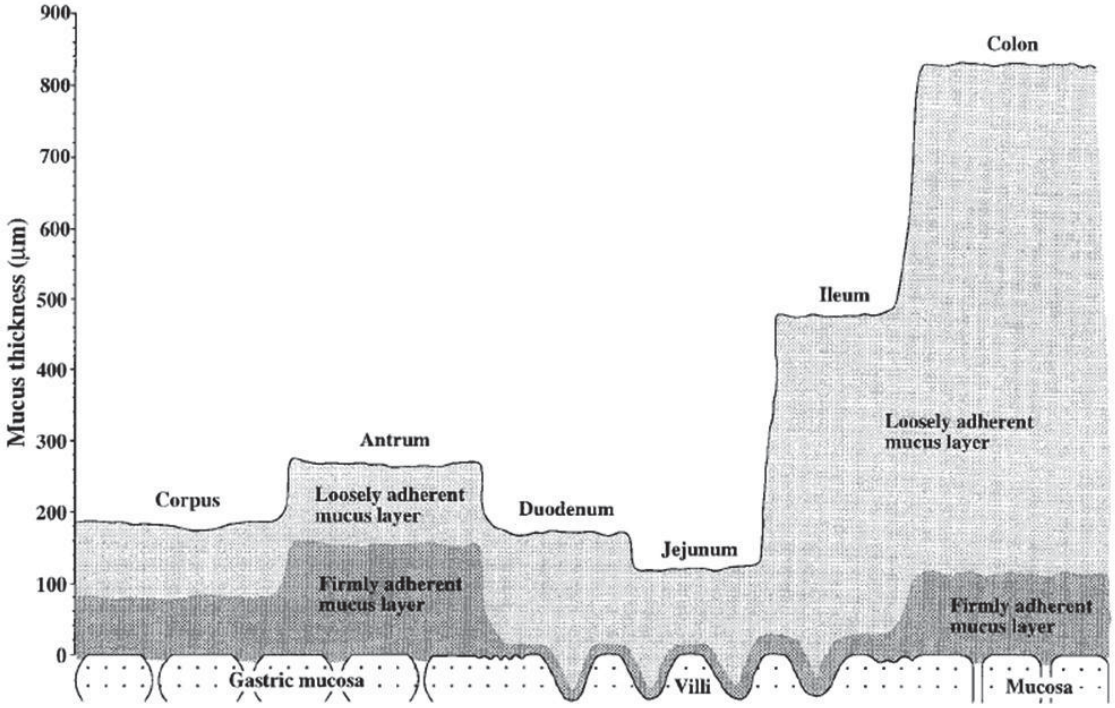

Figure 2-15: Thicknesses of the 2 mucus gel layers *in vivo* in the corpus, antrum, midduodenum, proximal jejunum, distal ileum, and proximal colon of the rat gastrointestinal tract (GIT) (adapted from Atuma et al. 2001).

Although mucin constitutes a small percentage of the overall mucus composition, the properties of mucin are directly responsible for the function of mucus as a whole (Strous and Dekker 1992).

2.4.1. Regional variation of mucin type

Given that different parts of the GIT have unique functions and specific roles in the process of digestion, it is conceivable that mucus produced in each section would have unique properties. One of the ways in which mucin may vary are by the different Muc (i.e. mucin) genes being expressed at the given site along the GIT (Robbe et al. 2003). Mucins have generally been classified into two classes on the basis of their localization post-secretion. The first are secretory mucins that lack a transmembrane domain that are

secreted into extracellular regions while the second are membrane-bound mucins that are also secreted by but bound to their cell of origin due to the presence of a single transmembrane domain on the mucin structure (Singh and Hollingsworth 2006; Johansson et al. 2011a). Mucin that is secreted into the small intestine and colon by goblet cells is largely coded by Muc2 genes (Johansson et al. 2008; Ermund et al. 2013). Conversely, mucin that is secreted and adherent to enterocytes were thought to be predominantly coded by the Muc3, Muc12, and Muc17 genes (Johansson et al. 2011a).

Differences in the concentration of a given type of mucin in the different mucus phases have been reported. For example, it has been reported that the mobile and adherent mucus layer of the colon have differing concentrations of Muc2 expressed mucin where the adherent mucus layer of the colon was observed to have four times the concentration of Muc2 mucin as compared to the mobile layer (Johansson et al. 2008). While such differences could be attributed with the degree of Muc2 mucin secreted to a particular region, it is also possible that the reduction of Muc2 mucin observed in the mobile mucus of colon is due to more proteolytic cleavage through its exposure into the gut lumen (Johansson et al. 2011b).

In addition, the type of mucin located at a given locale may also vary by the degree of and type of post-translational modification of the basic mucin monomer (Rose and Voynow 2006). The following are some examples that make references to the structure of a mucin (mucin structure will be outlined in greater detail in sub-section 2.4.3). A) It has been reported that the side chains of Muc2 mucin in the small intestine has a greater proportion of sialylated oligosaccharides as compared with that in the large intestine. Conversely, Muc2 mucin in the colon was observed to have a greater proportion of sulphated oligosaccharides as compared to the small intestine (Karlsson et al. 1997). B)

The O-acetylation of sialic acids of mucin was also observed to increase from the small intestine to the colon (Robbe et al. 2003). C) The composition of O-glycosylated side chains of mucin was observed to be different for the small intestine and the colon. The O-glycosylation of Muc2 mucin of colon was observed to be dominated by high-charged fucosylations while there were fewer fucosylations on the Muc2 mucin of the small intestine. The specific structure of mucin glycosylation was important given that the type of mucin glycosylation were thought to play a role in the maintenance of commensal microbiota (Holmén Larsson et al. 2013). There may be other effects and reasons for the observed variation that have yet to be determined.

Given the regio-specification of mucin types, it is also likely that glands along the GIT would also exhibit specialism in the type of mucin produced. A recent example of this form of mucin variation can be drawn from a study of the disposition of mucin contents in the gastric gland of the rat. High pressure freezing techniques employed by Sawaguchi et al. (2002) have shown that zymogenic granules (an inactive enzyme precursor) that are secreted from the neck and base of the gland are enveloped by MNC mucins that ascend to the pit of the gland (Figure 2-16).

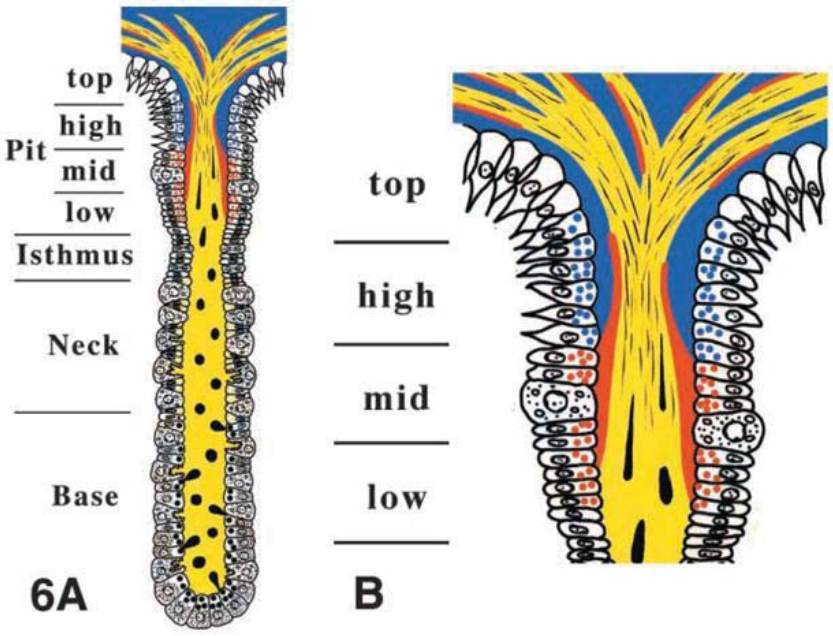

Figure 2-16: The disposition and flow of the various types of mucins and gastric gland secretions. The secreted gastric zymogenic contents (black – elongated and circular) are enclosed by MNC mucins (yellow) and sulfated mucins (red), which are subsequently laminated into channels by RGM11 mucins at the upper region of the rat gastric gland (Sawaguchi et al. 2002).

At the pit of the gland, the MNC mucin was observed to form stratified layers of alternating mucin types along with sulfated and RGM11-positive mucin (Sawaguchi et al. 2002). Such local disposition of mucin types was thought to play a role as a preventive barrier over the local stomach mucosa against denaturation and autolysis (Lentle and Janssen 2011).

2.4.2. Mucogenesis and organization of secreted mucin

The following are highlights of the current knowledge available on the genesis and organization of secreted mucin especially those secreted by goblet cells that are the predominant mucin type of the small intestine. It is noteworthy that baseline mucin secretions differs to mucin secreted as a result of abnormal external stimulation (Kemper and Specian 1991). Upon abnormal external stimulation of cells, especially

those that result in apical cell membrane disruption, it was observed that most if not all of the mucin and even some cytoplasmic contents of the cell fuse together to form a large bolus of mucin that is released from the cell (Miyake et al. 2006). Given the sudden and massive deposition of goblet cell contents, it is highly likely that mucin secreted under such circumstances would have abnormal attributes (e.g. incomplete post-translational modifications). This suggests some inherent shortcomings of previous work determining the function and attributes of mucus that is present in the gut lumen as a result of abnormal stimulation (e.g. physical challenges to the gut mucosal wall that differ to those normally applied *in vivo*).

In this respect, it is noteworthy that to date, studies conducted to determine the function and characteristics of mucus have largely utilized mucus from the following sources; re-constituted 'off the shelf' porcine gastric mucin (PGM) (Dawson et al. 2004), 'scraped off' mucus from the GIT (e.g. stomach, small intestine and colon of animals) (Sellers et al. 1991; Celli et al. 2005) and human sputum (Dawson et al. 2003; Suh et al. 2005). Such mucus samples would not be reflective of the mucus encountered by nutrients *in vivo* or show the postulated diversity of mucin oligomer configurations and their varying manifestations once secreted from goblet cells (see sub-section 2.4.2.3 below). Previous work has already called into question the use of re-constituted 'off the shelf' PGM with the finding that the physical properties of PGM, were dissimilar to that of native porcine gastric mucin (Kočevar-Nared et al. 1997) whereas mucus sampling by means of scraping the mucus off the gut wall would probably cause trauma to the gut wall. This would result in the ejection of copious amounts of mucus that may not have completed post-translational modifications and thus not representative of mucus that might be encountered *in vivo* under normal physiological conditions. A similar conclusion may also be drawn regarding the mucus samples that originate from 'waste'

human sputum where the human airways have undergone trauma during the process of expectorating the sputum or that the mucin secreted were a product of a pathological condition in the airways. Furthermore, the stratification of the individual mucin types observed over the gastric gland by immunohistochemical staining (Sawaguchi et al. 2002) would not be able to be determined by the use of such mucus samples.

2.4.2.1. Biogenesis of mucin secretory granules

The process of mucin biogenesis and discharge are summarized in Figure 2-17 below. Mucin monomer genesis in the goblet cell begins with the synthesis of precursor peptides in ribosomes and transport of these nascent polypeptides into the endoplasmic reticulum (ER) (Forstner 1995). Mucin dimers are formed in the ER by the fusion of two similar mucin monomers by disulphide bridges typically at their COOH terminals (see sub-section 2.4.3) (Perez-Vilar 2009). The process of N- and O-glycosylation that begins in the ER and the process of oligomerization by the fusion of multiple mucin dimers are completed in the Golgi apparatus (Roth 1996). Only the proline-theorine-serine (PTS) domains bound for extracellular regions (see sub-section 2.4.3) of trans-membrane mucin (e.g. mucin secreted and adhered to the surface of enterocytes) were glycosylated (McGuckin et al. 2011). Especially within the *medial*- and *trans*- regions of the Golgi apparatus, post-translation modification of the mucin oligomer occurs – modifications such as the addition of sulfate and sialylic acid groups to form the negatively charged bottle-brush mucin side-chains occurs (see sub-section 2.4.3) (Perez-Vilar and Hill 1999). In addition, the mucin oligomer is also enriched with Ca^{2+} to facilitate the process of oligomer condensation that prevents the repulsion of negatively charged side-chains (Perez-Vilar 2007). Following processing, the mucin polymers form nodular dilatations, randomly distributed throughout the *trans*-surface of the Golgi

apparatus and bud out as immature secretory granules (i.e. condensing granules) into the cell cytoplasm (Sandoz et al. 1985).

Subsequently, these condensing granules (i.e. immature secretory granules) are concentrated by homotypic fusion (i.e. fusion of multiple condensing granules) and remodelling of the cluster to produce mature mucin secretory granules (MSG) in which the mucin is highly condensed (Tooze et al. 2001). MSG's are then transported to the apical cell membrane by microtubules (Davis and Dickey 2008) awaiting exocytosis and consequent degranulation (Verdugo 1991) while membrane-bound mucins are transported to the cell membrane (McGuckin et al. 2011). The size of mucin granules before discharge from goblet cells were observed to be between 0.6 – 2.5 μm in diameter (Davis et al. 1992).

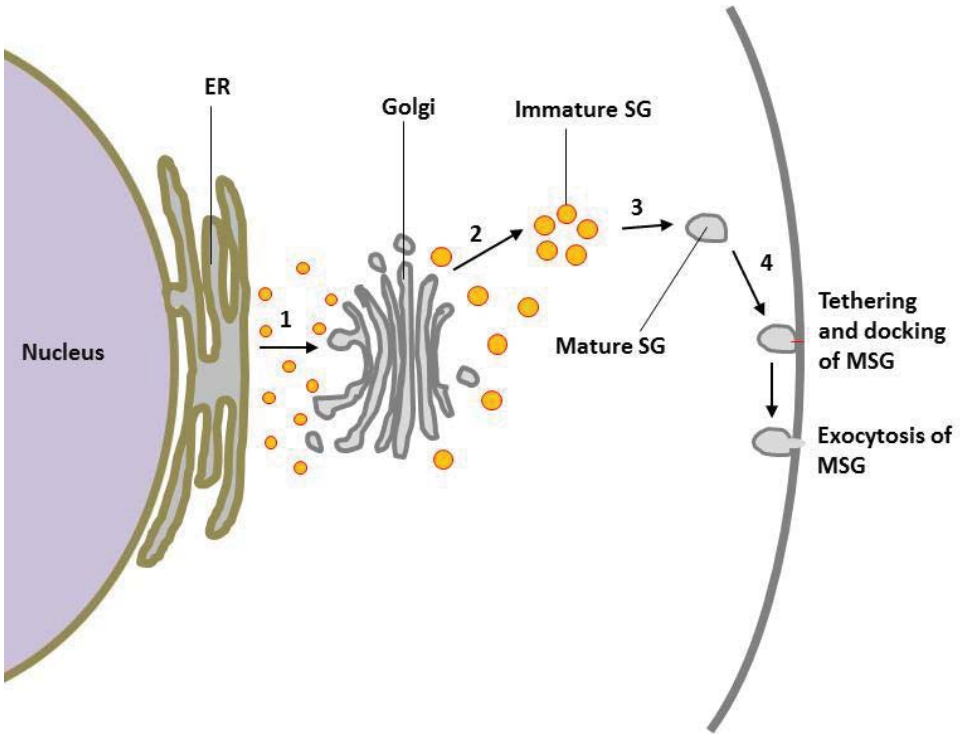

Figure 2-17: The process of biogenesis of a goblet cell mucin granule to its exocytosis.1) Mucin dimers emerge from the endoplasmic reticulum (ER) to enter the Golgi apparatus for the completion of N- and O- glycosylation. 2) Mucin oligomers nodules bud out of the Golgi apparatus as immature SG's. 3) Immature SG's undergo homotypic fusion and remodelling to form mature mucin secretory granules (MSG). 4) MSG's are transported to the apical cell membrane for exocytosis and dischange of its contents (adapted from Davis and Dickey 2008).

2.4.2.2. Discharge and expansion of mucin granules

There are two main types of mucin secretion; single MSG exocytosis (i.e. baseline secretion) and regulated stimuli driven compound exocytosis (i.e. accelerated degranulation of mucin granules) (Specian and Oliver 1991). During baseline secretion of single MSGs, synthesized MSGs are transported to the goblet cell apical membrane for immediate exocytosis. MSGs for baseline secretion are typically located at the periphery of the granule mass in goblet cells and may also participate in compound exocytosis (Forstner 1995). Conversely, compound exocytosis occurs as a result of changes in the environmental conditions around the intestinal mucosa (i.e. pH and/or osmolarity fluctuations) (Kim and Lee 1991) or by stimulation of goblet cells receptors

(Davis et al. 1992). Receptor driven triggers of compound exocytosis include; bacteria proteases (Klinger et al. 1989), cholinergic agonists (Specian and Neutra 1980), anaphylaxis of the intestine (Lake et al. 1980), as well as physical challenges (Neutra et al. 1982). As mentioned earlier, it is highly likely that the mucin secreted by goblet cells during compound exocytosis is different to the baseline secretions of mucin. This means that mucin secreted during compound exocytosis may be lacking of post-translational modification to a degree due to the sudden release of goblet cell contents or that the post-translational modification of goblet cell mucin were altered by a change in gene expression (e.g. as a defensive response to microbial invasion) (McGuckin et al. 2011).

Each goblet cell measuring 30 μm in length and 6 – 8 μm in diameter can contain upward of 100 MSGs at one time (Davis et al. 1992) ready for discharge (Steyer et al. 1997). MSG's are stored in the theca (i.e. a filament rich cytoplasm) at the luminal end of the goblet cell prior to exocytosis and degranulation. The MSG storage is located in the apical section of the goblet cells above most of the remaining cell cytoplasm (e.g., Golgi regions) (Specian and Oliver 1991).

The exocytosis and degranulation of MSGs does not occur by a straightforward diffusion of the granule contents through a fusion pore on MSGs at the apical surface of goblet cells (Forstner 1995). The following are details on the mechanisms of MSG transport and docking at the apical membrane of goblet cells. Most of the information is derived from studies conducted with airway goblet cells.

The regulation of MSG secretion may be initiated by the presentation of agonist substances such as ATP and UTP to goblet cells receptors (other agonist substances that would affect intestinal goblet cells are mentioned in preceding text above) (Davis et al. 1992; Kim and Lee 1991). This is followed by a disruption of the theca actin filament

cyctoskeleton, which frees the MSGs to be transported to the plasma membrane. The disrupted actin filaments are then remodelled to facilitate transport of the MSG to the target site at the cell apical plasma membrane. Upon reaching the target site, MSG's are tethered and docked at the target site along the plasma membrane by a protein complex. Concurrent to the tethering and docking step, the MSG is primed through the formation of a core complex with an attachment protein to allow fusion to the plasma membrane in preparation for exocytosis (Davis and Dickey 2008).

Given that MSG contents are of high viscosity, it is conceivable that an ejecting force is necessary for the degranulation of MSG contents (Forstner 1995). Docked MSGs contain mucin that exists in a condensed form due in part to the cationic shielding agent Ca^{2+} that shields its polyionic charges. Prior receptor activation by agonist substances establishes a secretory pore on the MSG and cell apical membrane allowing for the exchange of intragranular Ca^{2+} with Na^{+} from the extracellular environment. Exocytosis subsequently occurs by a 'jack-in-the-box' mechanism due to the sudden hydration of the mucin network that is driven by charge repulsion of the polyionic chains that are no longer shielded by Ca^{2+} to form mucus islands (Verdugo 1990, 1991) (Figure 2-18).

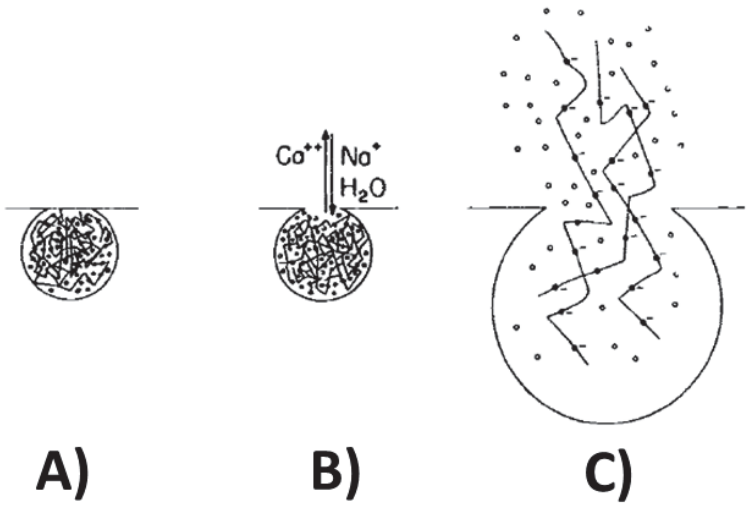

Figure 2-18: The 'jack-in-the-box' mechanism of exocytosis of a mucus secretory granule (MSG). A) The establishment of a secretory pore on the MSG and the cell apical membrane exposes the MSG contents to the extracellular compartments. B) This process facilitates the exchange of intragranular Ca^{2+} with Na^{+} from the extracellular environment. C) Electrochemical energy stored in the mucin polymer network is transformed into mechanical energy that drives the expulsion of MSG products (adapted from Verdugo 1991).

2.4.2.3. Annealing and organization of secreted mucin

There are two possible models of the goblet cell secreted mucin oligomer structures that have been proposed (Verdugo 1990; McGuckin et al. 2011). In the first model, the mucin monomer was thought to assume a branched configuration with multiple (i.e. more than 1) mucin monomers fused at their terminals (see sub-section 2.4.3) of the protein core for the formation of the mucin three-dimensional (3D) oligomer matrix (Gibbons and Mattner 1966; Perez-Vilar and Hill 1999). In the second model, the mucin oligomer was thought to be a linear chain of multiple mucin monomers that were bound with only one other mucin monomer at both their terminals (Verdugo 1990). By the latter configuration, the 3D matrix would be formed through the establishment of an entangled network between the oligosaccharide bottle-brush side chains of the protein core of the mucin monomers (of a given oligomer) facilitated by low-energy

electrostatic interactions and hydrophobic bonds (Bansil et al. 1995). While recent biochemical (Ambort et al. 2011) and electron microscopy (Godl et al. 2002) studies provide evidence for a branched mucin oligomer, other recent atomic force microscopy (AFM) (Round et al. 2002) and dynamic light scattering studies (DLS) (Bansil and Turner 2006) have observed a linear mucin oligomer. It is possible that there is only one true structure of the mucin oligomer configuration and the discrepancies observed across studies may be due to the different analytical techniques or type of mucin samples used. However, to date, the validity of one model over the other has yet to be proven, and evidence for both models are still being gathered and evaluated.

It is also likely that both models are valid, in accordance with the requirements of mucus function for a given locale (Verdugo 2012). Tangled networks of mucin bottle-brush side chains (of a linear oligomer configuration) would convey greater flexibility in the axial movements of the mucin oligomers, allowing mucus islands to continuously swell and anneal thus forming a continuous layer of aqueous mucin in some locales (Perez-Vilar 2009). However, other sites may require more strict regulation of mucus island swelling. Branched mucin oligomers would only swell to a limit depending on the degree of interchain bonding of multiple mucin monomers (i.e. the level of linearity or 'branching' of the mucin oligomer chain) forming dense viscoelastic mucus islands (Verdugo 1990, 2012). The latter type of mucus may be a more desirable feature particularly in the proximal small intestine, given the requirement of mucus in this region to protect the mucosal surface against mechanical, chemical and pathogenic challenges (Verdugo 2012).

Mucus islands of which their mucin oligomers are formed by an entangled network would be more likely to anneal by the process of translational interdigitation of the oligosaccharide side chains of multiple mucin oligomers (Verdugo 1990). This process

of translational interdigitation is similar to the random movements of individual segments of a snake, giving rise to the term ‘reptative inter-diffusion’ to describe such a process (De Gennes 1971, 1979). Thus the annealing of linear oligomers was thought to occur by the ‘random walking’ of ‘free’ oligosaccharide side chains of mucin oligomers undergoing ‘reptative inter-diffusion’ with one another (Verdugo 1990, 2012). Conversely, it was thought that should mucin oligomers have a branched configuration, annealing may not occur between individual mucus islands. If so, this could be due to the saturation of the amount of disulfide bonds that have been formed between the terminals of the protein core presumably optimized within individual mucin oligomers (i.e. individual mucin oligomers are ‘locked into’ their respective networks) (Verdugo 1990). As such, the secreted branched mucin oligomer would likely appear as discrete individual mucus islands rather than a contiguous aggregate of mucus islands (Verdugo 2012).

Prior studies have postulated that mucus in the GIT is organized as a continuous layer (i.e. contiguous ‘blanket’) overlying the peripheries of the gut (Sellers et al. 1991; Specian and Oliver 1991; Atuma et al. 2001; Cone 2009) suggesting that annealing of mucin oligomers occurs at all sites of the GIT. However, on closer inspection, an alternative hypothesis of mucus organization in the GIT can be put forward – mucus in some parts of the GIT is discontiguously organized and heterogeneous especially in the small intestine.

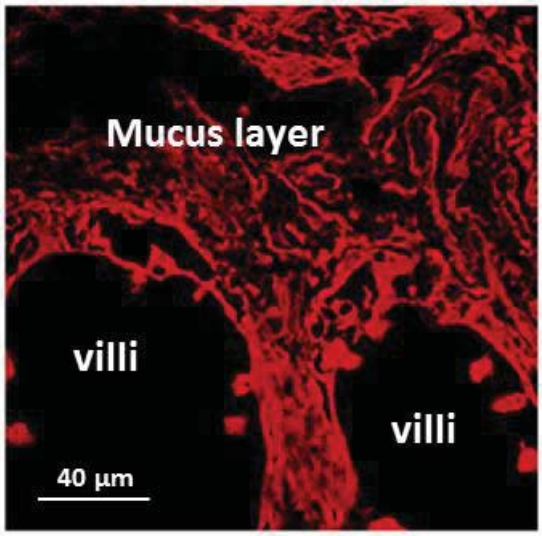

Figure 2-19: Confocal microscopy image of mucus overlying the apices of villi indicating that they are discontiguous and heterogeneous. The regions marked in red are mucus stained with Alexa-633-labeled wheat-germ-agglutinin (adapted from Sonaje et al. 2011).

For example, confocal microscopy images of mucus organization overlying small intestinal villi taken from the published work of Sonaje et al. (2011) suggest the discontiguity and heterogeneity of mucus (Figure 2-19). In addition, a contiguous layer of mucus was not observed in the small intestine and proximal colon of the rat (Szentkuti and Lorenz 1995) and in the small intestine of the cat (Florey 1933). The appearance of commensal bacteria in the proximal colonic crypts of mice also suggest that colonic mucus is not a contiguous layer overlying the mucosa (Swidsinski et al. 2007).

2.4.3. Mucin structure

Both secreted and trans-membrane mucins are glycoproteins that share similar basic structures. The formation of the mucin oligomer three-dimensional structure has been discussed in the prior sub-section. A mucin oligomer is tightly packed in the presence of high concentrations of Ca^{2+} and H^{+} prior to degranulation and discharge from the goblet cell. Several mucin dimers are bound covalently by disulphide bridges to form mucin

oligomers (Figure 2-20A). Each of the mucin dimers are formed by mucin monomers that are also bound by disulphide bridges (Figure 2-20B) (Bansil and Turner 2006). Overall, the mucin monomer consists of ~80% carbohydrates that form the mucin glycoprotein side-chains while the remaining 20% are the protein core (Johansson et al. 2011b). The mucin glycoprotein has a molecular weight of 0.5 – 20 MDa of which ~200 – 500 kDa is the molecular weight of its protein core (Bansil and Turner 2006).

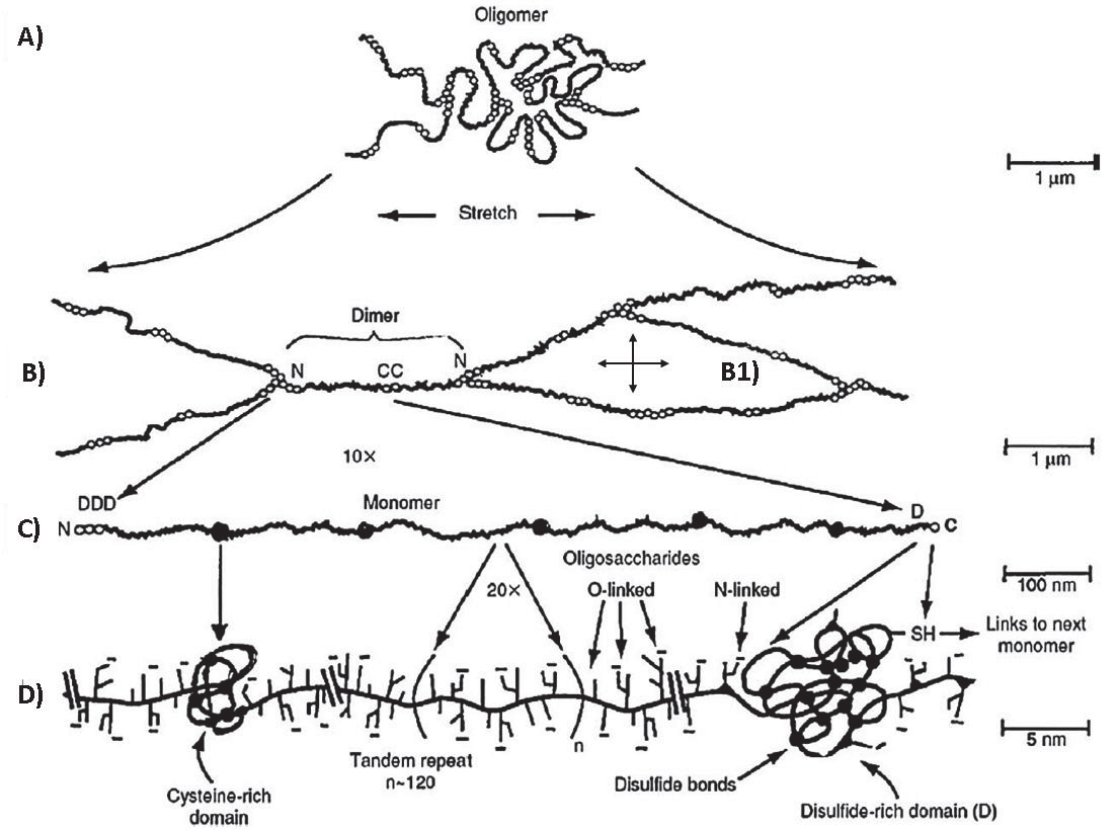

Figure 2-20: Possible mucin structure type taken at 3 different magnifications and 4 levels of detail.A) A mucin oligomer formed by B) multiple mucin monomers linked by disulphide bridges. A finite mucin mesh pore is indicated in B1. The oligomer configuration shown is derived from the assumption that a given mucin monomer terminal can bind to more than one monomer. C) A mucin monomer is composed of alternating proline-threonine-serine (PTS) amino acid domains and spherical 'bundles' of D) hydrophobic protein cysteine rich domains with an amine and carboxyl terminal at either end of the mucin monomer. Throughout the length of the mucin monomer are oligosaccharide branches with negatively charged tips (adapted from Cone (1999)).

The protein core of the monomer is thought to be composed of three distinct regions (Figure 2-20C and D). The first is a region situated centrally on the protein core that are composed of repeats of PTS amino acid, which are heavily glycosylated. The second region is their terminal where one terminal is composed of an amino H_2N group while the other terminal is composed of a carboxyl COOH group (Bansil et al. 1995; Bansil and Turner 2006) that contain disulphide-rich domains, which contribute to the binding of the monomer to other mucin monomers. The third region consists of 'naked' (due to the region lacking PTS amino-acid domains and being under-glycosylated) globular protein-like regions that are enriched by cysteine (i.e. to form cysteine-rich regions) (Perez-Vilar 2009). This region (i.e. the third) is typically found near the COOH or H_2N terminals of the mucin monomer (Sheehan et al. 1986; Perez-Vilar 2009). Oligosaccharide (i.e. glycans) chains are attached to the PTS domains predominantly by O-glycan bonds at the hydroxyl side chains of serine and theorine forming a 'bottle-brush' configuration about the protein core (Bansil and Turner 2006). Conversely, more glycosylation by N-glycan bonds could be observed at both terminals of the mucin monomer (Perez-Vilar 2009). For goblet cell mucins, O-glycan side-chains of the PTS domains forms what is known as 'mucin domains' that confers the mucin a high capacity to bind water that contributes towards their mucus island (i.e. gel) forming attributes during hydration of the secreted mucin (Johansson et al. 2011b). Most of the O- and N-glycans are negatively charged with sialic acids or sulphate groups (Van Klinken et al. 1995). The H^+ are thought to neutralize all the negatively charged sialic acid functional groups that branch out along the length of the mucin chains (see below), while the Ca^{2+} were thought to bind all other remaining negatively charged oligosaccharide side chains (Verdugo 1990).

2.4.4. Rheology of intestinal mucus

The determination of the mucus rheological properties sheds light on the role of mucus in protecting the mucosal surface from damaging levels of shear particularly in the proximal sections of the GIT (Bell et al. 1984; Bansil et al. 1995) as well as against invasion by foreign microbiota (Markesich et al. 1995) (discussed in sub-section 2.4.8). The protective attributes of mucus can be triggered as a result of changes to MUC genes expression or by feedback responses to inflammation and abnormal levels of shear forces (Lentle and Janssen 2011). This is in line with established knowledge that microbial invasion; mechanical as well as chemical challenges of the gut mucosa results in mucus production that is different to that expected during baseline secretions of mucin (Specian and Neutra 1980). Such mucus have been reported to be extensive, viscid (Atuma et al. 2001) and highly viscoelastic (Sellers et al. 1991) – attributes that would facilitate the protection of the underlying intestinal mucosal surface. Studies of porcine gastric, small intestine and colonic mucus that have been scraped of the mucosal wall suggested that mucus is a weak gel where both G' (elastic modulus) and G'' (viscous modulus) are dependent on shear rate (Bell et al. 1984; Sellers et al 1991). Such studies also showed that mucus at all three sites generally exhibited the mechanical deformation profile of a 'solid' viscoelastic gel as G' was greater than G'' over the shear rates tested (i.e. of between 10^{-2} and 10^{2} rad s^{-1}). Mucus at the three sites were reported to have the following ranges of G' and G'' values; gastric mucus (G' = 3.2 – 32 Pa, G'' = 0.63 – 13 Pa), small intestinal mucus (G' = 0.18 – 10 Pa, G'' = 0.05 – 6.3 Pa) and colonic mucus colon (G' = 63 – 160 Pa, G'' = 10 – 16 Pa) (Bell et al. 1982; Sellers et al. 1991).

The variation in the moduli of the three sites may be explained as follows. Colonic mucus is the most elastic-like given the need to maintain a barrier against a large

population of bacteria that can degrade mucus (Swidsinski et al. 2007) under high levels of shear by colonic wall contractile activity. In addition, colonic mucus would also need to be able to protect the colonic mucosa against abrasions by digesta that would have lost 80% of its original moisture content (Bowen 1995). For the gastric mucus, while not as elastic-like as colonic mucus, would also need to maintain a suitable barrier against foreign microbiota and to protect the stomach mucosa against low pH and acidic environments (Celli et al. 2007). Conversely, small intestinal mucus was the least elastic-like as the protective role of this mucus would need to be balanced by it also allowing for mass transfer of nutrients and pharmaceuticals to be absorbed at the epithelium.

A 'breakdown sweep test' of gastric mucus samples scraped from the pig mucosa across a range of shear rates has shown that the solid-like behaviour of mucus increased with increasing shear rates. For example, mucus demonstrated greater elastic tendencies during a sweep of shear stress at a shear rate of 0.5 Hz as compared to the same test conducted at a shear rate of 1 Hz (Taylor et al. 2003). The observed dependency of mucus properties with shear rates, though limited, may still have important implications for the protective role of the mucosal surface during the transit of digesta. With slower transit of digesta (i.e. lower shear rate) the mucus layer is more prone to be unsettled and will move with the digesta, hence the stress is not transmitted to the mucosal surface. Conversely, at more rapid shear rates, the mucus resists deformation by manifesting more solid-like properties (i.e. 'hardening'). This may then protect the underlying mucosal surface from abrasions by sharp particles appearing in digesta (Lentle and Janssen 2011).

To date, most rheological studies were conducted with porcine gastric mucin that were either scraped from the gut mucosa or 'purchased off the shelf'. Given that there are

already several studies indicating the heterogeneity of mucus and also variation across species, age and site (i.e. of the GIT) (Neutra 1987), it also is likely that both mobile and adherent mucus layers would have unique rheological properties. Hence caution is required when seeking to generalize the rheological data currently available.

2.4.5. Tribology of mucus

In addition to the mucus role as a physical protective barrier of the mucosal surface from abrasive damage during the transit of digesta, the rheological properties' of mucus also facilitates the transit of digesta. This function of the mucus layer is also known as the tribological function of the mucus layer (i.e. the lubrication of the transit of digesta) (Cone 2009). While the actual means by which mucus provides lubrication to the transit of digesta is not currently fully understood, there have been various suggestions put forward on the tribology of mucus in the GIT, which may be classified into two forms. In the first, the mucus interposes the digesta and the intestinal mucosa. A feature of this mucus interposing layer is its stratification into an outer mobile layer and an inner adherent mucus layer at some sites (e.g. colon) for the lubrication of digesta transit. This may occur by the formation of a slippage plane with digesta able to slide (i.e. flow) with the mobile more aqueous mucus layer over the more solid-like adherent layer (Cone 2009). Besides that, it has been suggested that the propulsion of viscid digesta by peristalsis requires mucus to possess thixotropic[2] properties (Lentle and Janssen 2008). The thixotropic properties of mucus enables it to remain a 'solid' like barrier during gut inactivity, but enables it to flow during the transit of digesta due to continuous high shear (as opposed to small *in situ* deformations) being generated from peristaltic contractions to propagate lumen contents in the gut (Lai et al. 2009).

[2] Thixotropy, is a shear thinning property of fluids. Such a fluid can remain in a viscous pseudo-solid like state under static conditions but will flow over time when a shear stress is applied.

Secondly, the mucus may also provide lubrication by adhering to digesta to facilitate the transit of digesta through the lumen (Andrews et al. 2009). Such properties of the mucus are especially important in parts of the GIT that do not secrete mucus e.g. oesophagus and anus (Bongaerts et al. 2007). One of the ways this may occur would be through the formation of liquid crystallinity on the surface of digesta providing lubrication (Lentle and Janssen 2011) in a similar way commercially available liquid crystals have been recently observed to provide markedly improved lubrication as compared with existing oil and synthetic lubricants (Bushby and Kawata 2011; Wen and Huang 2012). The critical experimental finding supporting this suggestion is that the concentrations of crude mucin required to form a liquid crystalline state have been observed in porcine gastric mucin secretory granule (Waigh et al. 2002). This concentration may be further augmented by the possible absorption of moisture from secreted mucins by digesta (Lentle and Janssen 2011). In addition, mucus may also lubricate the flow of digesta by adhering to it by the 'viscous boundary lubrication' mechanism (Yakubov et al. 2009). It was thus postulated that there will always be a film of mucus overlying digesta that would be able to reduce boundary friction by as much as 10-fold during the transit of digesta. With an increasing concentration of mucin adhered to digesta (i.e. by entangled annealing mechanisms between mucin oligomers), this would further increase the thickness of the mucus film, which should further reduce the boundary friction with the mucosal wall (Yakubov et al. 2009). Overall, it should be noted that both types of lubricating mechanisms (i.e. the facilitation of an interposing fluid layer and the adsorption of mucus to digesta) may occur at the same time for a given site in the GIT.

2.4.6. Mucus as a barrier (chemical)

The mucus layer may also function as a barrier against harmful chemical conditions. It was thought that the mucus facilitates a 'first-line barrier' defence against acidic challenges and luminal pepsin especially in the stomach and proximal small intestine (Allen and Flemström 2005). In earlier work on the protective role of the mucus in the protection of the mucosa against the diffusion of protons (i.e. H^+) from the gastric lumen, it was observed that a pH gradient existed from the mucus luminal surface through the mucus layer and to the mucosal surface (Ross and Turnberg 1983). Given the finding of superficial hardening of the mucus when exposed to acidic environments (Celli et al. 2007) it was postulated that the mucus formed a hydrogen ion repulsion barrier (Lentle and Janssen 2011) thus resulting in the pH gradient observed. However, recent research has shown that such suggestions were incomplete (McColl 2012); while mucus does form a barrier against hydrogen ions that does markedly retard its diffusion (Allen and Flemström 2005), bicarbonate (HCO_3^-) secretions from gastric parietal (i.e. acid-secreting) cells forms a bicarbonate concentration gradient within the mucus layer (Baumgartner and Montrose 2004), thus resulting in a 'dual-function' protective feature. While the gastric parietal cells secrete hydrogen ions into the gastric lumen, an equal number of bicarbonate ions are also released into the mucus adjacent to the gastric mucosa that would neutralize any backflux of hydrogen ions (McColl 2012).

As for the prevention of autolysis of the gastric and duodenal mucosa by pepsin, it has been postulated that this is due to the mucus providing a barrier that cannot be penetrated by pepsin within physiologically meaningful timescales. While pepsin does lyse mucus, this is balanced by fresh secretions of mucin into the lumen (Allen et al. 1986). It is noteworthy that for similar reasons, determination of the actual thickness of the mucus layer in such sites may be difficult.

2.4.7. Mucus as a barrier (physical)

The mucus layer also functions as a particle exclusion boundary (Cone 2009). The porcine gastric mucus layer are thought to have finite mucin mesh pores (Figure 2-20B1), brought about by the formation of mesh-like attributes through the alignment of mucin chains (Desai et al. 1992), which allow the passage of certain substrates. The existence of finite pores has also since been observed in varying sizes in the mucus of other sites of the GIT, cervico-vaginal regions as well as the trachea (Ensign-Hodges et al. 2013). The mucin pore size of cervico-vaginal (CVM) mucin was observed to be anywhere between 100 and 1000 nm (Chretien et al. 1975; Yudin et al. 1989) depending on the method of measurement, with an average mucin chain pore size of 340 (± 70) nm (Lai et al. 2010).

The permeability of a given substrate through the mucin mesh is also dependent upon the surface charges of the substrate (i.e. the measure of ionic interactions formed between the substrate and mucin chains) (Nicholas et al. 1991) or lipophilicity of the substrate (Larhed et al. 1997). There is currently debate on the effect of surface charges on the diffusivity of particles. Mildly cationic nano-particles (e.g. amine coated nano-particles) appeared to have increased diffusivity in mucus as compared to a stronger cationic charged nano-particle (e.g. carboxy coated nano-particles) (Dawson et al. 2003). However, similar studies conducted with the same nano-particles apparently resulted in the opposite effect (Crater and Carrier 2010).

However, there is consensus on the fact that particles that have an overall neutral charge may navigate through mucus almost as fast as in water (Dawson et al. 2003; Suh et al. 2007). While such particles that had a diameter almost twice the mean mucin pore size (e.g. 500 nm polyethyleneglycol coated particles) (Lai et al. 2007) have also been

reported to navigate the mucus with similar times, it has been demonstrated that particles larger than 1 micron will navigate through cervico-vaginal mucus several orders of magnitude slower than through water (Cone 2009). In such instances, the smaller pore size of the mucin chain mesh may be the main factor hindering the diffusivity of such particles. Conversely, the transit of particles smaller than the mean mucin mesh size (e.g. bovine serum albumin with <10nm) and immunoglobulins (e.g. IgM – 20 nm) are slightly slowed in mucus. The slowing of diffusion of such nano-sized particles may be caused by the formation of low affinity bonds with the mucin chain mesh (Olmsted et al. 2001).

In addition to its role of keeping away unwanted foreign particles and pathogens from the mucosa, mucus may also have a role in keeping nutrients and other useful substances close and adjacent to the epithelium (e.g. apical regions of enterocytes). Mucus may have a role in discouraging the back flux of lysed monomers towards the lumen (Pappenheimer 2001a). Smaller substrates would need to back diffuse through the mucus layer and as a consequence, are retained longer in the mucus layer adjacent to the mucosa (Pohl et al. 1998; Pappenheimer 2001a).

2.4.8. Mucus as a defence system against foreign microbiota

Mucus protects the mucosa of the GIT from the invasion of foreign microbiota by its semi-permeable barrier-like properties (e.g., with limited size and surface charge inclusivity) and hosts a variety of antimicrobial substances (Cone 2009). The presence of intestinal microbiota can alter the production (e.g. trigger compound exocytosis) and secretion of mucins for the defence of the underlying intestinal mucosa (Mack et al. 1999). There are thought to be two ways in which foreign microbiota may trigger the mucus production defence system of the intestinal mucosa; either by bioactive factors

produced directly by the microbes or by the bioactive factors of the host immunity system that were secreted as a response to the detection of microbes (Deplancke and Gaskins 2001). This may explain the finding of bacteria being excluded to the outer surface of the mucus layer overlying the apical epithelial surface (Matsuo et al. 1997; Johansson et al. 2009). However, even if an organism was smaller than the pores between individual mucin chains, it may still be trapped by its surface affinity to the mucin chains.

It is noted that the diffusion of infectious agents such as the Herpes-Simplex virus through mucus was partially hindered despite it being smaller than the pores between individual mucin fibres – a size of 180 nm (Olmsted et al. 2001). This is presumably due to the hydrophobic surfaces of the virus being incompletely shielded from the mucin chain domains causing the formation of low affinity bonds with the virus (Cone 2009). Trapped microorganisms and foreign agents are siphoned distally through a combination of gut contractile activity and the constant renewal of the mucus in the gut lumen (Tirosh and Rubinstein 1998). In addition, mucus may also reduce the harmful effects and spread of microbes by maintaining them in a 'planktonic' state that prevents their formation of biofilms (Caldara et al. 2012).

Another protective attribute of mucus against foreign microbiota is the potential for the mucus to host a variety of antimicrobial substances and immunoglobulins (e.g. IgA and IgB) (Hooper et al. 2012). Antimicrobial substances may indirectly target invasive microbes (Thim et al. 2002) while others directly target the microbes (Hecht 1999). Trefoil peptides are an example of the former type of antimicrobial peptide that protect the gut mucosa by 'physical' means such as by increasing the viscosity and viscoelastic properties of the mucus around invading microbes (Kindon et al. 1995; Thim et al. 2002). Examples of the second type of antimicrobial peptide include Reglly (Cash et al.

2006) and β-defensins (Harder et al. 2001) that both cause cell wall damage to microbes. Immunoglobulins such as IgA function is as follows: Dendritic cell (DC) processes sample microbes that penetrate the epithelial surface. Subsequently, microbe laden DC interacts with component cells of Peyer's patches and induces the production of IgA. IgAs that are secreted into the luminal regions adjacent to the epithelium then bind to microbes preventing bacterial translocation over the epithelium to basolateral regions (Macpherson and Uhr 2004).

It is noteworthy that membrane-bound mucins may also have a role in the defence of the intestinal mucosa. For example, it was observed that microbes that achieve contact with epithelial cell's apical surface by binding to the cell's membrane-bound mucin would be ejected from the apical cell surface along with the mucin (McGuckin et al. 2011).

2.4.9. Concluding remarks on the influence of mucus

In this section, the physical properties, function and origins of mucus have been presented. This section has also demonstrated why an understanding of the properties and disposition of mucus has an important bearing on our understanding of mass transfer in the small intestinal perivillous space. In addition, the regional variations of types of mucins secreted as well as the mechanics that underlay (e.g., Muc genes, extent and type of post-translational modification) those variations observed were also highlighted. It is unlikely that mucus at each site of the GIT and the airways would all manifest the same properties and function. It is more likely that the mucin produced at a given site is adapted for the specific function required at its locale. For example, the mucus in the colon is thought to be optimized to lubricate the rapid movement of semi-solid digesta while providing protection against microbial insults. Conversely, the

mucus in the distal small intestine may be optimized to facilitate luminal contents (e.g. nutrients) mixing and mass transfer.

Furthermore, several additional questions have been raised – Is the fluid environment in the gut really a gel-like contiguous blanket? If not, what does this mean for mass transfer in the perivillous space? If the currently accepted knowledge of the fluid environment at the gut peripheries is indeed true, it appears that the perivillous mucus would be a major limiter of mass transfer of nutrients and pharmaceuticals. The contiguous layer of gel-like material in the perivillous space would likely limit mass transfer times in this region to that of molecular diffusion (i.e. by restricting possible gains from advective mixing and mass transfer). However, gaps still remain in our knowledge as to the actual disposition and properties of mucus in the small intestine that would be encountered by nutrients during *in vivo* digestion. Future research to determine such parameters will complement the current knowledge available on mucus that has been largely studied *in vitro*.

2.5. Conclusion

In this chapter, the importance of the three identified factors that affect mass transfer in the perivillous space; postprandial gut motility, villi, and mucus, have been considered. In conclusion, from the survey of literature, there are four salient points and questions that would be be addressed in the following chapters:

A) An improved understanding on the effects of postprandial gut motilities such as pendular activity, on mixing and mass transfer is needed.

B) An improved understanding on the role of villi in the small intestine is also needed. It is still currently not known whether villi only plays a passive role in the absorption of nutrients (e.g. by the mere presence of enterocytes on it) or if it also may have a role in the augmentation of mixing and mass transfer in the small intestine?

C) An improved understanding on the mucus disposition (e.g., properties of the various mucus layers and their disposition upon secretion from epithelial cells) and physical properties (e.g. rheology) is needed *in situ* on living animals so that the role of mucus during *in vivo* digestion may be determined. Current work conducted on mucus scraped from the mucosa of dead animals or purchased off the shelf does not provide a thorough understanding on this subject.

D) Computational models that better reflect actual physiological conditions are needed to complement experimental work.

Experimental and computational modelling work on the three principal factors that may influence mass transfer in the perivillous space (mucus, villi and mixing mechanism during postprandial activity) are developed and discussed in the following five chapters.

Chapter Three -

Studies of the microrheology and fluid environment of the perivillous space

3.1. Foreword

This chapter details studies on the microrheology of the fluid environment in the perivillous space. Firstly, the methodology used by other workers in this field will be reviewed. Subsequently, a detailing of the work and the results presented in the form of a published peer-reviewed paper will be provided. This will be followed by a presentation of additional information on the development, design and construction of the apparatus used in this work. Finally, ancillary experimental work, results and discussions that were not published together with the peer-reviewed paper will also be provided.

3.1.1. Background and methodology used by other workers in this field

Much of the early work on the rheological (Bell et al. 1982) and the physical (Desai et al. 1992) properties of mucus appears to pay little regard to the possibility of the regional variation of mucus properties (Robbe et al. 2003) or *in situ* variation for a given section in the GIT (e.g. the stratification of mucus around the gastric pits in the stomach (Sawaguchi et al. 2002) and over the surface of the colon (Matsuo et al. 1997)). Studies of the physical properties of mucin have typically used either re-hydrated 'off-the-shelf' porcine gastric mucus (PGM) (Dawson et al. 2004) or mucus (gastric, small intestinal and colonic) scraped from the mucosal surface of gut components from dead animals (Sellers et al. 1991; Celli et al. 2007).

Among the studies that involved the use of the latter, some authors have stressed the importance of obtaining mucus samples that were free of debris (e.g. dead epithelial cells) (Sellers et al. 1988; Sellers et al. 1991; Dawson et al. 2003). These workers have centrifuged mucus samples to purify them (Taylor et al. 2004; Macierzanka et al. 2011); a process that involves the removal of considerable cellular material that would be

present in a physiological situation (e.g. exfoliated enterocytes from the tips of villi). Again, there is the question of the extent to which purified mucus represent the physical properties of mucus *in situ*. In addition, it is known that the mechanical stimulation of goblet cells causes them to discharge their contents by a process known as compound exocytosis (Specian and Oliver 1991). Given that the properties of such mucin differ from those released from un-stimulated cells (Miyake et al. 2006), it is highly likely that the properties of mucus sampled during these studies would not reflect that encountered during *in vivo* digestion. Indeed, the mucus present may be more similar to that under certain pathological conditions characterized by inflammation, such as those that result from mucosal wall challenges by *Escherichia coli* and cholera bacteria (Elliott et al. 1970; Moon et al. 1971). Furthermore, the rheological properties of the mucus sampled in such manner (i.e. scraped from the gut wall) would vary according to the manner in which the various mucus layers are mixed on sampling.

Histological and immuno-histochemical methods have also been used to determine the disposition of the mucus layer (Sheth et al. 2010; Gouyer et al. 2011). The work done in these studies has contributed to the hypothesis that mucus is a contiguous blanket of viscoelastic material (Atuma et al. 2001; Ensign-Hodges et al. 2013). However, such histochemical techniques require embedding, staining and sectioning techniques to be applied to gut samples, all of which could initiate goblet cell degranulation and the breakdown of existing physical structures.

Hence there is a need for assessments of the perivillous fluid environment at a microscopic level on living tissue. This can be achieved by micro-rheological techniques notably by the tracking of the Brownian motion of fluorescent microbeads. In the work detailed in this chapter of the thesis, the microbeads were suspended and applied to tissue in a sample of Newtonian fluid (Earle-Hepes solution). This mimics

the particulate suspension encountered by the mucosa under normal physiological conditions (Takahashi 2011).

MASSEY UNIVERSITY
GRADUATE RESEARCH SCHOOL

STATEMENT OF CONTRIBUTION TO DOCTORAL THESIS CONTAINING PUBLICATIONS

(To appear at the end of each thesis chapter/section/appendix submitted as an article/paper or collected as an appendix at the end of the thesis)

We, the candidate and the candidate's Principal Supervisor, certify that all co-authors have consented to their work being included in the thesis and they have accepted the candidate's contribution as indicated below in the *Statement of Originality*.

Name of Candidate: Ian LIM Yuen Feung

Name/Title of Principal Supervisor: Prof. Roger G. Lentle

Name of Published Research Output and full reference:

Lim, Y. F., M. A. K. Williams, R. G. Lentle, P. W. M. Janssen, B. W. Mansel, S. A. J. Keen and P. Chambers (2013). "An exploration of the microrheological environment around the distal ileal villi and proximal colonic mucosa of the possum (Trichosurus vulpecula)." Journal of the Royal Society Interface 10(81): 20121008

In which Chapter is the Published Work: Chapter 3

Please indicate either:

- The percentage of the Published Work that was contributed by the candidate: 65%

  and / or
- Describe the contribution that the candidate has made to the Published Work:

Ian Lim Yuen Feung — Candidate's Signature — 27/6/2014 — Date

Roger Lentle — Principal Supervisor's signature — 27/6/2014 — Date

3.2. Copy of the paper: An exploration of the microrheological environment around the distal ileal villi and proximal colonic mucosa of the possum (*Trichosurus vulpecula*).

The following pages contain a copy of the published journal article with the following bibliography;

Lim, Y. F., Williams, M. A. K., Lentle, R. G., Janssen, P. W. M., Mansel, B. W., Keen, S. A. J., and Chambers, P. (2013). An exploration of the microrheological environment around the distal ileal villi and proximal colonic mucosa of the possum (*Trichosurus vulpecula*). Journal of The Royal Society Interface, **10**(81): 20121008.

The contents of the published peer-reviewed article with the above bibliography is reproduced in this section. All references cited in section 3.2 are listed in a separate sub-section after the main body of the article. These references would be reproduced in the main bibliography of this thesis (i.e. after the thesis appendix) only should they be used elsewhere beyond this section (i.e. of this published article). All further work beyond this section will be citing the work presented in this section where appropriate.

An exploration of the microrheological environment around the distal ileal villi and proximal colonic mucosa of the possum (*Trichosurus vulpecula*).

Y. F. Lim[1], M. A. K. Williams[2 3 4], R. G. Lentle[1 3*], P. W. M. Janssen[1], B. W. Mansel[2 4], S. A. J. Keen[2 4], and P. Chambers[5]

[1] *Institute of Food, Nutrition and Human Health, Massey University, Private Bag 11222, Palmerston North, New Zealand*

[2] *Institute of Fundamental Sciences, Massey University, Private Bag 11222, Palmerston North, New Zealand*

[3] *Riddet Institute, Massey University, Palmerston North, New Zealand*

[4] *MacDiarmid Institute of Advanced Materials and Nanotechnology, Wellington, New Zealand*

[5] *Institute of Veterinary, Animal and Biomedical Sciences, Massey University, Private Bag 11222, Palmerston North, New Zealand*

*Corresponding author

3.2.1. Abstract

Multiple particle tracking techniques (MPT) were used to quantify the thermally driven motion of ensembles of naked polystyrene (0.5 μm diameter) microbeads in order to determine the microrheological characteristics around the gut mucosa. The microbeads were introduced into living *ex vivo* preparations of the wall of the terminal ileum and proximal colon of the brushtail possum (*Trichosurus vulpecula*). The fluid environment surrounding both the ileal villi and colonic mucosa was heterogeneous; likely

comprising discrete viscoelastic bodies suspended in a continuous Newtonian fluid of viscosity close to water. Neither the viscosity of the continuous phase, the elastic modulus (G') nor the sizes of viscoelastic bodies varied significantly between areas within 20 μm and areas more than 20 μm from the villous mucosa nor from the tip to the sides of the villous mucosa. The viscosity of the continuous phase at distances further than 20 μm from the colonic mucosa was greater than that at the same distance from the ileal villous mucosa. Furthermore, the estimated sizes of viscoelastic bodies were significantly greater in the colon than in the ileum. These findings validate the sensitivity of the method, and call into question previous hypotheses that a contiguous layer of mucus envelops all intestinal mucosa and restricts diffusive mass transfer. Our findings suggest that, in the terminal ileum and colon at least, mixing and mass transfer are governed by more complex dynamics than were previously assumed, perhaps with gel filtration by viscoelastic bodies that are suspended in a Newtonian fluid.

Keywords: microrheology; mucosa; ileum; colon

3.2.2. Introduction

The fluid environment near the wall of the small intestine has a significant effect on the absorption of nutrients (Wilson et al. 1971, Westergaard and Dietschy 1974, Read et al. 1976). A body of experimental work shows that the rates at which soluble substances are passively absorbed from the lumen (Amidon et al. 1980, Levitt et al. 1984, Anderson et al. 1988) are generally slower than those that would be expected from simple direct diffusion through the surface of the enteral mucosa. It has been suggested that this could result from the effect of a so-called unstirred layer of fluid (UWL) interposed between the lumen and the surface of the intestinal cells (enterocytes) that restricts diffusion (Thomson and Dietschy 1977, Winne 1981, Thomson and Dietschy

1984). The operational thickness of such an UWL has thus been estimated from transport measurements to be between 74 – 600 μm in the small intestine depending on the specific technique by which it has been measured, the rate at which intestinal lumen is perfused (Westergaard and Dietschy 1974, Debnam and Levin 1975, Read et al. 1976, Winne 1978, Winne et al. 1979, Fagerhold and Lennernäs 1995) and the molecular volume of the solute (Pohl et al. 1998).

While it is conceivable that such a UWL results largely from a continuous layer of mucus that completely envelops the intestinal epithelium (Smithson et al. 1981, Sellers et al. 1991), a growing number of findings run contrary to this hypothesis. Firstly, such a hypothesis rests on the integrity of the mucus layer and a number of workers have reported that there are significant discontiguity in the mucus layer within several locations of the small intestine (Szentkuti and Lorenz 1995). Secondly, direct measurements of the thickness of the layer of mucus overlying the apices of enterocytes do not consistently reflect the calculated thickness of the UWL obtained from transport considerations (Atuma et al. 2001, Sugano 2009).

The work reported here uses multiple particle tracking techniques (MPT) to determine the patterns of local variation in the rheological properties at multiple sites in close proximity to living small and large intestinal mucosa, whilst avoiding the physical disruption of the mucin layer (Suh et al. 2005). One aim was to determine whether the patterns fit in with the hypothesis of a contiguous layer of viscoelastic material partitioning the lumen contents from the mucosa. The disposition and rheological properties at locations adjacent to the apical and lateral surfaces of the villi in the terminal ileum of the brushtail possum (*Trichosurus vulpecula*) were compared with those at locations adjacent to the colonic mucosa, which is of markedly different morphology (Atuma et al. 2001, Swidsinki et al. 2007a).

3.2.3. Materials and Methods

It is known that villous intestinal mucosa can be maintained *ex vivo* for significant periods of time, provided it is well oxygenated and adequately supplied with nutrients (Danielsen et al. 1982). We used mucosa from the digestive tract of the brushtail possum as in this species both the small intestine and proximal colon are of simple tubular configuration and of a diameter suitable for attachment to our superfusion apparatus. Further, the tissues are robust, can readily be maintained in an tissue bath, and the tubular form and length of the ileal villi of the brushtail possum (560 ± 10 μm; our observations) are similar to those in the human small intestine (500 – 1000 μm) (Ham 1969, Weinstein et al. 1969). All studies were conducted on tissue maintained *ex vivo* in oxygenated Earles-Hepes solution (HBS) as we had found in prior work that the mucosa promptly secreted copious quantities of mucus whenever the mucosa became anoxic.

3.2.3.1. Preparation of intestinal samples

Nine freshly trapped brushtail possums, of either sex and between 2 and 3 kg body weight were each fasted for a minimum of 4 hours and subsequently anaesthetized in an induction chamber with 5% halothane in 33% oxygen and 66% nitrous oxide. Following induction they were maintained on a mixture of 1.5% halothane in oxygen and nitrous oxide administered via a face mask attached to a Bain's circuit. The gut was accessed via a ventral midline abdominal incision. In six possums a 20 cm length of the terminal ileum up to and including the ileocaecal junction was excised. In a further three possums a 15 cm length of proximal colon immediately distal to the ileocaecal junction was excised. The possums were subsequently euthanized with intracardiac

pentobarbitone (125 mg/kg). All procedures were approved by Massey University Animal Ethics Committee (approval no. 11/45).

The segment of excised gut was opened by a lengthwise cut and immediately placed with mucosa uppermost in carboxygenated Earles-Hepes solution (HBS) (composition in mM: NaCl 124.0, KCl 5.4, $MgSO_4$ 0.8, NaH_2PO_4 1.0, $NaHCO_3$ 14.3, Hepes 10.0, $CaCl_2$ 1.8 and glucose 5.0) maintained at 37^{o}C. This procedure diluted any adherent digesta and allowed it to float clear of the mucosal surface. A 2 cm^2 piece of mucosa and adherent wall was cut from this with its center at 10 cm from the distal end of the section of terminal ileum or at 10 cm from the proximal end of the section of proximal colon, and tied over the 5 mm diameter sintered tip of the central tube in the superfusion apparatus (Figure 3-1) with the mucosal surface outermost. This whole procedure was undertaken with due care to avoid any direct mechanical stimulation of the mucosa. A 100 µl aliquot of a suspension of fluorescent microbeads (0.5 µm naked polystyrene – see below), was applied to the mucosa and left *in situ* for 1 minute to allow the microbeads to settle onto the mucosal surface. The tube was then installed in the superfusion apparatus (Figure 3-1) with its tip immersed in a cylindrical bath so that the exposed mucosal surface and associated fluid were in the focal plane of an inverted microscope (Nikon Eclipse TE2000-U). A 0.5 ml dose of verapamil solution was then added to the bath to inhibit any spontaneous smooth muscle induced movement in the tissue, which could interfere with the observation of Brownian motion.

The bath was perfused at 500 ml min^{-1} with carboxygenated (95% O_2 – 5% CO_2) HBS (Figure 3-1) maintained at a temperature of 37^{o}C. The bath had a capacity of 70 ml and excess HBS overflowed the rim into an outer compartment (i.e. bath) from where it was then recirculated. HBS was also drawn at 2 ml min^{-1} through the sintered tip of the tube adjacent to the point where the excised gut wall was tied. The apparatus was designed

so that shear rates would not approach those encountered *in vivo* (Lentle et al. 2005) and any flow-induced mucin loss would be likely to be lower than that encountered *in vivo*.

The inverted microscope was equipped with a mercury fluorescent lamp (X-cite Series 120PC EXFO) and a x20 0.75 NA objective lens (CFI Plan Apo VC 20x), mounted on an air damped table (Photon Control). Image sequences were recorded with a Foculus FO124SC CCD camera. Bath circulation was halted 20 seconds before the commencement of imaging in order to prevent flow-induced oscillations of the beads. The assumption that all bulk motion in the tissue bath had ceased after 20 seconds was validated by the finding that the diffusivity of the microbeads was not detectably correlated with time. Image sequences were recorded for approximately 10 seconds with sampling at 20 – 43 Hz, depending on the clarity of the microbeads and villi or intestinal epithelium surface. It was not possible to conduct observations for periods greater than 10 seconds as microbeads in locations of low viscosity were able to move out of the focal plane after longer periods of time. Circulation of HBS was reestablished immediately on completion of several image sequences and maintained for a minimum of 5 minutes before further sequences were recorded.

At the conclusion of each experiment, the mucosa was removed from the tip of the probe and preserved in 10% formal saline pending histological processing, sectioning and staining with haematoxylin and eocin. Representative stained sections were subsequently examined for signs of necrosis.

3.2.3.2. Microrheological technique

The passive microrheological analysis used in this study enables fragile local environments that are of restricted volume (MacKintosh and Schmidt 1999) to be explored without disruption, and has been used previously to characterize mucus

microenvironments in the cavities of the small intestine and airways (Dawson et al. 2003, Crater and Carrier 2010, Macierzanka et al. 2011).

In each frame, X-Y coordinate data were extracted for the ensemble of microbeads using a Gaussian weighted polynomial fit to the image intensity (Rogers et al. 2007). It was not possible to survey Brownian motion directly in three-dimensions as such a procedure relies on consistency in the variation of the appearance of microbeads along the Z-axis as a result of its distance from the focal plane of the microscope. Such a technique may be applied to homogenous fluids but not to suspensions of translucent material such as mucus as their translucence would confound the consistency of this variation. However, the two-dimensional analysis used in our work was subsequently validated by the results showing isotropy in the three-dimensions insofar as there were no significant differences in the viscosities of the continuous phase between ensembles of microbeads measured around villi with their long axes orientated in the X-Z plane and those measured around villi with their long axes orientated in the X-Y plane. Any microbeads that exhibited excessive movement in the Z- axis, i.e. moved with respect to the focal plane, were omitted. The data from a given microbead were only retained if it could be tracked over the course of 75 to 150 successive frames, depending on the frame rate. In addition, microbeads were tracked only if they were identified as single particles and did not exhibit intimate interactions with other beads. The temporal resolution of the tracking was limited by the frame rate of the camera (1/43 Hz) and the spatial resolution of the 'center-of-mass' movement of the tracer particles was estimated from control experiments to be around 5 nm for the tracking algorithm used.

The mean squared displacement (MSD or $\langle r^2(\tau) \rangle$) of a microbead in the X-Y plane was calculated from the X-Y data using:

$$\langle r^2(\tau)\rangle = \langle [x(t+\tau) - x(t)]^2 + [y(t+\tau) - y(t)]^2 \rangle \quad (3.1)$$

where τ is the lag time over which the mean squared displacement is determined, t is time, and X and Y are the coordinates of the microbead (Gardel et al. 2005). The ensemble averaged MSD of microbeads under-taking thermally driven diffusive movement increases as a power law with lag time:

$$MSD \propto \tau^{\alpha} \quad (3.2)$$

where α is the exponent (Waigh 2005). In a purely viscous environment, the power law exponent is 1 and hence, a plot of the logarithm of MSD against the logarithm of lag time yields a slope of 1. Conversely, should the diffusion of microbeads be hindered by interaction with an elastic structure surrounding it, then its diffusive movement will be restricted and the slope will be reduced (Mason 2000). For the purposes of this work, the microbeads were taken to be situated in a predominantly Newtonian fluid environment if the slopes of the log plots were in the range 0.8 – 1.1. In these situations, the viscosity could be meaningfully determined by extracting the diffusion coefficient using a linear plot and applying the Stokes-Einstein equation (Waigh 2005).

When the slopes of log plots were less than 0.8, the component microbeads were considered to be situated in a viscoelastic fluid environment. In these cases, the MSD data were transformed to obtain a viscoelastic spectrum using a modified generalized Stokes-Einstein (GSE) equation (MacKintosh and Schmidt 1999, Mason 2000, Waigh 2005). This spectrum contains information on the relative viscous and elastic components of the material as a function of a lag time. Elastic moduli (G') values were calculated at a frequency of 1 Hz as this value was within the physiological range likely to be encountered by digesta in the intestine (Taylor et al. 2003, Lentle and Janssen 2011).

3.2.3.3. Assessing the homogeneity of the environments of bead ensembles

The homogeneity of the fluid environment within which each bead ensemble was moving was assessed by examining the distribution of displacements of the microbeads in the X-direction after a given lag time. Frequency distributions of the different displacements found over the ensemble, also known as van Hove plots, were prepared (Valentine et al. 2001). For a homogeneous system, where all the beads experience the same mechanical environment, the different displacements sampled by the ensemble arise simply from the stochastic nature of Brownian motion and the data are expected to fit to a single Gaussian curve centered on the point of origin and with the variance equal to the MSD calculated at the relevant lag time. Similarly, data that clearly fits to a sum of two Gaussian curves, each centered on the origin but with different breadths, can be taken to indicate that the component microbeads were distributed in two different micromechanical environments (Figure 3-2A to C). The suitability of such assignments was formally assessed by comparing the distribution pattern of residuals obtained after fitting with either a single or a double Gaussian function with Origin 8.5 software (OriginLab, Northampton, MA).

In cases where the method indicated that the beads in an ensemble were situated in a heterogeneous environment and were distributed between two regions of distinct mechanical properties, direct plots of microbead trajectories were prepared and these trajectories were color coded according to the magnitude of their displacements (Figure 3-3A). Local homogeneity within each environment was then confirmed by plotting separate van Hove plots (Figure 3-2B and C) of beads with MSDs of a given color-coding and ensuring these were Gaussian.

These trajectory plots also enabled the location of the individual beads in each of the two environments to be distinguished (Figure 3-3A) by the consistency of color-coding. A box-counting algorithm (BCA) was then implemented in MATLAB (Mathworks, Natick, MA) in order to examine areas of a particular colour coding where the motions of microbeads were more highly restricted (Figure 3-3B). The program evaluated the MSDs of all microbeads within a 'box' of set dimensions (96 pixels by 128 pixels – one fifth of the total visual field) that traversed the image in one pixel steps by row and column, and determined the densities of particles that fell within the narrower Gaussian curve in the two-component van Hove plots as the box progressed across the image. The resulting map was colour-coded with dark red to yellow shadings indicating regions containing higher densities of microbeads with restricted, i.e. sub-diffusive, MSDs and with blue indicating regions with higher densities of beads exhibiting unrestricted, i.e. purely diffusive, MSDs. An area was termed a viscoelastic body only when a region shaded red to yellow contained 3 or more microbeads with restricted MSDs. The sizes of these viscoelastic bodies were each estimated by determining the diameter of the largest circle centred on the geometric centre of the positions of the contributing microbeads that could be entirely contained within the 'viscoelastic' (red and yellow colour-coded) area. Only the diameters of bodies whose boundaries did not come into contact with the edges of the visual field were determined.

The areas of viscoelastic bodies as a percentage of the sampling area (0.064 mm^2) were also estimated by calculating the sums of the areas of the component circles within the sampling area based on these diameters.

3.2.3.4. Fluorescent microbeads

Naked polystyrene (NP) hydrophobic fluorescent microbeads (yellow fluorescent, excitation wavelength at 441 nm, emission wavelength at 486 nm) (Polysciences, Warrington, PA) of 0.5 μm diameter were applied to preparations obtained from a total of six distal ilea and three proximal colons. These beads were chosen on the basis that their movements would be relatively restricted when they were located in mucus as they would adhere to hydrophobic domains of mucin proteins (Lai et al. 2007).

The size of beads was chosen to exceed the mean reported distance, of around 100 nm, between component strands of mucin (Olmsted et al. 2001), so as to prevent them sampling voids between adjacent strands of the mucin matrix (Suh et al. 2005). Indeed, quantitative microrheology in such systems as these requires that the microbead size should be in excess of that of the polymer mesh.

3.2.3.5. Sampling and statistics

The viscosities of locations that exhibited Newtonian characteristics and the G' of material that exhibited viscoelasticity were determined separately for sub-ensembles of microbeads, both at distances within 20 μm and at distances greater than 20 μm from the intestinal epithelium. This distance classification was chosen on the grounds that the adherent mucus layer is reported to extend 29 ± 8 μm from the surface of the ileum (Atuma et al. 2001). A similar distance classification was used for microbeads located in the colonic mucosal environment for the purposes of comparison.

A series of image sequences of microbead motion were obtained at multiple sites within the focal plane of the microscope on a given sample of mucosa from a given animal over a period of two hours. Subsequent analysis was conducted on data from sites with a suitable density of microbeads and clarity of the villus edge.

The values obtained for the various parameters required transformation to render them suitable for parametric statistical analysis. This was carried out using the Johnson algorithm in the MINITAB package (Minitab Inc., State College, PA). Data was analyzed by nested ANOVA for the effects of distance from the mucosa, gut segment and animal in the SYSTAT package (Systat Software Inc., Chicago, IL). Hence the results are presented as raw data in box plots in the text along with statistical inferences drawn from the ratio of mean squares from ANOVA of the overall effect to that of the effect nested within animal.

3.2.4. Results

The continuation of contractile activity in the walls of *ex vivo* preparation of the colon and terminal ileum for a period exceeding one hour in a number of pilot experiments confirmed that the tissue remained viable for this time. Histological examination confirmed that the enterocyte epithelium had remained intact for the duration of the experiment and did not exhibit any signs of necrosis (Figure 3-4). Moreover, numbers of mucin bearing goblet cells were evident within the mucosa indicating there had been no general discharge of their contents stimulated by anoxia (Figure 3-4).

The determinations of the various rheological parameters at various sites in each preparation were conducted over a period of one hour after pharmacological blocking with the calcium channel blocking agent verapamil (0.5 ml dose) so as to eliminate any interference by contraction induced flow with the observed Brownian motion. Microbeads that were tracked were identified as single particles and did not exhibit intimate interactions with other beads, which would affect the MSD calculations.

Analyses of the behaviour of microbeads showed the environment around the ileal villi and the colonic mucosa were largely heterogeneous consisting of a continuous phase of

Newtonian liquid that contained viscoelastic material, which we termed ‘bodies’. The behaviour of ensembles of microbeads that exhibited average MSDs that scaled linearly with lag time and fitted with the broader of the two van Hove plots (Figure 3-2B) indicated that they were situated in liquid and could be used to determine local viscosity (Figure 3-2D). Similarly the behaviour of ensembles of microbeads that exhibited average MSDs that varied with lag time according to a local power law (Figure 3-2E) and fitted with the narrower of the two van Hove plots (Figure 3-2C) indicated that they were situated in a viscoelastic solid and could be used to determine elastic and viscous moduli. The dependence of the latter values upon frequency (or timescale) of perturbation was typical of that found in viscoelastic solutions of highly entangled polymer solutions (Williams et al. 2008).

3.2.4.1. Ileal mucosa

The continuous phase of the environment around the terminal ileal villi was a Newtonian fluid of viscosity similar to that of water (the viscosity of water measured by our methods was found to be close to 1 mPa.s as expected). The overall mean viscosity of the continuous phase obtained using transformed data from all preparations (Table 3-1 and Figure 3-5A) was not significantly different on nested ANOVA at distances less than 20 μm to those at distances greater than 20 μm from the mucosa. The mean viscosity of the continuous phase at distances greater than 20 μm above the apical epithelium of the villus tip (median value 1.49 mPa.s; interquartile range (IQR) 1.08 – 2.06, N = 15 replicates) did not differ significantly from that at distances greater than 20 μm from the sides of the villous (median 1.34 mPa.s; IQR 1.13 – 1.8, N = 59 replicates).

The mean elastic modulus (G') of viscoelastic bodies found in the continuous phase, obtained with transformed MSD data from all preparations, did not differ significantly at distances 20 μm or closer to the mucosa to that at distances further than 20 μm from the mucosa (Table 3-1 and Figure 3-5B). The diameters of viscoelastic bodies further than 20 μm from the ileal epithelium did not differ significantly from those of bodies situated 20 μm or closer to villus epithelium (Table 3-1 and Figure 3-6).

The numbers of viscoelastic bodies around the villous ileal epithelium were generally low. Of 26 replicates from locations that contained entire viscoelastic bodies, the visual fields in the majority contained one body per field of view whilst the visual field in one image sequence contained 3 bodies and those in a further three sequences contained two bodies. The percentage area per (0.064 mm^2) field of view occupied by viscoelastic bodies at distances greater than 20 μm from the ileal mucosa did not differ significantly from that of those situated at 20 μm or closer to the surface of the ileal mucosa (Table 3-1).

3.2.4.2. Colonic tissue

The viscosities of the continuous (Newtonian fluid) phase at sites that were situated further than 20 μm did not differ significantly from those 20 μm or closer to the colonic epithelium (Table 3-1). No median and IQR value was available for the viscosity at sites 20 μm or less from the epithelium of the colon as the bulk of microbead ensembles (11 out of 13) were located in viscoelastic material and those in bodies containing only Newtonian fluid were correspondingly low. However, these viscosity values were within the range of the values found at distances greater than 20 μm from the colonic epithelium.

The G' of bodies situated in the continuous phase at distances greater than 20 μm from the colonic epithelium did not differ significantly from those of bodies situated 20 μm or less from the colonic epithelium (Table 3-1). The diameters of viscoelastic bodies situated at distances greater than 20 μm from the colonic epithelium did not differ significantly to that of those situated 20 μm or less from the colonic epithelium (Table 3-1).

The numbers of viscoelastic bodies were generally low around the colonic epithelium. Of a total of 20 replicates from locations that contained entire bodies, the bulk of fields contained a single body, six contained 2 bodies and one contained 3 bodies. The percentage areas of the fields of view (0.064 mm^2) that were occupied by bodies at distances greater than 20 μm from the colonic mucosa did not differ significantly from that of those situated 20 μm or less from the colonic mucosa (Table 3-1).

3.2.4.3. Comparison of ileum and colon

The viscosities of the continuous Newtonian phase obtained at locations that were 20 μm or more from the colonic mucosa were significantly greater than those obtained at locations that were 20 μm or more from the ileal villous epithelium on ANOVA ($df = 8,131$, $F = 3.416$, $P < 0.01$) (Figure 3-4A). Note that the viscosities of the continuous phase obtained at locations that were less than 20 μm from the ileal or colonic mucosa could not be compared due to insufficient data being obtainable from this site in the colon.

The values for G' obtained from viscoelastic bodies that were situated 20 μm or closer to the colonic mucosa were not significantly different to the values obtained from bodies situated 20 μm or closer to the ileal villous mucosa (Figure 3-4B). Similarly, the values for G' obtained from bodies that were situated at distances greater than 20 μm

from the colonic mucosa were not significantly different to those obtained from bodies situated at distances greater than 20 μm from the ileal villous mucosa (Figure 3-4B).

The numbers of viscoelastic bodies identified in each visual field were generally low regardless of their distance from the mucosa or the location in the gut from which the image sequence was obtained (ileum or colon), the majority of sites contained only one body. However, while bodies that were situated above the ileal mucosa were always surrounded by the continuous Newtonian fluid phase, a significant number of bodies that were situated above the colonic mucosa filled the entire visual field and were also counted as a single body.

Taken overall, the diameters of the viscoelastic bodies in the colon were significantly greater on ANOVA ($df = 5, 42$, $F = 2.604$, $P = 0.05$) than those in the ileum[3]. However, the lack of any significance in the term for distance within the segment indicated that there was no significant variation in body size with distance from the surface of the mucosa in this analysis (Figure 3-6).

3.2.4.4. Further corroborative work

A series of further experiments were conducted on distal ileal and colonic samples from nine possums that yielded a total of 98 image sequences (63 of the ileal and 35 of the colonic mucosa) in which Brownian motion of amine coated polystyrene beads of 0.75 μm in diameter could be evaluated in a similar manner to the foregoing work. These beads were chosen as they adhered to mucin by electrostatic rather than hydrophobic interaction. The results obtained from this further work did not differ significantly from

[3] The difference between viscoelastic body sizes with site was conducted with pooled diameters of viscoelastic regions from both types of microbeads. The viscoelastic body diameters were pooled as the diameters of both types of microbeads were not significantly different from one another as shown in sub-section 3.4.3.4 to follow.

those detailed above, showing similar disposition of viscoelastic bodies of similar dimension in the two sites (ileum and colon).

3.2.5. Discussion

This is the first study to demonstrate that the material in bodies immediately adjacent to the small and large intestinal mucosa is rheologically heterogeneous, comprising circumscribed areas that exhibit viscoelastic behaviour similar to that of purified mucus and contained within a more extensive phase of low viscosity Newtonian fluid. In principle, either one or both of the two phases could form a percolating network. As the low viscosity phase percolates across most of the two-dimensional images it is reasonable to conclude that this phase is contiguous in three-dimensional space. However, the viscoelastic phase does not percolate the two-dimensional images and occupies a low percentage of the area per field of view (0.78 – 0.85% in the ileum and 1.4 – 2.9% in the colon). Such low percentages would require generally thin linkages were this phase to percolate through three-dimensional space. The lack of any long and thin viscoelastic components suggests the viscoelastic bodies are dispersed rather than linked.

In regard to the rheological characteristics of the continuous phase it is important to note that observations of the motions of beads were restricted to periods of less than 10 seconds. Hence, it is possible that fluid in these bodies could behave in a viscoelastic fashion over longer time scales, for example as a result of dispersal of extended molecules of mucin in dilute solution. However, given that flow within the intestinal lumen results from contractile events of short duration and is correspondingly short-lived, it is unlikely that such behaviour would be of physiological import.

Whilst further work is required to relate the nature of viscoelastic bodies to mucin secretions and their ability to anneal by reptative (snake-like diffusive motion of polymer chains within polymer entanglements) (De Gennes 1971) inter-digitation of polymer chains on adjacent mucus islands, the results fit in with a number of previous reports that the intestinal mucus layer is discontiguous (Szentkuti and Lorenz 1995) (Figure 3-7B). However, they run contrary to reports that the mucus layer forms a contiguous viscoelastic 'blanket' (Cone 2009) (Figure 3-7A) that overlies the absorptive surface of epithelial cells and restricts the rate at which nutrients are absorbed. The latter hypothesis is to some extent founded on the properties of mucus that have been 'purified' to remove cellular and other debris (Sellers et al. 1991, Macierzanka et al. 2011), and hence, may not reflect the heterogeneity that exists *in vivo*. Likewise, the lamellar structure of mucus found adjacent to the gastric (Sawaguchi et al. 2002) and colonic (Matsuo et al. 1997) mucosa may reflect a similar structure to that we report here comprising stacks of discrete islands of mucus that have become compacted and distorted by histochemical and immunohistological processing. Previous evidence regarding the contiguity of the mucus 'blanket' is equivocal. The tendency of particles to agglomerate within the lumen after being applied to living intestinal mucosa (Swidsinki et al. 2007b) suggests the mucus layer is impenetrable, while work showing that a commensal species *Enterobacter cloacae*, which is not equipped to navigate viscoelastic mucus, is found in murine colonic crypts (Swidsinki et al. 2007b) suggests the discontiguity of this layer and supports our hypothesis.

Given that NP microbeads have been found to adhere strongly to mucus (Dawson et al. 2003, Cone 2009, Crater and Carrier 2010), our results suggest, either that mucin secreted by individual mucosal goblet cells do not always 'anneal' to neighbours (Verdugo 1990) to form a contiguous layer, or that sites of translational diffusion and

reptative inter-digitation of adjacent mucus islands are more vulnerable to digestion by enteral micro-flora. It is known that small variations in the structure of constituent mucin polymer chains can disrupt their configuration, obstructing reptative interdiffusion and impeding annealing (Verdugo 1990). Similarly, the presence of high molecular weight polymers derived from nutrients can inhibit the expansion of mucin granules following their secretion by goblet cells (Whitaker and Zimmerberg 1987, Chandler et al. 1989).

Mucin granules from goblet cells in the respiratory epithelium of the rabbit are reported to expand 250 fold after their secretion (Verdugo 1993). The largest mucin granules within goblet cells are between 0.8 – 1.5 μm in size (Davis et al. 1992, Lethem et al. 1993, Jeffery and Li 1997). Hence, we may expect that the area of the expanded mucin from a single granule will lie between 100 and 370 μm^2. If viscoelastic bodies found in our study consist principally of mucins this suggests that the aggregation of mucin granules is somewhat limited.

The heterogeneity of the microrheological environment around the colonic and villous small intestinal mucosa may explain the variation in the functional thickness of the 'unstirred water layer' (UWL) with the molecular size of the probe (Pohl et al. 1998). Thus, larger molecules would tend to be more confined to the watery continuous phase whilst smaller molecules that are able diffuse into viscoelastic bodies would be retained for longer in a process akin to gel filtration. The extent of this effect will depend on the width of the channels in the continuous phase. Our estimates of the percentage area per field of view of the viscoelastic bodies suggest these channels are wide but this finding may have been influenced by a reduction in the rates at which water and contained nutrients are absorbed in an *ex vivo* mucosal preparation where subsequent vascular transport is necessarily inhibited. These heterogenous structures may similarly act to

confine fat micelles to the continuous phase allowing them to penetrate more readily to the villous mucosa. Similarly, it may allow membrane vesicles exocytosed from the enterocyte brush border to bypass the mucin layer and enter the lumen (McConnell et al. 2009).

The heterogeneous microrheological structure also has important consequences for the process of mixing within the intervillous space and our understanding of the transit and absorption of nanoparticles containing therapeutic substances that might adhere to viscoelastic bodies (Dawson et al. 2003, Dawson et al. 2004, Suh et al. 2005). Whilst previous reports have indicated that mucus can accumulate in the intervillous space (Atuma et al. 2001), the current work is the first to report the heterogeneous microrheology therein, its similarity to that around the villous tips suggesting that there is on-going admixture and transit of these elements between the lumen and the intervillous spaces during longitudinal (Lentle et al.2012) and circular (Grivel and Ruckebusch 1972) contractile activity.

Our finding that viscoelastic bodies are generally more extensive and the intervening continuous phase correspondingly reduced in sites less than 20 μm from the colonic epithelium, than at similar sites in the small intestine, suggest either that reptative diffusion and inter-digitation of polymer chains on adjacent mucus islands occurs more readily with colonic mucins, or that colonic sites are more mechanically resilient perhaps reflecting the greater diversity of colonic than small intestinal mucin structure (Matsuo et al. 1997, Robbe et al. 2003, Swidsinki et al. 2007b). The greater variance in the area and diameter of the bodies is similarly likely to reflect differences in the capacity for reptative interdiffusion of the different colonic mucins. The finding that the continuous phase in the colon has a greater viscosity than that in the ileal environment

may reflect a greater content of enteral micro-flora or concentration of oligosaccharides from bacterial degradation of dietary non-starch polysaccharides.

Whilst the size and form of possum ileal villi are similar to those of humans and the mucosal architecture is broadly similar over the range of laboratory species, notably the density of villi and effective surface area per unit villus (Kararli 1995), it is possible that the spatial pattern of aggregation of mucus islands varies between species. Hence caution is required pending completion of similar studies at other sites and in other species. However the results raise the possibility that the constituents of the mobile mucus layer are not always deployed to act as a contiguous barrier (Boshi et al. 1996) the strategy perhaps being sacrificed at sites of the gut where absorption of residual nutrients is at a premium.

3.2.6. Journal article references

Amidon, G. L., J. Kou, R. L. Elliott and E. N. Lightfoot (1980) Analysis of models for determining intestinal wall permeabilities. Journal of Pharmaceutical Sciences **69**: 1369-1373.

Anderson, B. W., A. S. Levine, D. G. Levitt, J. M. Kneip and M. D. Levitt (1988) Physiological measurement of luminal stirring in perfused rat jejunum. American Journal of Physiology **254**: G843-848.

Atuma, C., V. Strugala, A. Allen and L. Holm (2001) The adherent gastrointestinal mucus gel layer: thickness and physical state *in vivo*. American Journal of Physiology **280**: G922-929.

Boshi, Y., R. Nezu, J. Khan, K. Chen, L. Cui, H. Yoshida, M. Wasa, M. Fukuzawa, S. Kamata, Y. Takagi and A. Okada (1996) Developmental Changes in Distribution of the Mucous Gel Layer and Intestinal Permeability in Rat Small Intestine. Journal of Parenteral and Enteral Nutrition **20**: 406-411.

Chandler, D. E., M. Whitaker and J. Zimmerberg (1989) High molecular weight polymers block cortical granule exocytosis in sea urchin eggs at the level of granule matrix disassembly. Journal of Cell Biology **109**: 1269-1278.

Cone, R. (2009) Barrier properties of mucus. Advanced Drug Delivery Reviews **61**: 75-85.

Crater, J. S. and R. L. Carrier (2010) Barrier properties of gastrointestinal mucus to nanoparticle transport. Macromolecular Bioscience **10**: 1473-1483.

Danielsen, E. M., H. Sjöström, O. Norén, B. Bro and E. Dabelsteen (1982) Biosynthesis of intestinal microvillar proteins. Characterization of intestinal explants in organ culture and evidence for the existence of pro-forms of the microvillar enzymes. Biochemical Journal **202**: 647-654.

Davis, C. W., M. L. Dowell, M. Lethem and M. Van Scott (1992) Goblet cell degranulation in isolated canine tracheal epithelium: response to exogenous ATP, ADP, and adenosine. American Journal of Physiology **262**: C1313-1323.

Dawson, M., D. Wirtz and J. Hanes (2003) Enhanced Viscoelasticity of Human Cystic Fibrotic Sputum Correlates with Increasing Microheterogeneity in Particle Transport. Journal of Biological Chemistry **278**: 50393-50401.

Dawson, M., E. Krauland, D. Wirtz and J. Hanes (2004) Transport of polymeric nanoparticle gene carriers in gastric mucus. Biotechnology Progress **20**: 851-857.

de Gennes, P. G. (1971) Reptation of a polymer chain in the presence of fixed obstacles. The Journal of Chemical Physics **55**: 572.

Debnam, E. S. and R. J. Levin (1975) Effects of fasting and semi-starvation on the kinetics of active and passive sugar absorption across the small intestine *in vivo*. Journal of Physiology **252**: 681-700.

Fagerholm, U. and H. Lennernäs (1995) Experimental estimation of the effective unstirred water layer thickness in the human jejunum, and its importance in oral drug absorption. European Journal of Pharmaceutical Sciences **3**: 247-253.

Gardel, M. L., M. T. Valentine and D. A. Weitz (2005) Microrheology. In: Breuer KS, editor. Microscale Diagnostic Techniques: Springer. pp. 1-50.

Grivel, M. L. and Y. Ruckebusch (1972) The propagation of segmental contractions along the small intestine. Journal of Physiology **227**: 611-625.

Ham, A. W. (1969) Histology. Philadelphia: Lippincott:663.

Jeffery, P. K. and D. Li (1997) Airway mucosa: secretory cells, mucus and mucin genes. European Respiratory Journal **10**: 1655-1662.

Kararli, T. T. (1995) Comparison of the gastrointestinal anatomy, physiology, and biochemistry of humans and commonly used laboratory animals. Biopharmaceutics and Drug Disposition **16**: 351-380.

Lai, S. K., D. E. O'Hanlon, S. Harrold, S. T. Man, Y. Y. Wang, R. Cone and J. Hanes (2007) Rapid transport of large polymeric nanoparticles in fresh undiluted human mucus. Proceedings of the National Academy of Sciences **104**: 1482-1487.

Lentle, R. G., C. de Loubens, C. Hulls, P. W.M. Janssen, M. D. Golding and P. Chambers (2012) Organization of longitudinal and circular contractions during pendular and segmental activity; a comparison of duodenal contractile activity in the rat and guinea pig. Neurogastroenterology and Motility **24**: 686–e298.

Lentle, R. G. and P. W. M. Janssen (2011) Flow, mixing and absorption at the mucosa. In: Lentle RG, Janssen PWM, editors. Physical Processes of Digestion. New York: Springer.

Lentle, R. G., Y. Hemar, C. E. Hall and K. J. Stafford (2005) Periodic fluid extrusion and models of digesta mixing in the intestine of a herbivore, the common brushtail possum (*Trichosurus vulpecula*). Journal of Comparative Physiology B **175**: 337-347.

Lethem, M., M. Dowell, M. Van Scott, C. W. Davis, J. Yankaskas, T. Egan and R. C. Boucher (1993) Nucleotide regulation of goblet cells in human airway epithelial explants: normal exocytosis in cystic fibrosis. American Journal of Respiratory Cell and Molecular Biology **9**: 315.

Levitt, M. D., T. Aufderheide, C. A. Fetzer, J. H. Bond and D. G. Levitt (1984) Use of carbon monoxide to measure luminal stirring in the rat gut. Journal of Clinical Investigation **74**: 2056-2064.

Macierzanka, A., N. M. Rigby, A. P. Corfield, N. Wellner, E. N. Clare Mills, A. R. Mackie and F. Böttger (2011) Adsorption of bile salts to particles allows penetration of intestinal mucus. Soft Matter **7**: 8077-8084.

MacKintosh, F. C. and C. F. Schmidt (1999) Microrheology. Current Opinion in Colloid & Interface Science **4**: 300-307.

Mason, T. G. (2000) Estimating the viscoelastic moduli of complex fluids using the generalized Stokes-Einstein equation. Rheologica Acta **39**: 371-378.

Matsuo K, Ota H, Akamatsu T, Sugiyama A, Katsuyama T (1997) Histochemistry of the surface mucous layer of the human colon. Gut **40**: 782-789.

McConnell, R. E., J. N. Higginbotham, D. A. Shifrin Jr, D. L. Tabb, R. J. Coffey and M. J. Tyska (2009) The enterocyte microvillus is a vesicle-generating organelle. Journal of Cell Biology **185**: 1285-1298.

Olmsted, S. S., J. L. Padgett, A. I. Yudin, K. J. Whaley, T. R. Moench and R. Cone (2001) Diffusion of macromolecules and virus-like particles in human cervical mucus. Biophysical Journal **81**: 1930-1937.

Pohl, P., S. M. Saparov and Y. N. Antonenko (1998) The size of the unstirred layer as a function of the solute diffusion coefficient. Biophysical Journal **75**: 1403-1409.

Read, N. W., R. J. Levin and C. D. Holdsworth (1976) Proceedings: Measurement of the functional unstirred layer thickness in the human jejunum *in vivo*. Gut **17**: 387.

Robbe, C., C. Capon, E. Maes, M. Rousset, A. Zweibaum, J .P. Zanetta and J. C. Michalski (2003) Evidence of regio-specific glycosylation in human intestinal mucins. Journal of Biological Chemistry **278**: 46337-46348.

Rogers, S. S., T. A. Waigh, X. Zhao and J. R. Lu (2007) Precise particle tracking against a complicated background: polynomial fitting with Gaussian weight. Physical Biology **4**: 220-227.

Sawaguchi, A., K. Ishihara, J. Kawano, T. Oinuma, K. Hotta, T. Suganuma (2002) Fluid dynamics of the excretory flow of zymogenic and mucin contents in rat gastric gland processed by high-pressure freezing/freeze substitution. Journal of Histochemistry and Cytochemistry **50**: 223-234.

Sellers, L. A., A. Allen, E. R. Morris, S. B. Ross-Murphy (1991) The rheology of pig small intestinal and colonic mucus: weakening of gel structure by non-mucin components. Biochimica et Biophysica Acta **1115**: 174-179.

Smithson, K. W., D. B. Millar, L. R. Jacobs and G. M. Gray (1981) Intestinal diffusion barrier: unstirred water layer or membrane surface mucous coat? Science **214**: 1241-1244.

Sugano, K. (2009) Estimation of effective intestinal membrane permeability considering bile micelle solubilisation. International Journal of Pharmaceutics **368**: 116-122.

Suh, J., M. Dawson and J. Hanes (2005) Real-time multiple-particle tracking: applications to drug and gene delivery. Advanced Drug Delivery Reviews **57**: 63-78.

Swidsinski, A., B. C. Sydora, Y. Doerffel, V. Loening-Baucke, M. Vaneechoutte, M. Lupicki, J. Scholze, H. Lochs and L. A. Dieleman (2007b) Viscosity gradient within the mucus layer determines the mucosal barrier function and the spatial organization of the intestinal microbiota. Inflammatory Bowel Diseases **13**: 963-970.

Swidsinski, A., V. Loening-Baucke, F. Theissig, H. Engelhardt, S. Bengmark, S. Koch, H. Lochs and Y. Dörffel (2007a) Comparative study of the intestinal mucus barrier in normal and inflamed colon. Gut **56**: 343-350.

Szentkuti, L. and K. Lorenz (1995) The thickness of the mucus layer in different segments of the rat intestine. Histochemical Journal **27**: 466-472.

Taylor, C., A. Allen, P. W. Dettmar and J. P. Pearson (2003) The gel matrix of gastric mucus is maintained by a complex interplay of transient and nontransient associations. Biomacromolecules **4**: 922-927.

Thomson, A. B. and J. M. Dietschy (1977) Derivation of the equations that describe the effects of unstirred water layers on the kinetic parameters of active transport processes in the intestine. Journal of Theoretical Biology **64**: 277-294.

Thomson, A. B. R. and J. M. Dietschy (1984) The role of the unstirred water layer in intestinal permeation. In: Csaky TZ, editor. Pharmacology of Intestinal Permeation. New York: Springer-Verlag. pp. 165-269.

Valentine, M. T., P. D. Kaplan, D. Thota, J. C. Crocker, T. Gisler, R. K. Prud'homme, M. Beck and D. A. Weitz (2001) Investigating the microenvironments of inhomogeneous soft materials with multiple particle tracking. Physical Review E **64**: 1-9.

Verdugo, P. (1990) Goblet cells secretion and mucogenesis. Annual Review of Physiology **52**: 157-176.

Verdugo, P. (1993) Polymer gel phase transition in condensation-decondensation of secretory products. Advances in Polymer Science **110**: 145-156.

Waigh, T. A. (2005) Microrheology of complex fluids. Reports on Progress in Physics **68**: 685-742.

Weinstein, L. D., C. P. Shoemaker, T. Hersh and H. K. Wright (1969) Enchanced Intestinal Absorption After Small Bowel Resection in Man. Archives of Surgery **99**: 560-562.

Westergaard, H. and J. M. Dietschy (1974) Delineation of the dimensions and permeability characteristics of the two major diffusion barriers to passive

mucosal uptake in the rabbit intestine. Journal of Clinical Investigation **54**: 718-732.

Whitaker, M. and J. Zimmerberg (1987) Inhibition of secretory granule discharge during exocytosis in sea urchin eggs by polymer solutions. Journal of Physiology **389**: 527-539.

Williams, M. A. K., R. R. Vincent, D. N. Pinder and Y. Hemar (2008) Microrheological studies offer insights into polysaccharide gels. Journal of Non-Newtonian Fluid Mechanics **149**: 63-70.

Wilson, F. A., V. L. Sallee and J.M. Dietschy (1971) Unstirred water layers in intestine: rate determinant of fatty acid absorption from micellar solutions. Science **174**: 1031-1033.

Winne, D. (1978) Dependence of intestinal absorption *in vivo* on the unstirred layer. Naunyn-Schmiedebergs Archives of Pharmacology **304**: 175-181.

Winne, D., S. Kopf and M. L. Ulmer (1979) Role of unstirred layer in intestinal absorption of phenylalanine *in vivo*. Biochimica et Biophysica Acta **550**: 120-130.

Winne, D. (1981) Unstirred layer as a diffusion barrier in vitro and *in vivo*. In: Skadhause F, Heintse K, editors. Intestinal Absorption and Secretion. Lancaster: MTP-Press. pp. 21-38.

3.2.7. Journal article figures and tables

Figure 3-1: Tissue bath.The excised mucosal tissue is mounted with villous surface outermost on the sintered tip of the hollow tube in the center of the tissue bath. The focal plane of the objective can be adjusted to lie at different points along the axes of the projecting villi. The circular weir allows carboxygenated HBS superfusate to overflow into the outer compartment with minimal turbulence.

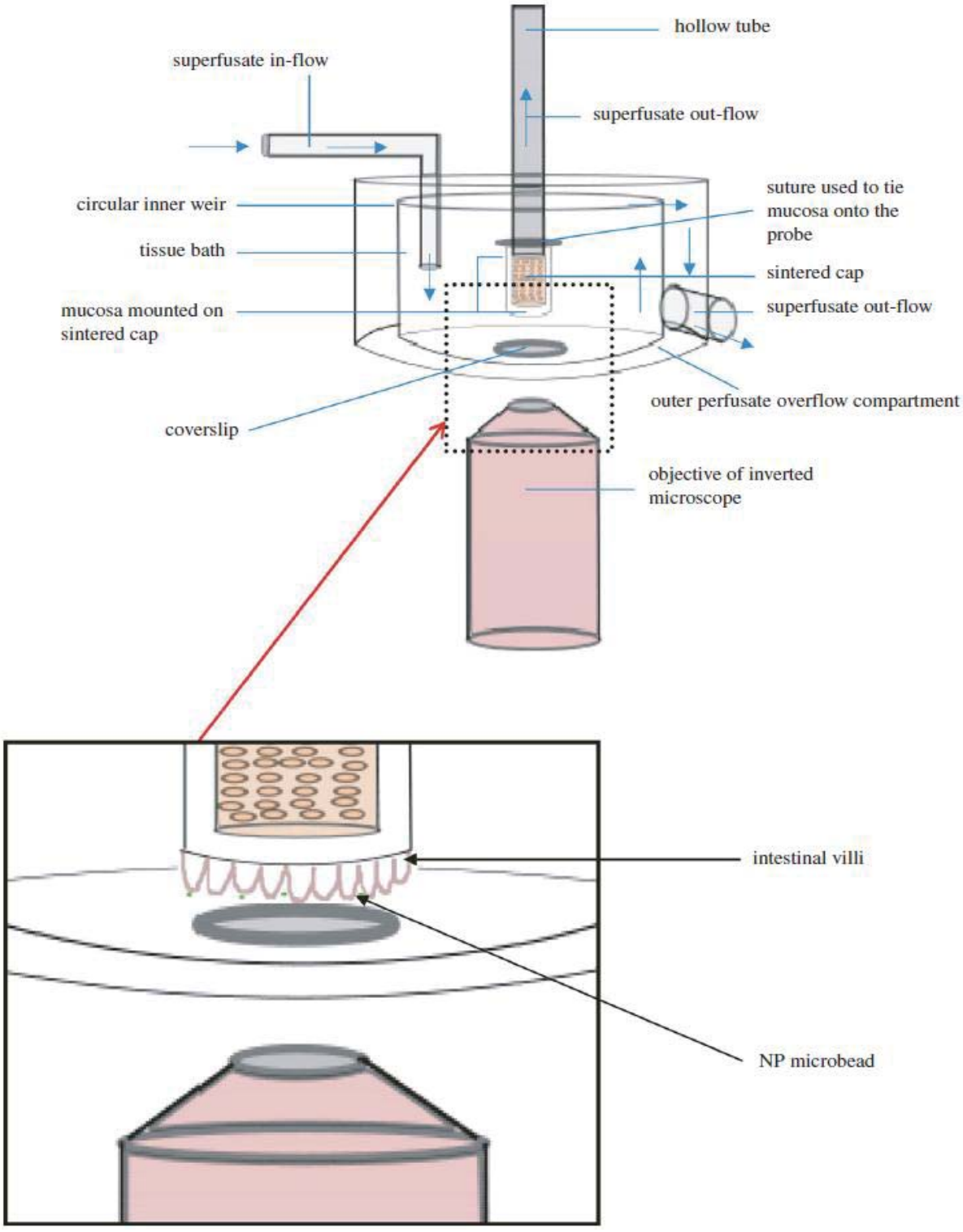
hollow tube
superfusate in-flow
superfusate out-flow
circular inner weir
suture used to tie mucosa onto the probe
tissue bath
sintered cap
mucosa mounted on sintered cap
superfusate out-flow
outer perfusate overflow compartment
coverslip
objective of inverted microscope
intestinal villi
NP microbead

Figure 3-2: Spatial analyses of microrheological environments.An initial van Hove plot of the combined mean squared displacement (MSD)s from the trajectories of all beads in a field showing a composite form (A).The data are better fitted by two Gaussian curves (B and C) than a single curve. Data from the broader curve (B) plotted as log MSD (microns) vs. log lag-time (D) yields a straight line indicating bead motion in a Newtonian fluid and allowing viscosity to be calculated from the slope. Data from beads in a viscoelastic body contribute to the narrower curve (C). Here a plot of log MSD (microns) vs. log (E) yields a curve indicating viscoelasticity. In this case, G' (elastic modulus) and G" (viscous modulus) can be derived (F).

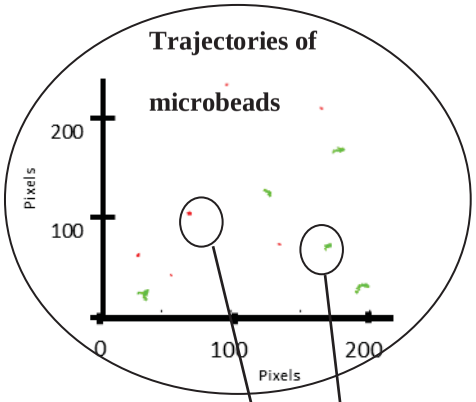

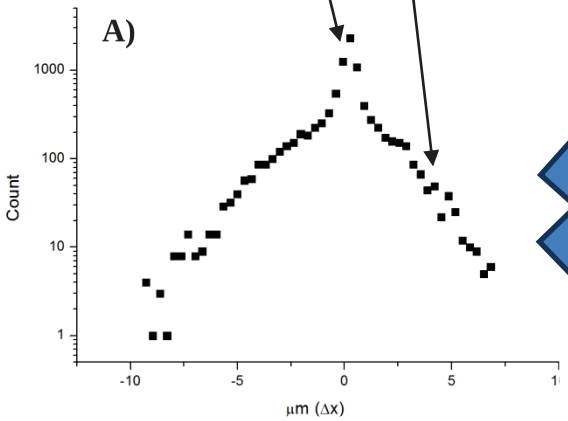

van Hove plot of microbead ensembles

Separation into two micro-mechanical environments

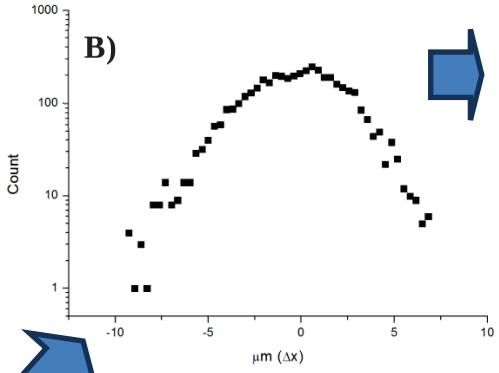

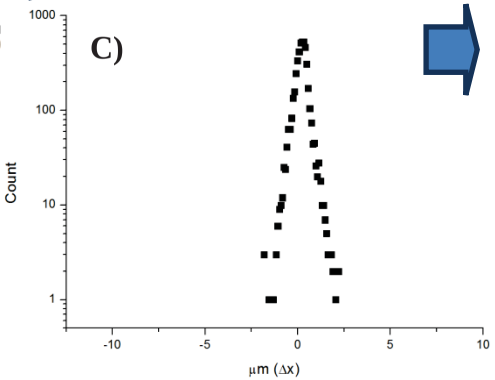

Environment 1, slope = 1

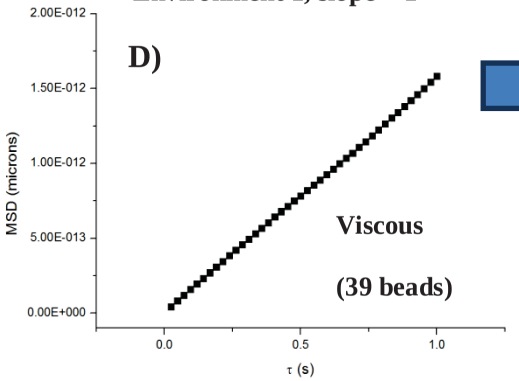

η = viscosity

Environment 2, slope = 0.3

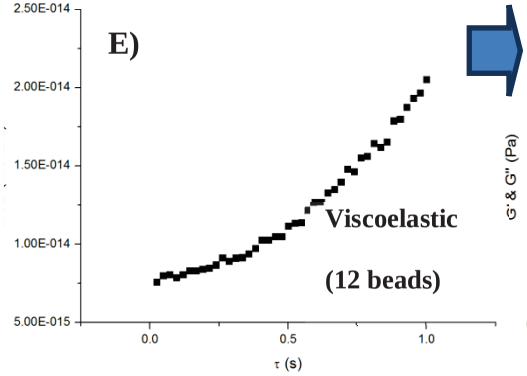

G' = viscoelastic component

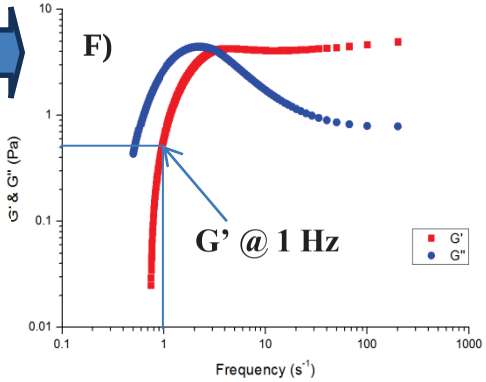

Figure 3-3: Mapping of viscoelastic bodies.A) Photomicrograph showing the location of the villi and the distribution of microbeads. B) A direct plot of the trajectories of a field of microbeads allows the sub-diffusive trajectories (coded red) of beads within viscoelastic bodies to be distinguished from the more extensive diffusive trajectories of microbeads (coded green) within the continuous fluid phase. C) Output from the box-counting algorithm (BCA) that delineates viscoelastic bodies containing groups of beads with sub-diffusive mean squared displacement (MSD)s.

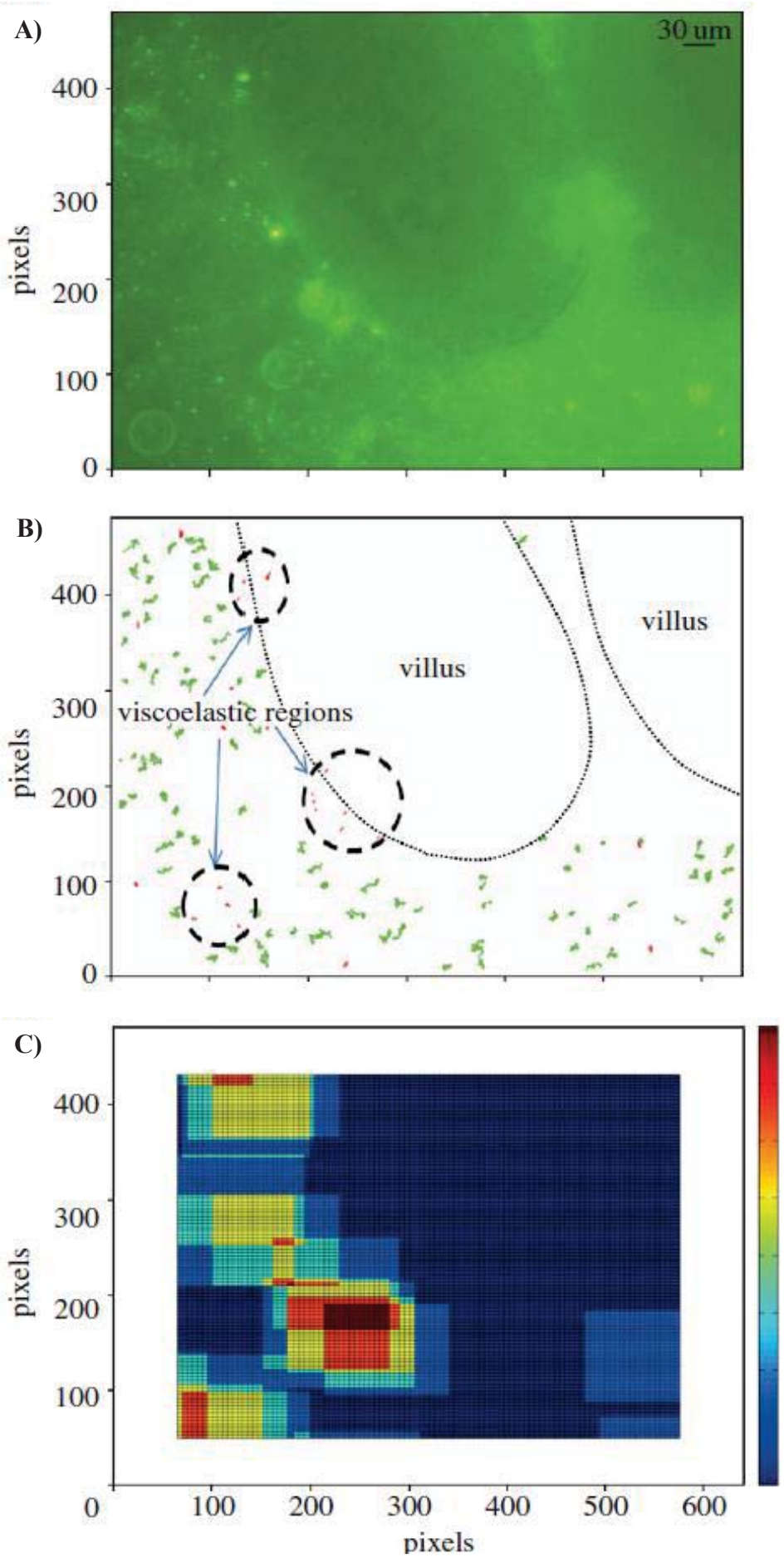
A)
30 um
400
300
200
100
0
pixels
B)
villus
villus
viscoelastic regions
C)
0
100
200
300
400
500
600
pixels

Figure 3-4: Stained sections of villi from mucosal sample following passive microrheology. Stained sections show preservation of tissue structure with no evidence of necrosis (Haematoxylin and Eocin stain). The red arrows indicate mucin granules lying within intact goblet cells.

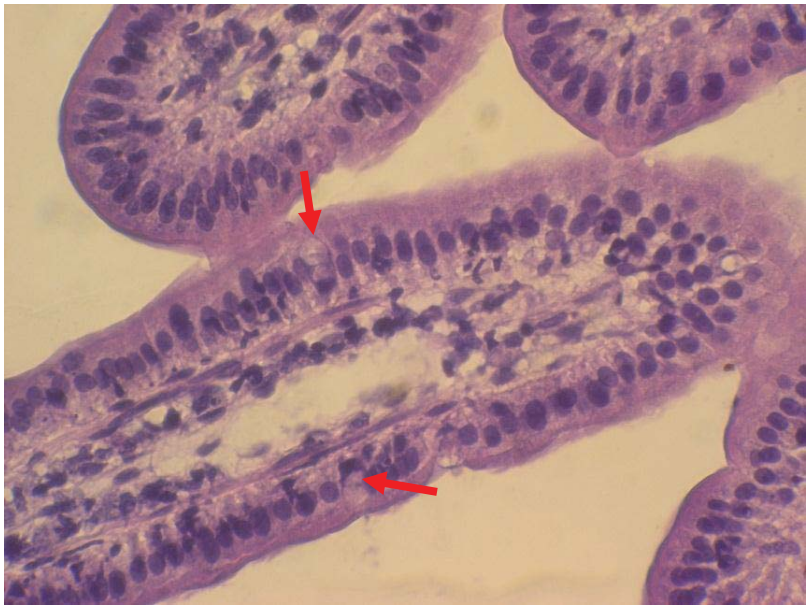

Figure 3-5: Variation in the rheological properties of the continuous phase and viscoelastic bodies with intestinal segment, distance from the mucosa and location around intestinal villi (i.e. tips and sides of villi) shown using boxplots. (A) Viscosity of continuous phase, (B) elastic moduli of bodies (G'), (C) comparison of viscosity of continuous phase > 20 µm from the tip and the sides of ileal villi. The following are the definitions of the various symbols on the boxplots: The maximum and minimum values of the dataset are indicated by the longer horizontal lines usually found on the extreme ends of the plot, the diagonal crosses (X) indicates the 1% and 99% percentile of the dataset, the shorter horizontal lines connected to the rectangle box by a vertical line is the 5% and 95% percentile of the dataset, the longest horizontal line forming the upper and lower boundaries of the box indicates the 25% and 75% percentile (i.e. the lower and upper quartile respectively) of the dataset, the longest horizontal line within the box is the median value of the dataset whilst the square (□) indicates the mean of the dataset.

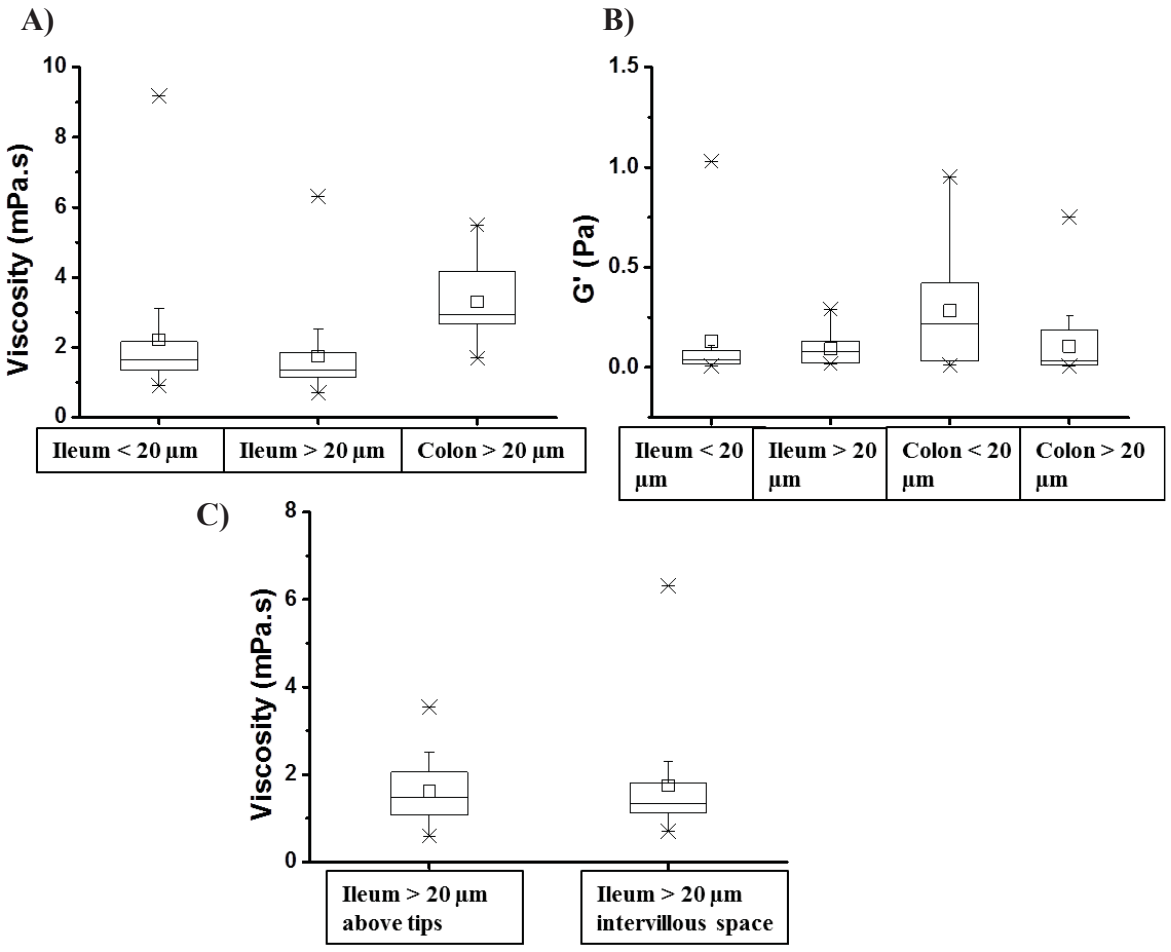

Figure 3-6: Variation in the diameter and projected area of viscoelastic bodies near the ileal villous and colonic mucosa.(A) Variation between the ileum and colon in diameters of viscoelastic bodies and, (B) variation between the ileum and colon in the areas of viscoelastic bodies. The following are the definitions of the various symbols on the boxplots: The maximum and minimum values of the dataset are indicated by the longer horizontal lines usually found on the extreme ends of the plot, the diagonal crosses (X) indicates the 1% and 99% percentile of the dataset, the shorter horizontal lines connected to the rectangle box by a vertical line is the 5% and 95% percentile of the dataset, the longest horizontal line forming the upper and lower boundaries of the box indicates the 25% and 75% percentile (i.e. the lower and upper quartile respectively) of the dataset, the longest horizontal line within the box is the median value of the dataset whilst the square (□) indicates the mean of the dataset.

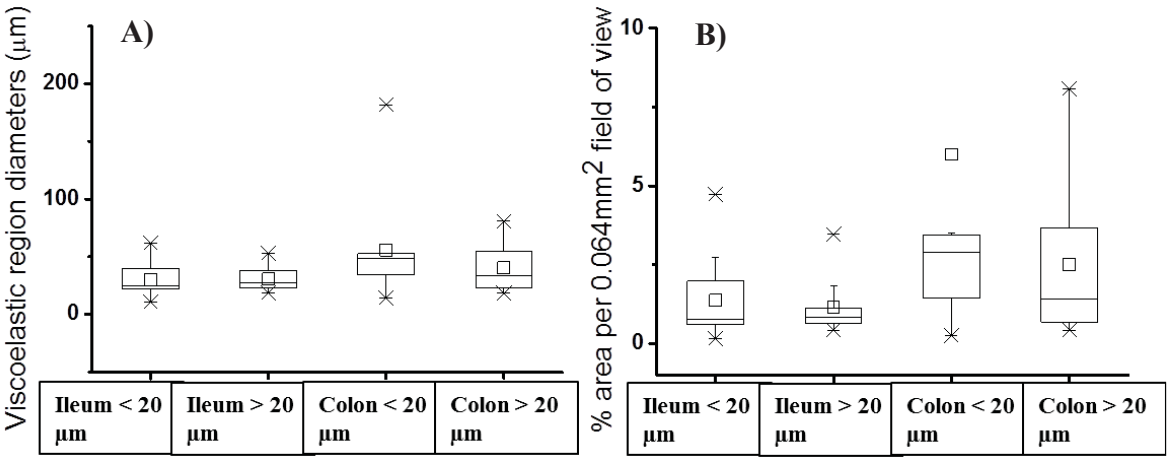

Figure 3-7: Alternatives for disposition of mucin around villi. A) Extensive reptative interdiffusion between mucus islands to form a continuous layer. B) Limited reptative interdiffusion between secreted mucin of mucus islands leading to discontiguity.

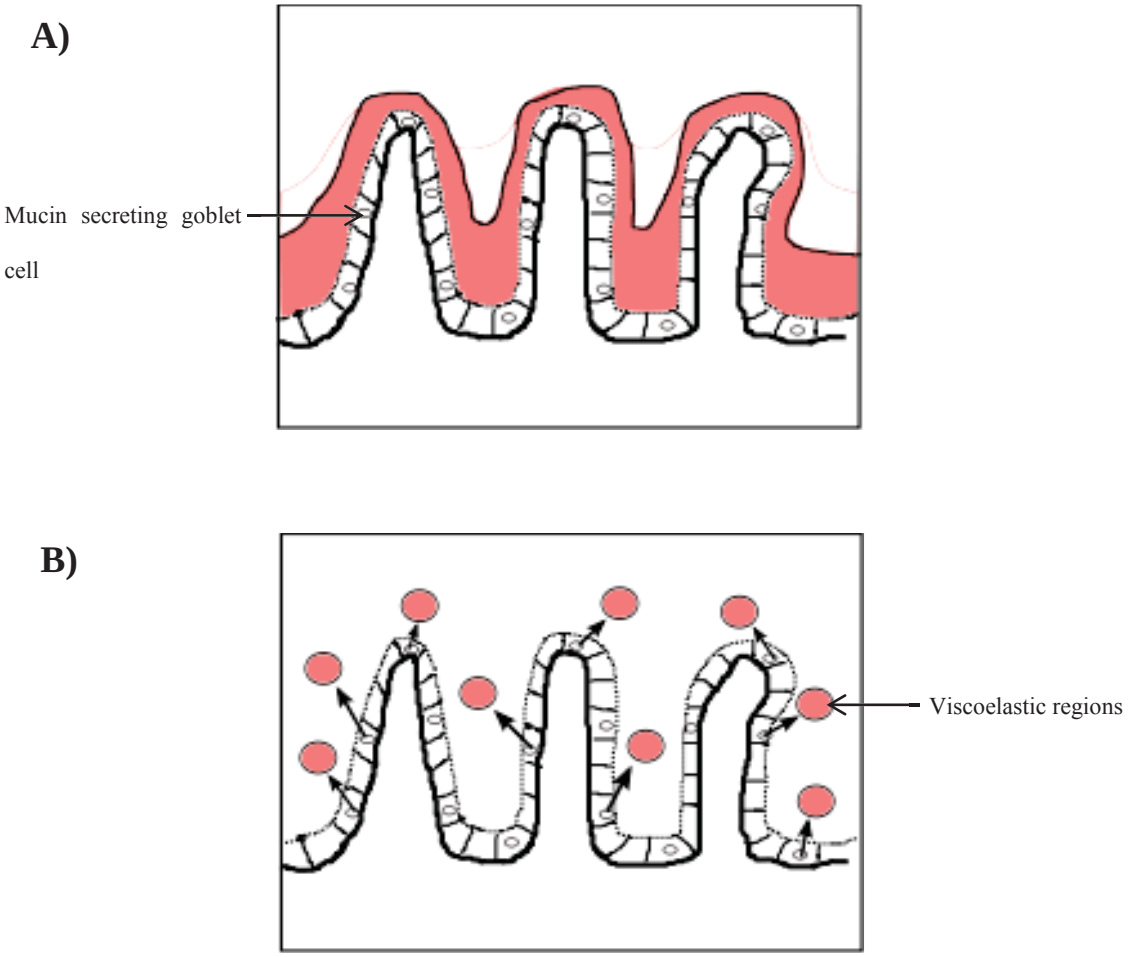

Table 3-1: Summary of the micro-rheological properties (viscosity and elastic moduli) of the continuous phase of Newtonian fluid and viscoelastic bodies, body diameters and percentage area occupied by viscoelastic bodies per 0.064 mm^2 field of view.The third entry of the table which stipulates the viscosity of the continuous Newtonian phase at less than 20 μm from then colonic surface, has been labelled with '*'. This is due to insufficient values for the calculation of median and interquartile range (IQR). It is included for comparison with other viscosity values.

Measured parameter	Site	N (replicates)	Median	IQR
Continuous Newtonian Phase Viscosity (mPa.s)	Ileum <20	50	1.68	1.34 - 2.18
	Ileum >20	66	1.35	1.14-1.85
	Colon < 20	2	3.18-5.22*	
	Colon > 20	16	2.94	2.67-4.16
Viscoelastic Bodies Elastic moduli (Pa)	Ileum <20	19	0.036	0.017-0.085
	Ileum >20	10	0.077	0.023-0.13
	Colon < 20	11	0.22	0.032-0.42
	Colon > 20	20	0.03	0.01-0.19
Viscoelastic Bodies Diameter (μm)	Ileum <20	12	25.1	22.2-40
	Ileum >20	14	27.8	22.7-53
	Colon < 20	12	48.4	34.1-52.9
	Colon > 20	8	33.8	23.5-54
% area occupied by viscoelastic bodies per 0.064mm2 field of view	Ileum <20	12	0.78	0.6-2
	Ileum >20	14	0.85	0.6-1.1
	Colon < 20	12	2.9	1.4-3.5
	Colon > 20	8	1.4	0.7-3.7

3.3. Additional details on the equipment and methods used for micro-rheology studies

The material in this section was not provided in Lim et al. (2013). The following are presented: the design of the tissue bath used, layout of experimental apparatus and additional details of the micro-rheology technique used.

3.3.1. Tissue bath design

A tissue bath was constructed to allow the disposition and microrheology of the fluid environment in the perivillous space of a sample of terminal ileum and proximal colon of the brushtail possum to be studied. The apparatus was designed to be attached to an inverted microscope that was adapted to function as an optical microrheometer. The tissue bath was constructed to fulfil the following requirements:

A) The excised gut wall sample must be maintained viable at a temperature of 37^{o}C and immersed in recirculated carboxygenated Earle-Hepes (HBS) solution.
B) The excised gut wall sample and its associated perivillous environment must be positioned in the optical plane of the inverted microscope. There should also be some method of adjustment of the sample position in the vertical and horizontal directions so as to allow as much of the mucosa as possible to be positioned in the optical plane of the microrheometer.

The design of the tissue bath probe facilitated the exposure of both sides of the gut wall to carboxygenated HBS (see sub-section 3.3.1.2). The design of the tissue bath allowed it to be positioned in a recess located on a manual substage of the inverted microscope. The manual substage allowed the horizontal translation (with an X-Y travel of 70 x 50

mm) of the whole tissue bath over the microscope objective. That, together with the vertical translation capability of the microscope hub containing the microscope objectives (a coarse adjustment of 4.9 mm/rotation and a fine adjustment of 0.1 mm/rotation), the focussing of the optical plane of the micro-rheometer to traverse the length of the villi in three directions was enabled. The imaging of the villi by the inverted microscope was enabled by an aperture at the underside of the bath. The final design of the tissue bath used for experiments can be seen below (Figure 3-8). The following sub-sections detail the various components of the tissue bath.

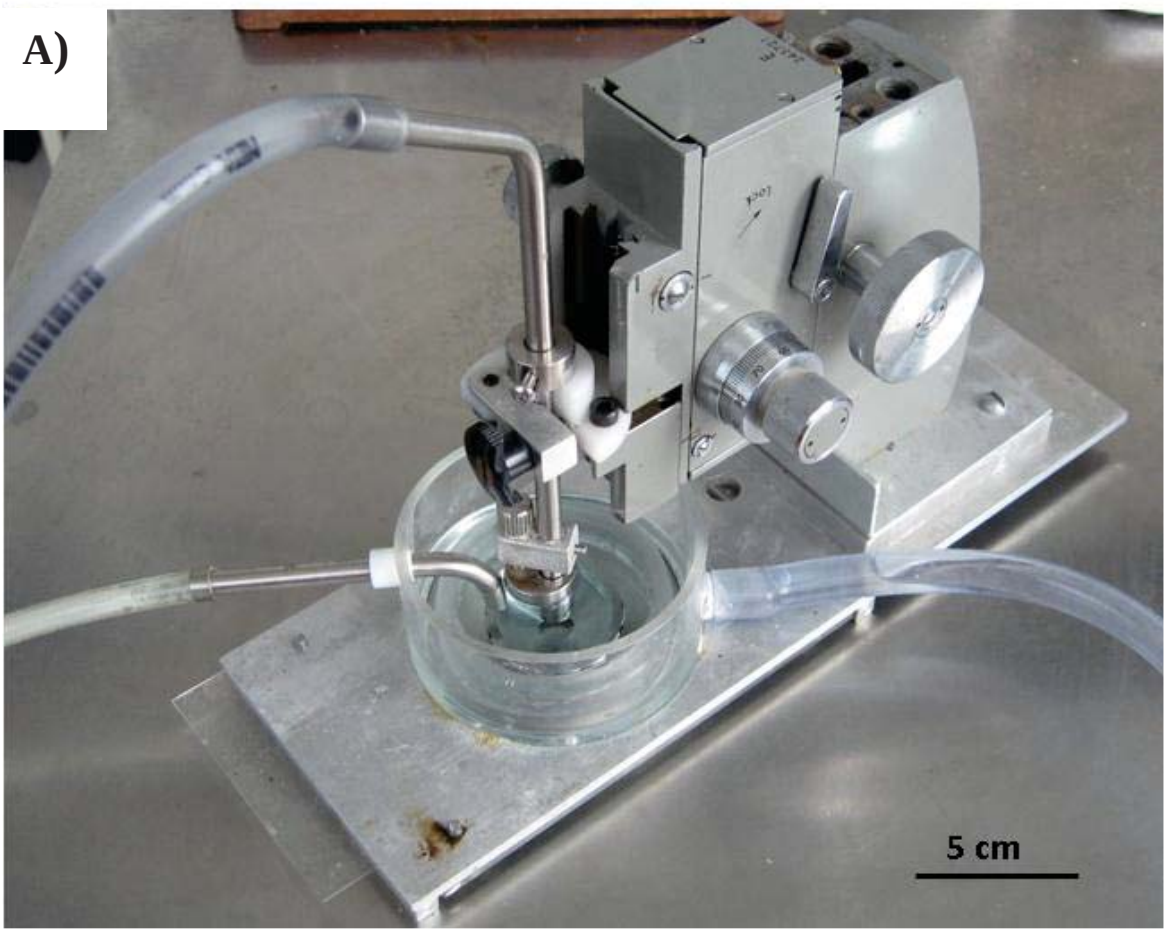

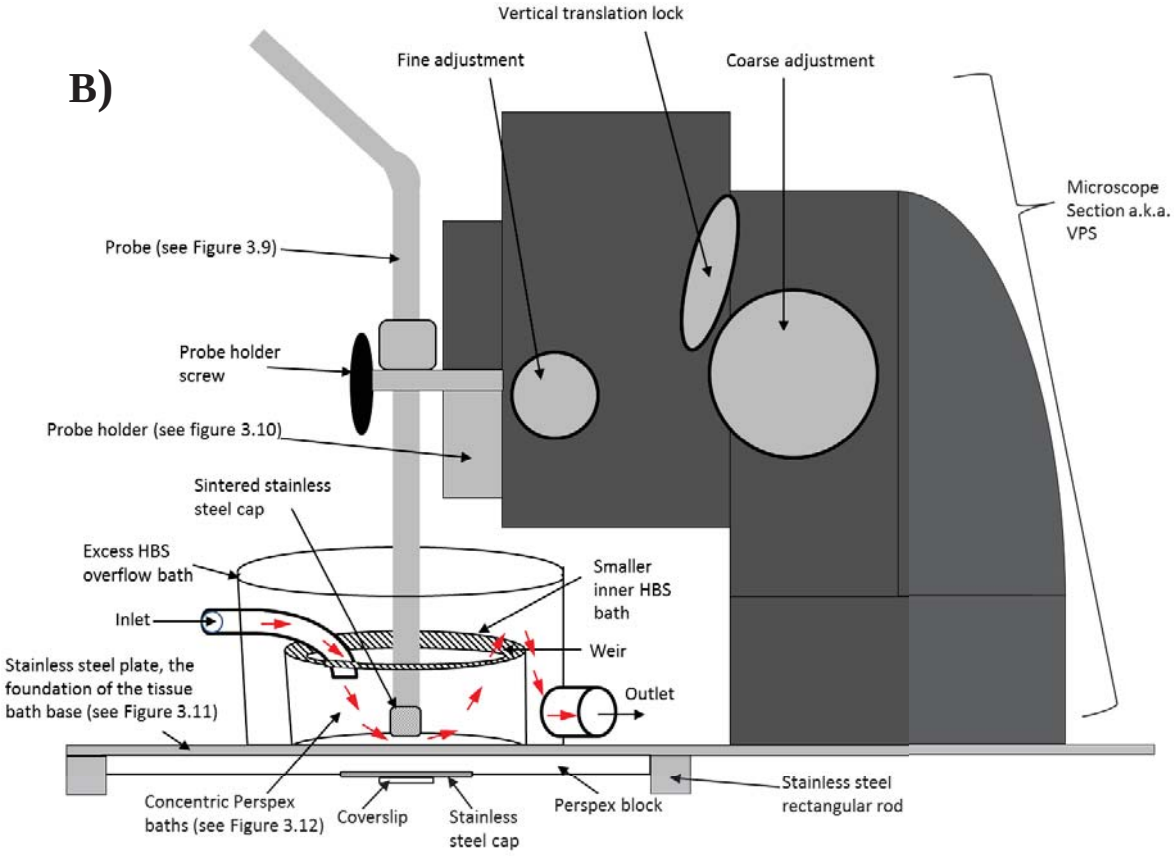

Figure 3-8: Final design of the tissue bath.A) A photographic view while B) is a layout of the tissue bath main components. The flow of Earle-Hepes solution (HBS) into and out of the baths is depicted by red arrows. The component marked in dark grey is the probe vertical positioning structure (VPS) was actually the top section of an old light microscope.

The tissue bath consisted of four main components: a probe (see sub-section 3.3.1.2), the probe vertical positioning structure (VPS, see sub-section 3.3.1.1), two circular Perspex baths of different size (see sub-section 3.3.1.4) and the tissue bath base (see sub-section 3.3.1.3).

3.3.1.1. Probe vertical positioning structure (VPS)

The VPS comprised the rack with its attached pinion gears, which were formerly the focussing adjustment of a light microscope. The purpose of VPS (Figure 3-8) was to be able to position the probe (see sub-section 3.3.1.2) with the mounted gut sample in the Perspex baths (Figure 3-8, the smaller inner HBS bath and excess HBS overflow bath),

which would contain carboxygenated and heated HBS. The tissue bath probe was secured to the VPS by a probe holder (see Figure 3-10 for the probe holder). The VPS allowed the probe tip to be additionally adjusted along the Z-axis (i.e. vertically with a coarse adjustment of 20 mm/rotation and fine adjustment of 0.1 mm/rotation). A vertical translation lock on the VPS was used to secure the probe once it had been adjusted preventing any further vertical movement. The distance between the VPS and the Perspex baths was such that the probe could be positioned over an area in the baths that lay in the optical plane of the inverted microscope. In addition, the probe and the attached gut wall sample could be easily detached and mounted onto the VPS.

3.3.1.2. Tissue bath probe

The main components of the probe were a hollow stainless steel tube, a stainless steel plug and a stainless steel outer casing. The stainless steel plug capped the tube and was enclosed by the outer casing (Figure 3-9A). The length of the plug that was enclosed by outer casing could be adjusted by a screw twist mechanism that allowed the height of outer casing along the length of the probe to be adjusted (Figure 3-9B). Hence the gut sample mounted over the probe tip could be stretched by the screw mechanism thus allowing the space between adjacent villi to be increased. The upper half of the steel tube of the probe was angled slightly to prevent the kinking of the pipe that connected to the peristaltic pump (Cole-Parmer, Illinois, US) that applied the vacuum.

The way in which the gut wall sample was obtained from the brushtail possum has been detailed in the peer-reviewed paper presented in section 3.2. Following that, the gut sample was mounted everted (i.e. the mucosal surface facing away from the probe) onto the surface of the outer casing by the following methods: the probe was first secured to a retort stand with the lower tip of the probe (i.e. the sintered plug enclosed by an outer

casing) facing upwards. The mounted gut sample was upheld over the probe using four hemostats while a suture was applied to secure the gut sample into a grove on the stainless steel outer casing (Figure 3-9C).

To enable the under-surfaces of the gut sample to be exposed to carboxygenated HBS solution, the following system was developed. A vacuum was generated on the upper end of the steel tube of the probe so that carboxygenated HBS solution can be drawn from the inner Perspex bath via the exposed sinter. This bathed the under surfaces (e.g. the serosa) of the gut sample whilst the villi were submerged in the circulated freshly carboxygenated HBS solution in the inner Perspex bath.

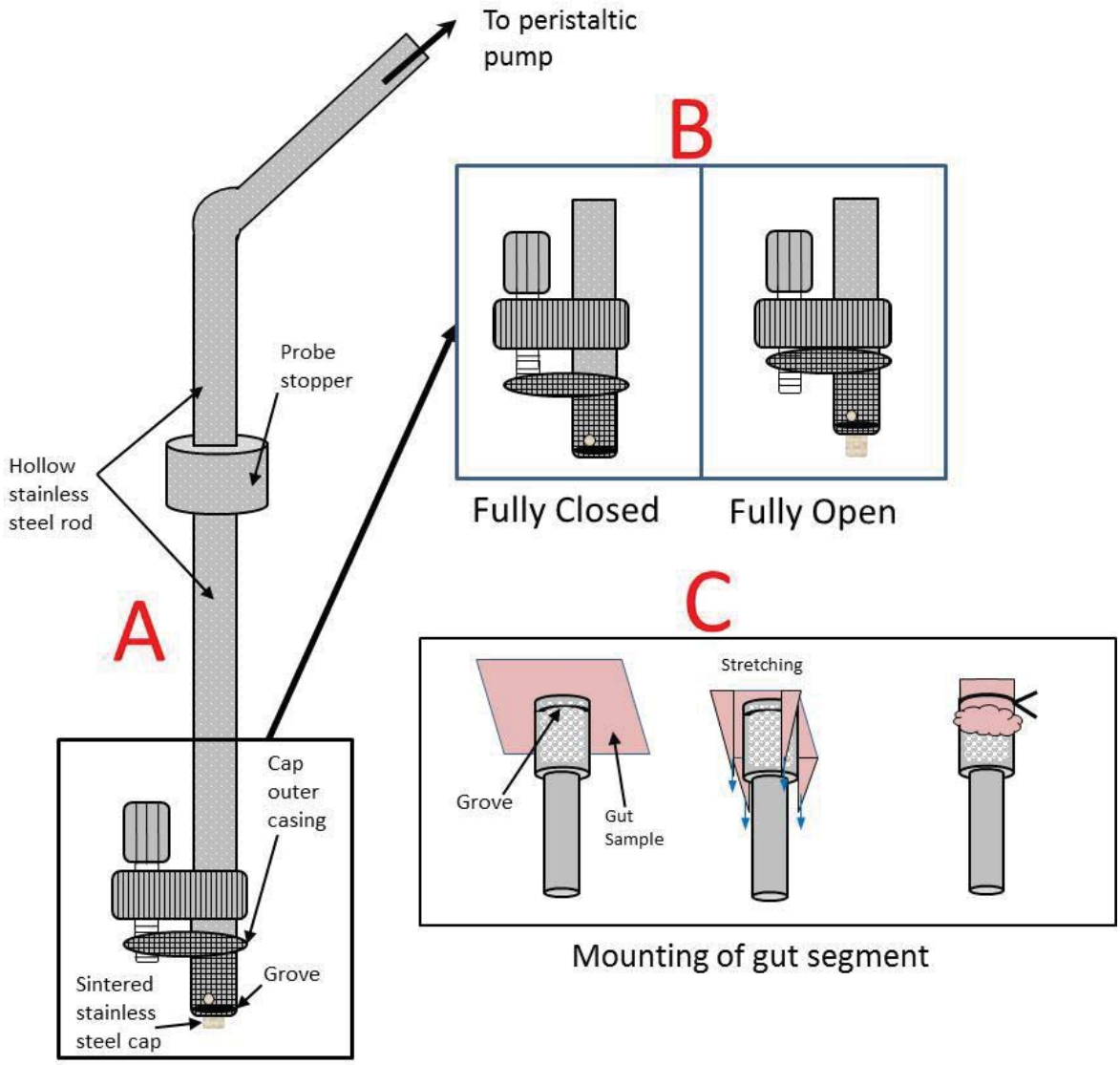

Figure 3-9: The tissue flow cell probe. A) The probe was composed of a hollow stainless steel tube, a sintered stainless steel plug that was enclosed by an outer casing. The probe stopper secured the probe in the probe holder at a pre-determined height in the baths and the upper half of the probe that was connected to the peristaltic pump was slightly bent to prevent the kinking of the pipe. B) The sintered plug outer casing was part of a stretching mechanism that was built into the end of the probe where the gut sample was to be mounted, which was operated by a screw-twist mechanism. C) The mounting of the gut sample onto the probe is also illustrated with the simplified design of the probe tip (i.e. without the outer casing). Photographs of the mounting of the gut sample on the probe* can be viewed in sub-section 6.2.1.1, Figure 6-8 (*while the probe portrayed in the photograph was different, the techniques used to mount the gut sample were same as the one utilized here).The grove allowed the gut sample to be secured to the apparatus by a suture.

The probe was secured to the VPS by a custom made probe holder (Figure 3-10). The probe was placed in the grove on the holder and held in place by a lever that was in turn secured to the probe holder by a screw. The lock located on the probe holder was used to secure the probe holder to the tissue bath.

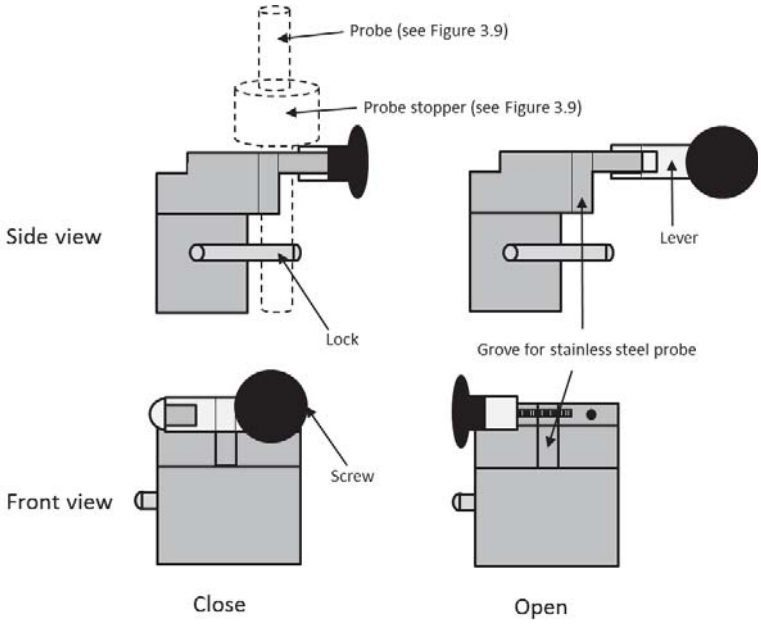

Figure 3-10: Custom made probe holder to secure the probe to the vertical positioning structure (VPS) of the tissue bath. The lock was used to secure the probe holder to the VPS. The complete tissue bath can be viewed in Figure 3-8.

3.3.1.3. Tissue bath base

The design and layout of the tissue bath base is presented below with dimensions (Figure 3-11);

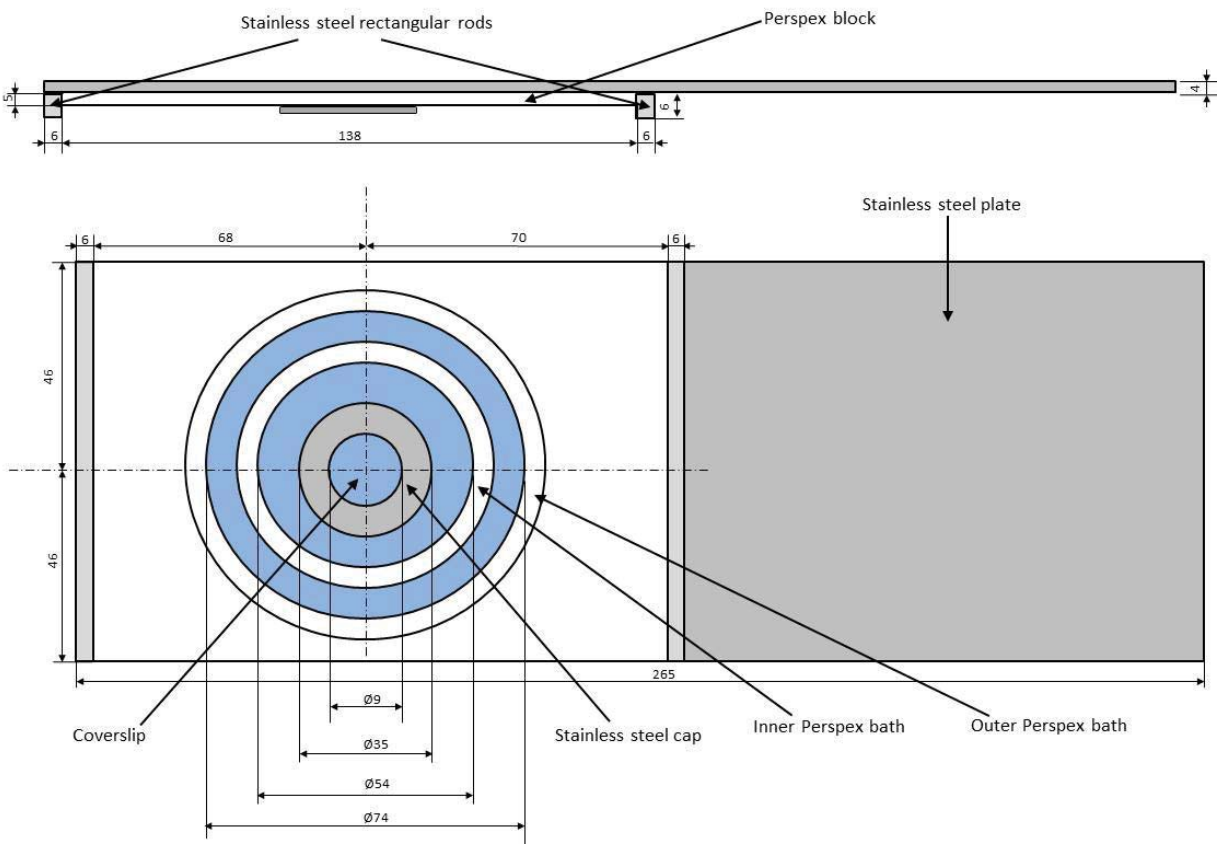

Figure 3-11: The base of the tissue. The upper picture is a side view while the lower picture is view of the underside of the base. The complete tissue bath can be viewed in Figure 3-8. All dimensions provided are in units of millimetres (mm). The regions marked in light blue are regions that would be filled with Earle-Hepes solution (HBS) during an experiment.

The foundation of the tissue bath base was a stainless steel plate (265 x 92 x 4mm). On one end of the plate (the end that would have the two Perspex baths attached), a Perspex (138 x 92 x 5mm) block was secured to the underside of the stainless steel plate (265 x 92 x 4mm) (Figure 3-11). An aperture the size of the outer diameter (78 mm) of the larger Perspex bath (see sub-section 3.3.1.4) was machined into the plate and together with the Perspex block attached to the underside of the plate, a recess was formed to facilitate the formation of the Perspex baths. Such a configuration enabled the viewing of the contents of Perspex baths from the underside of the base and the mounting of the tissue bath on to the manual substage of the inverted microscope with the Perspex block fitting into the recess in the substage.

A reamed aperture of 35 mm in diameter on the underside of the Perspex block was fitted with a stainless steel cap (Figure 3-11). The surface of the cap that was within the Perspex baths was sloped, leading to an aperture (9 mm in diameter) that was directly below the probe (Figure 3-11), which enabled the imaging of the villi by the inverted microscope. This sloped surface of the stainless steel cap facilitated the flow of carboxygenated HBS over all the exposed mucosal surface of the gut sample especially when the probe (with the mounted gut sample) was lowered to a distance within 1 mm from the aperture of the cap. On the under-surface of the cap was a recess that allowed for the engagement of a microscope coverslip of 0.16 mm in thickness. The use of the coverslip minimised the distance between the objective and the tip of the villi (approx. 600 μm).

A rectangular stainless steel rod (Figure 3-11) (92 x 6 x 6mm) was attached to the underside of the base at both ends of the Perspex block. The two rectangular rods acted as a stand for the tissue bath when the tissue bath was not attached to the inverted microscope substage. The rods could be easily detached from the base of the tissue bath when the tissue bath was to be positioned in the recess of the inverted microscope substage.

3.3.1.4. Perspex baths

The two baths were formed by securing two Perspex tubes of different sizes (Figure 3-12) to the Perspex block (using a solvent-based glue) that was attached to the underside of the stainless steel plate (that was the foundation of the tissue bath base). The smaller Perspex bath was concentrically positioned within the other larger Perspex bath. The Perspex bath that was innermost of the two baths was filled with freshly carboxygenated HBS solution via a inlet flow spout (Figure 3-12). Excess HBS solution

flowed over the rim of the inner bath (shaped as a weir) to the outer Perspex bath from which it was recirculated.

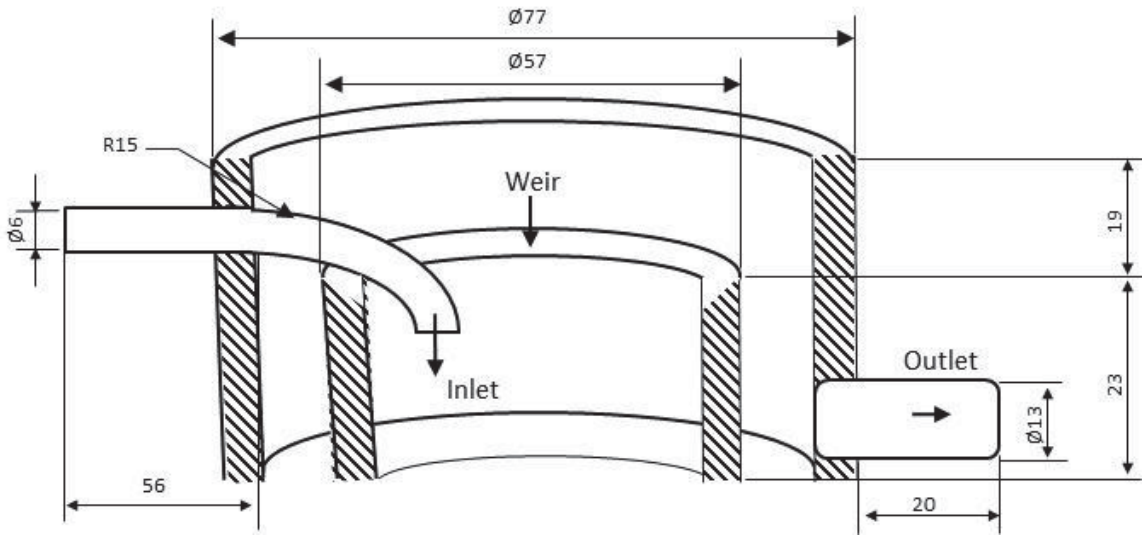

Figure 3-12: A sectional view of the Perspex baths through the baths centre showing the locations and diameters of the inlet and outlet flow spouts for carboxygenated and heated Earler-Hepes solution (HBS). The dimensions of both baths and the attachment baths components are also presented in this drawing. The rim of the smaller and inner bath was shaped as a weir to regulate the overflow of excess HBS.

The flow of freshly carboxygenated HBS solution was halted 20 seconds before image sequences were recorded as the influx caused the fluid around the villous tip to vortex and the microbeads to oscillate.

3.3.2. Layout of experimental apparatus

The perfusion pump, heating apparatus and the software processing computer were placed on separate tables from the air-damped table on which the inverted microscope was mounted.

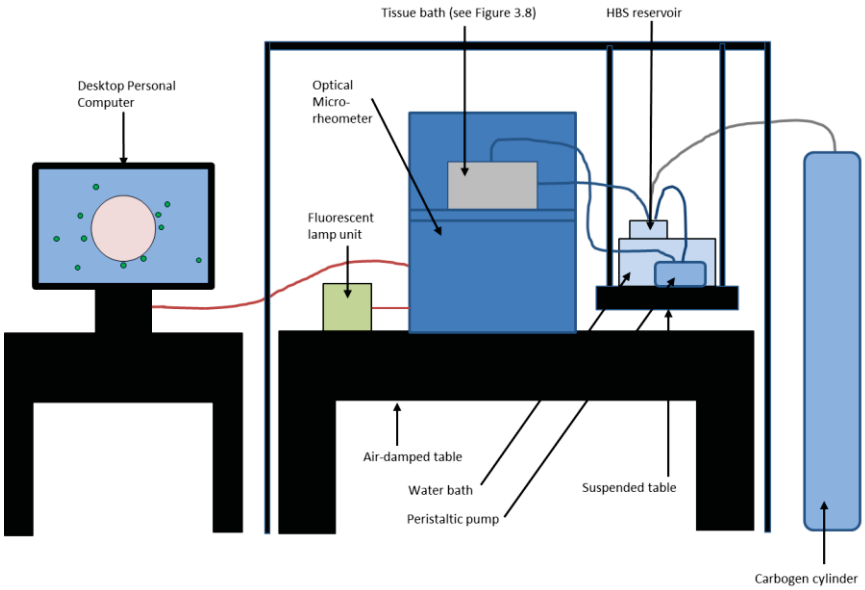

Figure 3-13: Basic setup of experimental apparatus on the optical microrheometer during recording of the Brownian motion of microbeads around villi on a live ileal segment. While the tissue bath has been represented as a rectangular block in this picture, the actual build of the bath may be viewed in Figure 3-8.

Hence, spent HBS from the excess HBS overflow bath (i.e. the larger outer bath) was recirculated to a HBS reservoir immersed in a heating bath, which was mounted on a suspended table that was separate from the inverted microscope. The pressure differential between the tissue bath and the HBS reservoir was generated by positioning the reservoir at a lower height than the tissue bath.

3.3.2.1. Optical Micro-rheometer

The optical microrheometer was based on a Nikon (Nikon Eclipse TE2000-U; Nikon Instruments, Melville, NY, USA) inverted microscope that was deployed on an air damped table (Photon Control, BC, Canada). The microrheometer was connected to an Intel Xeon 5140 Dual-Core (2.33 GHz per core, 2GB RAM) personal computer. LABRYX version 1.3.1 software (Arryx, University of Chicago, Illinois, USA) was used to visualize and capture images of microbeads located adjacent to villi on a living gut sample by a Foculus FO124SC CCD camera (Aegis Electronic Group, Arizona,

USA). Image sequences of the Brownian motion of microbeads were also recorded using this setup.

3.3.3. Additional details on micro-rheological technique

The process of tracking and recording the Brownian motion of microbeads in the perivillous fluid environment as well as the derivation of the mean squared displacement (MSD) value has been outlined in the main text of the journal article. The MSD value is a measure of the extent of spatial coverage by random (i.e. Brownian) motion of an ensemble of microbeads, describing the diffusivity of a microbead in a given fluid environment (Waigh 2005). When the MSD is linear with respect to time, the viscosity (η) can be calculated from the movement of spherical microbeads by the rearranged form of the Stokes-Einstein relationship (Waigh 2005) presented as equation 3.3:

$$\eta = \frac{kT}{6\pi aD} \tag{3.3}$$

where, T is the temperature (Kelvins), k is Boltzmann constant (1.38×10^{-23} m^2 kg s^{-2} K^{-1}), a is the hydrodynamic radius of the micro-bead(s) and D is the diffusion coefficient (a ratio of thermal energy to the frictional coefficient) that is obtained from the MSD. However, in the case of a more viscoelastic fluid environment, the Generalized Stokes-Einstein (GSE) equation must be used for the calculation. This accounts for the viscoelasticity of a complex fluid as a frequency dependent viscosity, resulting in (MacKintosh and Schmidt 1999):

$$\tilde{G}(s) = \frac{k_B T}{\pi a s \langle \tilde{r}^2(s) \rangle} \tag{3.4}$$

In the GSE (equation 3.4), $\langle \tilde{r}^2(s) \rangle$ is the Laplace transform of the MSD and $\tilde{G}(s)$ is the viscoelastic spectrum as a function of s, the Laplace frequency. Hence, MSD

measurements can then be transformed using the GSE into the rheological measurements of storage and loss moduli. This was calculated using a numerical method known for its ability to account for noisy data (Mason 2000). Firstly, the MSD data was fitted to a local power law and the power law exponent (α) may be calculated using equation 3.5:

$$\alpha(\tau) = \frac{d\ ln\langle \Delta r^2(\tau)\rangle}{d\ ln(\tau)} \tag{3.5}$$

where α describes the logarithmic slope of the MSD at t = 1/τ. This then allows the storage (i.e. elastic, G') and loss moduli (i.e. viscous, G'') with respect to frequency (ω) to be calculated:

$$G'(\omega) = |G^*(\omega)|cos\big(\pi\alpha(\omega)\big) \tag{3.6}$$

$$G''(\omega) = |G^*(\omega)|sin\big(\pi\alpha(\omega)\big) \tag{3.7}$$

where the frequency dependent complex shear modulus (G*(ω)) is:

$$|G^*(\omega)| \approx \frac{kT}{\pi a\langle \Delta r^2(1/\omega)\rangle\ \Gamma\ [1+\alpha(\omega)]} \tag{3.8}$$

where Γ is the gamma function that was approximated by; $\Gamma(1+\alpha) \approx 0.457(1+\alpha)^2 - 1.36(1+\alpha) + 1.9$ (Mason 2000).

3.3.3.1. Faxén's correction (boundary proximity considerations)

Errors in the determination of the calculated parameters that can result from local fluid drag in the proximity of local solid structures were also considered. These errors may be offset by the application of Faxén's correction (Leach et al. 2009). The estimated error in viscosity values derived from microbeads situated at a distance of 10 times their radius from a planar surface, would be approximately 10% (Leach et al. 2009). The

error would steadily increase with increasing proximity to the surface. However, the closest approach of microbeads to the mucosa was observed to be 10 μm, which is over 10 times the radius of the largest microbead used (the largest AC microbead had a diameter of 900 nm). Hence the correction was not applied as the calculated magnitude of such interactions was insufficient to greatly affect the experimental results. Further, the Brownian motion of all beads did not vary with orientation; the fluid environments were broadly isotropic. That is, microbead trajectories perpendicular or parallel to surfaces did not exhibit differing behavior.

3.3.4. Alternative micro-rheological techniques considered

In earlier pilot studies, a x60 1.2 NA (CFI Plan Apo VC 60x) objective was used to investigate the properties of mucus using a single particle tracking technique (Mason et al. 1997) with laser tweezers. However, due to insufficient lighting at regions below the villous tips to illumine the region of interest at such high levels of magnification, as well as the heterogeneity of the fluid environment adjacent to villi, it was decided that single particle tracking using laser tweezers would not be a suitable technique. Hence, multiple particle tracking was used to investigate the fluid environment around villi with the use of a lower magnification x20 0.75 NA (CFI Plan Apo VC 20x) objective (as detailed in Lim et al. (2013)). This magnification was the lowest that could still accurately track the Brownian motion of microbeads while allowing the surfaces of villi to be viewed.

3.3.5. Assessment of tissue viability

The viability of the gut segment used in the experiments was validated by histology. Hence the gut wall samples were histologically processed following their removal from the tissue bath probe by a Hematoxin and Eocin (H&E) staining. The gut wall sample

was stained and searched for signs of cellular necrosis and goblet cell degranulation. Hence as highlighted in Lim et al. (2013), no signs of cellular necrosis were observed and the goblet cells were observed to be intact. This suggests that the gut sample remained viable when image sequences of the Brownian motion of microbeads around villi were recorded.

In addition, another evidence for the viability of the gut sample during experimental work was the observation that the gut sample continued to exhibit contractile activity in pilot studies. In the main experimental runs, the contractile activity was halted through the use of the calcium blocker Isoptin (Abbot Laboratories, NSW, Australia) so as to not introduce artificial fluid oscillations to the fluid surrounding the microbeads.

3.3.6. Validation of the MPT technique

The multiple particle tracking (MPT) technique (a micro-rheological technique) detailed in this chapter may be validated by determining the properties of a 'simple material' using the techniques as outlined in Lim et al. (2013) and comparing the results obtained with that determined by a different technique. Given that MPT has only begun to be used to measure the micro-rheological properties of soft matter in the last 10 years (Waigh 2005), such technique may be compared with a more established (i.e. 'older') technique such as diffusing wave spectroscopy (DWS) (Pine et al. 1988). The mean squared displacement (MSD; the value used to calculate the viscosity and moduli of samples) of a 4wt% solution of 900kDa polyethylene oxide (PEO) was calculated using both techniques by Mansel et al. (2013).

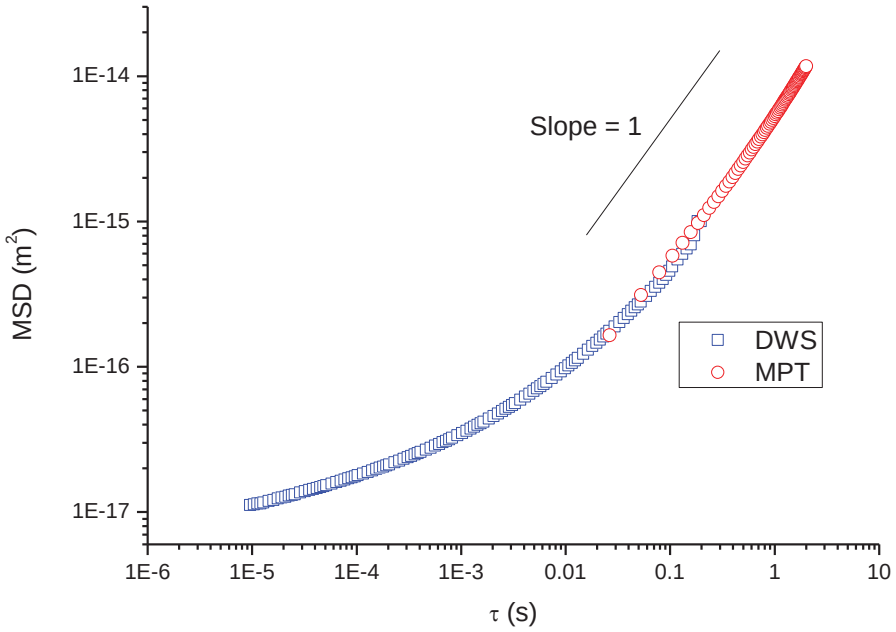

Figure 3-14: The mean squared displacement (MSD) plot for 4 wt% solution polyethylene oxide (PEO) showing an agreement between data obtained using multiple particle tracking (MPT) and diffusive wave spectroscopy (DWS). The results of both techniques were compared only at frequencies that were common between the two techniques.

It was observed that there was good agreement between the MSD values derived by both techniques (Figure 3-14). The comparison was limited only to time lags that were common between the two techniques of between 0.02 to 0.2 seconds. In addition, the results determined using both techniques have also been reported to be in good agreement with the results obtained by bulk rheology (i.e. macro-rheology) (Mansel et al. 2013).

3.4. Ancillary work: A comparison of the microrheological environment around distal ileal villi and proximal colonic mucosa of the possum (*Trichosurus vulpecula*) using two types of microbeads of differing surface chemistry.

The following are additional methods, results and discussions that were not published with the main text of the journal article (Lim et al. 2013).

3.4.1. Introduction

The NP (naked polystyrene) microbeads, used in the work by Lim et al. (2013) were thought to adhere to mucus. This reasoning was based on the reports that NP microbeads were completely immobilized by cervico-vaginal (CV) mucus (Olmsted et al. 2001; Cone 2009). Further, NP microbeads that were 59 nm (i.e. almost an order magnitude smaller than the average CV mucin chain pore size of 340 ± 70 nm (Lai et al. 2010)) did not penetrate CV mucus. These properties were attributed to the formation of polyvalent low-affinity bonds between the hydrophobic surfaces of NP microbeads and the hydrophobic naked globular protein domains (see below) of mucin (Cone 2009).

This section describes the work conducted with amine-coated (AC) polystyrene microbeads using the same multiple particle tracking techniques utilized by Lim et al. (2013). The objective of the work is to determine the patterns of local variation in the disposition and rheological properties of the brushtail possum (*Trichosurus vulpecula*) at multiple sites in close proximity to living small and large intestine taking care to avoid the physical disruption of the mucus layer (Suh et al. 2005). While the movements of AC microbeads are known to be restricted in airway (Dawson et al. 2003) and gastrointestinal mucus (Crater and Carrier 2010) by electrostatic interactions

with the hydrophilic domains of mucin monomers (of mucus), they were not completely immobilized (Crater and Carrier 2010) as were NP microbeads (Olmsted et al. 2001). The results of the work were compared with those using NP microbeads, which have been presented in section 3.2 (Lim et al. 2013).

3.4.1.1. Description of mucin structure

Mucin oligomers (i.e. polymers), such as those found in the small intestine, are glycoproteins that generally consists of a protein core densely coated by glycans (i.e. carbohydrate side-chains). This general description applies to both mucin that are secreted into the gut lumen by goblet cells and those that are secreted but remain adherent to the apical membrane of absorptive cells (i.e. enterocytes) (Perez-Vilar 2009).

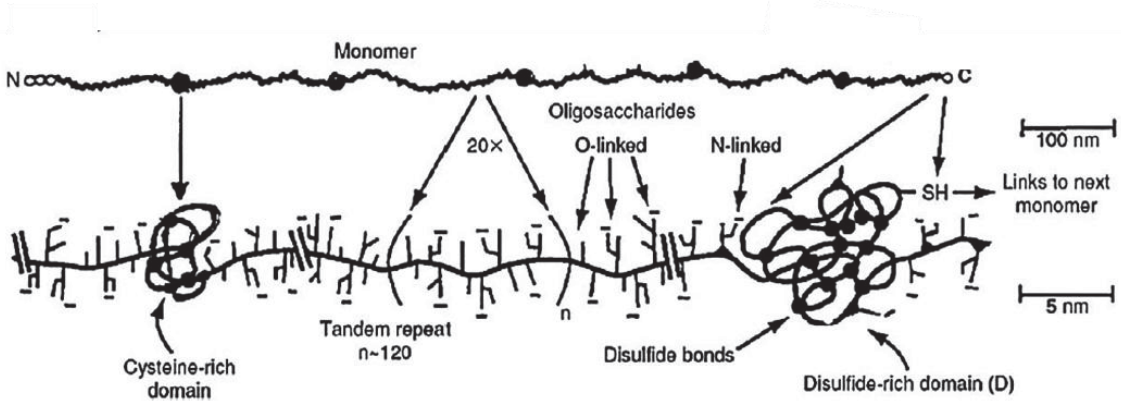

Figure 3-15: Main features of the mucin monomer glycoprotein that may be categorized into three main domains as highlighted in the text (adapted from Cone (1999)).

The protein core of mucin monomers (e.g. Muc2, the predominant type of mucin found in the small intestine) are composed of three main domains (Perez-Vilar 2009) (Figure 3-15). Firstly, there is a central domain of glycosylated (i.e. attached with glycans) tandem repeats of proline-theorine-serine (PTS) amino acids. The heavily glycosylated PTS domains of mucin are hydrophilic given the polar types of amino acid that form

this domain and the negatively charged tips of the glycans. Secondly, are the terminals on each end of the monomer where one is an amine (NH_2) group while the other a carboxyl (COOH) group. Finally, the third domain are the hydrophobic 'naked' sparsely glycosylated protein domains that are cysteine-rich, typically folded into a globular form and interspersed between PTS tandem repeats. The latter domain is typically found near the terminals on Muc2 mucin (Bansil and Turner 2006).

3.4.1.2. Mucus properties

It is postulated that mucus islands (formed through the hydration and subsequent expansion of Ca^{2+} sparse mucin secreted by goblet cells) are able to bind to particles by enveloping the particle with multiple low affinity bonds whether it be electrostatic interactions to hydrophilic domains or by hydrophobic interactions with the hydrophobic domains of mucin monomers that form the islands (Cone 2009). The enveloping of particles by mucin monomers is possible given the flexible nature of mucin resulting in particles being completely immobilized by 'dense cables' of mucin monomers as observed by Olmsted et al. (2001) using fluorescent labeled microbeads in cervico-vaginal (CV) mucus and Florey (1962) with particles of India ink in small intestinal mucus.

3.4.2. Methods

The same materials and methods that were used with NP microbeads, detailed in Lim et al. (2013), were used with the amine-coated (AC) microbeads. The AC microbeads were applied to a further six samples of distal ilea from 6 brushtail possums and three samples of proximal colon from 3 brushtail possums.

3.4.2.1. Choice of amine-coated (AC) microbeads

The amine-coated (AC) polystyrene microbeads (Spherotech, Illinois, USA) were labeled with nile red- fluorescence (excitation wavelength 515nm, emission 560 nm) and had a mean diameter of 0.75μm. The size was chosen, as was the size of the NP microbeads outlined in Lim et al. (2013), to exceed the mean reported distance between component strands of mucin (i.e. mucin mesh pores) (Lai et al. 2010) of around 340 nm. This is to prevent the microbeads sampling the voids between adjacent strands of the mucin matrix (Suh et al. 2005).

3.4.2.2. Sampling and statistics

The viscosities of locations that exhibited Newtonian characteristics and the G' of bodies that exhibited viscoelasticity were determined separately for sub-ensembles of microbeads, both at distances within 20 μm and at distances greater than 20 μm from the intestinal epithelium (e.g. villous surface; in the ileum). This distance classification was chosen on the grounds that the adherent mucus layer is reported to extend 29 ± 8 μm from the surface of the ileum (Atuma et al. 2001). Results were obtained from microbeads situated around villi that were orientated with their long axes at right angles to the focal plane of the inverted microscope and from those with their long axis parallel to this plane. For the microbeads used in the colonic mucosal environment, a similar distance classification was used for the purposes of comparison.

The micro-rheological results obtained with AC microbeads required transformation by the Johnson algorithm in the MINITAB package (Minitab Inc., State College, PA, USA) to render them suitable for parametric statistical analysis. The transformed data was analyzed by nested ANOVA for the effects of distance from the mucosa, gut segment, animal and in a separate analysis also for the type of microbead surface

chemistry along with the data for NP microbeads used in Lim et al. (2013), in the SPSS package (SPSS Inc., Illinois, USA). In the following text, the raw data from both studies reported as box plots and the statistical inferences drawn from the ratio of mean squares from ANOVA of the overall effect to that of the effect nested within animal are presented.

3.4.3. Results

All results presented in the following sub-sections were obtained using AC microbeads unless stated otherwise. This sub-section presents the micro-rheological results of the AC microbeads, which were not published in Lim et al. (2013). Overall, as was observed when using NP microbeads, the behaviour of AC microbeads showed that the environment around the ileal villi and the proximal colonic mucosa were largely heterogeneous consisting of a continuous phase of Newtonian liquid that contained viscoelastic material (see 'Microrheo Movie')[4], which have been termed 'viscoelastic bodies' (Lim et al. 2013).

3.4.3.1. Ileal mucosa

The continuous phase of the environment around the terminal ileal villi was a Newtonian fluid of a low viscosity similar to that of water. The overall mean viscosity of the continuous phase obtained using transformed data from all preparations (Table 3-2 and Figure 3-16A) was not significantly different on nested ANOVA at distances 20 μm or closer to the mucosa to that at distances greater than 20 μm from the mucosa. Similarly, the mean viscosity of the continuous phase at distances that were greater than 20 μm above the apical epithelium of the villus tip (median value 1.13 mPa.s; interquartile range (IQR) 0.8 – 1.4, N = 10 replicates) did not differ significantly from

[4] See http://youtu.be/V4M8SoAjxVQ, if the video does not play after a few minutes loading on a standard broadband connection, please try reloading the page.

that at distances greater than 20 µm from the sides of the villus (median 1.57 mPa.s; IQR 1.28 – 1.95, N = 33 replicates).

The mean elastic moduli (G') of viscoelastic bodies found in the continuous phase, did not differ significantly between those at distances 20 µm or closer to the mucosa to that at distances further than 20 µm from the mucosa (Table 3-2 and Figure 3-16B). The diameters of viscoelastic bodies further than 20 µm from the ileal epithelium did not differ significantly from those of distances 20 µm or closer to the villus epithelium (Table 3-3).

The numbers of viscoelastic bodies around villi of the ileal epithelium were generally low. Of 15 replicates from ileal sites that contained entire bodies, the visual fields in the majority of image sequences contained one body per field of view whilst the visual field in two sequences contained 3 bodies. The percentage surface area per (0.064 mm^2) field of view occupied by viscoelastic bodies at distance greater than 20 µm from the ileal mucosa did not differ significantly from those viscoelastic bodies situated 20 µm or closer to the surface of the ileal mucosa (Table 3-3).

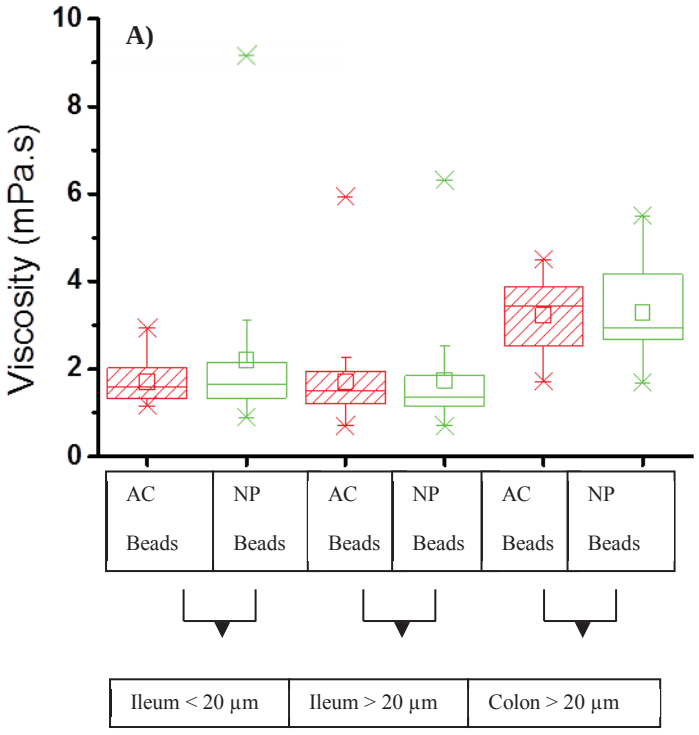

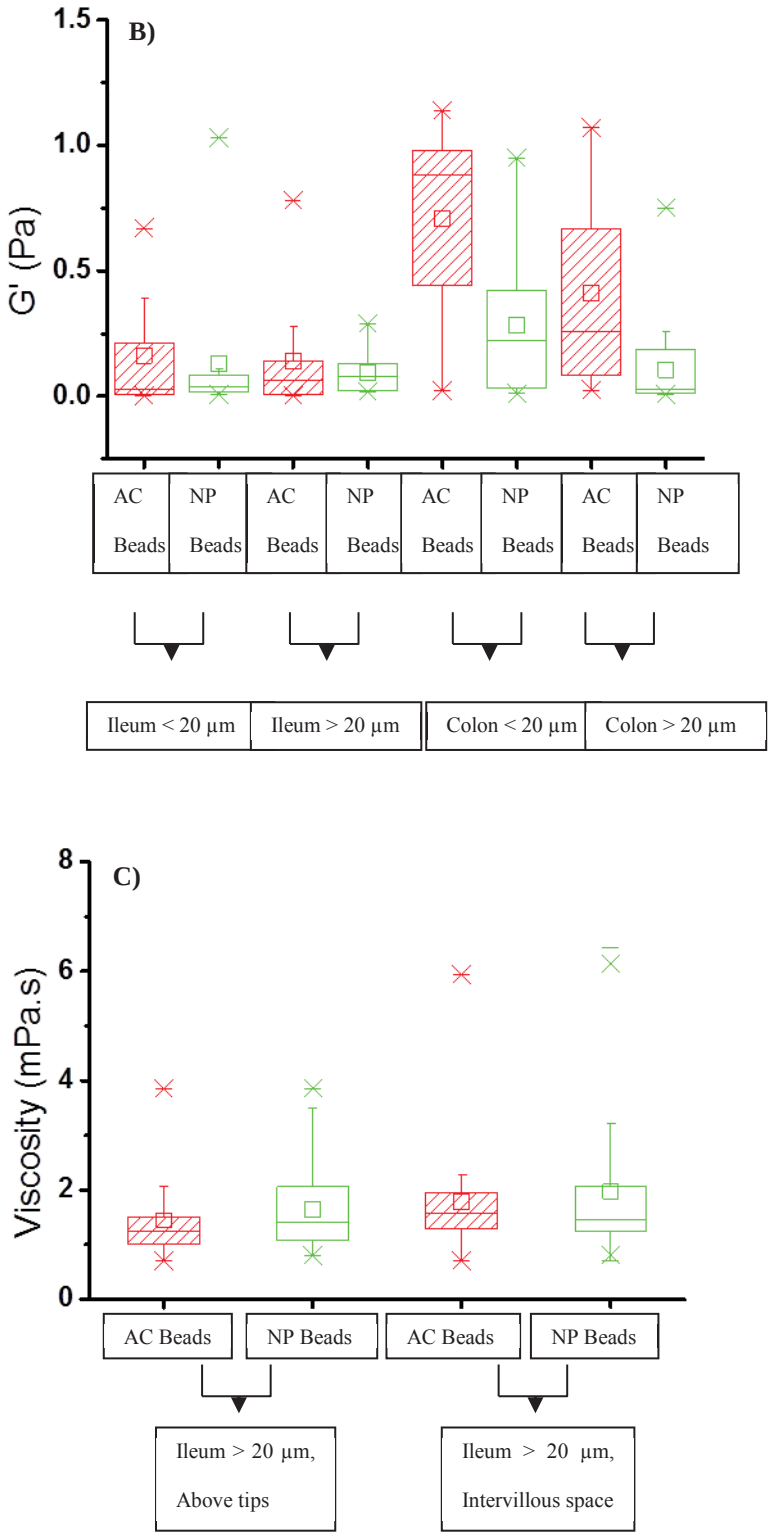

Figure 3-16: Variation in the rheological properties of the A) continuous phase and B) viscoelastic bodies near the ileal villus and colonic mucosa obtained using NP (naked polystyrene; green plots) and AC (amine coated; red plots) microbeads.While (C) is the comparison of the viscosity of the continuous phase > 20 µm from the tip and the sides of ileal villi. The results that were presented in Lim et al. (2013) were the results of the NP microbeads presented in

this section and were reproduced for ease of comparison for the reader. The following are the definitions of the various symbols on the boxplots: The maximum and minimum values of the dataset are indicated by the longer horizontal lines usually found on the extreme ends of the plot, the diagonal crosses (X) indicates the 1% and 99% percentile of the dataset, the shorter horizontal lines connected to the rectangle box by a vertical line is the 5% and 95% percentile of the dataset, the longest horizontal line forming the upper and lower boundaries of the box indicates the 25% and 75% percentile (i.e. the lower and upper quartile respectively) of the dataset, the longest horizontal line within the box is the median value of the dataset whilst the square (□) indicates the mean of the dataset.

			N (number of replicates)	Median	IQR
Continuous	Ileum <20	AC	28	1.61	1.33 - 2.06
Newtonian phase		NP	50	1.68	1.34 - 2.18
viscosity (mPa.s)	Ileum >20	AC	35	1.53	1.25-1.96
		NP	66	1.35	1.14-1.85
	Colon < 20	AC	1	2.73[a]	
		NP	2	3.18-5.22[a]	
	Colon > 20	AC	11	3.44	2.54-3.87
		NP	16	2.94	2.67-4.16
Viscoelastic bodies	Ileum <20	AC	20	0.025	0.007-0.21
elastic moduli (Pa)		NP	19	0.036	0.017-0.085
	Ileum >20	AC	21	0.064	0.007-0.14
		NP	10	0.077	0.023-0.13
	Colon < 20	AC	9	0.88	0.44-0.98
		NP	11	0.22	0.032-0.42
	Colon > 20	AC	14	0.26	0.08-0.67
		NP	20	0.03	0.01-0.19

Table 3-2: Summary of the microrheological properties (viscosity and elastic moduli) of the continuous Newtonian fluid phase and viscoelastic bodies. [a]A range or a single value is given for this site as there were insufficient values for the calculation of median and interquartile range (IQR). It is included for comparison with other viscosity values.

3.4.3.2. Colonic tissue

The viscosities of the continuous (Newtonian fluid) phase at sites that were situated further than 20 μm did not differ significantly from those situated 20 μm or closer to the colonic epithelium (Table 3-2). No median and IQR value was available for the viscosity of the continuous phase at distances 20 μm or less from the epithelium of the

colon as the bulk of microbead ensembles (9 out of 10) were located in viscoelastic bodies and those in locations containing only Newtonian fluid were correspondingly low. However, the viscosity values of the continuous phase that were available were within the range of the values of the continuous phase at distances greater than 20 μm from the colonic epithelium (Table 3-2).

The G' values of viscoelastic bodies at distances greater than 20 μm from the colonic epithelium did not differ significantly from those at distances 20 μm or less from the colonic epithelium (Table 3-2). The diameters of viscoelastic bodies situated at distances greater than 20 μm from the colonic epithelium were significantly smaller (df = 1, 19, F = 9.53, P = 0.006) than those of the locations situated 20 μm or less from the colonic epithelium (Table 3-3).

The numbers of viscoelastic bodies were generally low around the colonic epithelium. Of a total of 20 replicates from sites that contained entire bodies, the bulk of fields contained a single body, one contained 3 bodies and one contained 5 bodies. The percentage surface area per (0.064 mm^2) field of view occupied by viscoelastic bodies at distances greater than 20 μm from the colonic surface was significantly less (df = 1, 19, F = 10.1, P = 0.005) than that of those situated 20 μm or less from the colonic surface (Table 3-3).

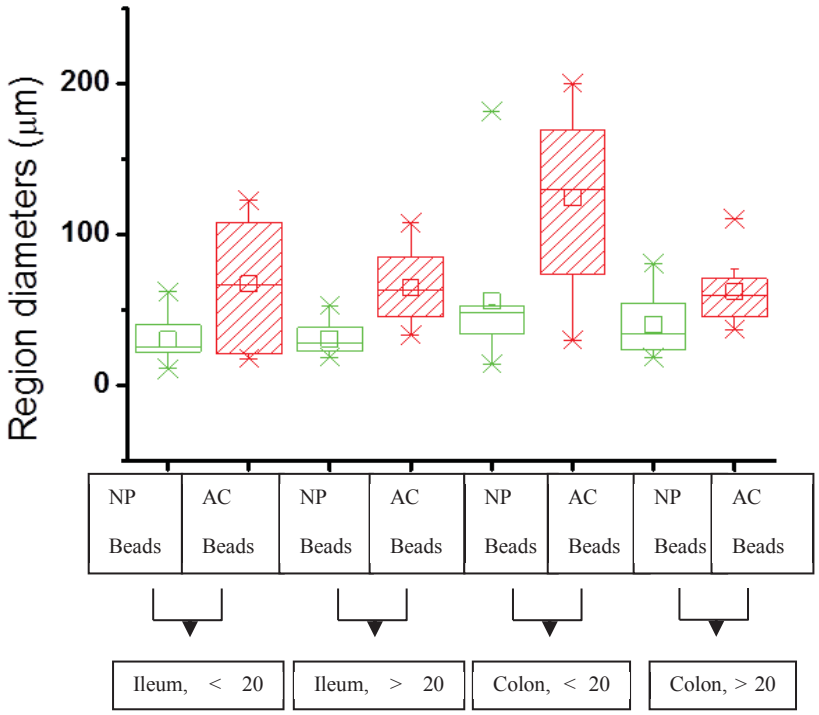

Figure 3-17: Variation in the diameter of viscoelastic bodies with intestinal segment, distance from the mucosa and type of microbead. The following are the definitions of the various symbols on the boxplots: The maximum and minimum values of the dataset are indicated by the longer horizontal lines usually found on the extreme ends of the plot, the diagonal crosses (X) indicates the 1% and 99% percentile of the dataset, the shorter horizontal lines connected to the rectangle box by a vertical line is the 5% and 95% percentile of the dataset, the longest horizontal line forming the upper and lower boundaries of the box indicates the 25% and 75% percentile (i.e. the lower and upper quartile respectively) of the dataset, the longest horizontal line within the box is the median value of the dataset whilst the square (□) indicates the mean of the dataset.

			N (number of replicates)	Mean	Standard Error
Viscoelastic bodies diameter (μm)	Ileum <20	AC	6	67.1	18.1
		NP	12	36.9	6.8
	Ileum >20	AC	9	63.6	11.8
		NP	14	31.3	3.6
	Colon < 20	AC	11	96.8	25.2
		NP	12	49.1	10.0
	Colon > 20	AC	9	69.4	9.4
		NP	8	40.9	8.9
% area occupied per 0.064mm^2 field of view	Ileum <20	AC	6	3.4	(0.6, 19.5)*
		NP	12	1.4	(0.5, 3.8)*
	Ileum >20	AC	9	5.6	(2.3, 14.0)*
		NP	14	0.9	(0.6, 1.4)*
	Colon < 20	AC	11	7.6	(1.6, 36.2)*
		NP	12	2.3	(0.6, 8.2)*
	Colon > 20	AC	9	5.5	(2.8, 10.5)*
		NP	8	1.7	(0.6, 4.6)*

Table 3-3: Summary of the viscoelastic body sizes (i.e. viscoelastic body diameters and the percentage area per (0.064 mm^2) field of view) occupied by viscoelastic bodies for both types of microbeads at both distances in both the ileum and the colon.*As the data had to be logarithmically transformed for it to be normally distributed, the 95% confidence interval was presented rather than the standard error.

3.4.3.3. Comparison of ileum and colon

The viscosities of the continuous Newtonian phase at distances greater than 20 μm from the colonic mucosa were significantly larger than those at distances greater than 20 μm from the ileal villous epithelium (df = 1, 38, F = 6.00, P = 0.05) (Figure 3-16A and Table 3-2). Note that the viscosities of the continuous phase at distances less than 20 μm from the ileum could not be compared with the viscosities of the continuous phase at a similar location in the colon due to insufficient data.

The values for G' of viscoelastic bodies that were situated 20 μm or closer to the colonic mucosa were not significantly different to the values at distances 20 μm or closer to the ileal villous mucosa (Figure 3-16B). Similarly, the values for G' of bodies

that were situated at distances greater than 20 μm from the colonic mucosa were not significantly different to those at distances greater than 20 μm from the ileal villous mucosa (Figure 3-16B).

The numbers of viscoelastic bodies identified in each visual field were generally low regardless of their distance from the mucosa or the location in the gut from which the image sequence was obtained (ileum or colon), the majority of sites contained only one body. However, it is noteworthy that while bodies that were situated above the ileal mucosa were always surrounded by the continuous Newtonian fluid phase, a significant number of bodies that were situated above the colonic mucosa filled the entire visual field and were also counted as a single body.

Taken overall, the diameters of the viscoelastic bodies in the colon were not significantly different than those in the ileum. Similarly, the lack of any significance in the term for distance within the segment indicated that there was no significant variation in size of the body with distance from the surface of the mucosa in this analysis (Figure 3-17).

3.4.3.4. Comparison of the results obtained with NP and AC microbeads

Continuous phase viscosity – There were no significant differences between the viscosity of the continuous phase obtained with the AC from those obtained with NP microbeads whether in the ileum and colon or at distances greater than 20 μm from the mucosa and distances 20 μm or closer to the mucosa (Table 3-2 and Figure 3-16A).

Elastic moduli (G') of viscoelastic bodies – There were no significant differences in the G' values obtained with the AC from those obtained with NP microbeads whether in the ileum and colon or distances greater than 20 μm from the mucosa and distances 20 μm or closer to the mucosa (Table 3-2 and Figure 3-16B).

Viscoelastic body sizes – There were no significant differences in the diameters of viscoelastic bodies obtained using AC from those obtained using NP microbeads whether in the ileum and colon or at distances greater than 20 μm from the mucosa and distances 20 μm or closer to the mucosa. Similar results were obtained for the percentage areas per (0.064 mm^2) field of view occupied by viscoelastic bodies (Figure 3-17) for AC and NP microbeads.

3.4.4. Discussion

Only the results obtained using amine-coated (AC) polystyrene microbeads that were not published together with Lim et al. (2013) and the comparisons with the results obtained with NP microbeads are discussed in this sub-section. The results obtained with AC microbeads showed that the material at locations immediately adjacent to the terminal ileal and proximal colonic mucosa is rheologically heterogeneous comprising circumscribed areas that exhibit viscoelastic behaviour termed 'viscoelastic bodies' suspended in a low viscosity Newtonian fluid.

The finding that the viscoelastic bodies at distances 20 μm or less from the colonic mucosa had a larger surface area as compared to distances greater than 20 μm from the colonic mucosa using AC microbeads suggests that there is greater opportunity for reptative interdiffusion closer to the mucosa. Conversely, the finding that there are no such differences in the surface area sizes of viscoelastic bodies in the ileum may be indication of the differing mechanisms of mixing and mass transfer that exists in the ileum and the colon. In the ileum, fluid may be ejected from the intervillous space by the actions of postprandial gut motility patterns (Lentle and Janssen 2011) or by the concerted motility of villi (Womack et al. 1987). Hence given the existence of such mechanisms in the ileum, it is unlikely that annealing of mucins by reptative

interdiffusion could take place. Reptative interdiffusion of mucus islands is a relatively slow process and is not detectable at times below 40 seconds in respiratory mucins (Puchelle et al. 1986) whereas slow wave induced, pendular activity in the longitudinal muscle of the small intestine is around 0.5 cps (Lentle et al. 2012; de Loubens et al. 2013). This would result in viscoelastic bodies (within the Newtonian fluid phase) located in the intervillous spaces to be forcibly ejected approximately every 2 seconds, making them less likely to anneal.

Concurrently, the differences in viscoelastic body sizes at different distances from the colonic mucosa may be attributed to the degree to which the glycans (that could interact with AC microbeads) of mucin (assuming that the viscoelastic bodies are mucus islands) has been degraded by glycosidases or been used as a food source by commensal bacteria (Holmén Larsson et al. 2013). Viscoelastic bodies that are situated further away from the colonic mucosa would be more likely to encounter enzymes and bacteria (Matsuo et al. 1997). The degradation of the glycans of the mucins may result in a reduced capability to anneal by reptative interdiffusion of their 'bottle-brush' glycan side-chains. In addition, it is also possible that the mucin of mucus located at greater distances from the colonic mucosa have been bound by larger quantities of water with fewer negatively charged glycans available to interact with AC microbeads. These suggestions assume that the two types of mucus observed are of the same type and origin – a hypothesis derived from recent experimental work (Johansson et al. 2008). While it is also possible that the two types of mucus in the colon are of a different type and origin, evidence for such a hypothesis has so far not been found.

These findings run contrary to those of Atuma et al. (2001) who postulated that there are two types of mucus throughout the GIT from the stomach to the colon – a viscid and thick mucus located closer to the mucosa that was not able to be removed by suction

with a pipette and a watery mucus situated at a greater distance away from the mucosa that could be easily removed. Moreover, these workers also suggest that mucus in the terminal ileum and proximal colon is a continuous layer, a view that is in opposition to the conclusions that could be drawn from the work outlined in this chapter. However, it is unlikely that such layers of mucus would be found in the small intestine during digestion *in vivo* under normal physiological conditions. While these workers used live animals under anaesthesia, their method of mucus extraction by suction using a pipette may have caused sufficient trauma of the goblet cells to trigger them to undergo compound exocytosis (i.e. degranulate prematurely). Given that the mucin secreted under such conditions may be lacking of post-translational modification to a degree due to the sudden release of goblet cell contents or that the post-translational modification of goblet cell mucin were altered by a change in gene expression (McGuckin et al. 2011), such mucins may have a higher tendency to anneal by reptative interdiffusion.

The absence of such observations made when using NP microbeads may be attributed to the differences in the surface chemistry between AC and NP microbeads – AC microbeads have a polar surface coating (Dawson et al. 2003) while NP microbeads are always apolar (Olmsted et al. 2001). It has been reported that Muc2 mucin is the main mucus island forming mucin in the colon at least in the rat (Johansson et al. 2008) and that the polar hydrophilic domains (i.e. the charged glycans attached to the PTS domain of the mucin protein core) compose more than half of Muc2 mucin (Gum et al. 1994). Hence it is likely that AC microbeads would be more sensitive to the differences in the disposition of mucus in the colon as compared to NP microbeads. It is noteworthy that the size of AC microbeads was one and a half times larger than the NP microbeads and alternatively could also be the cause of the discrepancies in the results between AC and NP microbeads.

Besides that, it is noted that only 12 possums were used for work in their terminal ileum while only 6 possums were used for work in their proximal colon. Hence, given the low numbers of animals used, it is possible that the finding that the results of the AC were not significantly different to that of the NP microbeads (other than those mentioned earlier) may be attributed to a shortfall of possums sampled and the difficulties in detecting and measuring parameters such as the viscoelastic body diameters with the current techniques available. Future work may seek to sample a greater number of animals so that any differences (or lack thereof) in the fluid environment of the ileum and proximal colon using microbeads with differing surface chemistry may be more thoroughly ascertained.

Overall, the results detailed in this section serve to further strengthen the case made in Lim et al (2013) despite the use of a microbead of a different surface chemistry. Both works together call into question previous works that have suggested that mucus in the small intestine is a contiguous ‘blanket’ of viscoelastic material. At the same time, the findings of this chapter deliver a model of mucus rheology and disposition that facilitates mixing and mass transfer in the terminal ileum of the brushtail possum using novel techniques.

3.5. Chapter conclusion

From the findings of this chapter, the microrheology of the fluid environment in the perivillous space of the terminal ileum and proximal colon were determined. The observed conditions were thought to be able to facilitate mixing and mass transfer of luminal contents in the perivillous region of the terminal ileum of the brushtail possum at least. Based on the various similarities between the viscoelastic material and mucus that have been presented in the previous sections of this chapter it is likely that the viscoelastic bodies detected were in fact mucus islands. However, given that the viscoelastic bodies have not been tested with immuno-staining methods to verify its composition of mucin, the viscoelastic material observed adjacent to the terminal ileal and proximal colonic mucosa will be addressed as 'viscoelastic bodies' for the rest of the thesis.

While the findings of this chapter have shown that there were differences in the disposition and microrheology of mucus with site (e.g. terminal ileum and colon) and with distance from the mucosa especially in the proximal colon, more work needs to be done to more accurately characterize the different types of mucus observed. The experimental setup outlined in this chapter does not permit environments of different scales to be investigated (e.g. locations within 10 μm of the villi and/or mucosal surface and the glycocalyx, which is reported to be less than a micron in thickness (Snoeck et al. 2005)). Again, with the current experimental setup, locations more than 300 μm below the villous tips could not be analysed. It is possible that the numbers of viscoelastic bodies could be greater near the villous crypts given that there may be greater numbers of mucin secreting goblet cells in the crypts (Ermund et al. 2013), assuming that these bodies are mucus islands.

Finally, the results obtained relate to a single section of small intestine in a single species. More work is needed to determine whether the viscoelastic bodies in other sites and species have similar properties. For example, it is likely that mucus in the duodenum, especially at its proximal sections, would be different in that it would be required to protect the intestinal mucosa from acidic material exiting the pylorus (Flemström and Kivilaakso 1983). Thus, mucus in this site may be formed by mucin oligomers of a more linear configuration that would facilitate annealing between individual adjacent mucus islands by reptative interdiffusion to generate a contiguous mucus layer (Perez-Vilar 2009). More work would also need to be conducted to determine the disposition and microrheology of mucus in the small intestine of other mammals as it is likely that animals that have a more abrasive diet may require mucus that has greater lubricating properties (Lentle and Janssen 2011).

Chapter Four -

LBM of mixing and mass transfer in the small intestine

4.1. Foreword

This chapter outlines the computational modelling of mass transfer in the perivillous space of a small mammal using a simplified boundary condition of pendular contractions of the gut wall in two-dimensions (2D). The chapter begins with an outline of the physical formulation (i.e. the modelling strategy and rationale of physical parameters used) of the model followed by the details of the numerical modelling technique – Lattice Boltzmann modelling (LBM). Subsequently, the experimental parameters (i.e. numerical and physiological parameters that will be used in the models) will be described. Finally, the results and discussions of the models run will be presented.

4.2. Modelling strategy

The computational model was developed with the purpose of evaluating whether mass transfer could be enhanced during non-propagating pendular contractions of gut wall in the perivillous region. Previously, by assuming that the gut lumen could be approximated as a cylinder, a computational model developed by Dr. Clement de Loubens and colleagues (2013) found that 'real-time' non-propagating pendular contractions (derived from actual video sequences of pendular activity from the rat duodenum) generates little *in situ* mixing of viscous fluids and augments mass transfer at the periphery of the gut (i.e. perivillous region). However the model did not incorporate the actions of villi. Hence the question remains whether villous structures located on the gut wall contribute further to mixing and mass transfer in the perivillous region.

However, as the models described in this chapter are a first approximation of the effect of villi on mass transfer at the gut periphery, 'real-time' data of *ex vivo* preparations of the rat duodenum were not used in order to reduce the computational load. With the help of Dr. de Loubens, his model of 'simplified pendular activity' (de Loubens et al. 2013) was further developed to incorporate villi to see if villi would further enhance mass transfer at the gut periphery. The model also incorporated the latest findings of the actual mechanical properties of the fluid environment in the perivillious space of the brushtail possum terminal ileum (Lim et al. 2013).

4.3. Physical formulation of the computational models developed

The small intestine was modeled as a half tube of radius R (mm) and length L (mm) (the length of a single spatial domain of non-propagating pendular contraction, see sub-section 4.4.3.1). The flow fields generated by non-propagating pendular contractions in the presence of intestinal villi were described by Navier-Stokes equations modeled by LBM. Formulation of the dimensionless Navier-Stokes equations of fluid flow in the model is outlined in a later section.

The physiological parameters used for the model were taken from a number of sources. The profile of simplified non-propagating pendular contractions was derived from spatio-temporal maps of the rat duodenum (de Loubens et al. 2013). As for the diameter of the small intestine, villous density and dimensions, these were determined from measurements on the ileal mucosa of freshly euthanized rats (see below). Conversely, the mucus disposition and micro-rheology were taken from work on the perivillous fluid environment of the brushtail possum ileum (Lim et al. 2013). This was necessary owing to the contemporary availability of data precluding the construct of models based on a single site (in the small intestine) and species.

4.3.1. Fluid environment of the model

In the initial model developed by Dr. de Loubens (2013), the viscosity of the fluid environment in the gut lumen was assumed to be viscous and Newtonian. This assumption was validated by micro-rheological work carried out as part of this thesis (see chapter three) showing that the fluid phase in the perivillous space of the terminal ileum of the brushtail possum was predominantly a Newtonian liquid of low viscosity. The behaviour and disposition of the viscoelastic bodies that were contained within it was not incorporated into the model.

4.3.2. Determination of villous architecture and density

All of the experimental procedures were approved by the Massey University Animal Ethics Committee (MUAEC approval no 11/36), and complied with the New Zealand Code of Practice for the 'Care and Use of Animals for Scientific Purposes'. Five male Sprague Dawley rats were each anaesthetized and dissected using the methods outlined in the previous chapter (chapter three).

4.3.2.1. Determination of villous density

A 5 cm segment of terminal ileum was excised from each rat and the segment's exact length and diameter was immediately measured. The ileal segment was then opened by a lengthwise cut along the abmesenteric border and placed on a glass slide with the mucosa uppermost. Tension was applied to the edges of the sample until the dimensions increased up to approximately twice the original dimensions. The exact dimensions of the stretched excised ileal wall were then determined to calculate a 'stretch factor' to correct calculations of villous density. Three drops of 1% Bromothymol-Blue (BTB) were applied onto the stretched ileal mucosa to delineate the outlines of intestinal villi. This solution is thought to be absorbed into the cells along the length of villi (Nakamura et al. 1978).

A dissection microscope (Olympus, Tokyo, Japan) was used to visualize the villi so as to determine the density, length and width of villi. The villi were measured using an eyepiece graticule over a number of 1 mm^2 areas on each ileal segment. The equation used to calculate the intervillous space for a given rat gut sample was developed in-house and derived in the following;

These derivations and the final equation used (equation 4.1) assume that villi are arrayed in a symmetric and consistent manner over a mm^2 area of gut sample and that the intervillous size is the same in all directions. Hence we can calculate N_{vil}, the number of villi per 1 mm length;

$$N_{vil} = \sqrt{D_{vil}}$$

where D_{vil} is the area density of villi (i.e. number of villi per mm^2 area of gut mucosa). Hence the total widths of N_{vil} villi located along a 1 mm length of mucosa w_{TOT}, is given by

$$w_{TOT} = \sum_{w_{vil}}^{N_{vil}} w_{vil}$$

where w_{vil} is the width of a single villous.

The values of Ivs_{TOT} , the total intervillous space in between all villi located on the 1 mm length of mucosa can be calculated by the following equation;

$$Ivs_{TOT} = 1\ mm\ length\ of\ gut\ mucosa - w_{TOT}$$

Hence Ivs_{vil} , the intervillous space in between any two villi is given by

$$Ivs_{vil} = \frac{Ivs_{TOT}}{N_{vil}}$$

and

$$Ivs_{vil} = \frac{1-(\sqrt{D_{vil}} \times w_{vil})}{\sqrt{D_{vil}}} \qquad (4.1)$$

Additionally, in the use of equation 4.1, it was also assumed that there was little change in the dimensions of the wall of each segment between the time of harvesting from the

animal to the time the principal dimensions was first determined. However, this assumption may be the source of the largest errors as any residual tone would induce immediate changes in dimensions of the gut wall sample.

4.3.3. Villous profile

The villous profile (Vil_p) in the Lattice Boltzmann modeling (LBM) environment were modeled as a 2D structure by a polynomial equation to the fourth power and calculated by the equation below. This was based on observations of the profile of ileal villi from the rat and reports on the profile of human ileal villi (Holmes et al. 1961).

$$Vil_p = h_{vil} - \frac{l}{{R_{vil}}^4}(X^4 + Y^4) \tag{4.2}$$

where h_{vil} is the length of a villous, R_{vil} is half its width while X and Y were the coordinates on the LBM mesh (Figure 4-2). Villi in the models described in this chapter were assumed to be static and rigid. While villi have previously been reported to exhibit contractile activity (e.g. waving 'left and right' as well as piston-like 'up-down' motions) (Womack et al. 1987), such movements were not incorporated into the model in the interest of reducing computation time.

4.4. Lattice Boltzmann numerical formulation of mathematical model

The computational fluid dynamics (CFD) technique that was chosen to model mixing and mass transfer in the intestinal lumen was based on a Lattice Boltzmann formulation (i.e. Lattice Boltzmann modeling – LBM). This technique was chosen on the basis of its superior capabilities in modelling flow with complex boundaries over a uniform Cartesian mesh as compared to other CFD techniques (Chen and Doolen 1998; Aidun and Clausen 2010). Unlike other CFD techniques that solved the discretization of macroscopic continuum equations (e.g. Navier-Stokes equation), the LBM technique models fluid dynamics by a combination of microscopic and mesoscopic level kinetic equations. At the fundamental level, LBM functions via a simplified kinetic model, which includes the physics of microscopic processes that are averaged but can accurately inform macroscopic fluid dynamics, consistent with macroscopic level equations (Chen and Doolen 1998). Hence the macroscopic fluid dynamics determined from LBM summarizes the collective behavior of an ensemble of microscopic processes (Kadanoff 1986).

The geometry and flow of fluid was modeled 2D using the LBM D2Q9 (i.e. 2 dimensions, 9 discrete velocities where the '9^{th}' velocity is the particle at rest) scheme in order to reduce computational time (Figure 4-1A). The 9 velocities are discrete 'bins' that together describes a density distribution function (f) (see sub-section 4.4.2 for more details). The function may be considered as a typical histogram that represents the frequencies of direction-specific densities (f_i) (Figure 4-1B) for each finite discretized velocity (i). The LBM model outlined in this chapter simulates the continuous streaming and collision processes of a specified number of particles interacting on a network of nodes that result from the radial movement of gut walls and/or diffusion. The process of

streaming is the movement of f_i to the nearest neighbor lattice node while collision is the relaxation of f_i towards a local equilibrium, (see equation 4.12 in sub-section 4.4.2 for the equilibrium density distribution function).

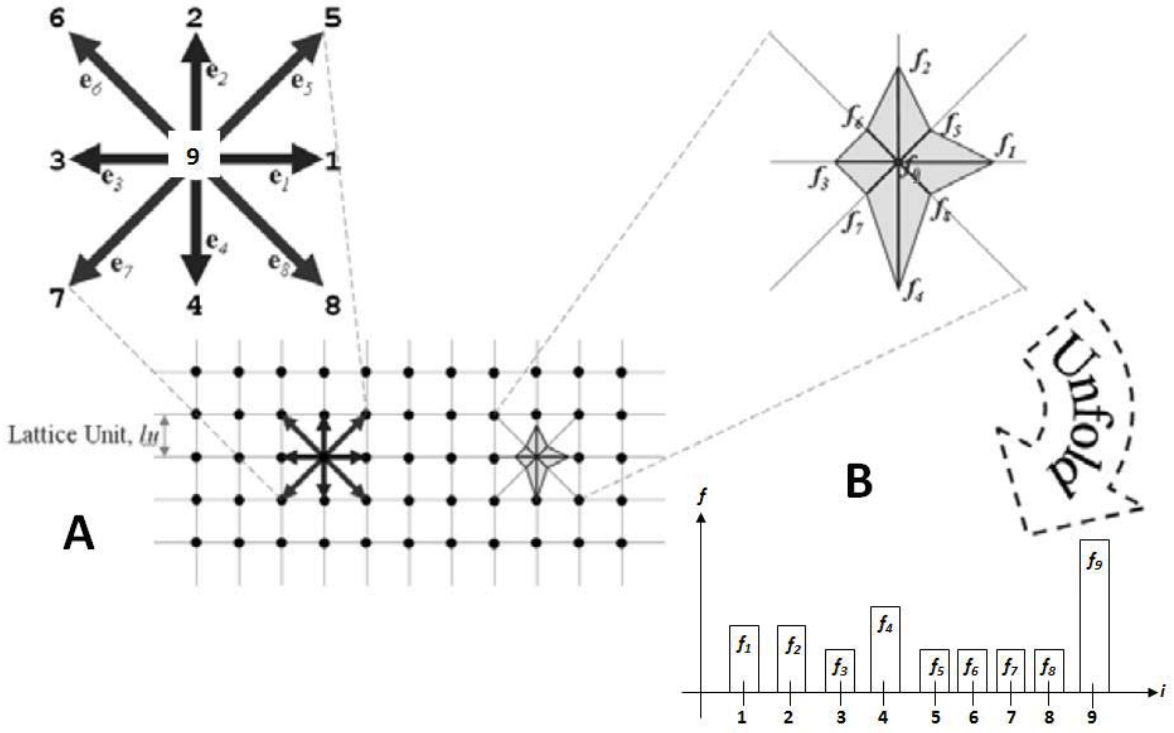

Figure 4-1: Lattice Boltzmann modelling (LBM) scheme used and the basic proceedings of any LBM algorithm. A) Is the on-lattice view of the 2 dimensions and 9 discrete velocities used for the LBM outlined in this chapter. B) Is the histogram view of the discrete single particle (i.e. direction specific) distribution function (f_i), for each of the finite discretized velocities (i) (adapted from Sukop and Thorne 2007).

4.4.1. Dimensionless formulation

In order to determine the fluid field (e.g. magnitude and fluid flow patterns) in the simulated gut by LBM, the Navier-Stokes equation was reformulated in a dimensionless form. Physical environment parameters were linked to their equivalent dimensionless LBM environment variables by dimensionless characteristic values. Characteristic values used included a characteristic velocity V_c value (m/s) that defined the maximum

magnitude of longitudinal velocity of the wall, the diameter D (m) of the rat small intestine and fluid density ρ that is assumed to be the density of water of 10^3 kg/m^3. Dimensionless values are identified with the symbol ‘′’. Thus, LBM environment values are linked to physical environment values by the following relationships;

$$\vec{u}' = \frac{\vec{u}}{V_c} \tag{4.3}$$

$$t' = \frac{t}{D/V_c} \tag{4.4}$$

$$p' = \frac{p}{\rho V_c^2} \tag{4.5}$$

where $\vec{u}$ is the velocity field (m/s), t the time (s) and p the pressure (Pa). The dimensionless Navier-Stokes equation of fluid flow is therefore;

$$\nabla.\vec{u}' = 0 \tag{4.6}$$

$$\frac{\partial \vec{u}'}{\partial t'} + \nabla.(\vec{u}'.\vec{u}') = -\nabla p' + \frac{1}{Re}\nabla^2\vec{u}' \tag{4.7}$$

where Re is the Reynolds number that represents the ratio of inertial forces to the viscous forces for a given flow condition. *Re* is thus defined as;

$$Re = \frac{\rho \vec{u} D}{\mu} \tag{4.8}$$

where μ is the dynamic viscosity of the fluid environment. While flow in a tubular channel can often be turbulent leading to the formation of unstable eddies of various sizes that promote mixing of the contents, in reality, flow in the small intestine has often been characterized with small Reynolds number never exceeding 200 (Jeffrey et al. 2003; Love et al. 2013). For that reason, flow in the small intestinal model will be laminar (Sakiadis 1984) and it would be expected that mixing and mass transfer by advection would be limited.

As flow is pulsatile due to pendular contractions varying cyclically with time at a frequency Fq (Hz) dictated by the slow wave (Lentle et al. 2012), it may be described by a Strouhal number (Sr). *Sr* is a dimensionless number describing oscillating fluid mechanical conditions and corresponds to the ratio of the time scale of the longitudinal activity $1/Fq$ to the time scale of flow D/V_c, thus defined by;

$$Sr = \frac{FqD}{V_c} \tag{4.9}$$

A more common way of characterizing pulsatile flows in a physiological environment is the dimensionless Womersley number, *Wo* (Loudon and Tordesillas 1998). It can be defined as a function of the *Re* and *Sr* numbers (i.e. pulsatile flow frequency associated with viscous effects). *Wo* numbers have originally been utilized in the characterization of blood flow in the arteries (Womersley 1955).

$$Wo = D\sqrt{\frac{Fq\rho}{\mu}} = \sqrt{ReSr} \tag{4.10}$$

4.4.2. LBM modeling of flow by LBGK

To resolve the LBM model of 2D incompressible fluid flow (i.e. the density of the fluid does not change during its motion) by the Navier-Stokes equation, the Lattice Bhatnagar-Gross-Krook (LBGK) derivation developed for use on a LBM Cartesian mesh by Guo et al. (2000) was utilized. This derivation of the LBGK method, unlike others, allows the incompressible Navier-Stokes equations to be exactly recovered (Guo et al. 2000). In 2D LBM, $f_i(\vec{x}, t)$ is the density (i.e. probability) distribution function, which is the probability of finding a particle at discretized positions $\vec{x}$ on a network of nodes at a given time (*t*) with a given velocity ($\vec{u}$, where $\vec{u} = c\vec{e_i}$). While $\vec{e_i}$ is the local particle velocity (Chen and Doolen 1998) where i is quantified through 1 of 8

discretized finite velocities (i = 1,…,8) that point to an adjacent node, or a zero velocity (i = 0) on the distribution function $f_i(\vec{x}, t)$. The equations used are as follows;

$$\overrightarrow{e_i} = \begin{cases} \langle \cos\left[\frac{(i-1)\pi}{2}\right], \sin\left[\frac{(i-1)\pi}{2}\right] \rangle & \textbf{if } i = 1,2,3,4 \\ \sqrt{2}\,\langle \cos\left[\frac{(i-5)\pi}{2} + \frac{\pi}{4}\right], \sin\left[\frac{(i-5)\pi}{2} + \frac{\pi}{4}\right] \rangle & \textbf{if } i = 5,6,7,8 \\ (0,0) & \textbf{if } i = 0 \end{cases} \quad (4.11)$$

The LBM density distribution function by the LBGK model is as follows;

$$f_i(\vec{x} + c\overrightarrow{e_i}\Delta t, t + \Delta t) - f_i(\vec{x}, t) = -\frac{1}{\tau}\left[f_i(\vec{x}, t) - f_i^{eq}(\vec{x}, t)\right] \quad (4.12)$$

where $c = \Delta x/\Delta t = 1$, Δx and Δt are the lattice grid spacing and the time step respectively, while $f_i^{eq}(\vec{x}, t)$ is the equilibrium density distribution function determined by;

$$f_i^{eq} = \begin{cases} \lambda\frac{p}{c^2} + s_i(\vec{u}) & \textbf{if } i = 1,2,3,4 \\ \gamma\frac{p}{c^2} + s_i(\vec{u}) & \textbf{if } i = 5,6,7,8 \\ -4\sigma\frac{p}{c^2} + s_i(\vec{u}) & \textbf{if } i = 9 \end{cases} \quad (4.13)$$

where p is pressure, λ = 1/3, γ = 1/12, σ = 5/12 (Guo et al. 2000) and;

$$s_i(\vec{u}) = \omega_i\left[3\frac{\overrightarrow{e_i}.\vec{u}}{c} + \frac{9}{2}\frac{(\overrightarrow{e_i}.\vec{u})^2}{c^2} - \frac{3}{2}\frac{|\vec{u}|^2}{c^2}\right] \quad (4.14)$$

where $\vec{u}$ is the fluid velocity in the LBM environment and ω_i is the weighting co-efficient, which varies conditionally as follows;

$$\omega_i = \begin{cases} 1/9 & \textbf{if } i = 1,2,3,4 \\ 1/36 & \textbf{if } i = 5,6,7,8 \\ 4/9 & \textbf{if } i = 9 \end{cases} \quad (4.15)$$

The velocity ($\vec{u}$), pressure (p) and kinematic viscosity (ν) values in LBM environment are defined as follows;

$$\vec{u} = \sum_{i=1}^{8} c\vec{e}_i g_i \quad (4.16)$$

$$p = \frac{c^2}{4\sigma}[\sum_{i=1}^{8} g_i + s_9(\vec{u})] \quad (4.17)$$

$$\nu = \frac{2\tau-1}{6} c\Delta x \quad (4.18)$$

where τ is the dimensionless relaxation parameter (i.e. time), describing the relaxation of the density distribution function to its equilibrium state.

4.4.3. Boundary conditions used in LBM environment

Three types of boundary conditions were developed and incorporated into the LBM of the small intestine. The first two were developed to determine the position of the intestinal villi and the axial velocity of the underlying walls of the gut during contractile activity; while the third boundary condition was developed in order to reduce computational time required for simulations to be completed.

4.4.3.1. Pendular contractions of gut wall in LBM environment

The length of the gut modeled was dependent on the number and length of spatial domains of contraction (i.e. domains of contractile activity) (de Loubens et al. 2013). The LBM of simple non-propagating pendular contractions described in this chapter of rat small intestine was for 1 domain (i.e. 2 half radial domains) (Figure 4-2) of length $2l$ facilitated by the use of the 'symmetry' boundary condition (see below). By assuming that the small intestine comprises multiple domains of contractile pendular activity in conjunction with the use of symmetry boundaries (see sub-section 4.4.3.3), the simplified model may be extrapolated over an infinite length of intestine. It was assumed that the phase lag between adjacent domains of contraction was 180° out of phase (de Loubens et al. 2013). However, it is noteworthy that the phase lag may vary

over successive longitudinal contractions (Lentle et al. 2012). When one domain of contractile activity is contracting, the immediately adjacent domain (on both ends) will be in its relaxation phase (Lentle et al. 2012; de Loubens et al. 2013).

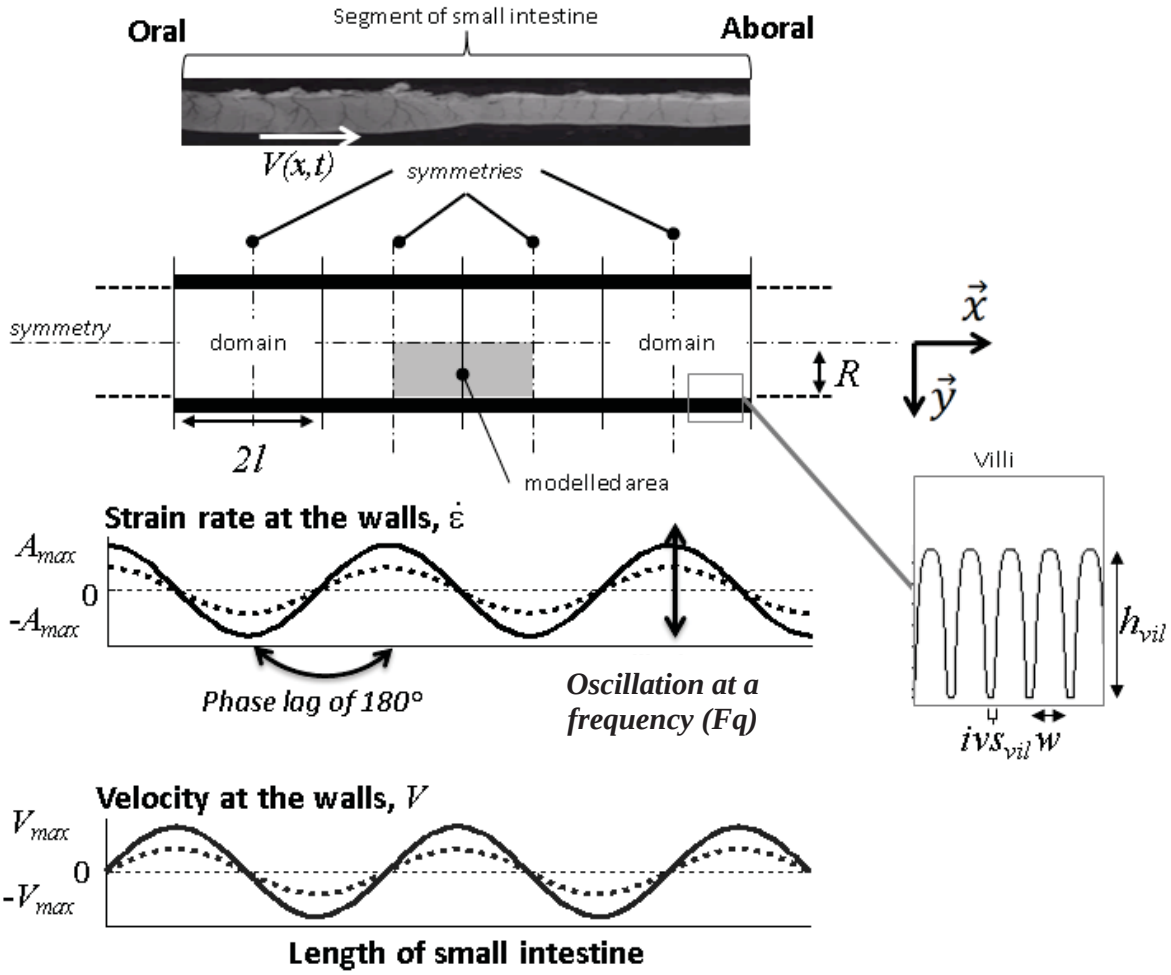

Figure 4-2: The simplified small intestinal model of 1 spatial domain of contraction (2*l*) of the rat duodenum (Lentle et al. 2012). At the mesenteric and abmesenteric surfaces, the strain rate $\dot{\boldsymbol{\varepsilon}}$, with which the walls contracts, oscillates at a frequency (*Fq*) and with an assumed phase lag of 180° between adjacent domains. The velocities V (used as boundary conditions in the model) were directly determined by integration of the strain rate $\dot{\boldsymbol{\varepsilon}}$ along the length of the gut. Villous dimensions of width ($w = R_{vil}$), length (h_{vil}) and intervillous space 'ivs_{vil}' were determined experimentally (sub-section 4.3.2) and translated into Lattice Boltzmann modelling units.

The cyclic variation of the longitudinal strain rate $\dot{\varepsilon}$ ($\partial\varepsilon/\partial t$), i.e. the rate of local lengthening (if $\dot{\varepsilon} < 0$) or shortening (if $\dot{\varepsilon} > 0$), for the specific domain (2*l*) modeled was represented by a sinusoidal function:

$$\dot{\varepsilon} = A_{max} \sin(2\pi f t) \sin(\frac{\pi}{l} x) \quad (4.19)$$

where A_{max} is the maximal amplitude of the longitudinal strain rate, t is the time, l is the length of the half domain of contraction while *X* is the longitudinal abscissa in the LBM. Thus relaxation and contraction of the gut wall defined by equation 4.19 occurs between the time intervals of 0 to T/2 and T/2 to T respectively where 'T' is the period (s) during one cycle of contraction. The velocity of the gut wall was derived from the integrated form of the strain rate equation with a maximal longitudinal velocity V_{max} defined by the equation below;

$$V_{max} = A_{max} \frac{2l}{\pi} \quad (4.20)$$

The results (e.g. flow parameters) depended on the time relative to one cycle of contraction and hence the parameters, such as the velocity $\vec{u}$, were averaged over the specified time interval of one-half of a cycle;

$$\bar{\vec{u}}_{T/2}(x) = \frac{2}{T}\int_0^{T/2} \vec{u}(x,t)dt \quad (4.21)$$

4.4.3.2. Simulating moving and curved boundaries

The 'bounce-back' boundary condition (i.e. the direction of travel of a particle is reversed when it encounters a solid boundary) scheme with interpolations (Bouzaidi et al. 2001) was utilized to detect moving and curved boundaries on a regularly sized Cartesian mesh. A q value is used to represent the position of a boundary as it intersects arbitrarily between two adjacent nodes, one in the fluid and the other in the non-fluid region within the boundary (Figure 4-3).

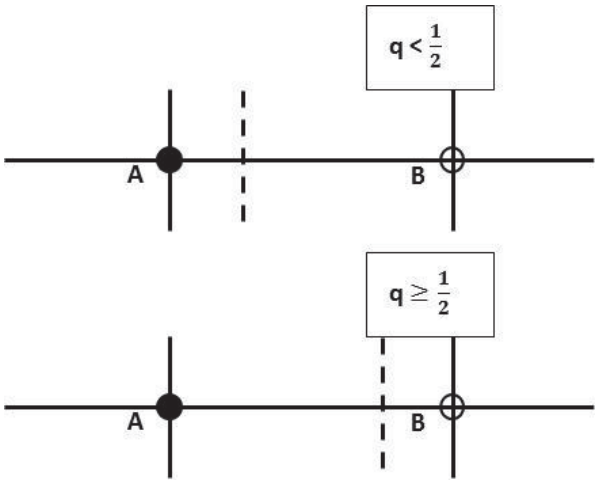

Figure 4-3: Two situations where the standard 'bounce-back' scheme (Sukop and Thorne 2007) was needed to be modified to address the density distribution function when the propagation of a particle encounters a boundary that is less than a lattice unit from the last fluid node. Node A is the last node in the fluid before the boundary while B is the first node behind the boundary (i.e. solid node), which is indicated by the dotted line.

Bouzaidi et al. (2001) describes two situations when interpolations to the density distribution function were required where either q < ½ or q ≥ ½ where at q = ½, the standard 'bounce-back' scheme (Sukop and Thorne 2007) without interpolations may also be used. Hence for all non-stationary velocities (i = 1,…,8), the equations for the respective conditions are below.

$$g_i(\vec{x},t) = 2q g_i^c(\vec{x},t) + (1-2q) g_i^c(\vec{x}-\vec{e}_i,t) - 6\omega_i(\vec{e}_i.\vec{u}_s),\ for\ q < \frac{1}{2} \tag{4.22}$$

$$g_i(\vec{x},t) = \frac{1}{2q} g_i^c(\vec{x},t) + \frac{(2q-1)}{2q} g_i^c(\vec{x},t) - \frac{3}{q}\omega_i(\vec{e}_i.\vec{u}_s),\ for\ q \geq \frac{1}{2} \tag{4.23}$$

where g_i^c is the density distribution function post-collision, $\vec{u}_s$ is the wall velocity while the third and last term of both equations represents the momentum exerted by the moving boundary onto the fluid. This method of detecting moving boundary conditions was used for dealing with complex geometry and arbitrary curvatures (i.e. intestinal villi) as it had a numerical accuracy consistent with LBM of incompressible flow while being simple to implement (Bouzaidi et al. 2001; Lallemand and Luo 2003). When

lattice nodes were uncovered by the moving boundary, the pressure at these nodes was evaluated by the average pressure of their nearest fluid nodes.

4.4.3.3. Symmetry boundaries

As compared to the model of pendular contractions developed by de Loubens et al. (2013), this LBM work required a significantly larger mesh size to account for the various size scales considered (e.g. the relative dimensions of the intestinal villi as compared with the dimensions of the adjacent lumen). This resulted in a substantial increase of computational time required. The use of the symmetry boundary condition outlined below allows the size of the small intestinal model to be reduced (e.g. by facilitating the extrapolation to multiple spatial domains of contraction while only actually modeling one) while ensuring that results generated could still be scaled and applied to the physical (i.e. 'real world') dimensions in a meaningful manner.

A symmetry 'east-west' boundary was implemented so that only one spatial domain of contraction would need to be modeled (Figure 4-2). The implementation of this boundary again assumes (see sub-section 4.4.3.1) that adjacent spatial domain of contractions would be in an opposite phase to the one modeled (i.e. if the modeled domain was contracting; adjacent spatial domains of contraction would be in its relaxation phase and vice versa). The computation time was reduced by at least 50% by only accounting for 1 domain of spatial contraction as compared to a previous model that accounted for 2 domains.

It was also assumed that fluid flow profiles generated at a given 2D slice of the tubular gut were identical for the whole circumference of the gut. Hence, the dimensions of the modeled small intestine of a small mammal were of length L and height $D/2$ with a symmetry boundary implemented to the 'north' of the LBM environment. Flow profiles

generated at the modeled region was therefore assumed identical to those at the 'north' of the gut section modeled.

4.4.4. Multi-scale meshing considerations

Multi-scale grids were not used in the final version of the LBM of the small intestine. This was because more extensive use of symmetry boundaries (see above) meant that the domain size that was modeled could be reduced to the point at which the use of multi-scale grids incurred a greater simulation time as compared to simulations conducted with uniform grid sizes. The increase of computational time through the use of multi-scale grids was attributed to the need for additional spatial and temporal interpolations that were part of the computational procedure during transfer of information from the coarse to fine grids and vice versa.

4.4.5. Code validation

All results were reported when the pseudo-steady state condition has been achieved. This condition was met when the relative error (E) with the analytical solution was less than 1%. The relative error was calculated by the following equation (Loudon and Tordesillas 1998);

$$E = \frac{\left(\sum(u_i - u_{i-1})^2\right)^{\mathbf{1/2}}}{\left(\sum u_{i-1}^2\right)^{\mathbf{1/2}}} \tag{4.24}$$

Where u is the magnitude of the velocity vector calculated with the model and i the number of iterations (i.e. cycle of contraction). The condition was met typically after 3 cycles of contraction. The final algorithm was also validated using different benchmarks (e.g. Poiseuille and Couette flow) to check for any errors.

4.5. Experimental parameters

The previous sections have outlined the physical and numerical formulation of the computational model that underlies the development of the LBM model of a length of small intestine that is undergoing cyclical pendular contraction. This section outlines the experimental parameters of the LBM model; the physiological parameters, LBM environment numerical parameters and the details of the subsequent computational experiments.

4.5.1. Physiological parameters

The size of the model was characterized by the length of one spatial domain of pendular contraction. To minimize the computational time required to perform simulations, the model was developed for a spatial domain of contraction of 7 mm, which is the minimum size of a domain observed in the rat duodenum (Lentle et al. 2012). The mean length of rat ileal villi was calculated to be 700 ± 20 μm while the median villous width was 150 μm with an interquartile range (IQR) of 30 μm (n = 47). The mean intervillous space was estimated to be 36 ± 11 μm (obtained by subtraction of the cumulative longitudinal and transverse villous width from dimensions of a 1 mm^2 mucosal sample; see sub-section 4.3.2.1).

All statistical analyses were conducted using SPSS version 20.0.0 (SPSS Inc., Chicago, Illinois) in this chapter. A Lillefors test of all the viscosity values of the perivillous fluid in the terminal ileum of the possum (the values obtained from Lim et al. 2013) found that the distribution was not normal (df = 1, 178, F = 0.236, P = 0.000). Hence a non-parametric distribution study was conducted on those values, yielding a first quartile (Q1) value of 1 mPa.s and a third quartile (Q3) value of 2 mPa.s. These two viscosity values were among the physiological parameters evaluated in the model (Table 4-1). In

addition, normality of the villous heights, widths and intervillous space values in the terminal ileum of the rat were also assessed by a Lillefors test. Data sets that were not normally distributed were reported as median and interquartile range (IQR) values (Table 4-1).

The range of values that were used for the model of simple pendular contractions of the small intestine can be seen below in Table 4-1:

	Symbol	Value(s) tested	References
Maximal amplitude of strain rate	A_{max}	0.09 or 0.21 s^{-1}	Lentle et al. 2012
Diameter of gut lumen	D	6 mm	
Frequency of longitudinal contraction	Fq	0.56 or 0.64 Hz	Lentle et al. 2012
Length of contractile domain	$2l$	7 mm	Lentle et al. 2012
Number of domains	N	1	
Maximal longitudinal velocity	V_{max}	0.4 or 1.6 mm/s	Lentle et al. 2012
Viscosity of lumen fluid environment	μ	1 or 2 mPa.s	Lim et al. 2013
Mean villous length	h_{vil}	700 ± 20 μm	
Median villous width	d_{vil}	150 (IQR = 30) μm	
Mean intervillous space	'ivs_{vil}'	36 ± 11 μm	
Number of cycles of contraction	N_{cycle}	3	
Calculated number of villi per domain	n	36	
Calculated Reynolds number	Re	0.3 or 1.2	equation (4.8)
Calculated Strouhal number	Sr	3.4 or 7	equation (4.9)
Calculated Womersley number	Wo	1.45 or 2.02	equation (4.10)

Table 4-1: Physical and dimensionless parameters used in the Lattice Boltzmann modelling (LBM) models described in this chapter.

4.5.2. Numerical Parameters

A relaxation parameter (τ) (see equation 4.18 in sub-section 4.4.2) of 0.9 with 40 mesh units was used as a base case. This τ value was used as it was reported to have a truncation error of less than 1% for low Reynolds numbers (Holdych et al. 2004). The use of any relaxation parameters less than 0.9 would increase simulation time. While it was favourable to increase the relaxation parameter in order to lower the simulation time, it was calculated that an increase of the relaxation parameter, which facilitates the order magnitude decrease in simulation time, also resulted in an order magnitude increase of errors. This was demonstrated by comparing how the resulting velocity fields generated over a range of relaxation parameters deviated from the velocity fields generated with the base case (Figure 4-4).

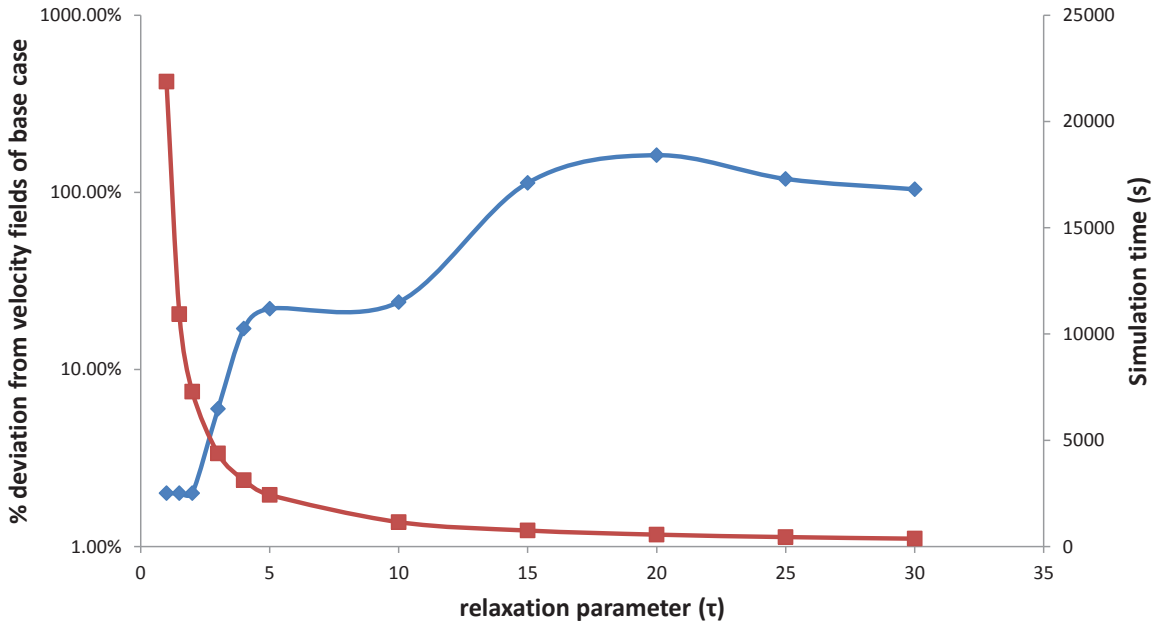

Figure 4-4: Relationship between '% deviation from velocity fields of the base case' (left Y-axis; blue plot with diamond shaped points) and simulation time (right Y-axis; red plot with square shaped points) against a range of assumed relaxation parameters (X-axis). The increase of relaxation parameters resulted in an order magnitude reduction of simulation time but also caused an order of magnitude increase of errors in the velocity fields generated as compared with the base case.

Further testing was then conducted to determine a suitable relaxation parameter that would reduce simulation time while maintaining a level of accuracy of 5% from the base case. The use of a suitable relaxation parameter had to be balanced also with a suitable choice of LBM mesh size. This was done by specifying the number of LBM units that would represent the combined width of an intestinal villus (at its base) and the intervillous space in the LBM environment. A mesh size of 20 was the minimum that could be used, where a fifth of the mesh size was always allocated as the width of the intervillous space (i.e. 16 units representing the villous width and 4 the intervillous space). Two other mesh size values were tested; 30 and 40 units along with a range of relaxation parameters between 0.9 and 3 (Figure 4-5).

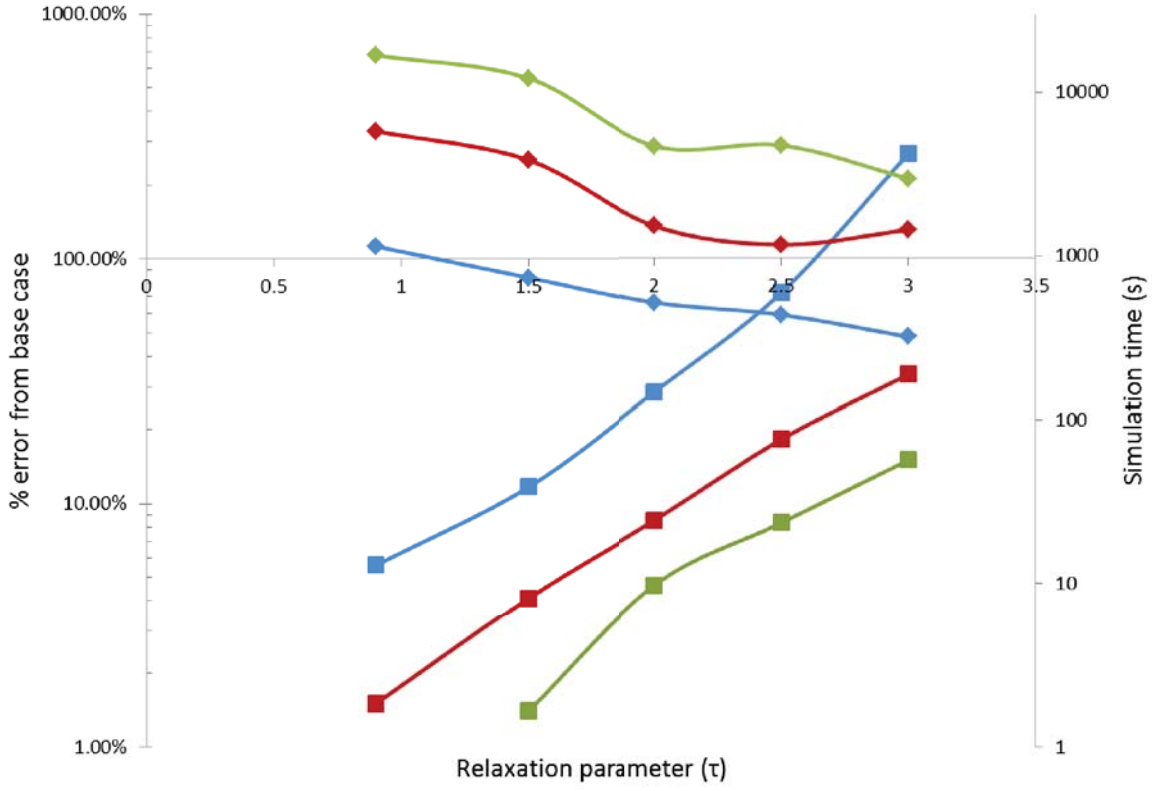

Figure 4-5: Relationship between '% error from the base case' (left Y-axis; square shaped points plot) and simulation time (right Y-axis; diamond shaped points plot) against a range of relaxation parameters (X-axis). The base case had a relaxation parameter of 0.9 and a mesh size of 40. The blue plot represents a mesh size of 20, the red plot a mesh size of 30 while the green plot represents a mesh size of 40.

While a relaxation parameter as high as 3 with a mesh size of 40 units would have reduced the simulation by more than 7 times as compared to the base case, the accumulated numerical errors would be as high as 15% from the base case would render the resulting flow profiles untrustworthy. The optimum combination of τ and mesh size that gave the lowest numerical error while keeping simulation time to a minimum was τ = 0.9 with a mesh size of 20 units and was used in all subsequent simulations. This optimum setting deviated from the base case by just over 5% but was 15 times faster than the base case (Figure 4-5).

4.5.3. Model's experimental parameters

The base case model had a Womersley number of 1.45, spatial domain of contraction size of 7 mm with 36 villi, and villous lengths of 700 μm. The following computational models were developed with the purpose of evaluating whether mass transfer was enhanced by varying combinations of parameters that deviated from base case values. The first two sets of models took into account only advective mass transfer while the third set of models simulated both advective and diffusive mass transfer of a solute tracer:

A) Comparison between a model run with villi and a model run without villi

B) Comparison between models run with various combinations of flow and characteristics of villi (see below).

C) Comparing the mass transfer of a solute tracer in a model run with non-propagating pendular contractions of the gut wall (advective and diffusive mass transfer) against a model run with stationary boundaries (only diffusive mass transfer).

The comparisons were made on the basis of the difference in radial velocity field at the end of the simulation (i.e. qualitative comparison). This parameter was used as it would reflect the movement of luminal contents into and out of the intervillous space during postprandial gut motility as would occur during *in vivo* digestion. In addition, quantitative comparisons were also conducted using plots of the relationship between '% increase in radial velocity' (X-axis) with respect to distance in the gut lumen (Y-axis).

Given that the number of villi simulated would be varied between some models, only radial velocity values that were in regions in between the lumen centre and regions directly above villi were considered. This was done as models with varying villi numbers may not be easily compared with the model simulated with the base case number of villi. To compare radial velocity fields that were of the same grid size, the larger velocity field was spatially interpolated by a 2D cubic spline algorithm. An example of the use of the interpolation is presented to illustrate the point: The grid size of velocity fields of the base case was 720 x 324 lattice units in length and height respectively, while the grid size of the velocity field generated from a model run without villi was 140 x 50 lattice units. Therefore, the velocity fields of the base case were interpolated into a grid size of 140 x 50 lattice units that allowed the magnitude of the radial velocity fields to be quantitatively compared.

4.5.3.1. Flow and villi characteristics compared

The effect of the following flow and villous characteristics were explored:

A) Villous height; a model run with villi at the length found in the rat ileum (700 μm) was compared with a model run with villi at half the length found in the rat ileum (350 μm).

B) Density of villi; models were run at three-quarters (27 villi), half (18 villi) and one-quarter (9 villi) of villi numbers per spatial domain of contraction. Their flow fields were compared with the base case model run with all 36 villi per spatial domain of contraction.

C) Flow characteristics are defined by a Womersley number (*Wo*) that is a result of a combination of Reynolds number (*Re*) and Strouhal number (*Sr*) (equations for *Wo*, *Re* and *Sr* numbers are in sub-section 4.4.1). *Re* is a function of maximal amplitude of strain rate (A_{max}) and viscosity of the fluid (μ) while *Sr* is a function of A_{max} and frequency of pendular activity (*Fq*). Combinations of A_{max}, μ and *Fq* that minimized the *Re* and *Sr* number generated a *Wo* number of 1.45 while the maximization the *Re* and *Sr* number of generated a *Wo* number of 2.02. Hence the flow fields of two scenarios were test, one at $Wo = 1.45$ and the other at $Wo = 2.02$.

4.5.3.2. Simulation of advective and diffusive mass transfer of a solute tracer

This experiment simulated the mass transfer of a solute tracer that had the same diffusion coefficient as a simple sugar (e.g. mannitol). As 30 cycles of contraction were needed to complete the simulation, which took 15 days to complete, only 2 experimental runs of this simulation were conducted. The runs compared the extent of mass transfer of the solute tracer firstly in the presence and similarly in the absence of non-propagating pendular contractions of the small intestine. In the simulations conducted in the absence of gut contractile activity, the mass transfer of the solute tracer was reliant solely on diffusion. Conversely, in simulations conducted in the presence of the gut wall pendular contractions, the movement of the solute tracer was influenced by advection. The models evaluated the mass transfer of a solute tracer without absorption of the tracer on villi.

The models were based on a particular family of LBM schemes developed by Ginzburg (2005) known as the 'optimal advection solution' that was used to solve the advection-diffusion equation (see below).

$$\frac{\partial s}{\partial t} + V.\frac{\partial s}{\partial x} = D.\frac{\partial^2 s}{\partial x^2} \quad (4.25)$$

In the context of the LBM environment of the model developed in this chapter, s is the concentration profile of the solute tracer undergoing mass transfer, V advection velocity, D is the diffusion coefficient of a mannitol-like solute of 1.5 10^{-10} m^2/s, and X is the distance in lattice units. This method of simulating the advection and diffusion of a solute tracer improved facilitation of anisotropic diffusion and allowed the use of high Péclet (*Pe*) numbers (i.e. up to 3 orders of magnitude) with LBM methods (Stiebler et al. 2008). The Péclet number is a dimensionless number that represents the ratio of advection to diffusion effects with the following relationship;

$$Pe = \frac{L.V}{D} \quad (4.26)$$

where L is the characteristic length. Two lines of solute tracers were positioned above the villi at time zero. One line was directly above the villi and the other line was a villous length above the villi. For both experiments, the concentration of the solute tracer remaining at its origin was determined after 30 cycles of contraction.

4.6. LBM results

The effects of villi in promoting radial flow in the gut as compared to a previous model that was developed without the incorporation of villi (de Loubens et al. 2013) can be seen in Figure 4-6.

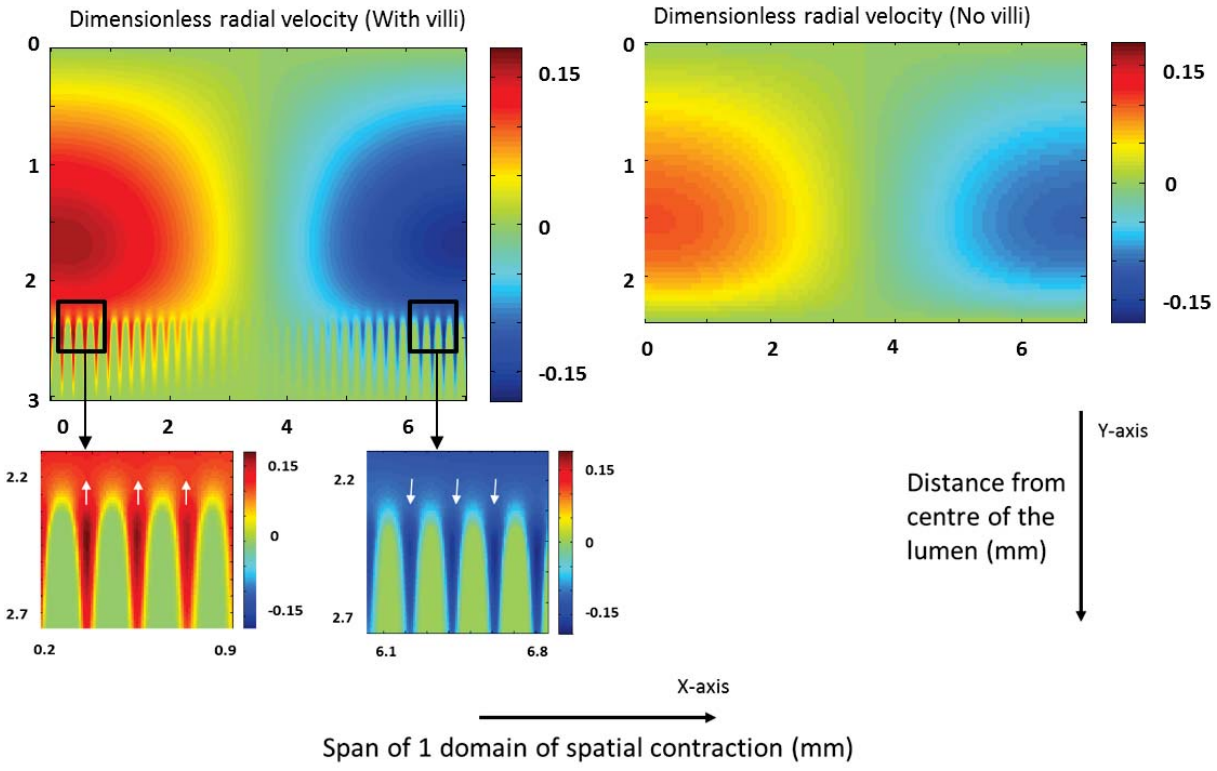

Figure 4-6: Radial velocity intensity plots comparing the base case model against a model run without villi. The colour maps attached to each image gives an indication of the magnitude of dimensionless velocity. The red colour represents flow moving in the direction of the lumen while blue represents flow moving towards the periphery of the gut.

Fluid expressed from the intervillous space was pulsatile over a cycle of contraction as would occur *in vivo*. While a similar radial velocity profile was also predicted in the output of the model without villi, it was of a lower intensity than that with villi (Figure 4-6). From a quantitative comparison as seen in Figure 4-7, it was evident that the presence of villi increased the radial velocity of fluid flow by approximately 4% at the centre of the lumen and up to 85% in regions near the villous tips.

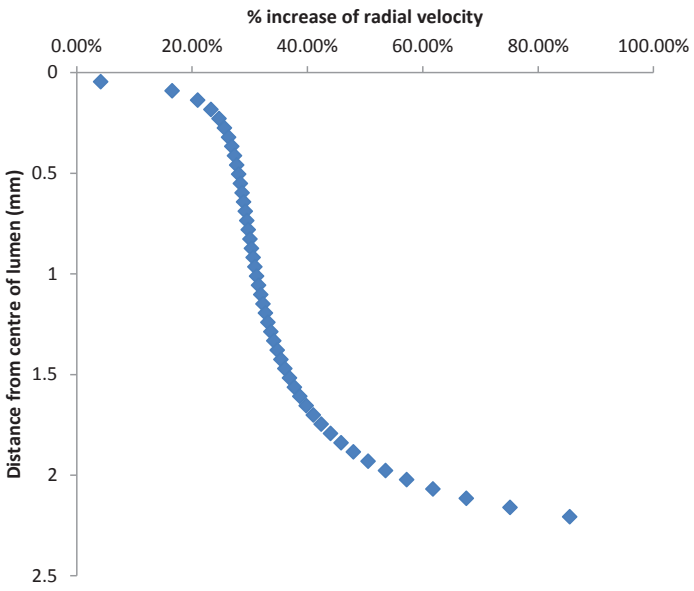

Figure 4-7: The percentage difference of radial velocities between the model run with villi and the other without. The positive '% increase of radial velocity' shows that the radial velocities of the model run with villi were larger than the model run without villi. The plot shows that the increase of radial velocity in the model run with villi against the one without villi was exacerbated with increasing proximity to regions directly above villous tips.

The qualitative and quantitative comparison between models with villi and those without suggests that villi significantly augment advective mass transfer in the peripheral gut lumen during non-propagating pendular contractions.

4.6.1. Effect of villous length

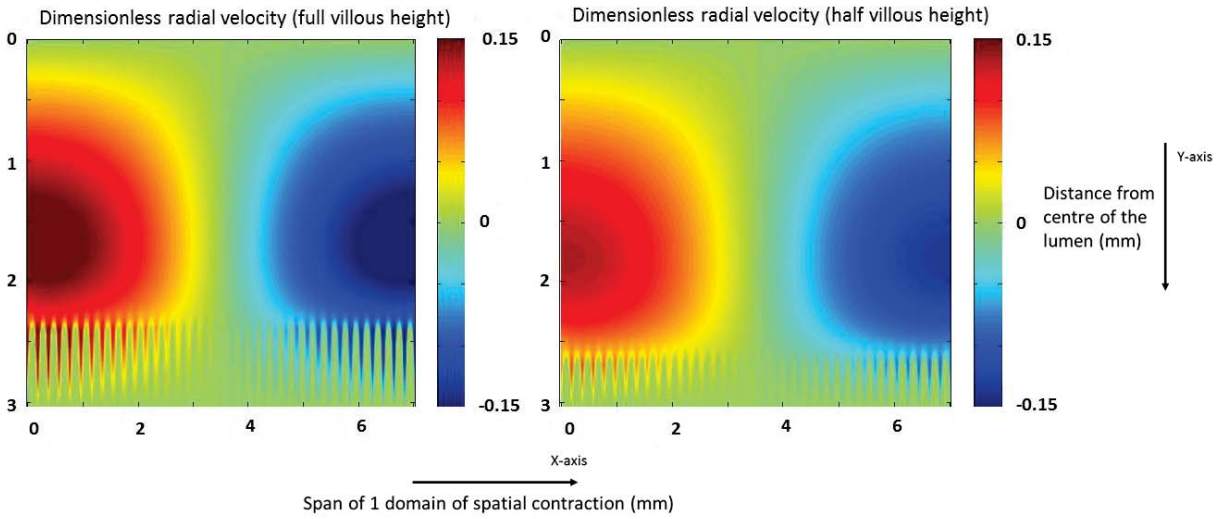

Figure 4-8: Radial velocity intensity plots comparing the base case model against a model run with villi of half the full length. The colour maps attached to each image gives an indication of the magnitude of dimensionless velocity. The red colour represents flow moving in the direction of the lumen while blue represents flow moving towards the periphery of the gut.

For the purposes of the discussion, the model run with full length villi (700 μm) will be termed FL while the model run with shortened villi (half the full villous length of 350 μm) will be termed HL. While a similar radial velocity intensity profile was also predicted in the output of the model HL (Figure 4-8) it was of a lower intensity than that of FL. Quantitative comparisons showed that the radial velocities of the model FL were larger than those from HL by 23% at the center of the lumen (Figure 4-9). This value persisted for the first 1.5 mm from the center of the lumen where it sharply decreased with increasing proximity to regions directly above the villous tips. In regions directly above villi, the radial velocities of model FL were the same as those of model HL.

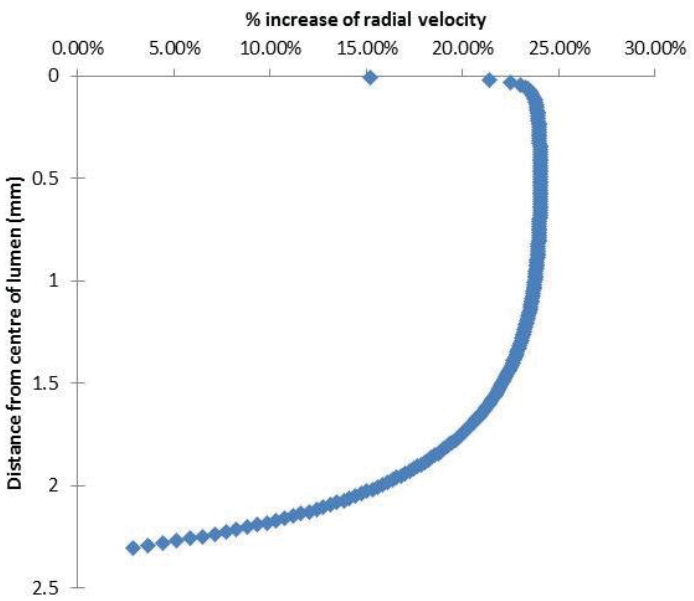

Figure 4-9: The percentage difference in radial velocities between the full length villi (FL) and half length villi (HL) model. The FL model had higher radial velocities (indicated by positive '% increase of radial velocity' values) at the centre of the lumen but their gains over the HL model decreased with proximity to the villous tips.

The results of this study suggest that fluid flow mass transfer in the gut would be marginally improved with longer villi.

4.6.2. Effect of villous numbers

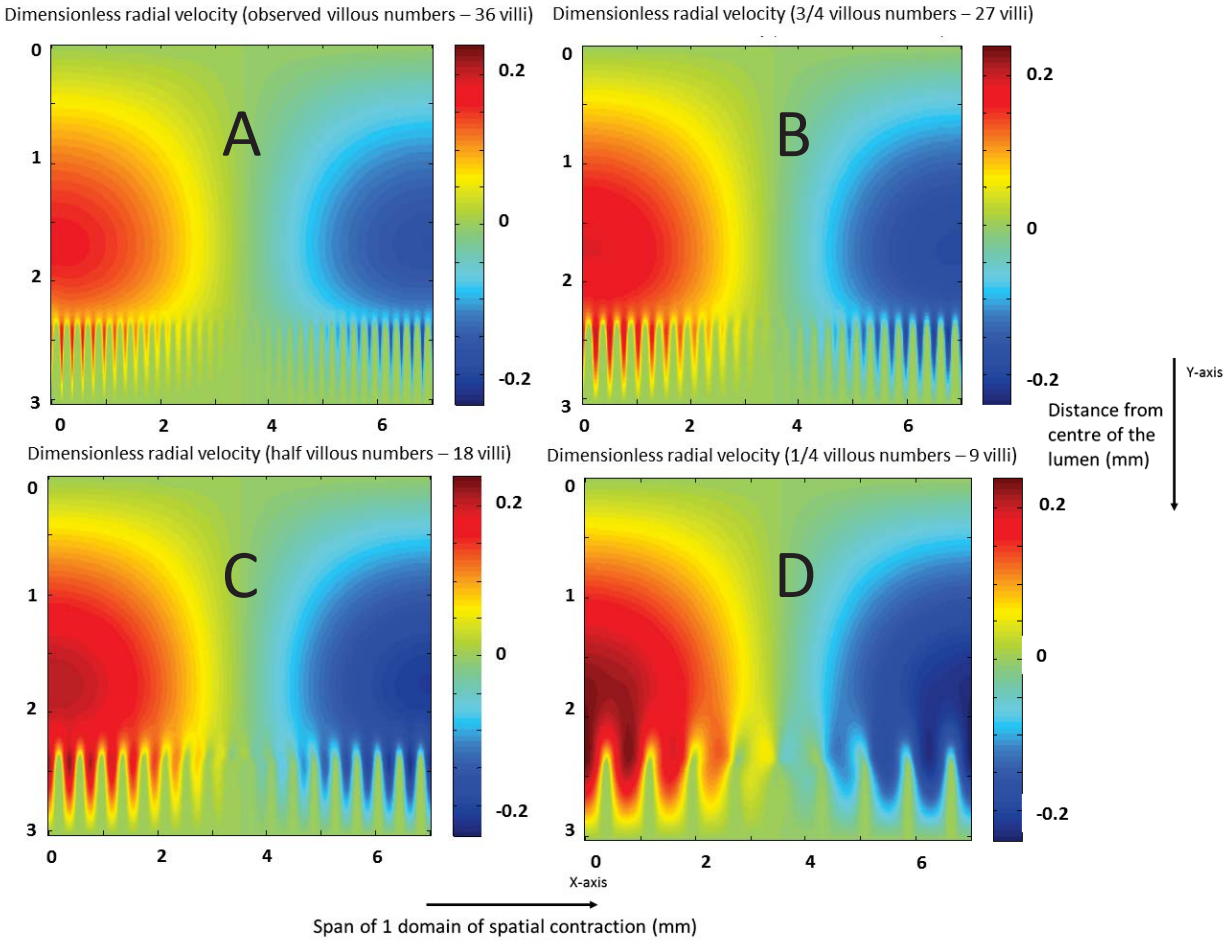

Figure 4-10: Radial velocity intensity plots comparing models with different densities of villi. A) All 36 villi were incorporated in the first model, a density that was determined from experimental studies of rat ileum mucosa. B) Three quarters of the observed number of villi were incorporated within the second model, C) half the numbers of villi in the third model and D) a quarter of villi numbers in the fourth model. The colour maps attached to each image gives an indication of the magnitude of dimensionless velocity. The red colour represents flow moving in the direction of the lumen while blue represents flow moving towards the periphery of the gut.

The magnitude of fluid flow mass transfer increased with the reduction in villi density (Figure 4-10). The radial velocity intensity plots suggest that the model that was run with a quarter of the observed number of villi (9 villi), generated the largest velocities of those investigated. A quantitative comparison of the base case and the model run with 9 villi showed that the latter model had radial velocities that were 25% larger than those

of the former at the centre of the lumen (Figure 4-11). The differences in the velocities subsequently increased markedly with increasing proximity to the periphery of the gut wall to being almost 70% larger in regions directly above the villous tips.

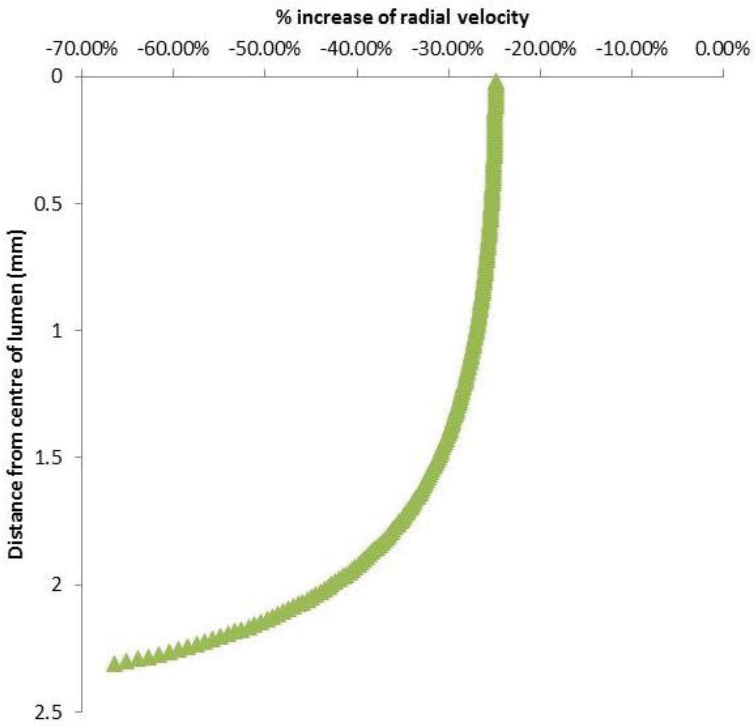

Figure 4-11: The percentage difference in radial velocities between the model run with all 36 villi and a model run with just 9 villi. The model run with 9 villi had very high radial velocities (indicated by negative '% increase of radial velocity' values) at the villous tips as compared to the model run with 36 villi but these gains decreased with proximity to the lumen centre.

4.6.3. Effect of varying flow parameters

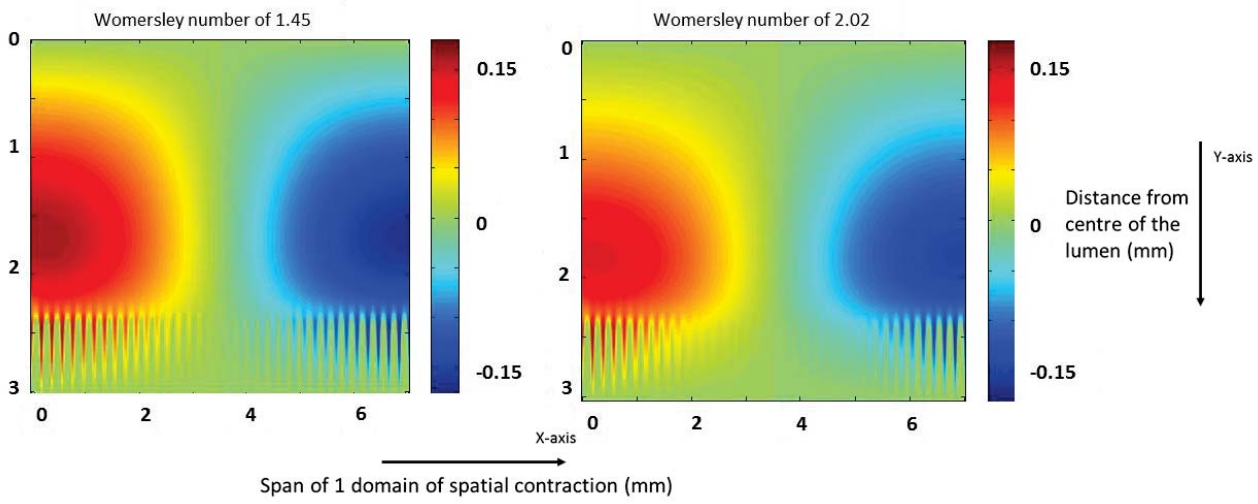

Figure 4-12: Radial velocity intensity plots showing flow profiles characterized by different combinations of dimensionless parameters. The plot on the left was run with a *Wo* number of 1.45 while the plot on the right was run with a *Wo* number of 2.02. The colour maps attached to each image gives an indication of the magnitude of dimensionless velocity. The red colour represents flow moving in the direction of the lumen while blue represents flow moving towards the periphery of the gut.

Combinations of A_{max}, Fq and μ (see Table 4-1 for definitions) that generated minimal *Re* and *Sr* numbers resulting in a *Wo* number of 1.45 appeared to facilitate a general increase in radial velocities in the gut as compared with the model run with $Wo = 2.02$ as observed from the intensity images of radial velocity (Figure 4-12). Quantitative comparisons of the model run with the lower *Wo* number and the model run with the higher *Wo* number showed that the former model had radial velocities that were 31% larger at the centre of the lumen (Figure 4-13). This value steadily decreased until there were no differences in radial velocity values at regions directly above the villous tips.

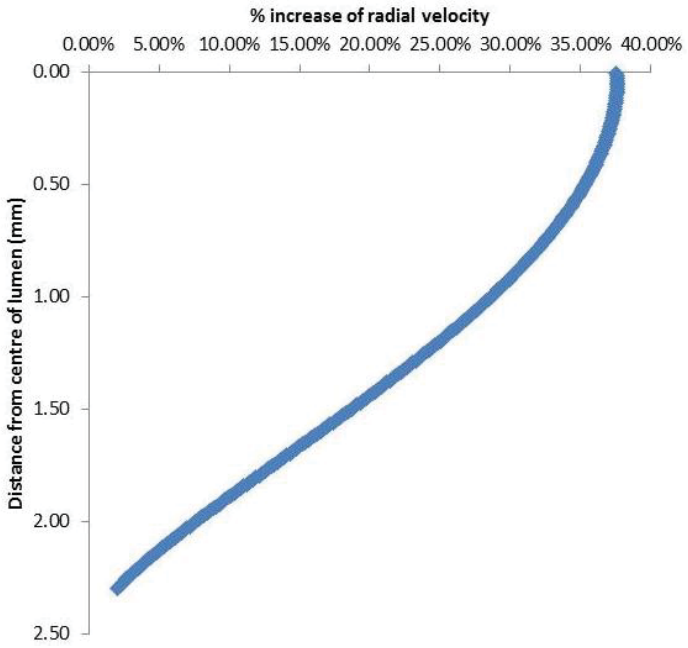

Figure 4-13: The percentage difference of radial velocities between the model run with *Wo* = 1.45 and the model run with *Wo* = 2.02. The model run with *Wo* = 1.45 had higher radial velocities (indicated by positive '% increase of radial velocity' values) at the centre of the lumen but their gains over the model run with *Wo* = 2.02 decreased with proximity to the villous tips.

Thus it was predicted that a lower *Wo* number facilitated the transmission of radial velocities generated in the intervillous space over a larger radial dimension of gut. This is thought to be attributed to a greater dominance of viscous over inertial forces (i.e. lower *Re* number).

4.6.4. Mass transfer of a solute tracer

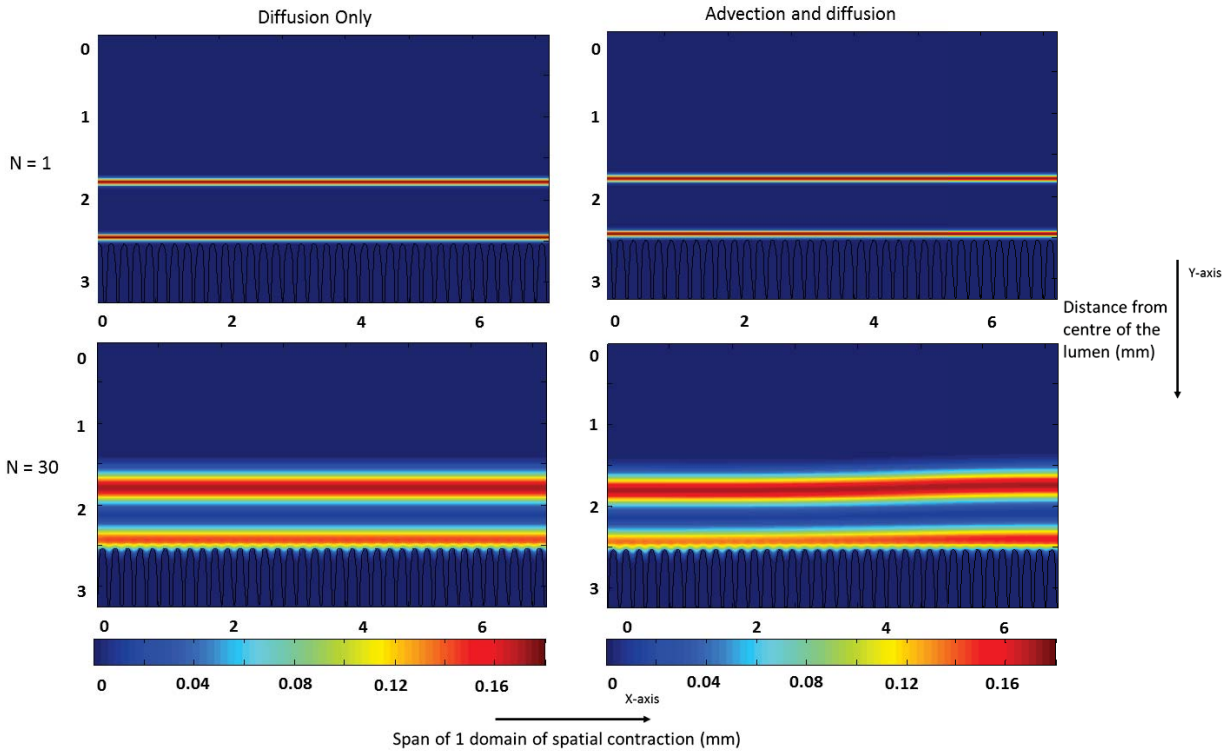

Figure 4-14: Plots of the advection and/or diffusion of a solute tracer that has the same diffusion coefficient as mannitol. A model run with non-propagating pendular contractions thus allowing for mass transfer of the tracer by advection and diffusion (right) is compared with a model run where the mass transfer of the tracer would only occur by diffusion. N is the number of cycles of contraction.

The impact of advective mixing on the mass transfer of a solute tracer positioned in horizontally oriented lines above villi was assessed over 30 cycles of contraction (N_{cycle}). Hence a model of mass transfer with non-propagating pendular contractions of the gut wall to generate advective flow (Figure 4-14 – right) was compared with that of a model run where the mass transfer of the solute tracer would occur only by diffusion (Figure 4-14 – left). Intensity plots of the dimensionless concentration of solute tracer show that the model run with non-propagating pendular contractions marginally improved solute tracer mass transfer. This was detected by the slightly fainter solute

tracer line toward the left of the image of the tracer line that is closer to the villous tips in comparison to that in the model run without pendular contractions (Figure 4-14).

To verify the minimal improvements of the solute tracer mass transfer by advective mixing engendered by pendular contractions, the concentrations of the solute tracers were also compared quantitatively (Figure 4-15).

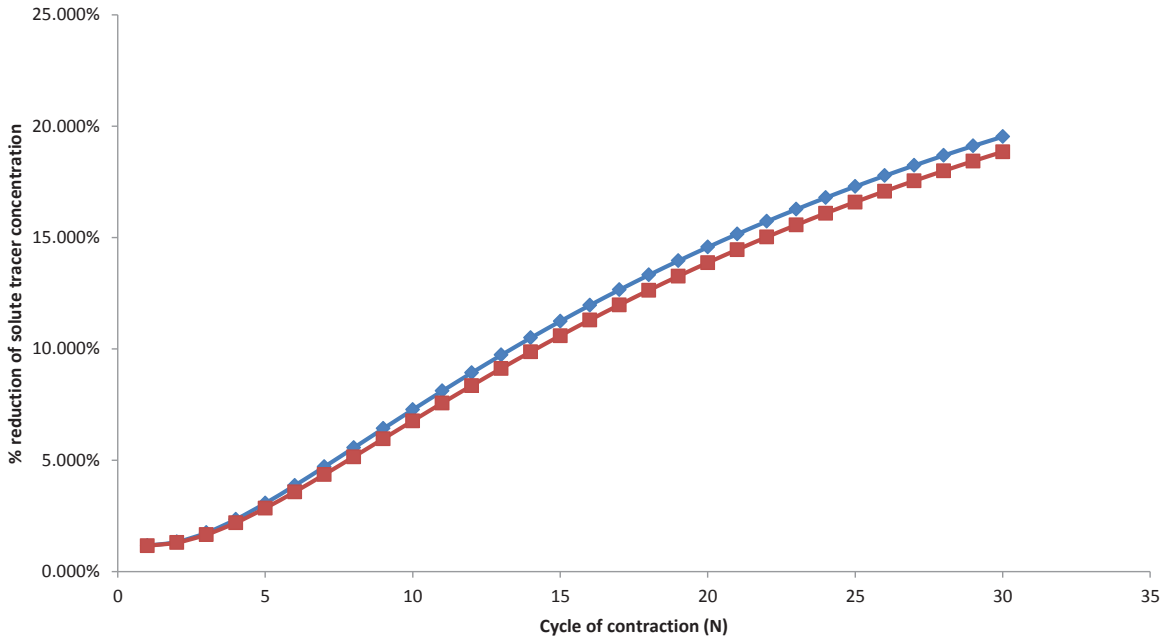

Figure 4-15: Plot comparing the percentage reduction of solute tracer concentrations between the model of pure diffusive mass transfer (red plot) of tracer and the model of advective and diffusive mass transfer (blue plot) of tracer.

Again the mass transfer of the solute tracer in the model with pendular contractions was marginally greater than in the model run without pendular contractions. Hence by the 30^{th} cycle of contraction, the concentration of the solute tracer at its point of origin in the model run with pendular activity of the gut wall was 19.5% less than its original value as compared to the model run with only pure diffusion where it was 18.8% less than the original value.

4.7. Discussion

In this chapter, 2D computational models of mass transfer in the perivillous region of the small intestine of a small mammal showing the effect of villi have been presented. The models described in this chapter assumed that villi were rigid (an assumption that would be investigated in more detail in chapter six) and that the movement of gut wall when undergoing non-propagating pendular contractions assumed only horizontal translations of the gut mucosa and associated villi. The results suggest that villi may have a role in improving the mass transfer of solutes in the perivillous space. Evidence of this is predicted from the comparison of models run with and without villi (see section 4.6).

Further comparison of models with various densities of villi demonstrates that the density of villi influenced the efficiency of mass transfer of solutes to the absorptive surface. Whilst it appeared that a density of villi that was lower than the normal physiological density further augmented mass transfer, this would reduce the area available for absorption. Hence this would be a functional trade-off between surface area and augmentation of advective flow.

Villous length also exhibited slight influences on mass transfer. While longer villi appear to increase the magnitude of radial velocity and propagate more into the centre of the lumen, longer villi may be more vulnerable to shear at the periphery and more prone to damage.

In addition, different characteristics of the fluid within the gut lumen also affected the magnitude of radial velocities and mass transfer. While it would appear that a lower *Wo* number facilitated the propagation of radial velocity within the lumen of the gut, this does not mean that mixing was augmented. A lower *Wo* value may result from a lower

frequency of vortex formation and shedding (Sundén 2011) over the tips of villi leading to the reduction in pulsatile flow and hence the mixing achieved.

The finding that advection did not distinctly augment mass transfer as compared with a situation with only molecular diffusion, may be due to the absence of asymmetry in the vortices. Conversely, this would favour the formation of symmetric vortices leading to alternate cycles of mixing and 'un-mixing' through each successive non-propagating pendular contractions (de Loubens et al. 2013). Such conditions would be compounded especially in a low *Re* number environment (e.g. as was used in the models described in this chapter) where the likelihood for the generation of turbulence would be significantly reduced.

The discussions above demonstrate that a thorough understanding of the fluid mechanical properties of the perivillous region (e.g. whether the perivillous environment is enveloped by a contiguous mucus layer or predominantly a Newtonian fluid of low viscosity) (Lim et al. 2013) and digesta (Lentle et al. 2002; Lentle et al. 2005) is important when seeking to determine the degree of mixing and mass transfer possible in this region. Indeed a computational model has shown that differences in the fluid mechanical properties of digesta may influence the effectiveness of different types of non-propagating patterns of gut motility – segmentation is thought to be more effective in mixing digesta of a high solid content (de Loubens et al. 2013).

Improved mixing and mass transfer could be augmented by a phenomenon known as 'geometric mixing' where different patterns of contraction occur at the same time to discourage the occurrence of mixing and 'un-mixing' in a given cycle of contractile activity as has been observed in the stomach (Cartwright et al. 2012) – a form of asymmetric mixing mechanism. Such mechanisms rely on the simultaneous contractile

activity of at least two types of motility patterns. However, such forms of asymmetric mixing are unlikely in the small intestine given that non-propagating pendular and segmentative contractions are mutually exclusive (Lentle et al. 2012). It is more likely that asymmetry in mixing mechanisms would come from stochastic (i.e. random) muscle contractions leading to stochastic variation in successive vortices formed (Lentle et al. 2012). Hence, asymmetric mixing may be reflected in computational simulations by the incorporation of 'real-time' longitudinal contractile activity as has been done in de Loubens et al. (2013). However, the single boundary condition implemented in the models that were described in this chapter does not reflect this effect as it would increase computation time, but could be considered in future work. Thus it is likely that mixing and mass transfer in the perivillous region in a living segment of small intestine would be augmented to a greater extent than has been demonstrated by the models described in this chapter.

In conclusion, the developed model of simple non-propagating pendular contractions indicate that an optimum number and length of villi is important in order that there be a balance between the mass transfer engendered and surface area that is available for absorption of solutes. However, the findings of this chapter also support prior work (de Loubens et al. 2013) indicating that whilst non-propagating pendular contractions facilitate mixing and mass transfer in the perivillous region, this does not necessarily translate to mixing in the centre of the lumen. The mechanisms of mixing and mass transfer in the lumen centre during the postprandial period are currently poorly described. Again, given that the computational model described in this chapter was conducted in 2D, it is important to note that such models may generate flow fields that may be restricted to only a single plane in the third dimension. Hence the flow field

patterns predicted that were generated in 2D require verification in a three-dimensional model.

4.8. Chapter Conclusion

In this chapter, computational models of simplified pendular contractions of the small intestine in a small mammal have been developed. The model incorporated the results from the previous chapter, which described the disposition and microrheology of the mucus environment in the perivillous space in the ileum of the brushtail possum. The effect of villi on mass transfer has also been highlighted.

Chapter Five -

Mucosal microfolding of gut wall

5.1. Foreword

This chapter describes previously unknown behaviour of the mucosal surface of the terminal ileum from the brushtail possum. The chapter begins with a consideration of the techniques used by previous workers in evaluating the mucosal movements and the utility of those techniques. This is then followed by a discussion of the design of experimental apparatus. This is followed by a published peer-reviewed paper discussing the results and conclusions of the work detailed in this chapter. Finally, additional material comprising computational modelling strategies based on the results of the paper, which examines the effect of mucosal microfolding on peripheral mixing and mass transfer will also be presented in this chapter.

5.1.1. Background and justification of experimental apparatus used

Mixing in the small intestine during the postprandial period is thought to result from a combination of contractile activity in the gut wall (Lentle and Janssen 2011) and by the motility of the intestinal villi of the mucosal lining (Strocchi and Levitt 1993). These mechanisms were thought to promote advective mass transfer of nutrients and pharmaceuticals in the perivillous space.

Previous studies indicate that pendular activity (Christensen 1984) and segmentation (Grivel and Ruckebusch 1972) were the main types of gut motility that occur during the postprandial period. Recent work indicates that segmentation may be effective in the mixing of luminal contents particularly those with a high solid volume ratio whilst non-propagating pendular contractions is only effective at promoting mixing at the periphery of the gut lumen (de Loubens et al. 2013). However, the work outlined in this chapter will largely focus on mixing during non-propagating pendular contractions. Given the possibility of villous motility promoting mass transfer of solutes in the perivillous

space, the initial experimental objective of this chapter was to determine the disposition and movements of villi during non-propagating pendular contractions. Previous work (Lee 1971; Womack et al. 1987; Mailman et al. 1990) had not considered villous motility in relation to that of the gut wall non-propagating pendular contractions of an intact gut segment.

There are various methods that may be used to achieve this aim especially in humans. Techniques such as endoscopy (Cammarota et al. 2004) or video-capsule (Ciaccio et al. 2012) provide direct evidence of the movements and disposition of villi *in vivo* but do not provide quantitative or qualitative evidence of any underlying contractile activity. Again the field of view of endoscopy is generally restricted to the region immediately caudad (i.e. towards the posterior or feet in humans) from to the fibre optic opening in the endoscope. Further, the use of endoscopy will require a fasted subject (i.e. one who is unlikely to exhibit postprandial gut motility). As for the video-capsule technique, while suffering from similar problems as endoscopy, it will also fail to provide a stable view of a given region of the gut wall as the video-capsule would be susceptible to the movements of the gut wall and the lumen (Kopylov and Seidman 2013).

The method used by Womack et al. (1987) and Mailman et al. (1989) observing movements of villi on exteriorized loops of gut segment of dogs that had been cut along its abmesenteric long axis and flattened could be used. However, it is likely that such flattening would impact the relative movement of mucosa in relation to the contraction of the muscle wall.

The novel techniques described in this chapter of observing the movement of villi in everted segments of intestine maintained *ex vivo* are thought to be the most suitable method. These techniques would allow sufficient separation of villous tips to enable the

movements and disposition of villi to be clearly visualized without impairment of contractile activity and relative movement of the villi and the mucosa. In addition, the contractile activity of the gut wall can still be distinguished and analysed to be compared with the activity of the uneverted gut wall.

5.2. Additional materials and methods

5.2.1. Eversion of gut segment

An everting probe was used to evert the gut segment. The main body of the probe was a metal rod that was of a cylindrical shape with the dimensions presented in the drawing below (Figure 5-1A). A screw was secured to one of the ends of the metal hollow rod (Figure 5-1B). The maximal radial dimension of the rod and screw-head (i.e. the everting probe) was smaller than that of the internal diameter of the gut segment of the brushtail possum that was 10 mm (our observations). This allowed for the expansion of the diameter of the gut segment to be everted by the mucosal thickness of the uneverted gut sections as the probe was pushed through the length of the gut segment without any undue compression to the gut mucosa.

The screw tip of the everting probe was inserted through the aboral end of the gut segment and secured to the wall with a suture placed around the screw shaft. The probe was then gently pushed into the lumen until it emerged from the oral end of the gut segment. The tip was then grasped and pulled through the remainder of the lumen with such action causing the gut to be everted. The aboral end of the everted gut segment was cut free from the everting probe and placed into the organ bath filled with heated and carboxygenated HBS. Both ends of the gut segment were cannulated before installation at the respective ends of the organ bath.

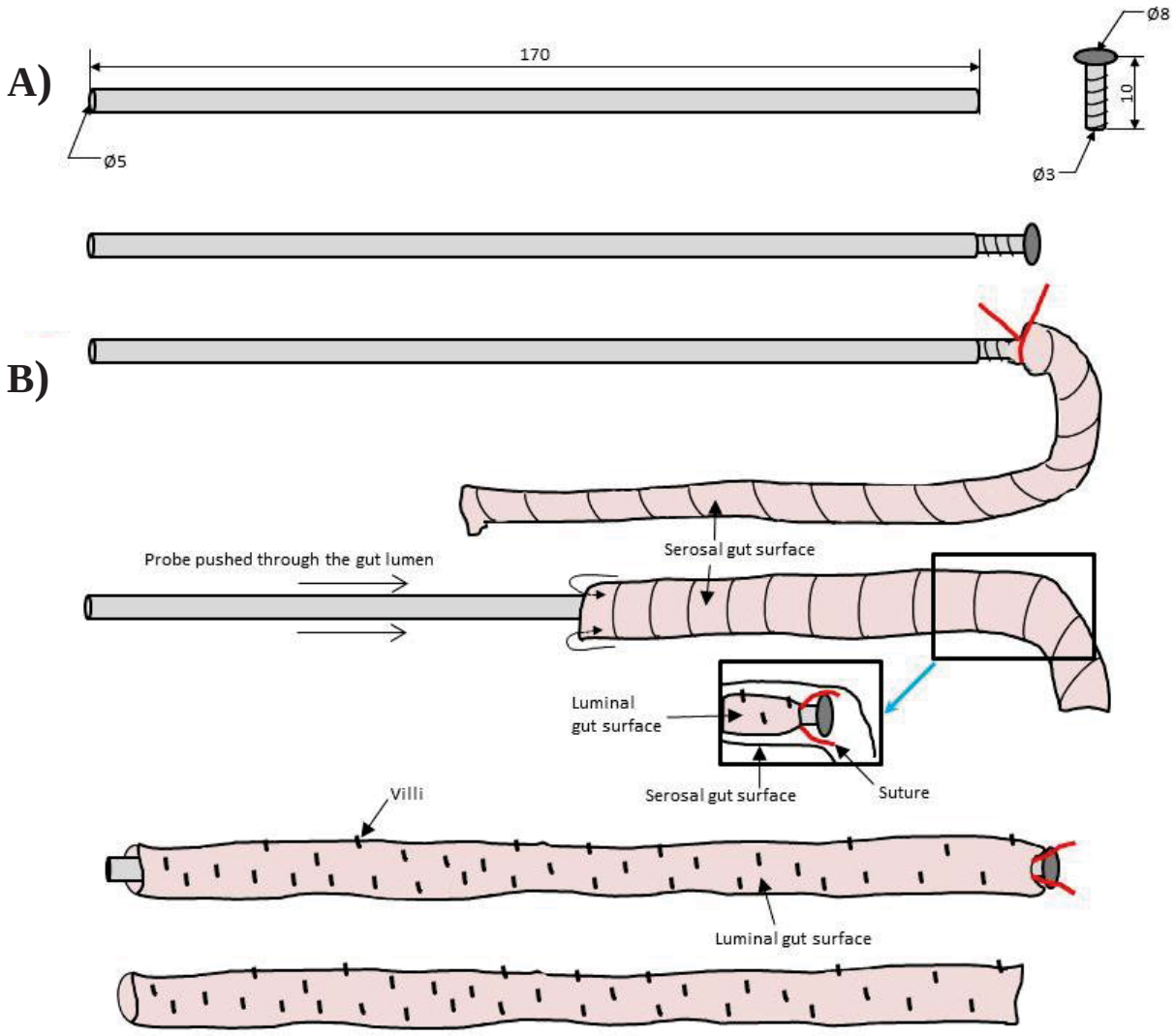

Figure 5-1: Everting probe used to evert gut segment samples.A) The dimensions of the two components that make up the everting probe; a metal rod and a screw. B) The assembled experimental apparatus with the aboral end of the gut segment secured under the screw head by a suture. Subsequently, the gut segment was then everted by wrapping the rest of the gut segment over the length of the metal rod. The aboral end of the everted gut segment was cut free from the metal rod so that the gut segment could be cannulated and placed into the organ bath.

The experimental procedure described here and those that are located in the methodology section of the journal article (in the subsequent section of this chapter) were also repeated with a rat terminal ileum. However, the absence of any contractile activity was observed on the everted rat gut segment. It is postulated that the gut eversion step was too invasive and stressful for the rat ileum to handle given the larger

angle of curvature that would arise when everting the rat ileum. It is noteworthy that the rat ileum was observed to have a thicker mucosal wall as compared with the possum ileum (our observations).

5.2.2. Organ bath design

The organ bath that was used to maintain everted segments of terminal ileum of the brushtail possum *ex vivo* was similar to that used in previous work (Lentle et al. 2007) (Figure 5-2). The back and bottom surfaces of the organ bath were darkened to enhance the contrast between the gut segment and the surfaces of the organ bath during image sequence recording of gut contractile activity.

Both the oral and aboral ends of the gut segment were cannulated to facilitate the ease of attachment of the gut segment in the organ bath. The cannula that would be connected to the oral end of the intestinal segment used in experiments was connected to a syringe pump so that carboxygenated and heated (37^{o}C) HBS could be perfused over the serosal surface of the everted gut segment. The cannula that was connected to the aboral end of the gut segment was connected to a plastic 'L' shaped pipe that had an internal diameter of 0.8 cm and a 3 cm outflow arm that was extendable to 5 cm with the addition of a tube. An in-built 'twist' mechanism of the 'L' shaped pipe allowed for alterations of the fluid level in the 'L' pipe outlet facilitating the regulation of the difference between the fluid level in the organ bath and the fluid level in the 'L' pipe outlet. Thus control of the amount of hydrostatic head (Δh) in the gut segment could be realized by the use of the 'L' pipe outlet system (Lentle et al. 2007) (Figure 5-2).

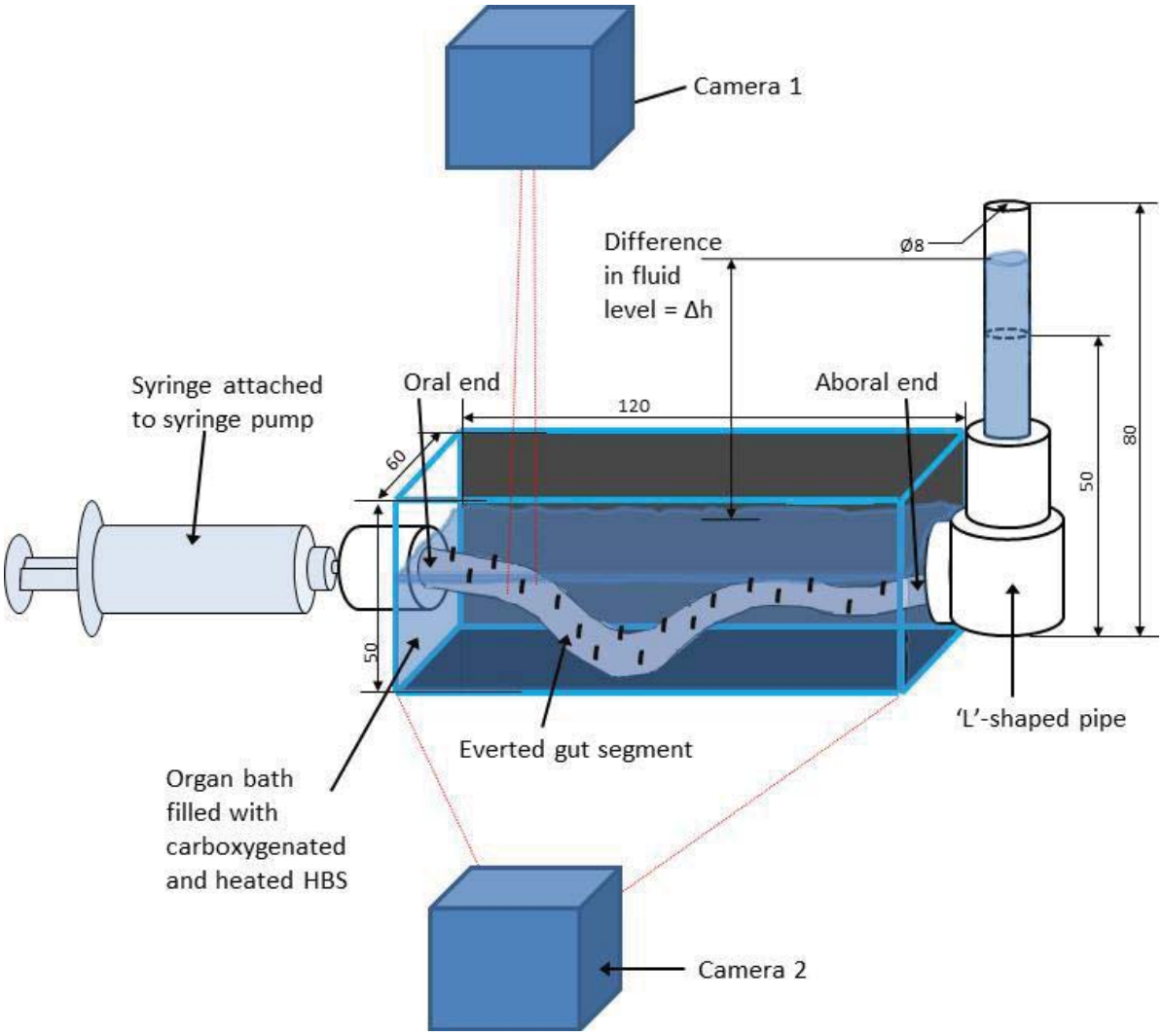

Figure 5-2: Basic setup of the experimental apparatus used for the recording of the disposition and movements of the mucosa and associated villi of gut segments maintained *ex vivo* during the recording of gut motility patterns of the everted gut. The organ bath contained Earle-Hepes solution (HBS) maintained at 37^{o}C and carboxygenated in a bath not seen in the figure. Circulation of fluid between the two baths was conducted by a peristaltic pump. The dimensions of the Perspex organ bath and the plastic 'L' shaped pipe that was used to maintain everted segments of the terminal ileum of brushtail possum *ex vivo* were also presented in units of millimetres (mm). A syringe pump was used to perfuse carboxygenated and heated HBS over the serosal surface of the gut segment. The level of the hydrostatic head (Δh) in the gut segment was regulated by the control of the difference between the fluid level in the organ bath and in the 'L' shaped pipe system. Two cameras were used to record postprandial motilities of the gut segment. Camera 1 recorded the disposition and movements of the mucosal wall and associated villi of a section of the gut segment at a x7 magnification while camera 2 recorded the whole length of the gut segment.

5.2.3. Experimental apparatus setup

The experimental setup was similar as was used in a previous experiment (Lentle et al. 2007). However this time, two cameras were used during recordings of the gut segment postprandial gut motility movements. Camera 1 recorded a section of the gut segment at a x7 magnification to allow for the visualization of a section of the segment with increased definition and resolution of the mucosal surface features (e.g. associated villi). Camera 2 recorded the whole gut segment used in these experiments so that the everted gut contractile activity could be assessed by spatio-temporal techniques (Lentle et al. 2007) (Figure 5-2).

5.2.4. Alternative method of determining mucosal microfolds dimensions

The following technique highlights an attempt at dimensioning the mucosal microfolds (see following section – '5.3'): A laser profiling technique was attempted to determine the dimensions (e.g. depths) of the mucosal microfolds during non-propagating pendular contractions of the gut segment of the terminal ileum from the brushtail possum. A beam from a laser light was projected onto the edge of the gut segment maintained *ex vivo* during the presence of gut contractile activity. Given that the length of the laser beam projected was kept constant throughout the whole process, any changes to the length of the projected beam would allow for the microfolds depth to be calculated. The formation of mucosal microfolds would alter the length of the projected laser beam where portions of the beam would be refracted through the formation of concavities on the mucosal surface. The measured reduction in the length of the projected beam would allow for an estimate of the microfolds' depths. However, due to the low quality of the results obtained, they were not published along with the peer-reviewed journal article. The quality of the results was limited by an inability to

accurately profile the dimensions of the microfolds due to the substantial presence of artefacts produced by the interferences of the laser beam by villi. The contents of the peer-reviewed journal article to follow, details an alternate image analysis technique used to obtain the dimensions of the mucosal microfolds.

MASSEY UNIVERSITY
GRADUATE RESEARCH SCHOOL

STATEMENT OF CONTRIBUTION
TO DOCTORAL THESIS CONTAINING PUBLICATIONS

(To appear at the end of each thesis chapter/section/appendix submitted as an article/paper or collected as an appendix at the end of the thesis)

We, the candidate and the candidate's Principal Supervisor, certify that all co-authors have consented to their work being included in the thesis and they have accepted the candidate's contribution as indicated below in the *Statement of Originality*.

Name of Candidate: Ian LIM Yuen Feung

Name/Title of Principal Supervisor: Prof. Roger G. Lentle

Name of Published Research Output and full reference:

Lentle, R. G., P. W. M. Janssen, C. de Loubens, Y. F. Lim, C. Hulls and P. Chambers (2013). "Mucosal microfolds augment mixing at the wall of the distal ileum of the brushtail possum." Neurogastroenterology & Motility 25(11): 881-e700

In which Chapter is the Published Work: Chapter 5

Please indicate either:

- The percentage of the Published Work that was contributed by the candidate: 20%

  and / or

- Describe the contribution that the candidate has made to the Published Work:

Ian Lim Yuen Feung
Candidate's Signature

27/6/2014
Date

Roger Lentle
Principal Supervisor's signature

27/6/2014
Date

5.3. Copy of the paper: Mucosal microfolds augment mixing at the wall of the distal ileum of the brushtail possum

The following pages contain a copy of the published journal article with the following bibliography;

Lentle, R. G., Janssen, P. W. M., de Loubens, C., Lim, Y. F., Hulls, C., and Chambers, P. (2013). Mucosal microfolds augment mixing at the wall of the distal ileum of the brushtail possum. Neurogastroenterology and Motility, **25**(11), 881-e700.

The contents of the published peer-reviewed article with the above bibliography is reproduced in this section. All references cited in section 5.3 are listed in a separate sub-section after the main body of the article. These references would be reproduced in the main bibliography of this thesis (i.e. after the thesis appendix) only should they be used elsewhere beyond this section (i.e. of this published article). All further work beyond this section will be citing the work presented in this section where appropriate.

Mucosal microfolds augment mixing at the wall of the distal ileum of the brushtail possum.

R. G. Lentle[1*], P. W. M. Janssen[1], C. de Loubens[2], Y. F. Lim[1], C. Hulls[1] and P. Chambers[3]

[1] *Institute of Food, Nutrition and Human Health, Massey University, Private Bag 11222, Palmerston North, New Zealand*

[2] *UMR 782 Génie et Microbiologie des Procédés Alimentaires, INRA, AgroParisTech, CBAI 78850 Thiverval Grignon, France*

[3] *Institute of Veterinary, Animal and Biomedical Sciences, Massey University, Private Bag 11222, Palmerston North, New Zealand*

*Corresponding author

5.3.1. Abstract

Background Recent work suggests that mixing in the small intestine takes place in central luminal and peripheral compartments. However, while movements of villi have been described, the mechanisms by which peripheral mixing are engendered remain unclear. **Methods** We examined the disposition and movement of mucosa and associated villi during contractions of the everted terminal ileum of the brushtail possum. We then simulated the effect of these movements on peripheral mixing. **Key Results** Compression of the intestinal mucosa by phasic longitudinal or radial contractions created short-lived microfolds, which were of similar scale to the attached villi. The packing density of the villous tips increased in the concavities and decreased on the crests of these microfolds. Simulations showed that these caused liquid digesta to be expelled from, or drawn into, intervillous spaces, significantly augmenting

peripheral, but not bulk, luminal mixing. **Conclusions & Inferences** We describe a mechanism by which peripheral mixing may be engendered by mucosal microfolds without requiring the coordinated contraction of individual villi or groups of villi.

Keywords: distal ileum, mucosal microfolds, peripheral mixing

5.3.2. Introduction

Nutrients are transported to the mucosa by a combination of diffusion and advective mixing, the latter depending principally upon the motility of the component structures of gut wall and the microrheological environment around the villi (Lim et al. 2013). While peristalsis is known to generate luminal mixing (Janssen et al. 2007), such activity is reduced during the postprandial period (Sarna 1985) when motility is largely restricted to pendular and segmentative contractions (Gwynne et al. 2004, Lentle et al. 2012), both of which have the potential to enhance digestive efficiency by generating local mixing without propelling the contents distally (Penry and Jumars 1987, Jumars 2000). However, recent modeling of the effects of real sequences of pendular contractions on the contents of a cylindrical segment of gut with a smooth mucosal surface indicates that they engender only limited mixing (de Loubens et al. 2013). Other workers have suggested that contractile movements of the villi themselves may augment mixing (King and Robinson 1945, Womack et al. 1988, Mailman et al. 1990), but this would require a high degree of coordination between groups of adjacent villi to forcibly eject material from the common space between them. While recent numerical simulations (Brasseur et al. 2009, Wang et al. 2010) indicate that intrinsic villous motility may augment mixing at the periphery of the lumen, there is considerable uncertainty as to the nature and extent of such motility *in vivo*. Other studies have assumed that villi are not motile and that the fluid held in the associated intervillous

spaces is correspondingly unstirred, a situation that would limit absorption (Levitt et al. 1992, Strocchi and Levitt 1993) and restrict it to the villus tip (Strocchi and Levitt 1993, Chang and Rao 1994).

In this work, we first examined the disposition and movement of mucosa and associated villi that are generated during contraction of the longitudinal and circular musculature in segments of the terminal ileum of the brushtail possum. Each segment was mounted in an organ bath with its length equal to that observed *in vivo*, with its mucosal surface outermost, i.e., everted, and with the villous tips stained with methylene blue to aid in their visualization. Subsequently, we simulated the effect of these movements on peripheral mixing in the intervillous spaces and on bulk mixing in the lumen.

The work is the first to show that mucosal folding associated with contraction of the longitudinal and circular musculature creates alternate regions of crowding and of separation of the tips of villi, and that this action may augment peripheral mixing around the tips of villi.

5.3.3. Materials and methods

5.3.3.1. Preparation of ileal segments

All procedures were approved by Massey University Animal Ethics Committee (MUAEC approval no 12/77) and complied with the New Zealand Code of Practice for the Care and Use of Animals for Scientific Purposes.

Thirteen freshly trapped brushtail possums (*Trichosurus vulpecula*) of either sex and between 2 and 3 kg bodyweight were each fasted for 2 h and anesthetized in an induction chamber with 5% halothane in 33% oxygen and 66% nitrous oxide. Following induction, they were maintained on 1.5% halothane in oxygen and nitrous oxide via a

face mask attached to a Bain's circuit during the surgery. A ventral midline incision was made in the abdomen and a 10 cm segment of ileum immediately oral to the ileocaecal junction was excised and immersed in carboxygenated Earle's Hepes buffer solution (HBS) maintained at 37 °C. The length of the segment that was to be taken was measured *in situ*, i.e., prior to excision and installation in the organ bath. The possums were subsequently euthanized with intracardiac pentobarbitone (125 mg/kg).

After flushing with carboxygenated Earle's HBS to remove any contained digesta, the ileal segment was usually (see below) everted so that its mucosal surface was outmost and serosal surface innermost. This was accomplished by passing a 0.5-mm diameter stainless steel probe along the length of the lumen from the proximal to the distal end of the gut, securing the tip of the probe to the distal end of the gut, and withdrawing the probe from the proximal end. The mucosal surface of the everted segment was flooded with stain solution (1% methylene blue and 2% glucose in deionized water) and left for 60 s before immersion in carboxygenated HBS for 2 min to remove excess stain. This procedure resulted in only the tips of villi taking up the stain (Figure 5-3), presumably from absorption of the dye only at sites where there are active enterocytes (Canto et al. 1996).

The everted segment was cannulated at the oral and aboral ends, and installed in the organ bath at the same length as it was *in vivo* and with the mesenteric attachment located at the upper edge of the video image. The organ bath contained 170 ml of HBS solution with the following composition in millimoles: NaCl 124.0, KCl 5.4, $MgSO_4$ 0.8, NaH_2PO_4 1.0, $NaHCO_3$ 14.3, Hepes 10.0, $CaCl_2$ 1.8, and glucose 5.0 and with a pH of 7.35. The solution was warmed to 37 °C, continuously carboxygenated (95% O_2, 5%CO_2), and recirculated at 60 ml/min. The lumen of the gut segment was perfused with HBS at a rate of 1 – 2 ml/min and the perfusion pressure was maintained at 0–2 cm

of water by appropriate adjustment of the height of the outflow at the distal end of the preparation.

To determine the effect of eversion on motility, the excised gut segments were either mounted directly in the organ bath or everted before mounting. In some cases, segments were removed from the bath after image capture, and again everted and remounted in the bath for further image capture. Excised segments of both everted and non-everted ileum were installed in the organ bath with length equal to that determined *in vivo*. Subsequently, the effect of the lengthening or shortening of a given segment on microfold formation was determined by changing the position of the distal cannula. A further series of experiments was conducted on unstained everted segments to determine whether the application of the methylene blue dye had influenced the formation of microfolds.

5.3.3.2. Image acquisition and spatiotemporal mapping

The movements of the mucosa and associated villi covering the external surface of the segment of ileum were recorded with a camera (Basler, SCA1000-20FC, Ahrensburg, Germany) and zoom lens (Cosmicar 12.5–75 mm) mounted 30 cm above the organ bath so as to give a magnified view of a short section of the ileum. A second camera (The Imaging Source DMK41AF02, Taipei, Taiwan) was mounted 40 cm to the side of the tank so as to give a view of the whole segment of ileum. Monochrome images were captured from both cameras at a rate of five frames per second and stored as uncompressed files. The images had scales of 0.02 and 0.08 mm per pixel for the high and low magnifications, respectively.

Sequences of images obtained from each camera and from each run were processed using a custom image processing program. The contraction of longitudinal muscles was

assessed using strain rate mapping (Janssen et al. 2009). In this method, cross-correlation between successive frames is used to quantify the displacement of reference points along the preparation based on the movement of surface textural patterns. These displacements are used to determine the longitudinal strain rates along the preparation at that time and yields a single row on the strain rate map on which regions undergoing shortening are represented by a shade of yellow and those undergoing extension by a shade of blue.

A form of spatiotemporal (ST) image intensity map was used to visualize the extent of villous apical crowding associated with transient microfolds. In the first image, a rectangular region of interest (ROI) was located axially on a section of ileum stained with methylene blue and undergoing pendular activity. The position of the ROI was moved in subsequent images to track the point at its center so as to counteract any axial movements associated with the pendular activity. The average pixel intensity for each column of the ROI generated a pixel on the ST map such that each image contributed a complete row to the map.

5.3.3.3. Measurement of villous and microfold geometry

The diameters and heights of villi were determined from the same segments of possum ileum as were used for motility studies in the organ bath. Full-thickness samples were taken from random sites and mounted with the villous surface outermost on a stainless steel holder with a 2-mm-diameter rounded tip. The holder was mounted in a cell with the sample immersed in carboxygenated HBS solution and viewed under dark field illumination with a Nikon Eclipse TE2000-U microscope (Nikon Instruments, Melville, NY, USA).

The number of villi per unit area of mucosa, i.e., density, and intervillous spacing were determined from randomly selected frames from the image sequences of motility of three stained everted ileum segments. Two 1 mm^2 ROIs were positioned on each image in a relaxed region that contained no microfolds. Villous density was determined by counting the number of villi within the ROI. Intervillous spacing was estimated by averaging the distances between each villus and its five to six nearest neighbours. As the villus density data were found to be normally distributed, the mean and standard error were determined directly. The intervillous space data required transformation using the Johnson algorithm in the MINITAB package (Minitab, Coventry, UK) to render them suitable for parametric analysis.

The scale of the microfolds was estimated from frames selected at the time when the longitudinal contractions of the stained everted ileum were at their maximum. The image was thresholded to highlight the microfolds along the top boundary of the ileum in the image. The pitch and depth of the microfolds were manually estimated from the thresholded image.

5.3.3.4. Modelling of peripheral and bulk fluid mechanics

We used computational fluid dynamics to assess whether apical crowding caused sufficient quantities of fluid to be displaced from between the villi to generate mixing in the intervillous spaces or lumen and to augment nutrient absorption (see supplementary material for method details). Two models were used that differed in scale. Both were solved by similar 2D lattice Boltzmann-based methods to those used in our earlier paper (de Loubens et al. 2013). The first model focused on the flow and mechanisms of absorption at the scale of a group of few villi (approximately 0.5 mm). The second

focused on the consequences of apical villous crowding on flow and mixing at the scale of the small intestinal lumen (approximately 10 mm).

The objective of the micro-scale model was to evaluate the flow generated by the villous apical crowding during longitudinal contractions independent of any bulk luminal flow, such as that generated by peristalsis. To reduce the computational load, the flow was assumed to be two-dimensional (2D), and the villi were maintained parallel and moved only in the longitudinal direction. These simplifications preserved the main characteristics of the movement of the villi, i.e., grouping and separation. The longitudinal mucosal strain rate was taken to be sinusoidal with period T; thus, the grouping and separation peaked at $t = T$ and $t = T/2$, respectively. The advection and diffusion of tracers with constant diffusion coefficient α was modelled to assess the influence of apical villous crowding on absorption of nutrients. We considered the situation where absorption was passive and not limited by epithelial permeability, i.e., the tracer was instantaneously absorbed when it reached the mucosa. At the initial time of the simulation ($t = 0$), the concentration of tracer was homogeneous in the flow domain. The total mass of tracer absorbed between the tips of the two outermost villi was calculated during one cycle of contraction. The strategy of the macro-scale modelling was an extension of our previous work (de Loubens et al. 2013), where real motility data were used as boundary conditions. The ileum was modelled as a segment of tube with no radial velocity components and pressures at the oral and aboral ends. Considering the presence of the villi in a model at the intestinal scale explicitly would be very computationally demanding. Instead, the influence of villous apical crowding on the macro-scale flow was modelled by the introduction of a radial velocity at the wall. During a contraction, the grouping of villi generates a radial flow from the wall into the lumen and during a relaxation, the flow is reversed. We examined the extent to

which deformations in the flow of the contents increased the lengths of interfaces between different elements of fluid and hence improved the diffusion process between them (de Loubens et al. 2013).

5.3.4. Results

5.3.4.1. Experimental

All preparations developed ongoing propagating phasic longitudinal, i.e., pendular, contractions (Figure 5-4A) as are discussed below and have been reported previously in this tissue (Lentle et al. 2007). At the sites of lengthwise shortening that were induced by these events, the mucosa became folded into a series of inwardly projecting rings, which we term microfolds (Figure 5-5D). The pitch (approximately 800 μm) and depth (100–300 μm) of these microfolds were of a similar scale to the villi (length 560 μm and diameter 160 μm), which did not appear to flex, but remained perpendicular to the mucosal curvature of the microfold. Hence, they became inclined toward each other in the concavities between adjacent microfolds so that their tips became crowded together forming dark radially orientated bands (Figure 5-5B) and they inclined away from each other, i.e., diverged, on the crests of microfolds so that their tips became separated forming lighter bands (see 'Microfold Movie1')[5]. The sites at which radial bands of villus tip crowding formed and dispersed were assessed using ST intensity maps (Figure 5-4B). These showed that individual radial microfolds reformed at the same site during successive pendular contractions.

When the overall length of the segment of intestine was maintained at that determined *in vivo*, most of the radial mucosal microfolds were formed at the height of each longitudinal contraction and disappeared during subsequent relaxation, i.e., were

[5] See http://youtu.be/F29dnnqIpBI, if the video does not play after a few minutes loading on a standard broadband connection, please try reloading the page.

transient. However, the numbers of the long-standing and the transient radial microfolds formed during each contraction were diminished when the length of the ileal segment was increased relative to that *in vivo*. Conversely, when the length of the segment was decreased relative to that in vivo, the numbers of both long-standing and transient radially orientated microfolds were increased. Longitudinally orientated mucosal microfolds were formed at times when segmentation or peristalsis generated radial narrowing of the lumen, the latter occurring only rarely under the experimental conditions used. At sites where radial and longitudinal contraction occurred concurrently, they intersected to create irregularly dispersed islands of villous crowding (Figure 5-5C).

The video recordings of four excised everted segments of ileum with unstained mucosa showed the same pattern as that which occurred when the mucosa was stained with methylene blue. These patterns were less distinct, but nevertheless recognizable as areas of darker and lighter shade that presumably resulted from crowding and separation of villi due to microfold formation (see 'Microfold Movie2')[6]. Hence, the application of methylene blue appeared to have no effect on mucosal mobility. In addition, there was no significant difference on ANOVA between frequencies of longitudinal muscle contraction before and after eversion (non-everted median 8.7 cpm, inter-quartile range (IQR) 8.7–12.1; everted median 9.1 cpm, IQR 8.8–10 cpm), indicating that the process of eversion did not alter contractile rhythm (Figure 5-4A). The distribution of the villi in the relaxed intestinal wall (mean density 15.8 ± 0.5 villi per mm^2, n = 6; median intervillous distance 162 µm, IQR 181 µm, n = 521) was notable insofar as the median intervillous distance was of the similar length to the mean diameter of the villi.

[6] See http://youtu.be/1-Q5ugAbC6c, if the video does not play after a few minutes loading on a standard broadband connection, please try reloading the page.

5.3.4.2. Modeling

The micro-scale model showed that the cyclic formation of mucosal microfolds noticeably augmented mixing and mass transfer in regions around the villi and mucosa. Molecules of high diffusivity were absorbed principally at the villous tips, whereas those of low diffusivity penetrated further into the intervillous spaces where they were also absorbed (Figure 5-6). Further, the rate of absorption decreased with shortening of the villus length (Figure 5-7), an effect that resulted more from reduction in pulsatile flow about the villi than from reduction in their surface area.

The macro-scale model indicated that the microfolds had little effect on mixing across the width of the lumen. The added effect of villous crowding caused only a slight augmentation of the radial velocity (x 1.3). As the resulting flow was pulsatile with a low Reynolds number (< 50 in the terminal possum ileum), there was only a slight influence of inertia and the flow was quasi-reversible. Hence, the point around which massless particles moved with the fluid travelled about 40 μm in the radial direction, the amplitude of oscillation being around 200 μm.

Plots of the effect of villous crowding on shear rate showed that the maximum radial component of the shear rate when villi were present, 1.6 x 10^{-2}/s, was increased only by a factor of 1.3 compared to that without villi, 1.2 x 10^{-2}/s, a value that is two orders of magnitude lower than that for the maximal longitudinal component for shear rate (1.2/s). Given that shear is responsible for deforming the luminal content, increasing the interfaces between the various elements of fluid and augmenting diffusion between them (de Loubens et al. 2013), this finding indicates that at the macro-scale mixing is generated principally by pendular contraction and not significantly augmented by villous tip crowding.

5.3.5. Discussion

This is the first study to show that short-lived folding of the small intestinal mucosa occurs at a micro-scale synchronous with pendular contractions. Previous theoretical studies have shown that reduction of either the radial or longitudinal dimensions of the outer layers of a two-layered cylindrical structure causes the inner layer to become progressively mechanically unstable and prone to folding (Yang et al. 2007, Moulton and Goriely 2011). Thus, the folding is influenced by the thickness and relative compliance of submucosa and mucosa layers (Yang et al. 2007, Li et al. 2011). Hence, the innermost thin and less compliant mucosal layer 'ruckles' when compressed, while the thicker and more compliant submucosa deforms to accommodate the change (Figure 5-5D).

Our work demonstrates that radial microfolds recur at the same site in successive cycles of longitudinal contraction. This suggests that folding of the mechanically unstable mucosa did not occur at random sites, but was influenced by inhomogeneity at a microscopic level in the mechanical properties of the underlying (submucosal) tissues. In addition, variation in the length of the intestinal lumen as a result of long-standing changes in the tone of longitudinal musculature could influence the number of sites at which such radial mucosal microfolds occur and hence the extent of any associated mixing. Although they were obtained from everted segments of gut, these results are robust. The process of eversion was more likely to reduce the capacity for microfolds to form as the compressive force that normally predominates in the mucosal layer (Gregersen and Kassab 1996, Dou et al. 2006) and is demonstrable when fresh sections of small intestine are cut (Gregersen and Kassab 1996, Gregersen 2003), would be to some extent relieved.

Given the dependence of folding on the state of the mucosa and submucosa, it follows that more extensive local morphological modification may create the conditions necessary for the formation of more longstanding folds, such as plicae circulares Kerkringi (Kopáčová et al. 2010), semilunar or circumferential folds (Junqueira and Carneiro 2005). Again, similar changes resulting from oedema and inflammation (Levine et al. 2008) may promote the formation of more prominent long-standing, or transient, mucosal folding.

The formation of microfolds is dependent on differences in the mechanical behaviour of the mucosa and submucosa from that of the underlying muscle during longitudinal or circular contraction. This difference is manifested by the fact that, on application of increasing longitudinal stretch to postmortem specimens of human small intestine, the mucosa prolapses following annular rupture of the muscular layers and is the last to rupture (Egorov et al. 2002). Hence, our work provides a functional explanation for a phenomenon that has hitherto been attributed to 'mitotic pressure' in the cells of the mucosa (Li et al. 2011).

The finding that the formation and dissolution of microfolds augments intervillous mixing does not exclude the possibility that mixing may be further augmented by 'wavy' or 'whip-like' intrinsic motions of villi, such as are described in a number of early report (Hambleton 1914, King and Arnold 1922). However, we found no evidence, either of individual or of concerted intrinsic motion of villi, in this or in our prior experimental work. It has also been suggested that villous motion could arise extrinsically from tonic or phasic contraction (King and Robinson 1945, Morgan et al. 1985, Uchida and Kamikawa 2007) of smooth muscle situated in the underlying muscularis mucosae (Wang et al. 2010), elements of which are inserted into the bases of villi. Again, we can find no reports of localized patterns of concerted contractions that

are capable of ejecting fluid from a set of contiguous intervillous spaces in a coordinated manner. Moreover, the mechanism demonstrated in our work in which mucosal folding induces such ejection requires no coordinated contraction of sets of villi and hence is more parsimonious. The finding that villous crowding can induce pulsatile flow may account for the lack of a contiguous mobile mucous layer covering the villus and restriction of mucins to islands that are of a similar volume to that secreted by individual goblet cells (Lim et al. 2013). Hence, pulsatile flow may propel such masses into the lumen and thus prevent them uniting in situ by interdigitation of the polymer chains (de Gennes 1971) on adjacent mucin masses.

It is noteworthy that the magnitude of the intervillous space was somewhat larger than that reported (40 μm) in the jejunum of the dog (Levitt et al. 1990), a value that is based on histological material. This greater separation between villi would presumably be accompanied by a correspondingly greater intervillous volume, which may serve to augment peripheral mixing. However, even with this greater distance incorporated into the models, there was little effect on bulk mixing in the lumen.

In conclusion, we were able to demonstrate that compression of the intestinal mucosa, generated by contraction of the muscle layers in the small intestinal wall, created mucosal microfolds that were of similar scale to the attached villi. Simulations showed that changes in the packing densities of the villous tips due to microfold formation cause liquid digesta to be expelled from or drawn into intervillous spaces, and that this process significantly augments peripheral, but not bulk, luminal mixing. This mechanism of inducing peripheral mixing is more parsimonious than one of coordinated contraction of groups of villi, i.e., requires fewer synchronizing components to function.

5.3.6. Journal article references

Brasseur, J. G., G. Banco, A. C. Ailiani, Y. Wang, T. Neuberger, N. B. Smith and A. G. Webb (2009) Motility and absorption in the small intestines: Integrating MRI with lattice Boltzmann models; Boston, MA.

Canto, M. I. F., S. Setrakian, R. E. Petras, E. Blades, A. Chak and M. V. Sivak-Jr (1996) Methylene blue selectively stains intestinal metaplasia in Barrett's esophagus. Gastrointestinal Endoscopy **44**: 1–7.

Chang, E. B. and M. C. Rao (1994) Intestinal water and electrolyte transport: mechanisms of physiological and adaptive responses. In: Johnson LR, ed. Physiology of the Gastrointestinal Tract. New York: Raven Press. 2027–2081.

de Gennes, P. G. (1971) Reptation of a polymer chain in the presence of fixed obstacles. The Journal of Chemical Physics **55**: 572–579.

de Loubens, C., R. G. Lentle, R. J. Love, C. Hulls and P. W. M. Janssen (2013) Fluid mechanical consequences of pendular activity, segmentation, and pyloric outflow in the proximal duodenum of the rat and the guinea pig. Journal of the Royal Society Interface **10**: 20130027.

Dou, Y., J. Zhao and H. Gregersen (2003) Morphology and stress-strain properties along the small intestine in the rat. Journal of Biomechanical Engineering **125**: 266.

Dou, Y., Y. Fan, J. Zhao and H. Gregersen (2006) Longitudinal residual strain and stress strain relationship in rat small intestine. Biomedical Engineering Online **5**: 37.

Egorov, V. I., I. W. Schastlivtsev, E. V. Prut, A. O. Baranov and R. A. Turusov (2002) Mechanical properties of the human gastrointestinal tract. Journal of Biomechanics **35**:1417–1425.

Gregersen, H. (2003) Biomechanics of the Gastrointestinal Tract: New Perspectives in Motility Research and Diagnostics. New York: Springer Verlag.

Gregersen, H. and G. Kassab (1996) Biomechanics of the gastrointestinal tract. Neurogastroenterology & Motility **8**: 277–297.

Gwynne, R. M., E. A. Thomas, S. M. Goh, H. Sjovall and J. C. Bornstein (2004) Segmentation induced by intraluminal fatty acid in isolated guinea-pig duodenum and jejunum. Journal of Physiology **556**: 557–69.

Hambleton, B. F. (1914) Note upon the movements of the intestinal villi. American Journal of Physiology **34**: 446–447.

Janssen, P. W. M., R. G. Lentle, C. Hulls, V. Ravindran and A. M. Amerah (2009) Spatiotemporal mapping of the motility of the isolated chicken caecum. Journal of Comparative Physiology B **179**: 593–604.

Janssen, P. W. M., R. G. Lentle, P. Asvarujanon, P. Chambers, K. J. Stafford and Y. Hemar (2007) Characterisation of flow and mixing regimes within the ileum of

the brushtail possum using residence time distribution analysis with simultaneous spatio-temporal mapping. Journal of Physiology **582**: 1239–1248.

Jumars, P. A. (2000) Animal guts as non-ideal chemical reactors: partial mixing and axial variation in absorption kinetics. The American Naturalist **155**: 544–55.

Junqueira, L. C. and J. Carneiro (2005) Basic Histology: Text and Atlas, 11th edn. New York: McGraw-Hill.

King, C. E. and L. Arnold (1922) The activities of the intestinal mucosal motor mechanism. American Journal of Physiology **59**: 23.

King, C. E. and M. H. Robinson (1945) The nervous mechanisms of the muscularis mucosae. American Journal of Physiology **143**:325–335.

Kopáčová, M., I. Tachecí, J. Květina, J. Bureš, M. Kuneš, S. Špelda, V. Tyčová, Z. Svoboda and S. Rejchrt (2010) Wireless video capsule enteroscopy in preclinical studies: methodical design of its applicability in experimental pigs. Digestive Diseases and Sciences **55**: 626–630.

Lentle, R. G., C. de Loubens, C. Hulls, P. W. M. Janssen, M. D. Golding and P. Chambers (2012) Organization of longitudinal and circular contractions during pendular and segmental activity; a comparison of duodenal contractile activity in the rat and guinea pig. Neurogastroenterology & Motility **24**:686–e298.

Lentle, R. G., P. W. M. Janssen, P. Asvarujanon, P. Chambers, K. J. Stafford and Y. Hemar (2007) High definition mapping of circular and longitudinal motility in the terminal ileum of the brushtail possum (*Trichosurus vulpecula*) with watery and viscous perfusates. Journal of Comparative Physiology B **177**: 543–556.

Levine, M. S.,S. E. Rubesin and I. Laufer (2008) Pattern approach for diseases of mesenteric small bowel on barium studies. Radiology **249**: 445–460.

Levitt, M. D., A. Strocchi and D. G. Levitt (1992) Human jejunal unstirred layer: evidence for extremely efficient luminal stirring. American Journal of Physiology **262**:G593–G596.

Levitt, M. D., J. K. Furne, A. Strocchi, B. W. Anderson and D. G. Levitt (1990) Physiological measurements of luminal stirring in the dog and human small bowel. Journal of Clinical Investigation **86**: 1540–1547.

Li, B., Y-P. Cao, X-Q. Feng and H. Gao (2011) Surface wrinkling of mucosa induced by volumetric growth: theory, simulation and experiment. Journal of the Mechanics and Physics of Solids **59**: 758–774.

Lim, Y. F., M. A. K. Williams, R. G. Lentle, P.W.M. Janssen, B. W. Mansel, S. A. J. Keen and P. Chambers (2013) An exploration of the microrheological environment around the distal ileal villi and proximal colonic mucosa of the possum (*Trichosurus vulpecula*). Journal of the Royal Society Interface **10**:20121008.

Mailman, D., W. A. Womack, P. R. Kvietys and D. N. Granger (1990) Villous motility and unstirred water layers in canine intestine. American Journal of Physiology **258**:G238–G246.

Morgan, K. G., F. Angel, P. F. Schmalz and J. H. Szurszewski (1985) Intracellular electrical activity of muscularis mucosae of the dog stomach. American Journal of Physiology **249**: G256–G263.

Moulton, D. E. and A. Goriely (2011) Circumferential buckling instability of a growing cylindrical tube. Journal of the Mechanics and Physics of Solids **59**: 525–537.

Penry, D. L. and P. A. Jumars (1987) Modeling animal guts as chemical reactors. The American Naturalist **129**: 69–96.

Sarna, S. K. (1985) Cyclic motor activity; migrating motor complex. Gastroenterology **89**: 894–913.

Strocchi, A. and M. D. Levitt (1993) Role of villous surface area in absorption science versus religion. Digestive Diseases and Sciences **38**:385–387.

Uchida, K. and Y. Kamikawa (2007) Muscularis mucosae - the forgotten sibling. Journal of Smooth Muscle Research **43**: 157–177.

Wang, Y., J. G. Brasseur, G. G. Banco, A. G. Webb, A. C. Ailiani and T. Neuberger (2010) A multiscale lattice Boltzmann model of macro- to micro-scale transport, with applications to gut function. Philosophical Transactions of the Royal Society Series B; Mathematical, Physical and Engineering Sciences **368**: 2863–2880.

Womack, W. A., P. K. Tygart, D. Mailman, P. R. Kvietys and D. N. Granger (1988) Villous motility: relationship to lymph flow and blood flow in the dog jejunum. Gastroenterology **94**: 977–983.

Yang, W., T. C. Fung, K. S. Chian and C. K. Chong (2007) Instability of the two-layered thick-walled esophageal model under the external pressure and circular outer boundary condition. Journal of Biomechanics **40**: 481–490.

5.3.7. Journal article figures and tables

Figure 5-3: Staining of villous tips following application and elution of methylene blue.

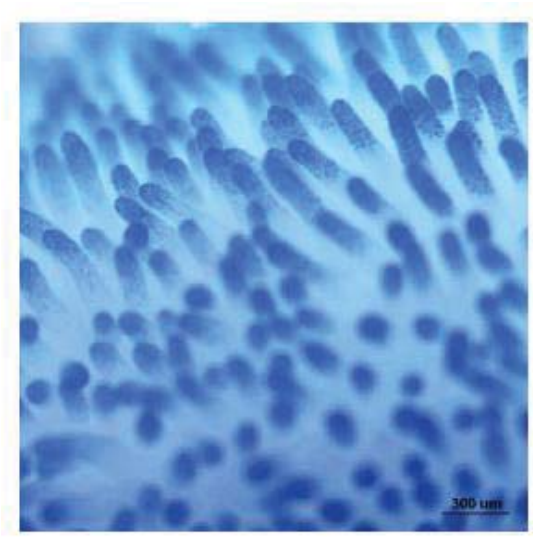

Figure 5-4: Spatiotemporal maps of pendular activity in the terminal ileum of the possum. A) Longitudinal strain rate maps prior to (upper) and after eversion (lower). Yellow and blue signify shortening and lengthening, respectively. The shallow slopes of the colored areas show that the regular phasic contractions in the longitudinal muscle layer are propagating aborally. (B) Map of image intensity in which darker regions indicate areas of apical villous crowding. A succession of dark bands forms between successive microfolds during longitudinal contractions (arrowed) and disperse during relaxation. These bands form at the same site during successive contractions. The two thicker, darker bands that are evident throughout the contraction relaxation cycle are from more permanent folds.

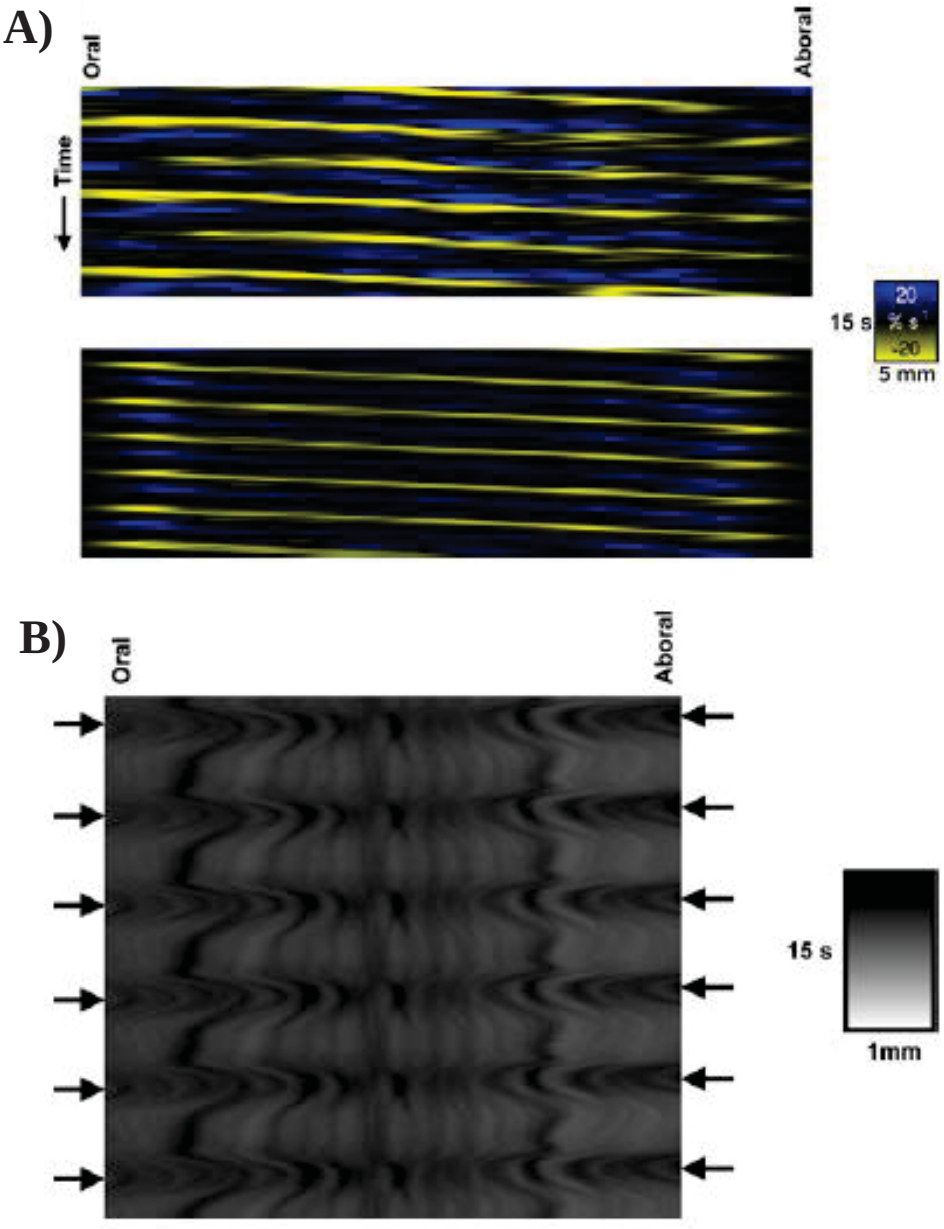

Figure 5-5: Everted mucosal surface of ileum at rest (A), and during a longitudinal (B), and a simultaneous longitudinal and circular (C) contraction. Radially orientated areas of apical crowding can be seen to develop between lighter areas on the crests of microfolds at the site (right) of longitudinal shortening (B). At sites of radial narrowing (C left), the regular radial pattern is interrupted by longitudinally orientated areas of apical crowding (C). (D) Schematic figure showing development of microfolds and associated apical crowding.

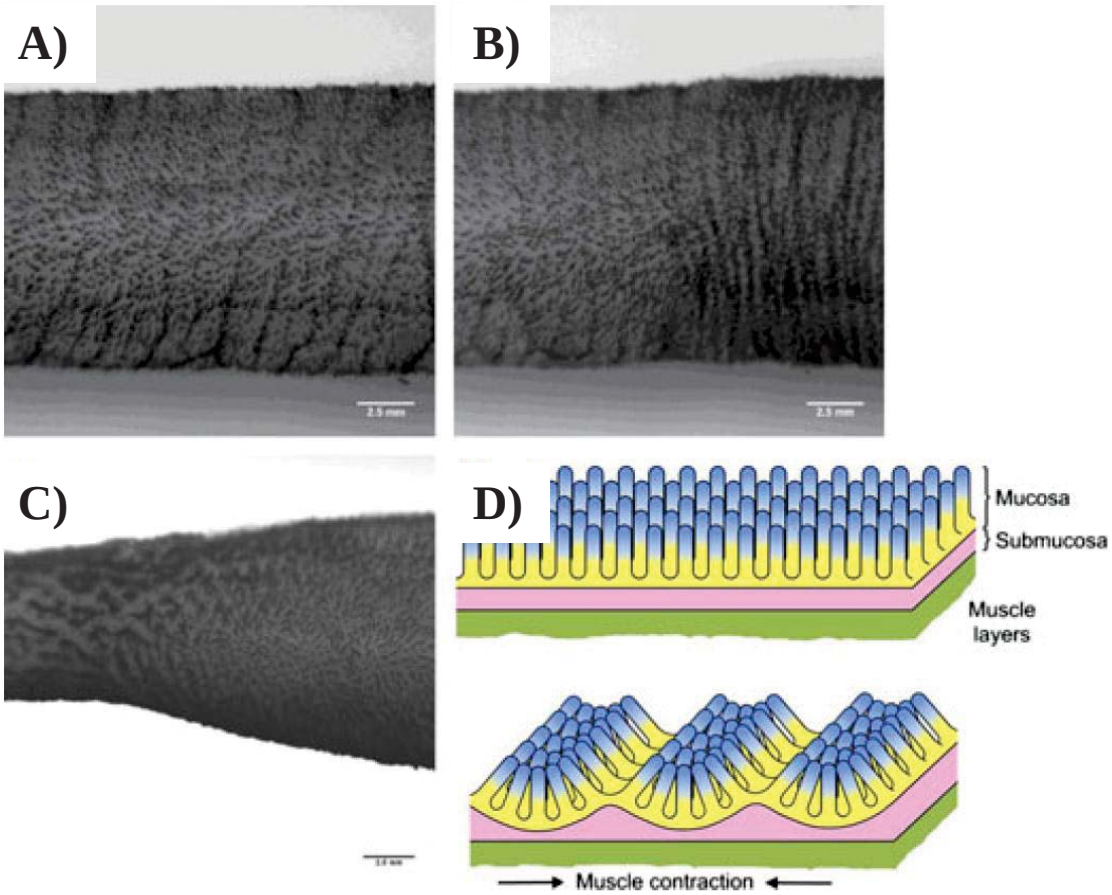

Figure 5-6: Micro-scale simulation of the effect of villous apical crowding on velocity and mixing adjacent to the mucosa during a complete pendular contraction cycle*. (A) Velocity plots show alternating flow between the intervillous spaces and the surrounding fluid. Concentration plots show that greater quantities of nutrient molecules of high diffusivity (B) are absorbed at the villous tips than are those of lower diffusivity (C).

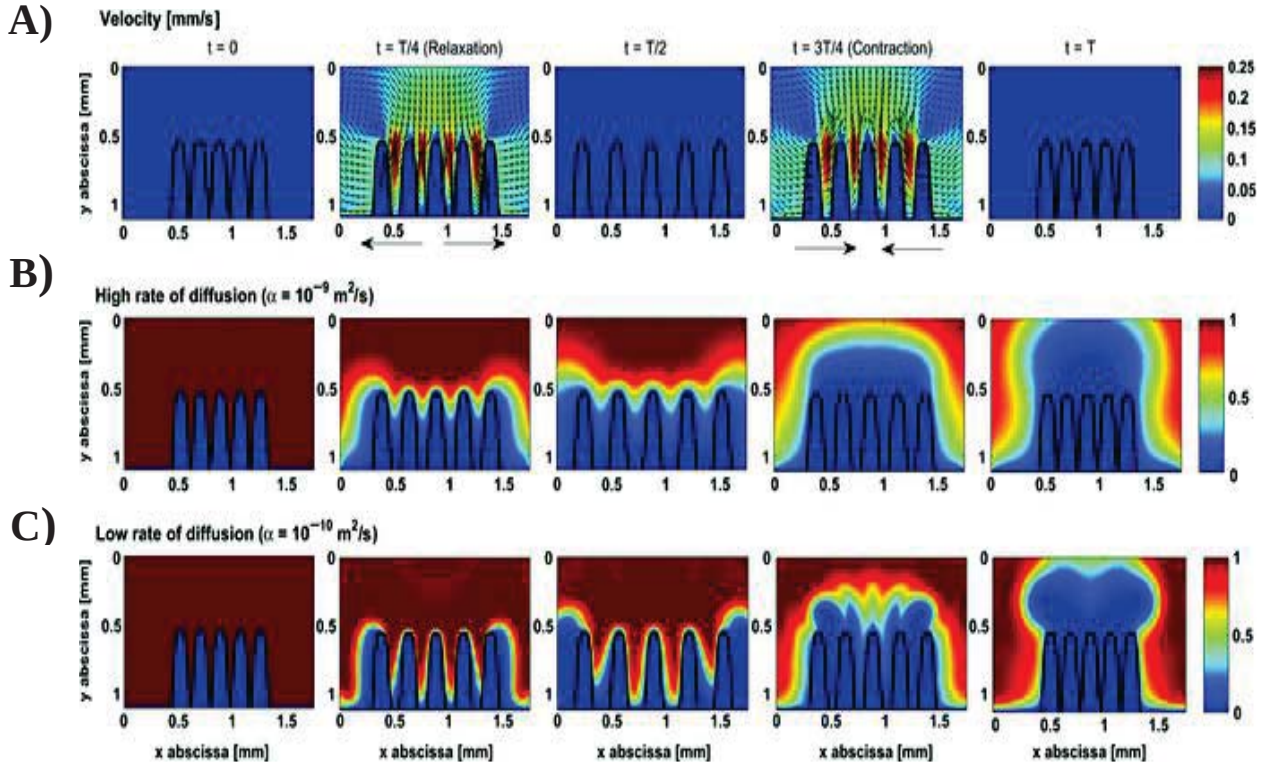

***A larger view of the figure is reproduce in the adjacent page.**

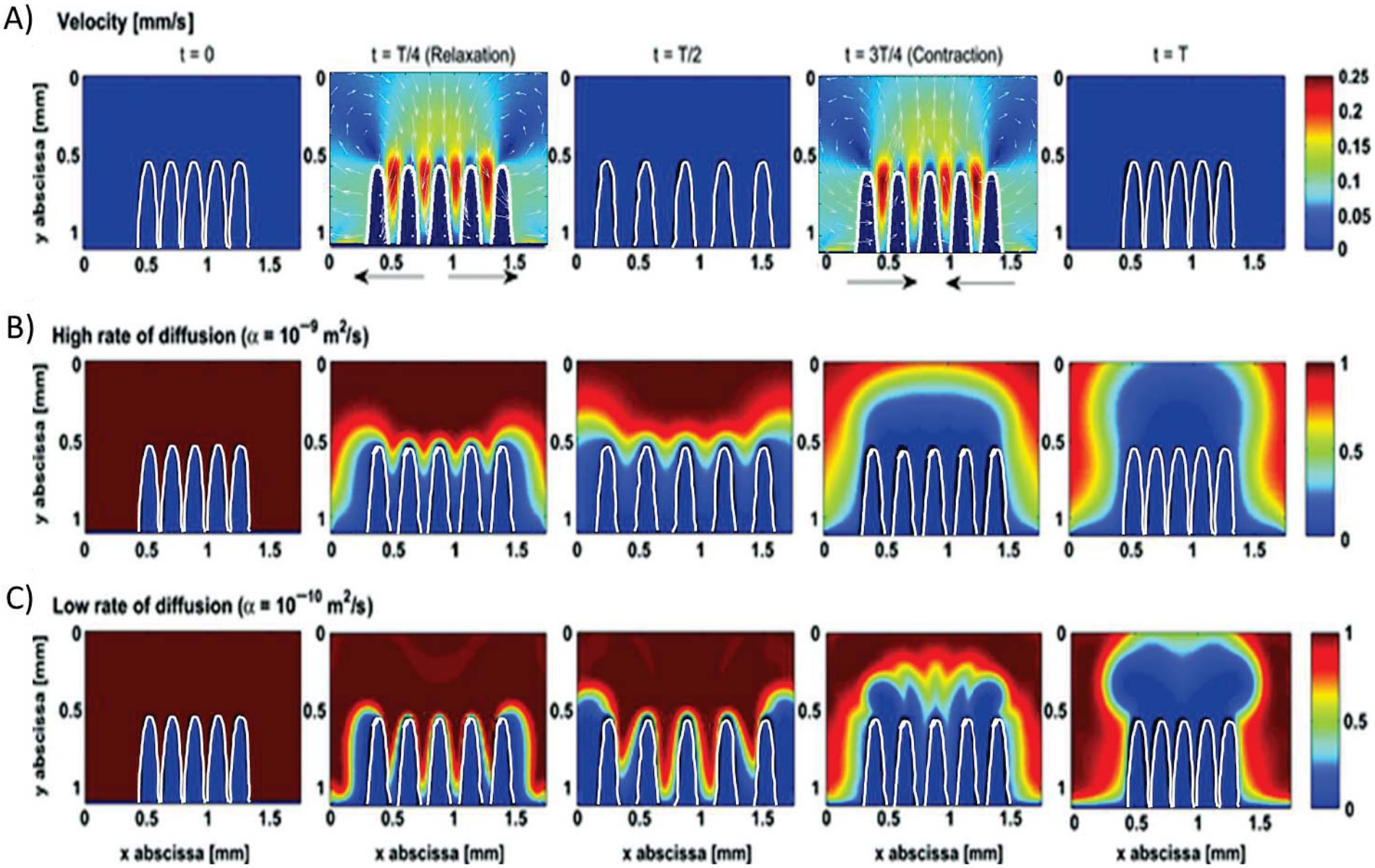
A) Velocity [mm/s]
t = 0
t = T/4 (Relaxation)
t = T/2
t = 3T/4 (Contraction)
t = T
y abscissa [mm]
0.25
0.2
0.15
0.1
0.05
0
B) High rate of diffusion (α = 10^−9 m^2/s)
1
0.5
0
C) Low rate of diffusion (α = 10^−10 m^2/s)
x abscissa [mm]

Figure 5-7: Simulated effect of villous length and molecular diffusivity on the absorption rate of readily absorbed compounds.

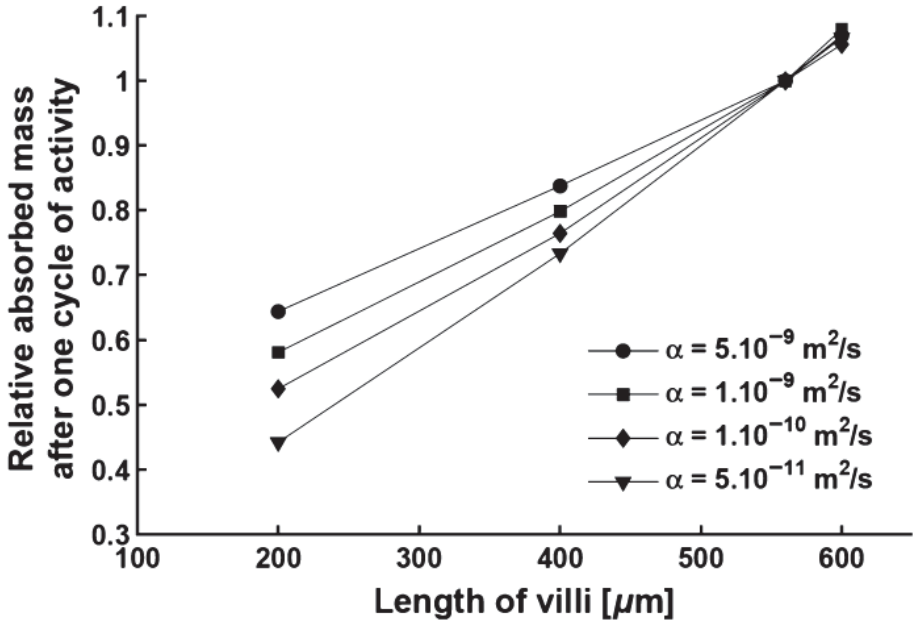

5.3.8. Journal article supplementary figures

Figure 5-8: Macro-scale simulation of the effect of villi on radial velocity and shear rate across the lumen. The simulation was run for a 40 s period using experimental data derived from spatiotemporal maps of propagating longitudinal contractions in the terminal ileum of the possum.

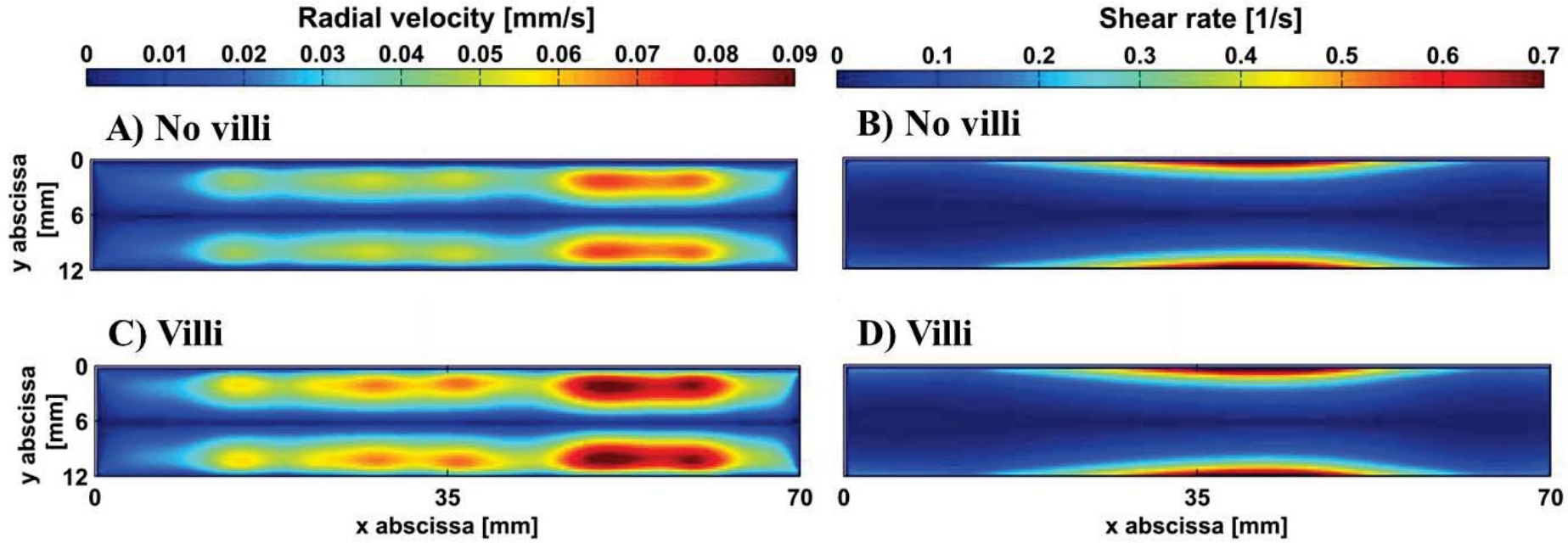

5.4. Journal article supporting information

This section describes the development and features of the computational model in more detail than was published in the peer-reviewed paper (Lentle et al. 2013). The influence of villous apical crowding (caused by mucosal microfolding during non-propagating pendular contractions) on mass transfer, nutrient absorption and mixing was analysed by two models. The first model focused on the mass transfer and mechanisms of absorption at the scale of a group of a few villi (~0.5 mm). The second focused on the consequences of apical villous crowding on flow and mixing at the scale of the small intestine lumen (~10 mm). Both models were numerically solved by lattice Boltzmann modelling (LBM) in two-dimensions (2D), a technique described in more detail in chapter four of this thesis.

5.4.1. Modelling strategy at the villous scale

The micro-scale model described in this chapter was an extension of the work detailed in chapter four, which was adapted to include the new experimental findings from Lentle et al. (2013). The objective of the micro-scale model was to evaluate the augmentation of flow in regions adjacent to the mucosa generated by the villous apical crowding during non-propagating pendular contractions.

5.4.1.1. Villous profile

Villi were assumed to be static and rigid structures for these simulations. Again, villi could conceivably be flaccid structures (i.e. low stiffness) with shafts that were prone to bend with their movements independent of the movements of the underlying mucosa. However, it is likely that the resulting mechanism of luminal mixing would be less effective. Any movement of the underlying mucosa would not translate to an equivalent

movement of the villi to advect fluid given that the drag forces applied onto the flaccid villi by the fluid would overcome the stiffness of the villi.

The villi in these simulations were described by a polynomial of degree 4 as was done in the models described in chapter four. This shape was consistent with the shape of possum ileal villi observed on gut segments maintained *ex vivo* during experimental work outlined in Lentle et al. (2013) and was similar to the shape of rat ileal villi observed in chapter four.

5.4.1.2. Villous dimensions and intervillous spacing

The villous dimensions (length = 560 μm and width = 160 μm) and intervillous spacing (160 μm) were determined from experimental observations of possum ileal villi (Lentle et al. 2013) (Table 1). It is noteworthy that the intervillous space used in the model described in this chapter was larger (up to four times) than the spacing size used in the model described in chapter four. It is possible that the size differences may be due to the differences in the species of the animal of which the observations were derived. However, it is more likely that the smaller intervillous spacing observed in the rat (chapter four) was due to the fact that the gut sample of which observations were derived from was no longer viable with further shrinking due to the loss of muscle tone that was unaccounted for. It was important to use the most accurate intervillous spacing size as different spacing size would likely result in varying fluid mechanical consequences – the findings of chapter four indicate that a larger intervillous space would increase the magnitude of radial velocities and hence the magnitude of advective mass transfer.

5.4.1.3. Villous movement

Apical villous crowding comprises the congregation and subsequent separation of arrays of villous tips. The actual movement of the villi is complex, and hence, some simplifications have been implemented to reduce the complexity of the problem and the computational load. In particular, the computational domain was reduced to two-dimensions (2D) and the small number of villi simulated (e.g. 5 villi) with movement only in the longitudinal direction (Figure 5-9). These simplifications preserved the main characteristics of the movement of the villi (i.e. grouping and separation) and make the model more computationally tractable. The group of villi were studied in an 'infinite space' (i.e. the model boundaries are far enough from the villi that they do not impact on the velocity flow fields in the perivillous region) in order to prevent any boundary effects affecting the flow near the villi.

While these simplifications do preserve the main characteristics of the movement and disposition of villi, the conditions simulated is still 'unphysiological' to a degree that actual flow patterns and impact of villous apical crowding on mass transfer is not predicted. It is likely that the extent of mass transfer predicted may be over-estimated given that the experimentally observed consequence of mucosal microfolding was villous apical crowding rather than the simulated crowding of whole lengths of villi.

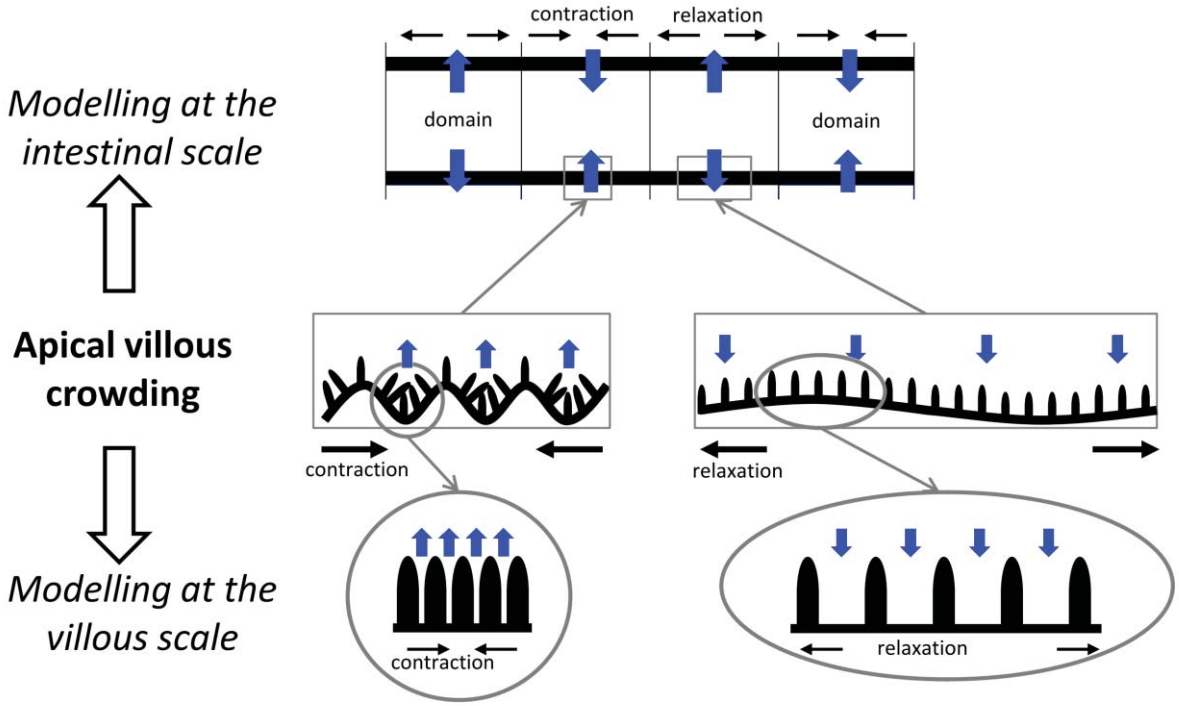

Figure 5-9: Overview of geometry used in both micro- and macro-scale simulations.

The strain in the longitudinal direction ε was defined by $\Delta L/L$, where L is the length of a segment of muscle and ΔL is its change of length due to muscle contraction. The cyclic variation of the longitudinal strain rate $\dot{\varepsilon}$ ($\partial\varepsilon/\partial t$), i.e. the rate of local lengthening (if $\dot{\varepsilon} < 0$) or shortening (if $\dot{\varepsilon} > 0$), was represented by a sinusoidal function:

$$\dot{\varepsilon}(Y,t) = \dot{\varepsilon}_{max} sin\left(\frac{2\pi}{T}t\right)(X - X_0) \quad (5.1)$$

where $\dot{\varepsilon}_{max}$ is the amplitude of strain rate (%s^{-1}), t is the time (s) and T is the period of the longitudinal contraction (s). X (µm) is the longitudinal abscissa while X_0 (µm) is the position in the middle of the spatial domain of contraction (see chapter four, sub-section 4.4.3.1). This equation of the longitudinal strain rate is a similar equation as was used in the work detailed in chapter four of this thesis and in de Loubens et al. (2013) but adapted to allow the simulation of a few villi in 'infinite space' (i.e. the model boundaries are far enough from the villi that they would not impact on the velocity flow

fields in the perivillous region). The longitudinal velocities of the villi were calculated by the integration of the longitudinal strain rate $\dot{\varepsilon}$ (%s^{-1}). Thus relaxation and contraction occurs during the time intervals of 0 to T/2 and T/2 to T respectively.

5.4.1.4. Simulation strategies of advective mass transfer

Advection of diffusive tracers was modelled using the advection-diffusion equations (ADE) with a constant diffusion coefficient α (m^2/s) in order to assess the influence of villous apical crowding on the absorption of nutrients and mass transfer. Absorption was considered to be entirely passive and not constrained by epithelial permeability (i.e. the tracer is instantaneously absorbed when it reaches the mucosa). At the initial time of the simulation (T = 0), the concentration of the tracer was homogeneous in the flow domain (i.e. perivillous region). The total absorbed mass of tracer between the tips of the two outermost villi was calculated during one cycle of contraction.

5.4.2. Modelling strategies at the Intestinal Scale

The strategy of the macro-scale modelling was an extension of previous work (de Loubens et al. 2013) where real motility data were used as boundary conditions. The terminal ileum was modelled as a segment of tube with no radial velocity components or pressures at the oral and aboral ends. Considering the presence of individual villi in a model at the intestinal scale explicitly would be very computationally demanding. Hence the influence of villous apical crowding at the macro-scale flow was modelled by the introduction of a radial velocity at the gut wall. Thus during a contraction, the grouping of villi generates a radial flow from the wall into the lumen and during a relaxation the flow is reversed. With the assumption that villi are rigid and remain straight, the radial velocity u_{vf} (m/s) of fluid exiting from the space between two neighbouring villi can be calculated by considering the conservation of mass:

$$u_{vf} = -\dot{\varepsilon} h_{vil} \tag{5.2}$$

where h_{vil} is the villi length (m) and $\dot{\varepsilon}$ is the strain rate (s^{-1}). Knowing the spatiotemporal evolution of the strain rate, the radial velocity can be calculated as a function of time and location. However, to obtain a mean radial velocity value, a correction must be included to account for the portion of the intestinal length L that is covered by N villi of diameter d, which do not generate any radial flow. Therefore:

$$u_{vf}(x,t) = -\dot{\varepsilon}(x,t) l \frac{L-Nd}{L} \tag{5.3}$$

The strain rate $\dot{\varepsilon}(x,t)$ input to the simulation was derived from a 40 second portion of the 'real-time' longitudinal strain rate map determined in a non-everted segment of the terminal ileum of the possum. The pressure and velocity field was zero at the commencement of the simulation.

The extent to which deformations in the flow of the luminal contents increased the interfacial areas between different solutes of the luminal contents (e.g. enzymes and nutrients), which improves the diffusion process between them was also examined (de Loubens et al. 2013). The parameter of interest in this case was the shear rate component of the strain rate tensor noted $\dot{\gamma}$ (s^{-1}):

$$\dot{\gamma} = \frac{1}{2}\left(\frac{\partial u}{\partial y} + \frac{\partial v}{\partial x}\right) \tag{5.4}$$

where u and v are the axial and radial velocity; respectively. The radial $\left(\frac{\partial v}{\partial x}\right)$ and axial $\left(\frac{\partial u}{\partial y}\right)$ components of the shear rate were also compared to determine the direction in which mixing was promoted. The absolute values of the radial velocity and the shear rate were averaged for each location over 40 seconds. The displacement of 200 small

massless particles, which were spaced regularly within the lumen, was calculated so as to assess the extent to which contained material was advected by the flow field.

5.4.3. Lattice-Boltzmann methods

The following features of the Lattice Boltzmann model outlined in this chapter were similar to that detailed in chapter four of this thesis: The NSE were solved using the methods of the Guo et al. (2000) variant of Lattice Bhatnagar-Gross-Krook (LBGK) collision method while for the villous scale model, the moving boundary conditions imposed by villi were calculated using the bounce-back boundary scheme (Sukop and Thorne 2007) with spatial interpolations for additional accuracy of delineating the non-regular boundaries of villi (Bouzaidi et al. 2001; Lallemand and Luo 2003). In addition, to describe the advection and diffusion of a solute tracer, the ADE were also solved by one particular member of the family of 2D advection-diffusion LBM algorithms described by Ginzburg (2005) called ‘optimal advection’.

The oral and aboral pressure and velocity conditions of the model at the villous scale were modelled by the methods of Guo et al. (2002). The implementation of such boundary conditions with LBGK schemes was reported to be second-order numerically accurate and also numerically stable for the relaxation parameters (see chapter four for description) used in the models described in this chapter.

The following features were unique to the models described in this chapter: The perivillous region was modelled in an ‘infinite space’. As such, the simulation layout was different to the model described in chapter four of this thesis that required the use of symmetry boundaries on the oral and aboral ends of the model. To measure effect of villous apical crowding on advective and diffusive mass transfer of a solute tracer, the villi were designated to instantaneously absorb the solute tracer when it reached the

villous mucosa (Lentle et al. 2013). This was done by the implementation of the Dirichlet boundary conditions (Huang et al. 2011) around the villi through a spatial interpolation (Bouzaidi et al. 2001) of the equilibrium distribution function.

In order to simulate the flow generated by villous apical crowding in an infinite space ('modelling at the villous scale'), two grids were used (Figure 5-10). The information communication and reconstruction at grid transitions was done using the coupling algorithms of Dupuis and Chopard (2003) and Stiebler et al. (2008) for the NSE and the ADE respectively. The final code was validated using different benchmarks, e.g. Poiseuille and Couette flow, and Taylor dispersion.

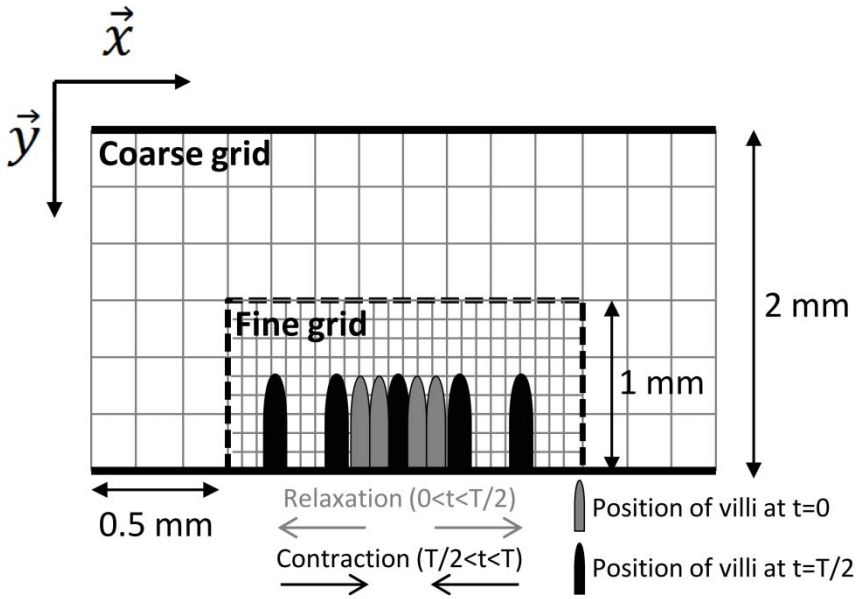

Figure 5-10: Coarse and fine grid dimensions used in the villous micro-scale simulation

5.4.4. Use of physiological and numerical parameters in simulations

The physiological parameters used in this work came from previous work or were specifically measured as required for this study (Table 5-1). Preliminary tests were done to choose the different numerical parameters of the models. To obtain a sufficiently high degree of computational accuracy, the radius of the ileum and the maximal width of villi

were meshed with 40 and 16 cells respectively. For the villous scale model using two LBM nodes of different sizes, the ratio of the size of the fine grid to the size of the coarse grid was 3 (Figure 5-10). The comparison of the flow generated by groups of villi of different numbers has shown that 5 villi were enough to obtain representative results. The height of the fine grid was two times the length of a villus (i.e. 1 mm).

Parameters	**Value**	**Reference**
Strain rate amplitude ($\dot{\varepsilon}_{max}$)	20 % s^{-1}	(Lentle et al. 2007)
Period of longitudinal activity (T)	6.66 s	(Lentle et al. 2007)
Dynamic viscosity (μ)	1.5 mPa.s	(Lim et al. 2013)
Length of villi (h_{vil})	560 μm	(Lentle et al. 2013)
Half width of villi (R_{vil})	80 μm	(Lentle et al. 2013)
Intervillous space	160 μm	(Lentle et al. 2013)

Table 5-1: Physiological parameters used for modelling at the villous scale.

5.5. Chapter conclusion

A novel mechanism that exists on the terminal ileum of the possum at least, has been detailed and its effects on mixing and mass transfer of perivillous luminal contents predicted using LBM in this chapter. However, the findings of this chapter were site specific for one particular type of animal. Given that different sites of the small intestine of the same species are of different size (e.g. the duodenum and jejunum typically larger in diameter than the ileum) (Levine et al. 2008) and subject to varying conditions (e.g. pH) (Daniel et al. 1989), it is likely that the mechanisms highlighted in this chapter may have different dynamics and dimensions or even not be available across the different sites.

The discussions in this chapter have predominantly considered the dynamics and contributions to mixing and mass transfer of radially oriented short-lived mucosal microfolding during non-propagating pendular contractions. However, longitudinally oriented short-lived mucosal microfolding have also been observed during gut wall radial contractions (e.g. from either segmentative- and peristaltic- like contractions). As demonstrated in Figure 5-11 below, it is likely that both types of mucosal microfolding may result in variations in the way perivillous mass transfer is augmented. The flow of digesta may likely affect only the upper regions of villi especially in the concavities of radially oriented mucosal microfolds (Figure 5-11A) – mass transfer in the upper intervillous regions being augmented by the formation of vortexes behind villi.

Conversely, it is likely that longitudinally oriented mucosal microfolds may promote the flow of digesta to all of the intervillous regions hence augmenting mass transfer even at the villi basses (Figure 5-11B). Given that all three postprandial gut motility patterns have been observed in a given animal (e.g. the brushtail possum) (Lentle et al. 2013), a

possible corollary of all this findings is that all three motility patterns may occur intermittently to augment perivillous mixing according to the local needs at a given point in time.

Overall, more studies would be needed to assess the existence of mucosal microfolding in other species or in different parts of the small intestine for a given animal as well as the dynamics of both types of microfolding.

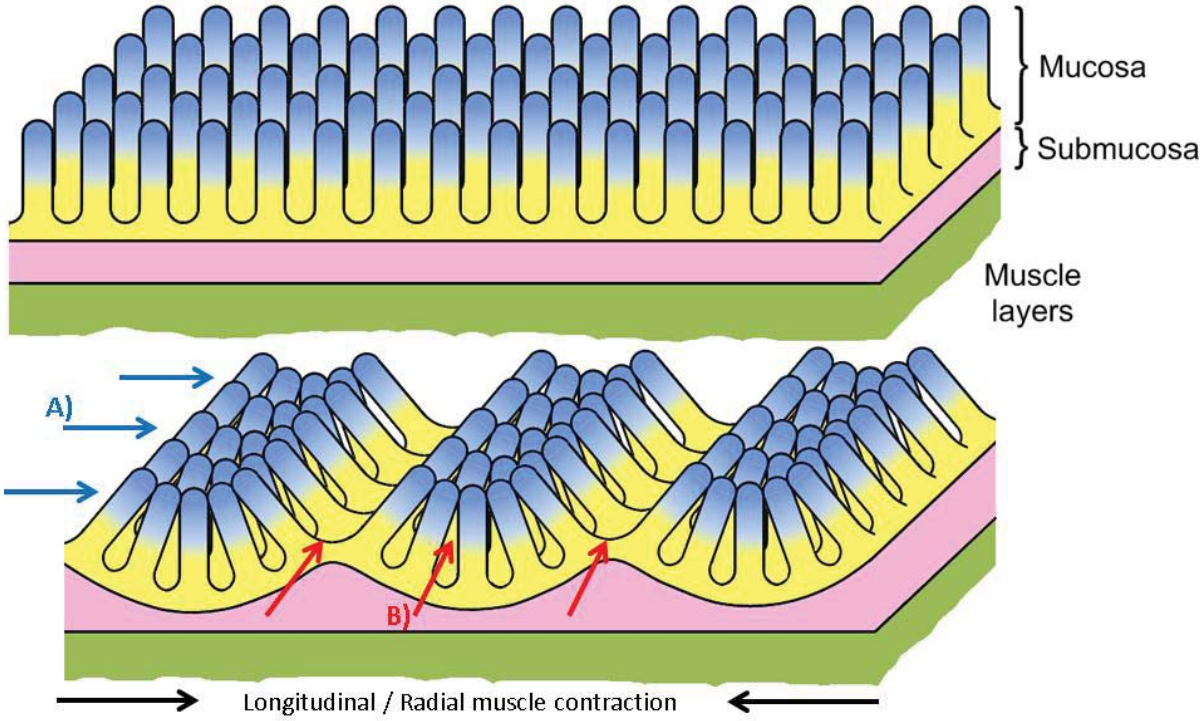

Figure 5-11: Contact and access locations of perivillous digesta flow during both axial and radially oriented mucosal microfolds. Digesta flow is always in the same direction (i.e. regardless of whether it is blue or red arrows, flow direction is always from the oral to aboral end of the gut) in the two situations depicted. The only difference in the two situations is in the orientation of mucosal microfolds formed during digesta flow. In situation A), villous apical crowding caused by non-propagating pendular contractions would likely result in digesta flow (blue arrows) encountering the upper section of villi especially villi in the concavity of the mucosal microfolds formed. In situation B), villous apical crowding caused by segmentative- or peristaltic- like gut wall contractions would likely result in digesta flow (red arrows) and its mass transfer and mixing being promoted in all regions of the intervillous space (adapted from Lentle et al. (2013)).

Chapter Six -

Passive mechanical properties of villi

6.1. Foreword

This chapter details studies on the flow patterns around and of the rigidity of villi at physiological levels of flow in the gut lumen. Firstly, a review of the methodology used by other workers in this field is presented. This is followed by information on the design of the experimental apparatus used in this study as well as a discussion of the experimental work and results that form a published peer-reviewed research article. Subsequently, the development of a computational model of flow around an infinite array of villi is detailed. Finally, additional methodology, results and discussions not included in the main text of the research article are provided.

6.1.1. Background and justification of experimental techniques used

To date, there has been no work conducted with the explicit purpose of determining the rigidity of villi. Published works purporting a role for villi in the process of intestinal mixing and mass transfer have assumed that villi are rigid structures (Wang et al. 2010; Takahashi 2011).

Other earlier published works also had the implied notion that villi are rigid structures and that they would pivot during lumen flow by the flexibility at the junction of the villous shafts and the underlying mucosa. Guldner et al. (1972) observed that smooth muscle fibres were aligned along the long axis of villi, perpendicular to the underlying mucosa. They also observed that smooth muscle fibres were denser at the villous base and were progressively less dense towards the villous tip. This suggests that villi are structures that have developed the capacity for pivoting (i.e. movement at the junction between villi and the underlying mucosa). In addition, the rigidity of villous shafts was also implied by works of Hosoyamada and Sakai (2005, 2007) who postulated that smooth muscles may act as intravillous scaffolds that maintains the integrity of the

shape of villi against osmotic pressures of fluid being absorbed into villi. Furthermore, the observed turgidity of interstitial tissue as a result of fluid absorption into villi is also evidence for the rigidity of villi (Westergaard and Dietschy 1974).

While the aforementioned works provide strong circumstantial evidence for the rigidity of villi, the actual response of villi to shear stress by the flow of luminal contents remains to be determined. Hence there is a need to determine the response of villi to shear stress during lumen flow. In addition, the influence of such phenomenon on intervillous space flow patterns would also be investigated given that there have been very few studies conducted for the said purpose.

6.1.1.1. Determination of flow velocity in the perivillous space

From the background provided in the prior sub-section, it is clear that there have so far been no studies conducted to determine the passive mechanical properties of living villi (i.e. villous rigidity). The work outlined in the following sections of this chapter outlines work done to determine the rigidity of and flow patterns around villi on an *ex vivo* maintained specimen of small intestine. Two techniques were considered for use in the calculation of flow velocity patterns in the perivillous region. The first was the utilization of the Polyparticletracker algorithm (Rogers et al. 2007), the same algorithm used in the study of the microrheology of the fluid environment in the perivillous space (chapter three). However it was found that Polyparticletracker was only able to accurately determine the velocity of fluid flow at flowrates of less than 0.4ml/min. This technique could not accurately determine the velocity of microbeads at higher perfusion rates possibly due to the inability of the Polyparticletracker particle linking algorithm to reliably map the movement microbeads at higher displacements. This was likely to be

due to microbeads being displaced by distances greater than the radius of the microbead itself across consecutive images (Rogers et al. 2007) at flowrates exceeding 0.4ml/min.

The second technique used to determine the velocity of flow in the pervillous space was known as PIVLab (Thielicke and Stamhuis 2013), which also required the use of microbeads to facilitate the delineation of the velocity of flow around villi. This technique determined the trajectories of microbeads by a method known as particle image velocimetry (PIV) (this method is described in more detail in the accompanying paper) and functioned by cross-correlating the average motion of particles in flow over successive images (Thielicke and Stamhuis 2014). Such a technique was able to accurately determine the velocity of the flow for all the perfusion rates used in the work described in this chapter (see section 6.2).

Conversely, the techniques used to determine villous rigidity were developed 'in-house' and will be detailed in the accompanying paper in the following sections. The following section outlines the supplementary methods and design of the equipment used to determine villous rigidity and flow velocities in the perivillous space.

6.2. Supplementary methods and design of the equipment used

A tissue flow cell was constructed that would allow villous rigidity to be determined at physiological (2 to 12.2 $ml.m^{-1}$) (Grovum and Williams 1973; Bueno et al. 1975) and supraphysiological perfusion rates (up to 3 times the upper physiological rate). The flow cell was designed to fulfill the following requirements;

A) The tissue flow cell was able to maintain a living sample of gut wall tissue.

B) The flow cell allowed the introduction of fluid flow at physiological and supraphysiological perfusion rates.

C) The flow cell could be positioned in the focal plane of an inverted microscope with enough focal length (i.e. microscope objective working distance) to visualize villi within it, as well as determine fluid flow patterns and velocities in the perivillous space.

D) The flow cell probe allowed sufficient tension to be introduced onto the mounted gut tissue so that the underlying mucosa will not move in relation to the flow. This allowed the rigidity of an individual villus to be determined in response to lumen flow.

6.2.1. Tissue flow cell design

A complete diagram of the tissue flow cell is provided in the peer-reviewed journal article presented in section 6.3 of this chapter as Figure 6-11 and a photograph of it is presented below (Figure 6-1).

A)

B)

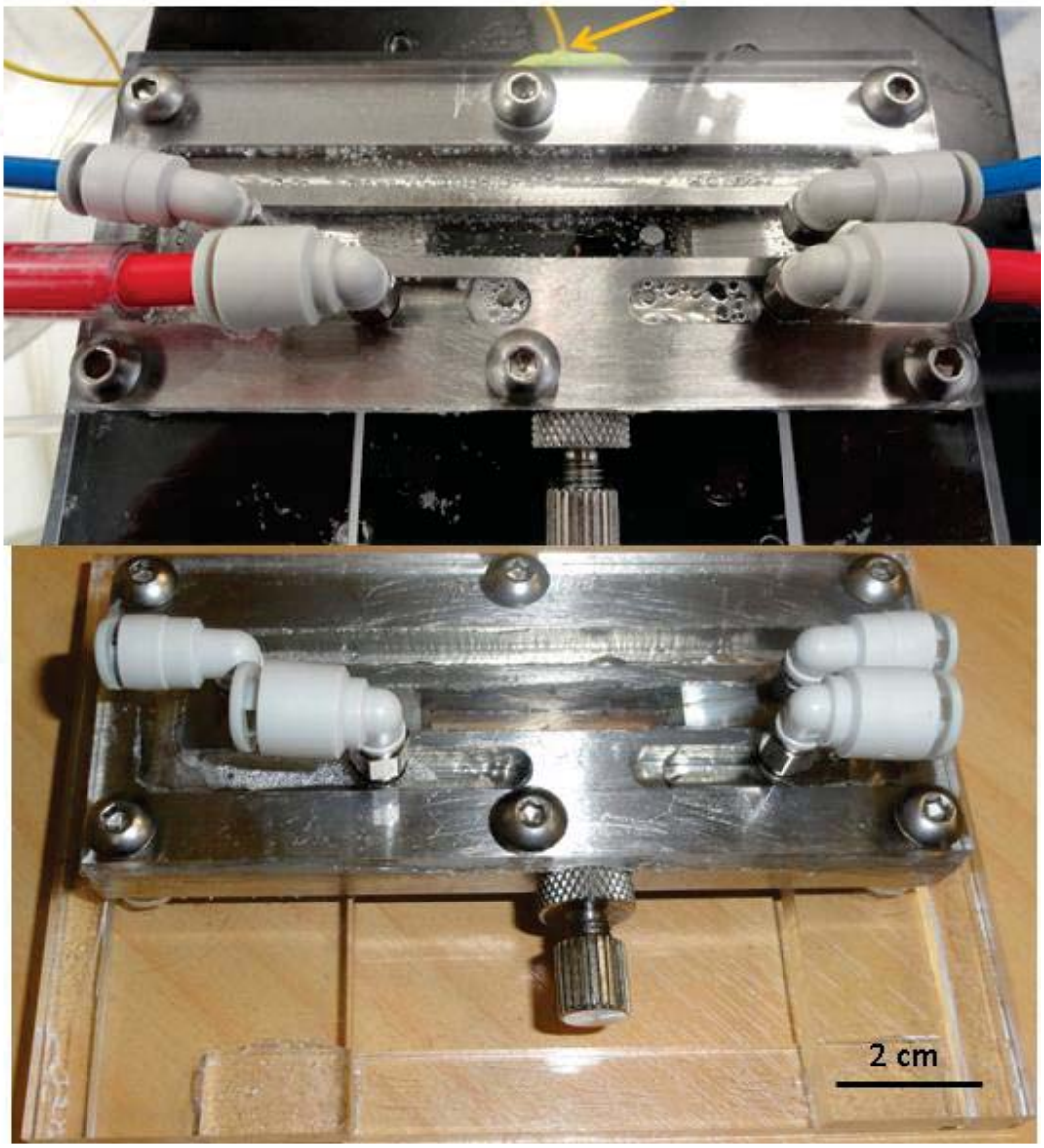

Figure 6-1: Photographs of the tissue flow cell. A) A close up image with pipes attached to the connectors (Figure 6-3) of the inner flow chamber (blue pipe) and outer (red pipe) flow channel as well as the yellow wire (indicated by the orange arrow) of the thermocouple used. Heating water flows through the outer channel while Earle-Hepes solution (HBS) flows through the inner channel. Image B) is an overview of the tissue flow cell with a scale bar.

The following figures describe the features and main components of the tissue flow cell. The core structure of the tissue flow cell was a machined block of stainless steel (115 x 49 x 8mm) (Figure 6-2). The stainless steel block contained two compartments; an inner flow chamber that contained the gut wall tissue that was perfused with carboxygenated and heated Earle-Hepes (HBS) solution and an outer channel through which heating

water was circulated. The inner chamber was positioned in the middle of the stainless steel block, was 82 mm in length and 8mm in width while its depth varied along its length. Both ends of the inner chamber sloped downwards towards a central section of 34 mm in length that occupied all 8 mm of the height (Figure 6-2B) of the stainless steel block. Hence, this inner chamber profile ensured that flow would be laminar by the time it reached the mounted gut sample.

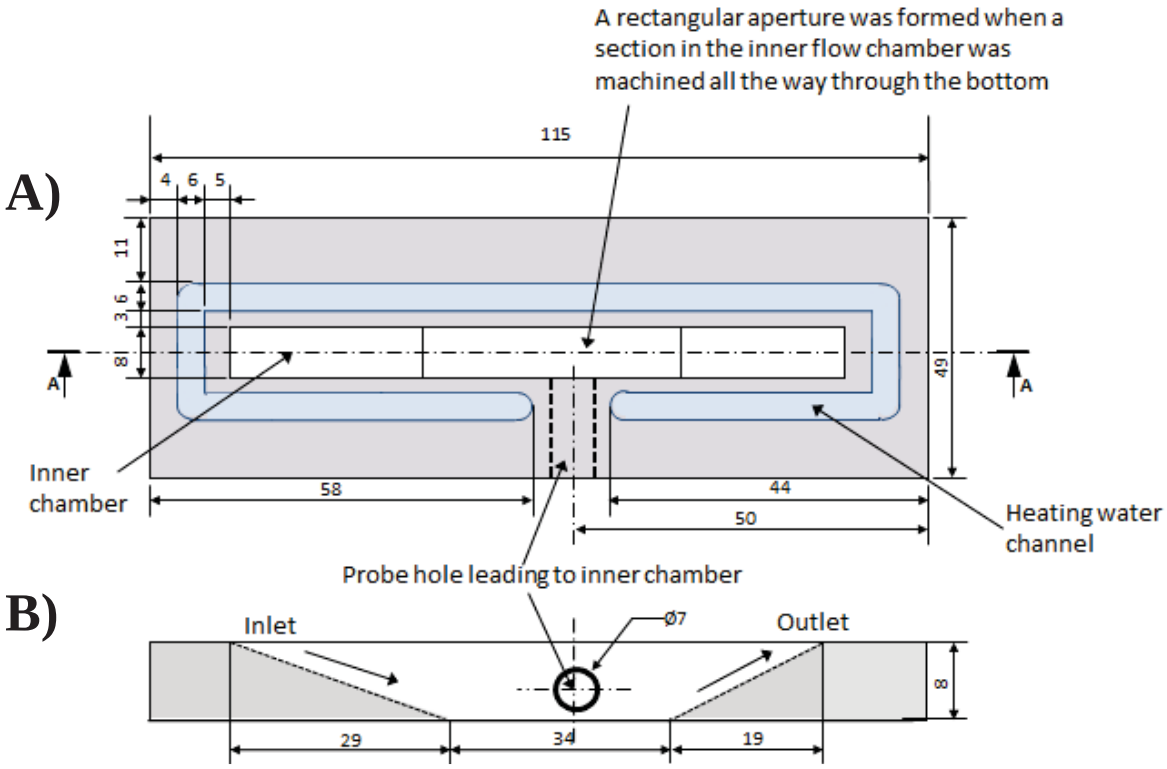

Figure 6-2: Tissue flow cell core structure with dimensions – a machined stainless steel block. A) Top view of the structure. While B) is a side-on sectional view of the structure at the midpoint marked in A). The regions marked in light blue indicates an outer heating water channel while the regions in white marks the inner chamber of the flow cell that would be filled with Earle-Hepes solution (HBS) during an experiment.

The outer channel had a width of 6 mm and was 3 mm from the long edge and 5 mm from the short edge of the wall of the inner chamber (Figure 6-2A). A 7 mm diameter probe hole was bored into the stainless steel block perpendicular to the length of the

stainless steel block channel in the middle of the section of the block, shown as dotted lines in Figure 6-2A and as a circle in Figure 6-2B.

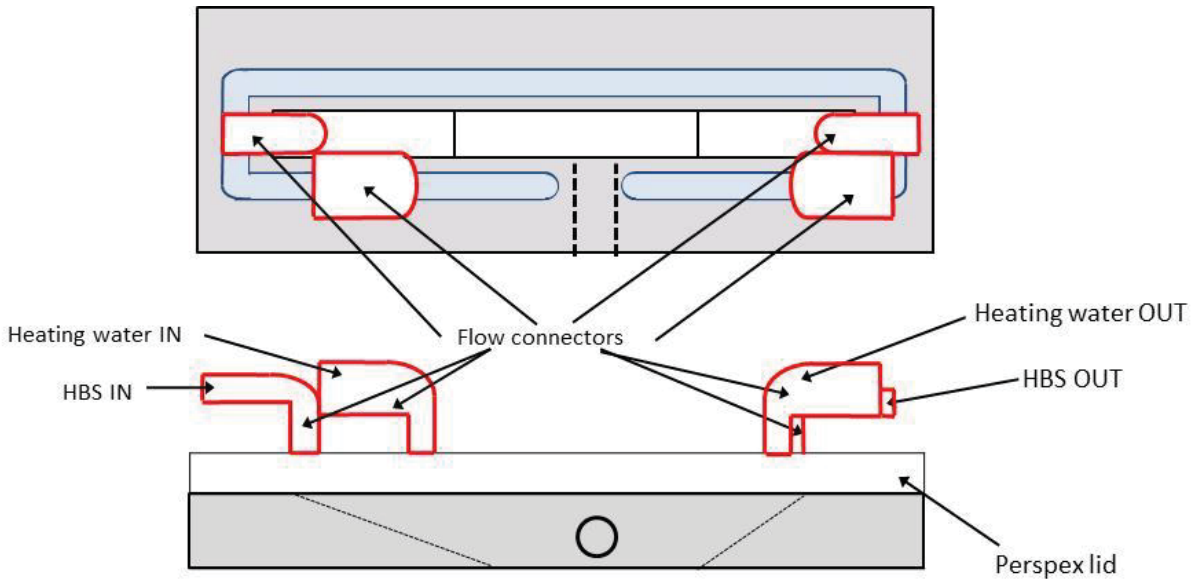

Figure 6-3: The elbow quick-fit flow connectors attached to the Perspex lid to be inlet and outlet points for the inner flow chamber and outer flow channel.

Four plastic elbow quick -fit flow connectors (PMC series, Colder Products Company, USA) were attached to the top surface of the Perspex lid to act as inlet and outlet points for both the inner chamber and outer channel (Figure 6-3).

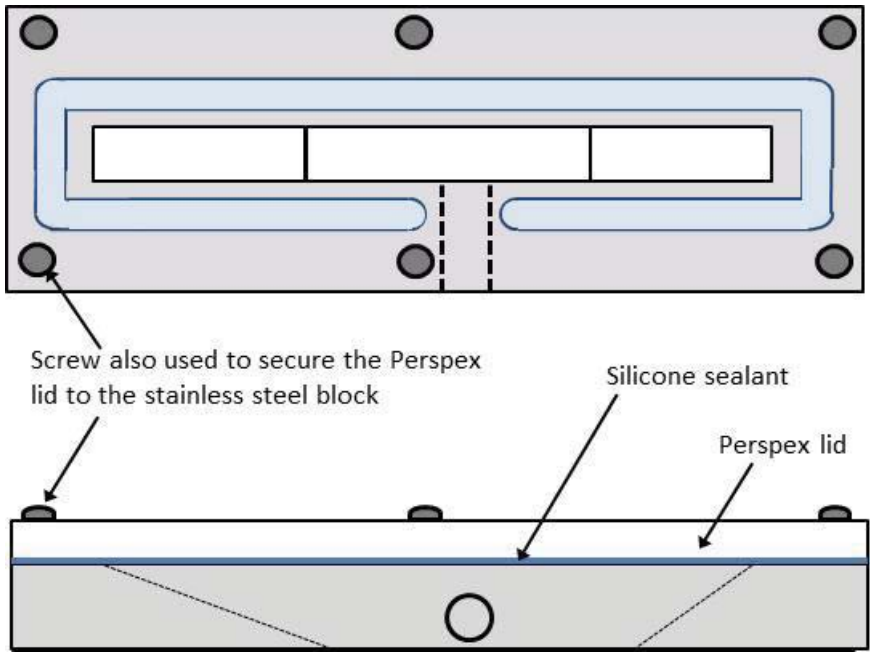

Figure 6-4: The silicone sealant and positioning of the screws used to secure the Perspex lid to the stainless steel block.

A 4mm Perspex lid with the same length and width as the stainless steel block was fixed onto the top of the stainless steel block thus enclosing the inner chamber and outer channel. The Perspex lid was secured to the stainless steel block by silicone sealant (Selleys, NSW, Australia) as well as by six screws of which three screws were positioned on each of the two long edges of the stainless steel block assembly (i.e. flow cell core structure with the Perspex lid attached to it) (Figure 6-4).

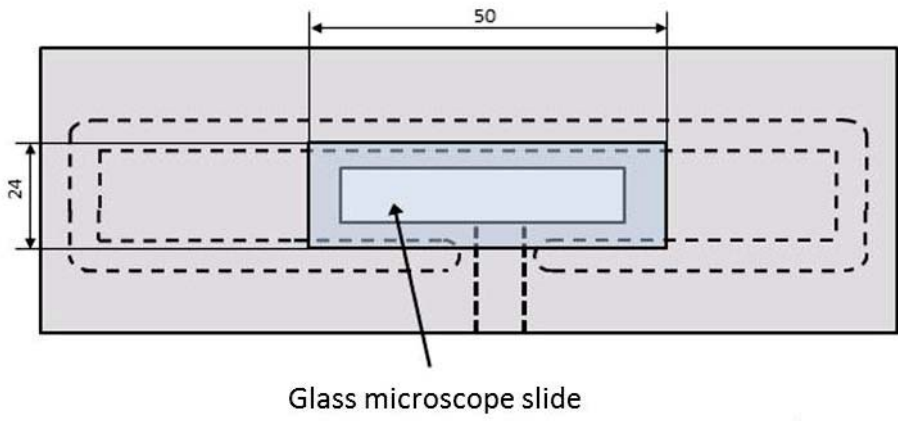

Figure 6-5: Underside of the stainless steel block. A microscope slide was used to cover the rectangular aperture in the block located at the inner chamber. The transparency of the microscope slide allowed the visual field of the inverted microscope to access villi positioned in the flow cell.

A rectangular aperture on the under surface of the flow cell core structure where the inner chamber was located was covered by a glass microscope slide (50 x 24 x 1mm) (Figure 6-5). This provided access for the visual field of the inverted microscope. The microscope slide was secured to the base of the stainless steel block with cyanoacrylate glue (Elephant, Jiangxi, China) and silicone sealant was used to seal its edges. The stainless steel block assembly was then fitted onto a Perspex base plate machined to fit the recess on the manual substage of the inverted microscope (Figure 6-6). The placement of the flow cell into the microscope substage allowed the flow cell to be moved in the x, y and z direction within the focal plane of the inverted microscope.

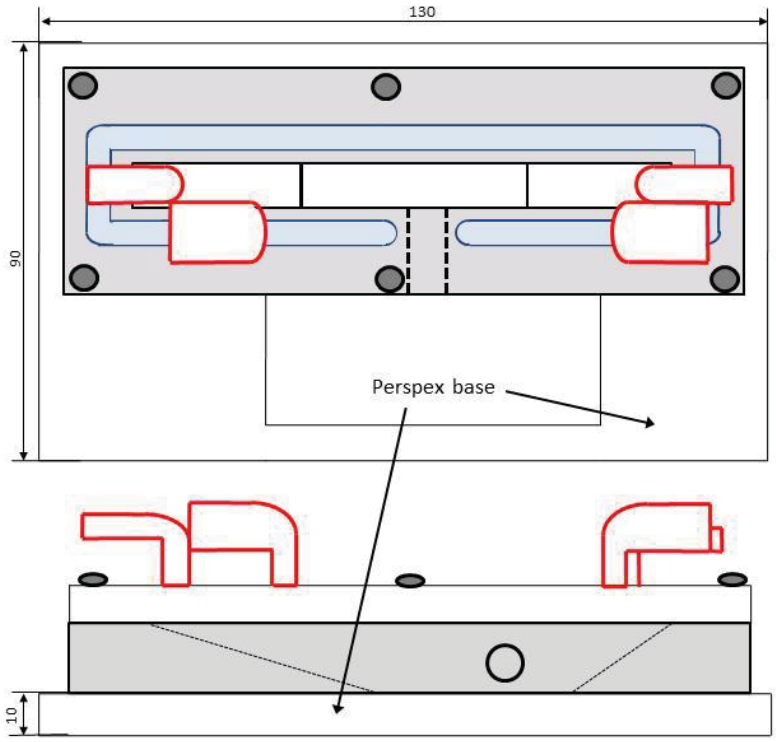

Figure 6-6: Perspex base plate and its dimensions, which was attached to the tissue flow cell.

6.2.1.1. Tissue flow cell probe

The distal ileal sample was mounted onto a stainless steel probe that was 41 mm in length from its base to tip (Figure 6-7).

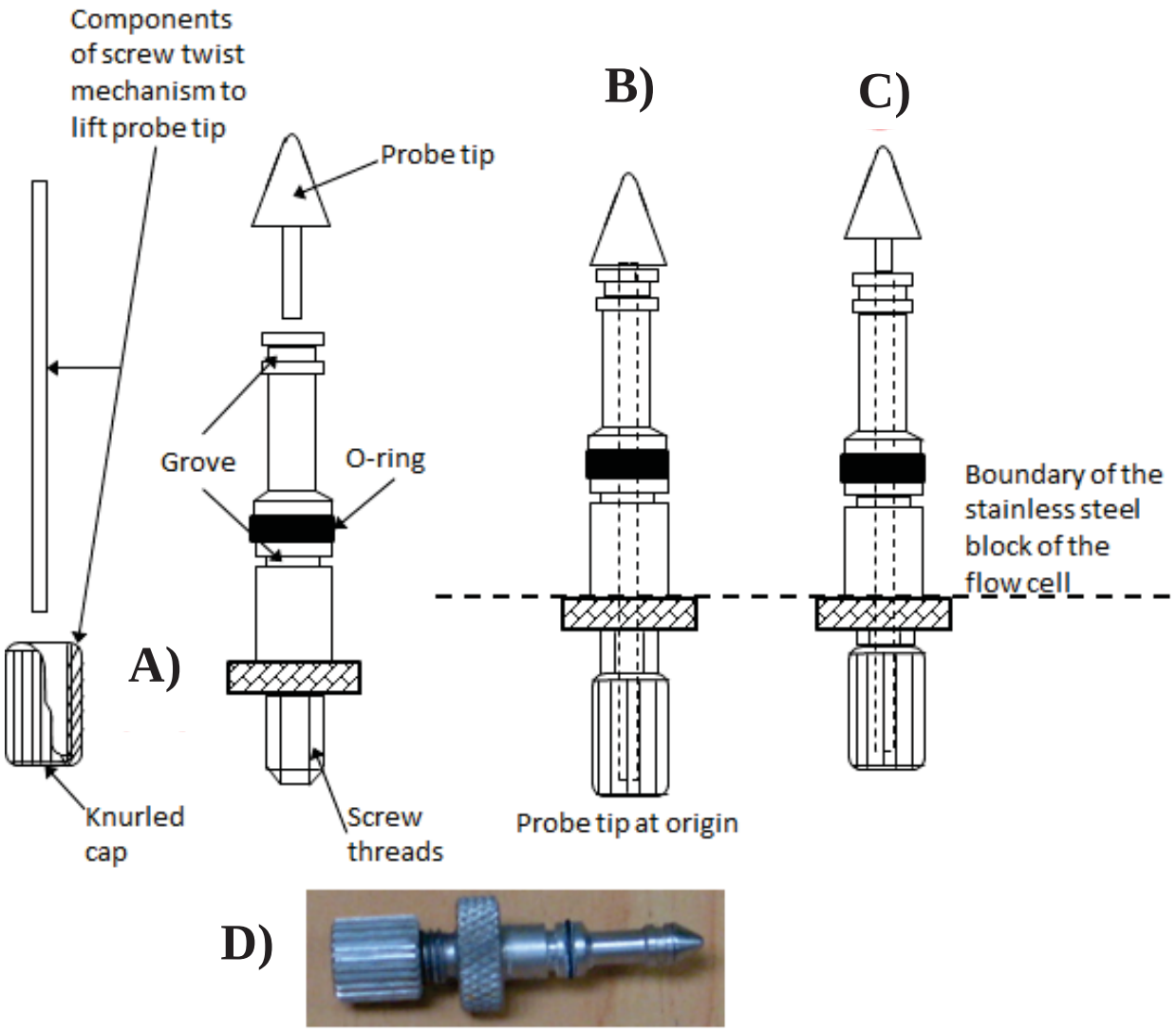

Figure 6-7: Tissue flow cell probe. A) Flow cell probe main components are indicated. The probe tip at origin B) and when it is semi-ejected C) to stretch a gut sample mounted onto the probe. Image D) is a photograph of the tissue flow cell probe.

The tip of the probe was machined to a cone shape to allow the gut sample to be mounted over it and tension applied without its perforation. A suture was used to secure the taut gut sample into a grove on the probe (Figure 6-7A). The gut sample was upheld over the probe using four hemostats (Figure 6-8A) (as was the gut wall tissue used in micro-rheological studies of the mucosal fluid environment; see sub-section 3.3.1.2, Figure 3-9C for a schematic drawing of the mounting of the gut sample on the probe) while the suture was applied.

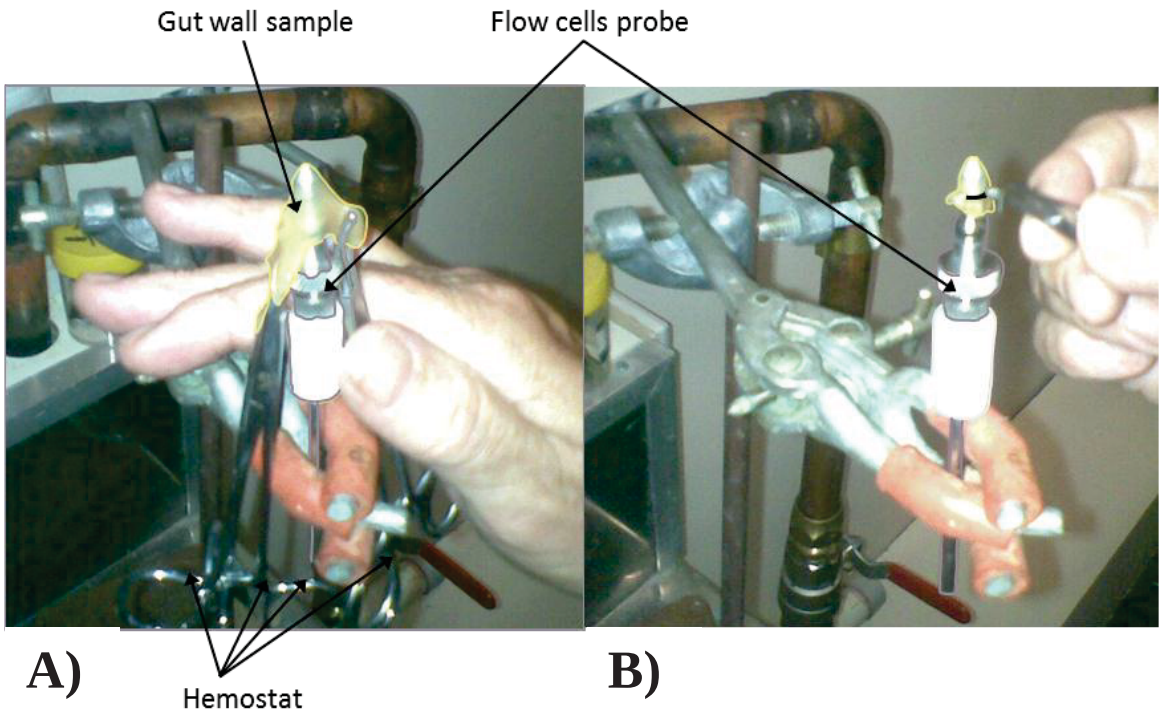

Figure 6-8: The process of the mounting of the sample of gut wall on the flow cell probe. A) The sample held by 4 hemostats. B) Trimming of the mentioned sample after it had been secured to the probe with a suture.

An O-ring (Figure 6-7A) was attached to the probe to allow it to be rotated and its depth to be varied within its housing after the tip of the probe had been inserted into the inner chamber. A threaded (i.e. knurled) cap (Figure 6-7A) was mounted at the back of the probe that allowed the probe tip to be extended or retracted thus varying the tension applied to the mounted tissue. This was used to properly tension the mucosa underlying the villi to prevent the mucosa from moving with the flow in the inner chamber.

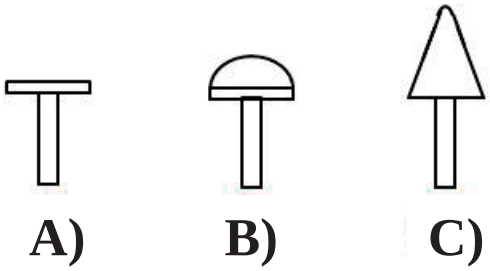

Figure 6-9: The various probe tips designs trialled during pilot study. A) The initial design of the probe tip was a circular flat surface, which did not separate villi sufficiently to determine villous rigidity during lumen flow. A subsequent modification to construct a pinhead tip i.e. a hemisphere B) improved villi separation marginally. A second modification to the probe tip to resemble a cone C) resulted in sufficient separation of villi. Design C) was used in all main experimental trials.

In order to assess the rigidity of an isolated villus and its surrounding flow patterns, it was important that the villus was not obstructed by any surrounding villi. There was difficulty in isolating a single villus with the first type of probe tip that was trialled, which was of a flat profile (Figure 6-9A). Despite tensioning the gut sample with the screw device, villi were unable to be separated to a distance that was sufficient to allow villous rigidity to be determined during lumen flow. The probe tip was subsequently modified to a hemispherical shape (Figure 6-9B) but this only marginally improved the intervillous spacing and the visualisation of individual villi. However, a cone shape probe tip in the final modification (Figure 6-9C) allowed sufficient separation of villi and was used in all subsequent experiments.

6.2.2. Overall setup of experimental apparatus

The basic setup of the experimental apparatus on the inverted microscope during recording of movements of villi during lumen flow and trajectories of microbeads in the perivillous space is shown in Figure 6-10. The perfusion and heating apparatus were placed on the floor below the vibration proof table (i.e. the air damped table highlighted

in subsection 3.3.2) and the software processing computer positioned on a separate table.

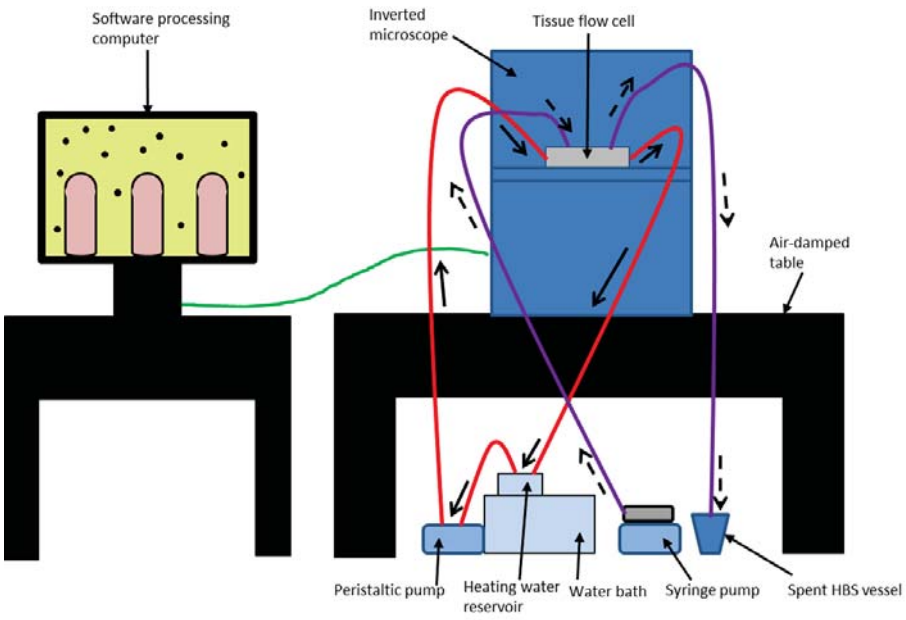

Figure 6-10: The basic setup of experimental equipment used for the recording of the movements of villi during lumen flow and trajectories of microbeads in the perivillous space. The bold arrows alongside the red pipe show the direction of flow into and out of the flow cell outer channel. The dotted arrows that accompany the purple pipe shows the direction of flow of heated and carboxygenated Earle-Hepes solution (HBS) into and out of the flow cell inner chamber.

The temperature of the HBS solution in the inner chamber of the flow cell was maintained at 37°C with water being driven by a peristaltic pump at a perfusion rate of 500 ml min^{-1} (Cole-Parmer, Illinois, US) through the outer channel. Spent heating water was recycled into the reservoir. A peristaltic pump was used in early work to pump carboxygenated HBS through the inner chamber. However, the pulsatile nature of flow was found to be unsuitable for the determination of microbead trajectories. Hence, a syringe pump was used instead. In the main experimental work, carboxygenated HBS with or without microbeads (see accompanying journal article and sections to follow for microbead type and concentration) was pre-heated to 37.5^{o}C and this temperature maintained by the heating system of the tissue flow cell.

6.2.2.1. Inverted microscope

The same inverted microscope and CCD camera that was used to determine the microrheological properties of the fluid environment in the perivillous space (see sub-section 3.3.2.1 for further details) was used in the experiments detailed in this chapter.

6.2.2.2. Microscope objective used

An extra-long working distance (ELWD) x20 0.45 NA (CFI S Plan Fluor ELWD 20x) objective was used initially for the first few experimental trials. The initial use of the same magnification that was used in prior work was based on the fact that it enabled clear visualisation of the villous tip. However, it became apparent that at the high velocities of flow used in this experiment, a larger field of view was required. Subsequently and in the main experimental work, a lower magnification of x10 0.3 NA (CFI Plan Fluor DL 10x) objective was used. The lower magnification was used as it required as much of the entire length of a villus and its response to flow to be analysed. Larger microbeads (3 μm in diameter) were also used to improve the clarity of visualisation when using the lower magnification objective.

This technique allowed imaging of up to 85% of the length of possum ileal villi along with the tracking of microbeads that were perfused even at supraphysiological rates (i.e. up to 3 times the physiological flow rate). When villi had very low movement, an additional x1.5 magnification was also used with the existing setup (by the use of the x10 objective with the x1.5 intermediate magnification lens setting).

MASSEY UNIVERSITY
GRADUATE RESEARCH SCHOOL

STATEMENT OF CONTRIBUTION
TO DOCTORAL THESIS CONTAINING PUBLICATIONS

(To appear at the end of each thesis chapter/section/appendix submitted as an article/paper or collected as an appendix at the end of the thesis)

We, the candidate and the candidate's Principal Supervisor, certify that all co-authors have consented to their work being included in the thesis and they have accepted the candidate's contribution as indicated below in the *Statement of Originality*.

Name of Candidate: Ian LIM Yuen Feung

Name/Title of Principal Supervisor: Prof. Roger G. Lentle

Name of Published Research Output and full reference:

Lim, Y. F., R. G. Lentle, P. W. M. Janssen, M. A. K. Williams, C. de Loubens, B. W. Mansel and P. Chambers (2014). "Determination of Villous Rigidity in the Distal Ileum of the Possum (Trichosurus vulpecula)." Plos One 9(6): e100140

In which Chapter is the Published Work: Chapter 6

Please indicate either:

- The percentage of the Published Work that was contributed by the candidate: 70%

  and / or
- Describe the contribution that the candidate has made to the Published Work:

Ian Lim Yuen Feung — Candidate's Signature — 27/6/2014 — Date

Roger Lentle — Principal Supervisor's signature — 27/6/2014 — Date

6.3. Copy of the paper: Determination of villous rigidity and intervillous flow in the distal ileum of the brushtail possum (*Trichosurus vulpecula*).

The following pages contain a copy of the published journal article with the following bibliography;

Lim, Y. F., R. G. Lentle, P. W. M. Janssen, M. A. K. Williams, C. de Loubens, B. W. Mansel and P. Chambers (2014). "Determination of Villous Rigidity in the Distal Ileum of the Possum (*Trichosurus vulpecula*)." Plos One **9**(6): e100140

The contents of the published peer-reviewed article with the above bibliography is reproduced in this section. All references cited in section 6.3 are listed in a separate sub-section after the main body of the article. These references are reproduced in the main bibliography of this thesis (i.e. after the thesis appendix) only if they are used in other parts of this thesis. All further work beyond this section will be citing the work presented in this section where appropriate.

Determination of villous rigidity in the distal ileum of the possum (*Trichosurus vulpecula*)

Y. F. Lim[1], R. G. Lentle[1 2*], P. W. M. Janssen[1], M. A. K. Williams[2 3 4], B. W. Mansel[2 4], C. de Loubens[1] and P. Chambers[5]

[1] *Institute of Food, Nutrition and Human Health, Massey University, Private Bag 11222, Palmerston North, New Zealand*

[2] *Institute of Fundamental Sciences, Massey University, Private Bag 11222, Palmerston North, New Zealand*

[3] *Riddet Institute, Massey University, Palmerston North, New Zealand*

[4] *MacDiarmid Institute of Advanced Materials and Nanotechnology, Wellington, New Zealand*

[5] *Institute of Veterinary, Animal and Biomedical Sciences, Massey University, Private Bag 11222, Palmerston North, New Zealand*

*Corresponding author r.g.lentle@massey.ac.nz

6.3.1. Abstract

We investigated the passive mechanical properties of villi in *ex vivo* preparations of sections of the wall of the distal ileum from the brushtail possum (*Trichosurus vulpecula*) by using a flow cell to impose physiological and supra-physiological levels of shear stress on the tips of villi. We directly determined the stress applied from the magnitude of the local velocities in the stress inducing flow and additionally mapped the patterns of flow around isolated villi by tracking the trajectories of introduced 3 μm microbeads with bright field micro particle image velocimetry (mPIV).

Ileal villi were relatively rigid along their entire length (mean 550 μm), and exhibited no noticeable bending even at flow rates that exceeded calculated normal physiological shear stress (> 0.5 mPa). However, movement of villus tips indicated that the whole rigid structure of a villus could pivot about the base, likely from laxity at the point of union of the villous shaft with the underlying mucosa. Flow moved upward toward the tip on the upper portions of isolated villi on the surface facing the flow and downward toward the base on the downstream surface. The fluid in sites at distances greater than 150 μm below the villous tips was virtually stagnant indicating that significant advective mixing in the lower intervillous spaces was unlikely. Together the findings indicate that mixing and absorption is likely to be confined to the tips of villi under conditions where the villi and intestinal wall are immobile and is unlikely to be greatly augmented by passive bending of the shafts of villi.

Keywords: small intestinal villi, rigidity, mixing, microfold, mPIV

6.3.2. Introduction

While villi have long been hypothesised to augment the absorption of nutrients by increasing the surface area of the small intestinal mucosa, the mass transfer of nutrients is also dependent upon the attendant fluid dynamics (Gruzkov et al. 1989). In the absence of villous motility, there may be stasis of fluid in the intervillous spaces (Ryu and Grim 1982, Holzheimer and Winne 1989) and absorption in the lower regions more dependent on diffusion than advection (Levitt et al. 1990, Pappenheimer 2001a).

Recent experimental evidence has shown that arrays of short-lived radially disposed mucosal microfolds are formed during static pendular contractions (Lentle et al. 2013). This action causes the tips of the attached villi to incline towards each other in the concavities and to diverge over the apices of microfolds. Further, fluid mechanical

simulations show that these actions cause fluid to be alternately expressed from and drawn into the intervillous spaces from alternate crowding and separation of villous tips, augmenting peripheral mixing and dispersion of luminal contents (Lentle et al. 2013). This mechanism is more parsimonious than one that requires coordinated endogenous contraction of groups of villi (King and Robinson 1945, Womack et al. 1988, Mailman et al. 1990, Wang et al. 2010) to induce such movement of fluid.

However, the efficiency with which peripheral lumen contents could be absorbed by crowding of the villous tips depends on the relative rigidity of the villous shaft. A high degree of flexibility in the shafts of villi would allow movement of their bases to occur independently of their tips. Conversely, a degree of laxity at the point of union of the base of the villus with the adjacent mucosa would allow villous shafts to pivot with respect to the plane of the underlying mucosa and thus to accentuate crowding within the concavity between adjacent mucosal folds. Given the turgor of the interstitial tissue within the shafts of villi (Westergaard and Dietschy 1974) that results from a combination of hydrostatic distension by absorbed fluids and opposing circumferential tension of the collagen fibres of the villous lamina propria (Hosoyamada and Sakai 2007), it seems unlikely that villous shafts would possess a high degree of flexibility. However, given the differences in the dispositions and densities of collagen fibres in the subepithelial network of the villous lamina propria from that in the pericryptal lamina propria (Hosoyamada and Sakai 2007), the junction between the two sites would likely allow a degree of pivoting. However to date, no work has been carried out to determine the flexibility of the villous shafts or the laxity of their bases during lumen flow.

The purpose of the current work was to determine the passive mechanical properties of villi in the absence of any villous contractile activity using microbeads to allow flow velocities and the imposed stresses to be determined directly. We also endeavour to

describe the flow patterns around villi in *ex vivo* tissue in a flow cell that was designed to replicate physiological and supra-physiological levels of shear stress acting on small intestinal villi. The rigidity of villi about their longitudinal axes during flow was assessed from a sequence of high definition image sequences. Micro particle image velocimetry (mPIV) was used to delineate fluid flow at a micro level and to derive velocity fields (Raffel et al. 1998, Prasad 2000) at various locations around villi. Further, spatiotemporal mapping techniques developed by our research group (Hulls et al. 2012, Janssen et al. 2013, Lim et al. 2013) were used to search for any intrinsic contractile movement within the shafts of villi.

6.3.3. Methods

6.3.3.1. Preparation of intestinal samples

This study was carried out in strict accordance with the 'New Zealand Code of Practice for the Care and Use of Animals for Scientific Purposes'. The brushtail possums are regarded as a pest in New Zealand and are widely killed by trapping and/or shooting. In this case the animals were caught humanely as part of a routine pest control operation in an approved box trap in areas of pasture in the Manawatu region of New Zealand. Permission to conduct a routine pest control operation of the brushtail possum in the stated regions was not required.

The possums were subsequently transported in the box trap to the Veterinary hospital in the Veterinary faculty of Massey University where they were with anaesthetized by a registered vet and the ileum removed prior to euthanasia with intracardiac pentobarbitone. All of these procedures were approved by the Massey University Animal Ethics Committee (MUAEC approval no 12/77), which is accredited within New Zealand and internationally.

We used sections of the wall of the terminal ileum of the brushtail possum (*Trichosurus vulpecula*) maintained *ex vivo* in a flow cell. Villous intestinal mucosa can be maintained *ex vivo* for significant periods of time, provided it is well oxygenated and adequately supplied with nutrients (Danielsen et al. 1982, Lim et al. 2013).

Seven freshly trapped brushtail possums (*Trichosurus vulpecula*), of either sex and between 2 and 3 kg body weight were each fasted for 4 hours and anaesthetized in an induction chamber with 5% halothane in 33% oxygen and 66% nitrous oxide administered via a face mask attached to a Bains circuit. The gut was accessed via a ventral midline incision and a 10 cm length of terminal ileum was excised. The segment of excised gut was opened by a lengthwise cut and immediately placed with mucosa uppermost in carboxygenated Earle's-Hepes solution (HBS) (NaCl 124.0, KCl 5.4, $MgSO_4$ 0.8, NaH_2PO_4 1.0, $NaHCO_3$ 14.3, Hepes 10.0, $CaCl_2$ 1.8, glucose 5.0 mM) maintained at 37^oC. This procedure diluted any adherent digesta and allowed it to float clear of the mucosal surface.

A 2 cm^2 piece of mucosa was cut from the opened segment with its center located 5 cm from the distal end of the section of terminal ileum. The rectangular piece of mucosa was then draped over the 5 mm diameter conical tip of the flow cell probe (Figure 6-11B) with the mucosal surface outermost, using four haemostats, one attached to each corner, and secured with a suture that was located over a grove situated just below the tip of the probe.

The tip of the probe was then extended until the overlying tissue was taut and the surplus mucosa around the suture trimmed off. The probe bearing the tautened mucosa was then mounted in a specially designed flow cell (Figure 6-11) that allowed the tip and overlying mucosa to be positioned in the inner flow channel of the flow cell that was perfused with HBS. The flow cell was maintained at 37^oC by the flow of an outer

channel of heated water (Figure 6-11B). The position of the probe was such that the tissue overlying the tip lay in the focal plane of an inverted microscope (Nikon Eclipse TE2000-U) and gave a lateral view of villi with the perfusate flowing at right angles to their long axes. Shear rates in species such as the rat and the possum during either pendular or peristaltic activity has been reported to be around 0.5 – 1 s^{-1} (Lentle et al. 2005, Lentle et al. 2013). Given that the viscosity in the continuous fluid layer around the tips of ileal villi of the possum is around 1.5 mPa.s (Lim et al. 2013), then by assuming Poiseuille flow we can calculate the shear stress acting on the villi at these shear rates to be between 0.7 – 2.5 mPa. The delivery of shear stress to villi was by perfusion of the flow cell with either HBS alone or HBS containing suspended microbeads delivered by a 50 ml syringe mounted in a syringe pump (Harvard Instruments). The syringe pump was adjusted to deliver perfusion at 3.8, 7.6, and 15.3 ml/min. The rates were chosen as they encompass reported physiological and supra-physiological levels of flow (Grovum et al. 1973, Bueno et al. 1975). Velocity profiles of the flow measured by mPIV above the villi subsequently confirmed these orders of magnitude (see Results).

The substage of the microscope on which the flow cell was mounted could be manually adjusted to view selected villi. The inverted microscope was mounted on an air damped table (Photon Control) and was equipped with a halogen bright field illuminator (Nikon), and a x10 0.3 NA (CFI Plan Fluor DL) objective lens. Image sequences for processing by micro-PIV (see below) were recorded with a Foculus FO124SC CCD camera (that was mounted on the microscope) for between 30 and 60 seconds at a frame rate of 43 Hz and a camera resolution of 640 x 480 pixels. In all cases, acquisition of image data commenced within 10 minutes of the time the segment was excised from the

ileum. The total time elapsed following excision was determined for all image sequences.

The circulation of the heating water was halted for at least 20 seconds prior to image capture to prevent interference from flow induced vibrations. Perfusion of the inner flow channel with HBS was halted one minute prior to image capture but recommenced 5 seconds after imaging had started. The latter procedure allowed the position of the villus under static conditions to be determined. Circulation of heating water was re-established immediately on completion of recording and maintained for a minimum of 5 minutes before further recording of image sequences. All image sequences were completed within 90 minutes of the time of excision of the ileal segment.

6.3.3.2. Micro-PIV

Polystyrene microbeads (Polysciences, Warrington, PA, USA) 3 μm in diameter were suspended at a concentration of 0.0005% (weight/volume) in the HBS perfusate. The magnitude and pattern of the two-dimensional (2D) fluid flow around intestinal villi were assessed from the movement of these microbeads as measured using micro particle image velocimetry (mPIV). It is noteworthy that the method of preparation effectively removed large digesta particles and also fine food particles while mucus islands, microflora and sloughed epithelial cells (Allen et al. 1993, Corfield et al. 2001) could be distinguished from microbeads and not inadvertently tracked. Again as such fine particles were of low mass, they would move with the microbeads during bulk flow and would be unlikely to hinder their passage.

The mPIV technique used was implemented using software (PIVlab v.1.32) (Thielicke and Stamhuis 2013) run in the MATLAB 2011b (MathWorks, Natick, MA) programming environment. The resolution of the velocity flow fields generated by mPIV was enhanced by a technique known as ensemble correlation (Santiago et al.

1998). This technique may be applied to image sequences by two methods. Firstly, arrays of particles in a series of closely spaced focal planes could be used to determine a mean vector. Secondly, ensemble images were formed from groups of images taken of the same field of view but at different times, when the population of beads contained within them were different (the initial population of beads having left the frame by being driven by the flow perfusion). A mean vector associated with each spatial region may then be derived from the superimposed images. For example, by the latter method, for two successive groups of 100 images, the first image in each group would be superimposed, the second on the second etc. (Thielicke 2013). Given that the first method could not be utilized with PIVlab, the second method of enhancing the resolution of the velocity field was used. Hence the flow field was evaluated using a series of interrogation windows in which the flow vector was ultimately determined (the areas occupied by the villi were masked). The software employed a series of four interrogation windows of decreasing size that were uniformly distributed over the image in order to increase spatial resolution of the generated velocity vectors while minimizing noise. Ultimately this method was able to simultaneously determine flow velocities that varied by 2 – 3 orders of magnitude (Thielicke 2013). The interrogation window used was always 4 times the size of the maximum expected particle displacement in accordance with the one-quarter rule of mPIV for optimum recoverability of flow field velocities (Keane and Adrian 1990, Raffel et al. 1998). The cross-correlation functions between successive superimposed images were evaluated by Fast-Fourier Transform (FFT) and the position of maximum in the cross-correlation was located to sub-pixel accuracy by fitting a Gaussian function to the peaks in the cross-correlation data. The velocity was determined by calculating the displacement of this maximum with respect to the prior superimposed image over a given time interval (dt = 1/43 seconds). This

procedure was repeated for all interrogation areas to determine their respective velocity flow fields. The above procedure was applied to at least 100 pairs of successive superimposed images and the resulting velocity fields to be used in further analysis were obtained by averaging the velocity fields over all instances of the same time interval.

6.3.3.3. Analysis of micro-PIV results

The magnitudes of the velocity vectors of microbeads were assessed at a number of differing volumetric flow rates, namely; at 2.0, 1.0, and 0.4 ml/min in open channel studies on the flow cell. This procedure recovered flow profiles that were close to that predicted assuming the law of Poiseuille. The same procedure was used with the tissue *in situ* to determine velocity profiles 200 μm above the tip of a chosen villus at volumetric flow rates of 38.2, 15.3, 7.6, 3.8, 1.9 ml/min. The distance of 200 μm was chosen as it was the maximum vertical distance from the villous tip that was visible in the apparatus. The mean velocity was calculated from between 20 and 30 values at perfusion flow rates between 1.9 and 7.6 ml/min, and from between 140 and 160 values for flow rates above this.

The gradation of the horizontal component of flow velocities at right angles to the long axis of the villi (U_x) was determined at HBS perfusion rates of 15.3, 7.6, 3.8 ml/min. Plots of the horizontal component of velocity of the flow at right angles to the long axis of the villi (U_x) were prepared from all image sequences that were suitable for the calculation of TD. Horizontal velocities were recorded at a distance of 30 μm lateral to the edge of the villous image, starting at a point 100 μm above the villous tip and at all available points below this as far down the length of the villus as was practicable (in some cases up to 400 μm below the villous tip). The starting distance of 100 μm above the villous tips was chosen as it was the greatest distance above them at which at least

15% of the mean villous length could be seen in the same visual field in all image sequences.

The gradation and flow direction of the component of flow velocity parallel to the long axis of villus (U_y) was also determined at the same three flow rates. This was done at distances between 5 – 15 μm from the lateral edge of the villous image at all available points along both the upstream and downstream longitudinal axes of villi, from the tip to as far down the length as practicable (in some cases up to 400 μm below the villous tip). Only image sequences that recorded streamlines of microbeads perpendicular to the long axis of villi for the whole length of villi that could be seen in the image, which had villous lengths of over 280 μm (greater than half the mean length of a villus) were suitable for this assessment.

As the technique used for determining velocity profiles around villi involved direct superimposition of video images taken prior to the commencement of perfusion and intervals thereafter, it also allowed direct comparisons of the villus profile. This allowed us to determine whether there had been any swelling of the tissue over the course of the experiment.

6.3.3.4. Mean villous length and width

Further samples of distal ileal mucosa, each of 2 cm^2 in surface area, were obtained from a further four possums. Each sample was tied to the probe from the tissue flow cell and stained with 1% Bromothymol-Blue (BTB) before being mounted in a micromanipulator, and immersed in a petri dish of oxygenated HBS situated in the focal field of a Diaphot inverted microscope (Nikon). The sample was illuminated using bright field illumination from a FL-150 fibre optic lamp (MeijiTechno) and images of villi captured with a Nikon DS-Fi1 Hi-Definition digital camera. The lengths of

component villi were measured along their long axis from their tips to the points where the cylindrical profiles of their shafts broadened at their junction with the basal mucosa. The width of each component villus was also determined at the midpoint of its length.

6.3.3.5. Total displacement (TD) of the villous tip

The overall movement of the tip of a villus, i.e. total displacement (TD), was determined as the linear displacement of a point located 20 μm below its tip from its original position (when there was no flow) to that when there was steady fluid flow of HBS at each of three perfusion rates (3.8, 7.6 and 15.3 ml/min). The TD will be the sum of any linear displacement of the villous tip from bending of its shaft plus that from any pivoting around the point of attachment of its base to the mucosa, that from any translational movement of the base of the villus with respect to the adjacent muscular wall and that from any change in its lateral profile by twisting about its long axis.

The point in time at which the maximum TD occurred following the commencement of flow was determined, from intensity based spatiotemporal mapping (Janssen and Lentle 2013) by assessing the displacement along a line of interest (LOI) drawn at right angles to the longitudinal axis of the villus across a point 20 μm below the tip. A reference line was drawn, using Image J software (NCBI), along the temporal axis of the spatiotemporal intensity map from the position of the upstream edge of the LOI when there was no flow (Figure 6-12A). The time of maximal TD could thus be identified as the point of maximum distance of the edge of the LOI from the marked line (Figure 6-12B), and the requisite video image then selected. A distinctive point was then identified on the tip of the villus in one of the initial frames taken during stasis and in the image acquired at the time of maximal displacement. The linear distance between

the two positions was then determined from the requisite cross-correlation data between the two images.

6.3.3.6. Assessment of bending of the villous shaft and angular displacement

This procedure was undertaken on a series of villi using the same images that were used to determine TD and the same cross-correlation techniques applied to each in the series of selected features. The contribution of bending to the total displacement of a given villous shaft (TD) was assessed from the displacements, in the image taken at maximum displacement, of a series of features along the length of the villus that were aligned with its longitudinal axis in the initial image. Were the villus a rigid structure that could be displaced only by pivoting, (i.e. hinging about its base) the displacement distance would be expected to decrease in a linear fashion with distance from the villous tip. Conversely, were displacement to be generated by bending, then the displacement distance would vary in a non-linear fashion according to the local elasticity at the point along its length at which it was determined. Hence, the displacements of individual villi plotted against the distance from the villous tip at which they were taken, would be linear in the first case (assuming that the mechanical properties of villi did not vary along their longitudinal axes) and non-linear in the second. Likewise, if bending occurred at higher velocities of flow, the fit would depart from linearity and influence the slope of the line of best fit.

The correlation coefficient (R^2) of the straight line regression (SLR) of the percentage displacement of the requisite TD against the distance from the villous tip was used as a basis of assessment of the quality of linear fit. Comparisons of the correlation coefficients obtained on SLRs of individual villi by ANOVA could then be used to assess whether the quality of linear fit declined significantly over the three flow rates that were used as would occur with bending.

Similarly, the difference between the slope of the line of the SLR in the plot of the displacement of the requisite TD in microns against the distance from the villous tip in microns will in each case indicate the angle with which the villus pivoted. Again comparisons by ANOVA of pivot angles of individual villi at the various speeds of flow will indicate whether pivoting continues to increase as flow increases.

6.3.3.7. Assessment of endogenous villous motility

The occurrence of any spontaneous longitudinal movement in individual villi was assessed from spatiotemporal maps of strain rate along three lines of interest (LOI) that were orientated along longitudinal axis of villi, i.e. on the upstream and downstream edges and along the central axis. The manner in which these maps are derived has been fully described elsewhere (Janssen and Lentle 2013). Briefly, the software identifies displacements of textural patterns within the images of the villi along the LOI, which are plotted row by row through time. Longitudinal strain rate is then derived by differentiation with respect to distance and similarly plotted. The resulting spatiotemporal map allows regions of contraction (negative strain rate) to be distinguished from those in which extension (positive strain rate) is taking place, through time (Janssen and Lentle 2013).

6.3.3.8. Sampling and statistics

All statistical analyses were conducted using the SPSS statistical package version 20.0.0 (SPSS Inc., Chicago, Illinois). Normality of the various data sets generated in this work was assessed by Lillefors test. Parameter values that were not normally distributed were converted via the Johnson algorithm in Minitab or by standard mathematical manipulation. Raw non-parametric data was summarised graphically as boxplots and reported as median and interquartile range (IQR) values in the text. Converted data was

compared by one-way ANOVA. The fits of displacements of various points along the shafts of villi expressed as a percentage of total tip displacement (TD) to the corresponding distance along the villus were explored by curve fitting using CurveExpert v.1.4 software (Hyams 2010) to determine whether the best fitting form of the regression line was linear.

6.3.4. Results

6.3.4.1. Villus length and width

Mean villous length (546 ± 3 μm) was normally distributed while mean villous width (156 ± 1 μm) was normally distributed only after logarithmic transformation (n = 234) in data obtained from the terminal ileum of four possums.

Direct superimposition of video images taken prior to the commencement of perfusion and intervals thereafter (see method for determination of villus bending) showed no tendency for the second image to be wider than the first i.e. no detectable change in villus width over time.

6.3.4.2. Flow profiles around villi

The relationship between perfusion rates, i.e. volumetric flow rates between 1.9 and 38.2 ml/min (as dictated by the syringe pump), and magnitude of the velocity of microbeads at a point 200 μm above the villous tips (Figure 6-13) was linear as expected. This indicates that the mPIV method was sensitive enough to detect changes in flow velocity under the experimental conditions.

At all three flow rates tested on villi, flow around the tips of isolated villi was characterised by streamlines moving upward toward the tip on the surface facing the flow and downward from the tip on the opposite surface. In the region located between

the base of the villus and a point 50 μm below the tip, the mean velocity of the flow in the two-dimensional (2D) plane examined (0.29 – 0.38 mm/s) was low compared to that at the tip (0.81 – 0.97 mm/s). These low values were likely from streamlines that had been deflected around the base of the villous.

Flow velocity profile perpendicular to the villous longitudinal axis

The velocity of flow at points 200 μm or more above the villi varied linearly with the distance from the tip. The approximate magnitudes of shear and strain rates acting on the villous tips could thus be calculated if it was assumed that this relationship could be extrapolated to the region at the villus tip. These shear rates varied between 1 and 7 s^{-1} and corresponded to shear stresses of 2 and 9 mPa (values that were calculated assuming Poiseuille flow in the flow cell) at perfusion rates of 3.8 and 15.3 ml/min respectively. These levels of shear stress exceeded those generated during normal peristaltic or pendular activity (see section 2.1 of Methods).

Plots of the horizontal component of velocity of the flow at right angles to the long axes of the villi (U_x) showed that flow declined rapidly below the villous tips at all three flow rates (Figure 6-14). The results from each experimental run (plotted as different symbols on Figure 6-14) differed in absolute values but all showed a pattern of exponential decline along the length of the villus regardless of flow rate. Hence, U_x varied somewhat between 1.5 mm/s and 0.25 mm/s in regions above the tips of the villi according to perfusion rate and declined rapidly and exponentially below the villous tips regardless of flow rate to a mean velocity of 0.11 mm/s at approximately 100 μm below the villous tips, and less than 0.05 mm/s at 200 μm below the tips (Figure 6-14).

Flow velocity profile parallel to the villous longitudinal axis

Of a total of 38 image sequences that were used for the calculation of TD, eight image sequences from a total of three villi from three animals were suitable (see experimental methods) for analysis of flow velocity profiles parallel to the villous longitudinal axis (U_y) at perfusion rates of 15.3, 7.6, 3.8 ml/min.

Lengthwise velocity (U_y) tended to decrease with distance from villous tip on both the upstream and downstream edges. Hence, at distances 50 μm below the villous tips, U_y varied between 1 and 400 μm/s whilst in regions between 50 μm and 300 μm below the villous tips, U_y was more than an order of magnitude lower, varying between 0.05 and 20 μm/s (Figure 6-15).

All three plots of the variation of U_y with lengthwise distance from the tip of the villus (Figure 6-15) showed a general trend of flow towards the villous tip on the upstream edge of the villus with some flow towards the base in the lower third of villus (notably between 250 and 400 μm from the villous tip). Conversely the velocity profile plot of the downstream edge of the villus showed a general trend of flow toward the villous base. Hence, volumetric flow at physiological rates was sufficient to establish a pattern of flow around the periphery of the villus although in all cases the flow rate was low.

6.3.4.3. Total displacement (TD) of the villous tip

It was possible to determine TD for a total of 26 villi from 7 animals over a total of 38 image sequences (Figure 6-16). The median TD was 5.07 μm with an interquartile range (IQR) of 5.29 (n = 12) at a volumetric flow rate of 3.8 ml/min; 6.46 μm with an IQR of 9.01 (n = 22) at 7.6 ml/min; and 10.59 μm with an IQR of 2.3 (n = 5) at 15.3 ml/min (Figure 6-16). Thus TD was generally small, being less than 7% of the mean width of a villus. There was no significant change ($P > 0.05$) in TD with flow rate on one-way-

ANOVA of logarithmically transformed data. There was no significant variation of TD with time over a period of 80 minutes.

6.3.4.4. Assessment of villous rigidity

The overall mean R^2 value obtained by SLR of percentage displacement of TD against distance down the villus for all villi was 0.82 ± 0.03. The R^2 values obtained from individual villi (0.80 at a flow rate of 3.8 ± 0.04 ml/min; mean 0.81 ± 0.04 at 7.6 ml/min; 0.88 ± 0.04 at 15.3 ml/min) did not vary significantly with flow rate. The overall mean pivot angle obtained from SLR of displacement in microns against distance down the villus in microns was 0.98^o with a 95% confidence interval (CI) between 0.73^o – 1.32^o. The pivot angles of individual villi required log transformation prior to ANOVA. The pivot angles of individual villi (mean 0.65^o; 95% CI 0.4^o – 1.06^o at a flow rate of 3.8 ± 0.04 ml/min; mean 1.15^o; 95% CI 0.76^o – 1.75^o at 7.6 ml/min; mean 1.27^o; 95% CI 0.03^o – 3.76^o at 15.3 ml/min) also did not vary significantly with flow rate (see also sub-section 6.3.8). Hence, there was no evidence of significant bending or any increase in pivot angle at any flow rate, the latter being no more than one degree in all readings.

Curve fits of pooled data (CurveExpert v.1.4) from all flow rates showed that the variation of displacement (expressed as a percentage of TD) against distance down the villus was best fitted by a linear function (Figure 6-17). At flow rates of 3.8, 7.6 and 15.3 ml/min significant linear regressions (Figure 6-17) with R^2 values of 0.73, 0.59, and 0.81 respectively were obtained. Moreover, the slopes of the linear fits at the three perfusion rates did not differ significantly on Student's t-test (d.f. = 29, T = 0.35, $P > 0.05$ between 3.8 and 7.6 ml/min, d.f. = 24, T = 1.41, $P > 0.05$ between 7.6 and 15.3 ml/min and d.f. = 13, T = 1.77, $P > 0.05$ between 15.3 and 3.8 ml/min). Together these findings indicate that the villi were effectively rigid and did not bend at physiological or

supra-physiological flow rates. Furthermore, the shafts of villi pivoted little around their bases. In regard to the latter finding it is important to note that the tension in the tightly mounted tissue (which was necessary to avoid movement of the entire mucosa on the probe) may have restricted such pivoting.

6.3.4.5. Spatiotemporal maps along the longitudinal axis of villi

The patterns of distribution of strain rate about the longitudinal axis of three villi on spatiotemporal maps taken at all three LOIs showed no coherent patterns of phasic change in strain rate that would be consistent with local phasic contractile activity that affected the longitudinal dimensions of the villi.

6.3.5. Discussion

This is the first study to assess the bending and passive mechanical properties of villi in the absence of any active villous motions in response to a flow of Newtonian fluid across living villous mucosa. It is noteworthy that the mucosa was harvested with minimal trauma and manipulation and was then maintained in a fluid environment similar to that *in vivo*. Hence whilst production of excess mucus by anoxic or mechanical degranulation of goblet cells was avoided, any material that is normally adherent or close to the villus (Maury et al. 1995, Lim et al. 2013) was maintained *in situ*.

The lack of any significant change in the profiles of lines of defined points on villi even when villi were exposed to supra-physiologically high levels of shear stress, indicates they would behave as rigid structures within the gut (see 'Villi bend Movie')[7]. Hence villi would be sufficiently rigid to allow their shafts to tilt in concert with folding of the underlying mucosa to generate crowding of the villous tips between adjacent folds

[7] See http://youtu.be/SybdXpWNCRo, if the video does not play after a few minutes loading on a standard broadband connection, please try reloading the page.

(Lentle et al. 2013). The ileal villi in this species were of similar lengths to those of other common laboratory animals such as rats (250 – 375 μm) (Daniel et al. 1989), pigs (275 – 310 μm) (Davidson et al. 1977) and dogs (460-550 μm) (Kuzmuk et al. 2005) and were within the range of villi lengths of the human small intestine (500-1000 μm) (Ham 1969, Weinstein et al. 1969). Further, they were tubular of form.

The finding that villi were relatively rigid structures fits with the dynamics outlined by previous workers (Hosoyamada and Sakai 2005). These workers concluded that villi would be in a turgid state as a result of absorbed fluid, the resultant interstitial pressure being opposed by tension of interstitial fibres and smooth muscle cells (Womack et al. 1988, Güldner et al. 1972) within and at the bases of these structures. Such turgor would render the villous shaft resistant to bending (Hosoyamada and Sakai 2005). It may be considered that this turgor was augmented in our *ex vivo* preparation, in the absence of any ongoing venous or lymphatic drainage. However, the finding that TD did not decrease significantly with time counts against such a hypothesis as does the finding that the widths of individual villi did not change appreciably over the course of the experimental determination of their bending and velocity profiles. Hence it seems likely that ongoing activity of smooth muscle in the villous shaft (Hosoyamada and Sakai 2005) prevented such engorgement. Whilst the villi in our experiment did not exhibit spontaneous movement, the phasic contraction of myocytes associated with any such action would presumably augment intravillous pressure and further limit the capacity of the villus shaft to bend. The absence of spontaneous villous contractions in the *ex vivo* preparations is in line with the findings of previous workers (Womack et al. 1988) who reported that spontaneous longitudinal movements only occurred *in vivo*.

Although the shafts of villi were rigid, there was detectable movement of the villous tip during flow (< 7% of the mean width of a villous). This movement was likely from

pivoting of the shaft of the villus around the point of the attachment of its base to the mucosa and from relative movement of the point of attachment across the underlying muscular wall of the ileum. Given the likely restriction of translational and pivoting movements of villi from the taut mounting of the tissue on the probe, it is probable that these movements would be of greater magnitude *in vivo*. The presence of such movements supports the hypothesis that submucosal laxity allows mucosal folding and that villi between mucosal folds may incline toward each other enhancing villous crowding (Lentle et al. 2013).

This is the first study to quantify flow patterns around living villi. Whilst much is known of the general nature of flow around rigid structures, notably the tendency for vortices to form between structures that project into a flow-stream (Tietjens 1935), the effects of the material properties of the villi and of the mucins around and between the villi have not been previously described. The fact that the velocity of flow in the perivillous spaces around the bases of villi was reduced to levels that approximate those of macromolecular diffusion, even at supra-physiological rates of perfusion, fits with previous work indicating that the bulk of absorption occurs in the upper third of the villus (Ryu and Grimm 1982), i.e. over a distance of 180 μm proximal to the tip of the villous. Any solvent drag (Pappenheimer 2001b) generated in the preparation, would similarly be around the villus tip and unlikely to influence mixing in the lower intervillous space. Thus advective mass transfer in these regions can only be secured by movements of the villi or mucosa (Levitt et al. 1990). Such mixing could be brought about by uncoordinated, i.e. spontaneous, contraction of villi (King and Robinson 1945, Womack et al. 1988, Mailman et al. 1990, Wang et al. 2010) or by mucosal folding (Lentle et al. 2013).

While the size and form of the ileal villi of the possum are similar to those of humans, and mucosal architecture, i.e. density of villi and effective surface area per unit villus, are also similar over a range of laboratory species (Kararli 1995), caution is required in generalising the findings from this study. It is likely that flow dynamics vary with the rate and character of mucus secretion where the latter varies regionally along the small intestine (Robbe et al. 2003). Again it is possible that ileal villi of other vertebrate species vary in their rigidity, for example according to the abrasive qualities of the diet.

In conclusion, our experiments provide new insights into the ability of static villi to augment mass transfer and absorption. The lack of significant advective mixing in the base of the intervillous space indicates that absorption is likely to be confined to the tips of villi under conditions when the villi and wall are immobile. The finding that villi are resistant to bending, even at supra-physiological flow rates, indicates that intrinsic movements of villi will be correspondingly limited but that relative movements of their shafts will be reflected in movements of their tips. Correspondingly, the finding of displacement of the tips by flow indicates that the shaft of the villi may become angulated relative to the mucosa and supports a mechanism of fluid displacement by villous apical crowding and consequent augmentation of mixing (Lentle et al. 2013).

Acknowledgement

We wish to thank William Thielicke of University of Applied Sciences Bremen, Bremen, Germany for his helpful advice regarding the mPIV technique used in the work.

6.3.6. Journal article references

Allen, A., G. Flemstrom, A. Garner and E. Kivilaakso (1993) Gastroduodenal mucosal protection. Physiological Reviews **73**: 823-857.

Bueno, L., J. Fioramonti and Y. Ruckebusch (1975) Rate of flow of digesta and electrical activity of the small intestine in dogs and sheep. Journal of Physiology **249**: 69-85.

Corfield, A. P., D. Carroll, N. Myerscough and C. S. J. Probert (2001) Mucins in the gastrointestinal tract in health and disease. Frontiers in Bioscience **6**: D1321-D1357.

Daniel, H., C. Fett and A. Kratz (1989) Demonstration and modification of intervillous pH profiles in rat small intestine in vitro. American Journal of Physiology **257**: G489-G495.

Danielsen, E. M., H. Sjöström, O. Norén, B. Bro and E. Dabelsteen (1982) Biosynthesis of Intestinal microvillar proteins. Characterization of intestinal explants in organ culture and evidence for the existence of pro-forms of the microvillar enzymes. Biochemical Journal **202**: 647-654.

Davidson, G., D. Gall, M. Petric, D. Butler and J. Hamilton (1977) Human rotavirus enteritis induced in conventional piglets. Intestinal structure and transport. Journal of Clinical Investigation **60**: 1402.

Grovum, W. L. and V. J. Williams (1973) Rate of passage of digesta in sheep. 1. The effect of level of food intake on marker retention times along the small intestine and on apparent water absorption in the small and large intestines. British Journal of Nutrition **29**: 13-21.

Gruzdkov, A. A., V. Gusev and A. M. Ugolev, editors (1989) Mathematical Modelling. Moscow: Mir. 228-234 p.

Güldner, F., J. Wolff and D. Keyserlingk (1972) Fibroblasts as a part of the contractile system in duodenal villi of rat. Cell and Tissue Research **135**: 349-360.

Ham, A. W. (1969) Histology. Philadelphia: Lippincott:663.

Holzheimer, G. and D. Winne (1989) Influence of distension on absorption and villous structure in rat jejunum. American Journal of Physiology **256**: G188-G197.

Hosoyamada, Y. and T. Sakai (2007) Mechanical components of rat intestinal villi as revealed by ultrastructural analysis with special reference to the axial smooth muscle cells in the villi. Archives of Histology and Cytology **70**: 107-116.

Hosoyamada, Y. and T. Sakai (2005) Structural and mechanical architecture of the intestinal villi and crypts in the rat intestine: integrative reevaluation from ultrastructural analysis. Anatomy and Embryology **210**: 1-12.

Hulls, C., R. G. Lentle, C. de Loubens, P. W. M. Janssen, P. Chambers and K. J. Stafford (2012) Spatiotemporal mapping of *ex vivo* motility in the caecum of the rabbit. Journal of Comparative Physiology B **182**: 287-297.

Hyams, D. (2010) CurveExpert software. URL http://www.curveexpert.net.

Janssen, P. W. M., R. G. Lentle (2013) Spatiotemporal Mapping Techniques for Quantifying Gut Motility. New Advances in Gastrointestinal Motility Research: Springer. pp. 219-241.

Kararli, T. T. (1995) Comparison of the gastrointestinal anatomy, physiology, and biochemistry of humans and commonly used laboratory animals. Biopharmaceutics and Drug Disposition **16**: 351-380.

Keane, R. D. and R. J. Adrian (1990) Optimization of particle image velocimeters. I. Double pulsed systems. Measurement Science and Technology **1**: 1202.

King, C. E. and M. H. Robinson (1945) The nervous mechanisms of the muscularis mucosae. American Journal of Physiology **143**: 325-335.

Kuzmuk, K. N., K. S. Swanson, K. A. Tappenden, L. B. Schook and G. C. Fahey (2005) Diet and age affect intestinal morphology and large bowel fermentative end-product concentrations in senior and young adult dogs. The Journal of Nutrition **135**: 1940-1945.

Lentle, R. G., P. W. M. Janssen, C. de Loubens, Y. F. Lim, C. Hulls and P. Chambers (2013) Mucosal microfolds augment mixing at the wall of the distal ileum of the brushtail possum. Neurogastroenterology & Motility **25**: 881-e700.

Lentle, R. G., Y. Hemar, C. E. Hall and K. J. Stafford (2005) Periodic fluid extrusion and models of digesta mixing in the intestine of a herbivore, the common brushtail possum (*Trichosurus vulpecula*). Journal of Comparative Physiology B **175**: 337-347.

Levitt, M. D., J. K. Furne, A. Strocchi, B. W. Anderson and D. G. Levitt (1990) Physiological Measurements of Luminal Stirring in the Dog and Human Small Bowel. Journal of Clinical Investigation **86**: 1540-1547.

Lim, Y. F., M. A. K. Williams, R. G. Lentle, P. W. M. Janssen, B. W. Mansel, S. A. J. Keen and P. Chambers (2013) An exploration of the microrheological environment around the distal ileal villi and proximal colonic mucosa of the possum (*Trichosurus vulpecula*). Journal of the Royal Society Interface **10**: 20121008.

Mailman, D., W. A. Womack, P. R. Kvietys and N. Granger (1990) Villous motility and unstirred water layers in canine intestine. American Journal of Physiology **258**: G238-G246.

Maury, J., C. Nicoletti, L. Guzzo-Chambraud and S. Maroux (1995) The filamentous brush border glycocalyx, a mucin-like marker of enterocyte hyper-polarization. European Journal of Biochemistry **228**: 323-331.

Pappenheimer, J. (2001a) Intestinal absorption of hexoses and amino acids: from apical cytosol to villus capillaries. Journal of Membrane Biology **184**: 233-239.

Pappenheimer, J. R. (2001b) Role of pre-epithelial "un-stirred" layers in absorption of nutrients from the human jejunum. The Journal of Membrane Biology **179**: 185-204.

Prasad, A. K. (2000) Particle Image velocimetry. Current Science **79**: 51-60.

Raffel, M., C. Willert and J. Kompenhans (1998) Particle Image Velocimetry: A Practical Guide. Göttingen, Germany: Springer-Verlag.

Robbe, C., C. Capon, E. Maes, M. Rousset, A. Zweibaum, J. P. Zanetta and J. C. Michalski (2003) Evidence of regio-specific glycosylation in human intestinal mucins. The Journal of Biological Chemistry **278**: 46337-46348.

Ryu, K. H. and E. Grim (1982) Unstirred water layer in canine jejunum. American Journal of Physiology **242**: G364-G369.

Santiago, J., S. Wereley, C. Meinhart, D. Beebe and R. Adrian (1998) A particle image velocimetry system for microfluidics. Experiments in Fluids **25**: 316-319.

Thielicke, W. (2013) Personal Communication.

Thielicke, W. and E. Stamhuis (2013) PIVlab - Time-Resolved Digital Particle Image Velocimetry Tool for MATLAB.

Tietjens, O. (1935) Applied Hydro-and Aeromechanics, based on Lectures by L. Prandtl. Bulletin of the American Mathematical Society **41**: 173-174.

Wang, Y., J. G. Brasseur, G. Banco, A. G. Webb, A. C. Ailiani and T. Neuberger (2010) A multiscale lattice Boltzmann model of macro- and micro-scale transport, with applications to gut function. Philosophical Transactions of the Royal Society Series B; Mathematical, Physical and Engineering Sciences **368**: 2863-2880.

Weinstein, L. D., C. P. Shoemaker, T. Hersh and H. K. Wright (1969) Enchanced Intestinal Absorption After Small Bowel Resection in Man. Archives of Surgery **99**: 560-562.

Westergaard, H. and J. M. Dietschy (1974) Delineation of the dimensions and permeability characteristics of the two major diffusion barries to passive mucosal uptake in the rabbit intestine. The Journal of Clinical Investigation **54**: 718-732.

Womack, W. A., P. K. Tygart, D. Mailman, D. N. Granger and P. R. Kvietys (1988) Villous motility: Relationship to lymph flow and blood flow in the dog jejunum. Gastroenterology **94**: 977-983.

6.3.7. Figures and Figure Legends

Figure 6-11: Tissue flow cell used in experimental work.

A) Lateral view, B) plan view

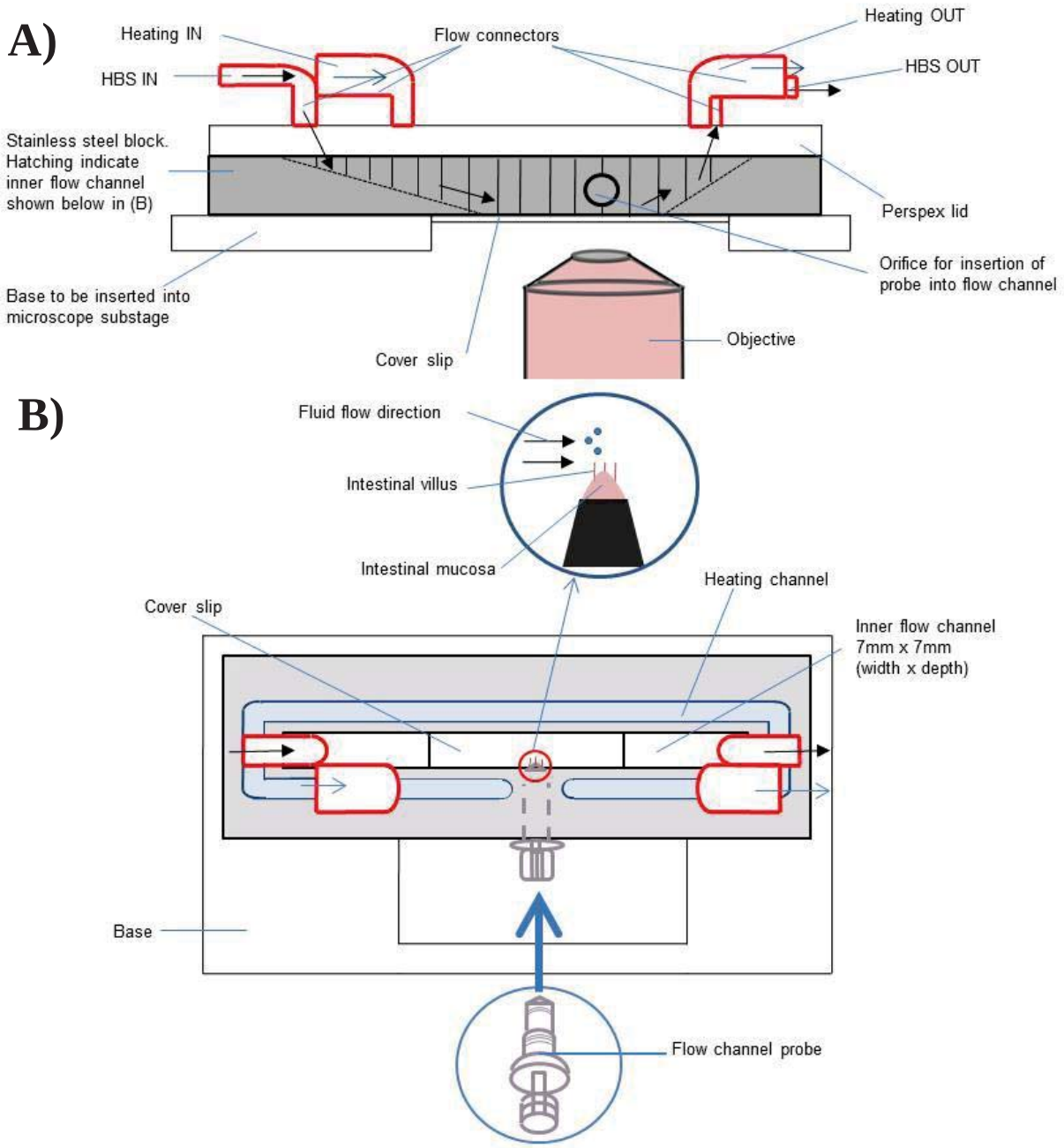

Figure 6-12: Method for determining the total displacement of villus tips (TD).

A) A spatiotemporal intensity (ST) map taken along a 'line of interest' (LOI - indicated by the dashed line in (B) situated 20 µm below the villus tip before flow commenced (left arrow on upper border of map) and at the time of maximum displacement (TD) (right arrow on upper border of map).

B) Views of the villus from which the ST map was taken before flow commenced and at the time of maximum displacement (right). The square marks a distinctive structural feature used as a reference point. The value of TD is calculated from the difference in the location of the same distinctive feature in the two images.

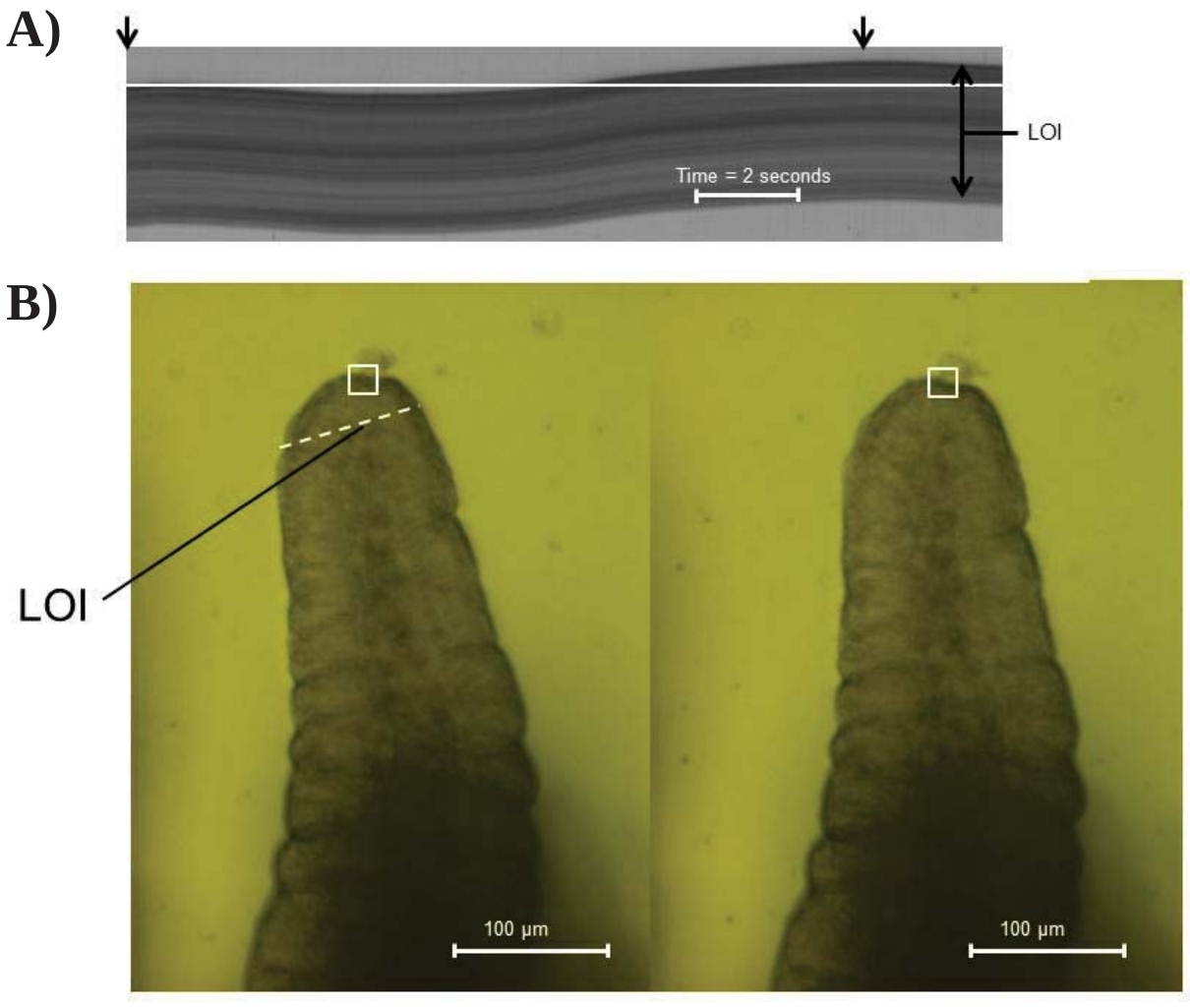

Figure 6-13: Relationship between local velocity of microbeads and the volumetric perfusion rate.

The local velocity of microbeads were taken in the region 200 µm above the villous tips and determined by mPIV. Physiological flow rates reported during the postprandial period (Grovum and Williams 1973; Bueno et al. 1975) are indicated by the shaded region in the plot.

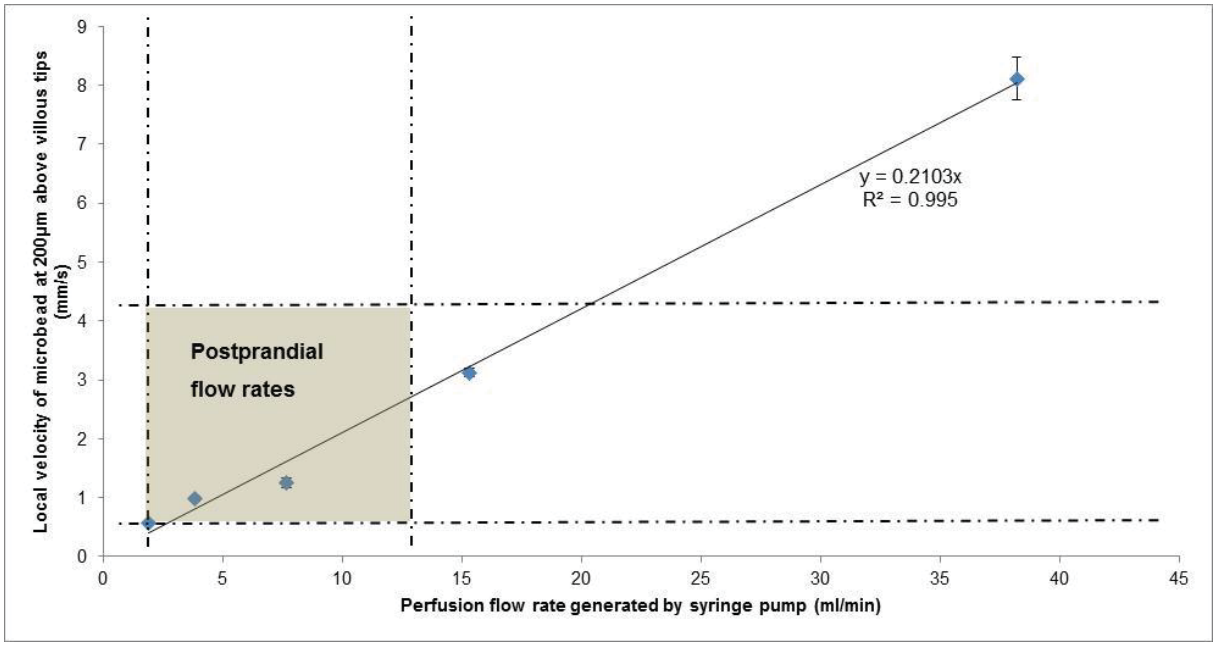

Figure 6-14: Variation of U_x with lengthwise distance from the villous tip.

Flow velocity component at right angles to the long axis of the villi (U_x) were determined 30 μm lateral to the villous image edge at three perfusion flow rates – A) 3.8 ml/min, B) 7.6 ml/min, C) 15.3 ml/min.

Zero on both Y axes corresponds to tip of the villus while negative distances are distances below the villous tip. Exponential fits (R^2 given on each plot) were obtained for all three perfusion rates. The different symbols on each plot represent a different experimental runs on different villi.

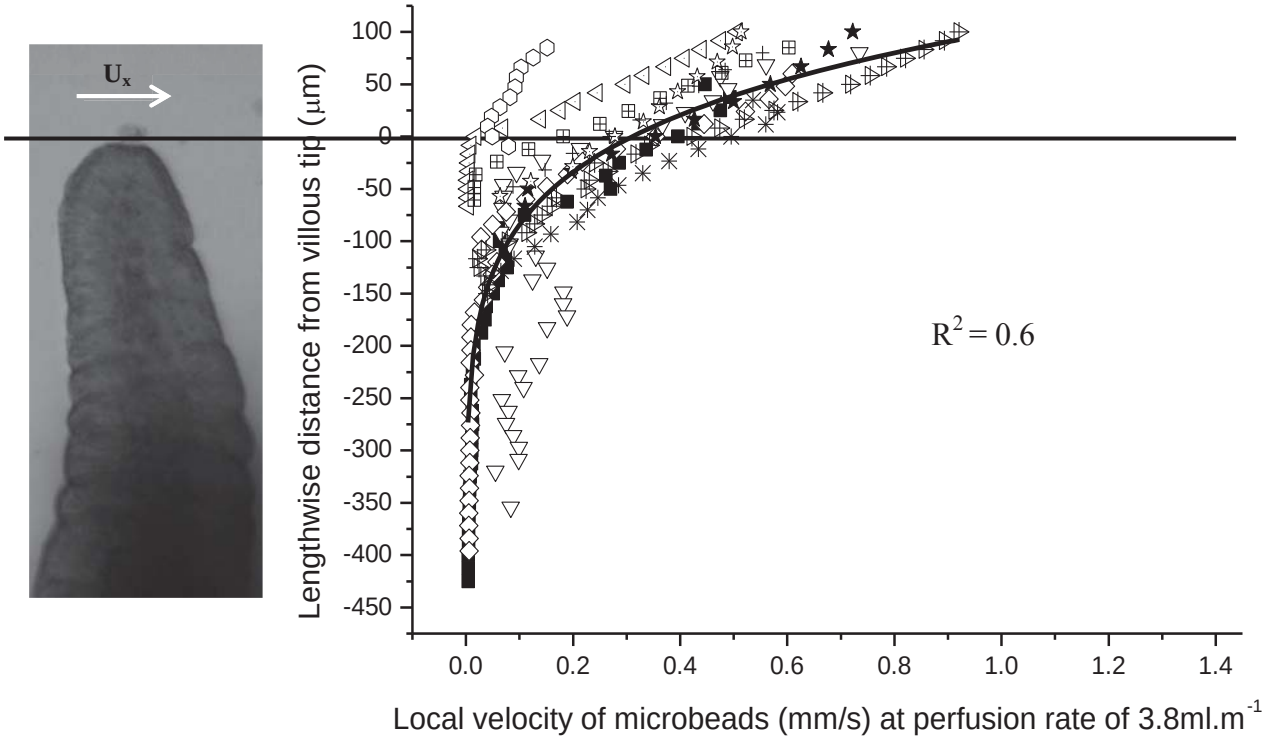

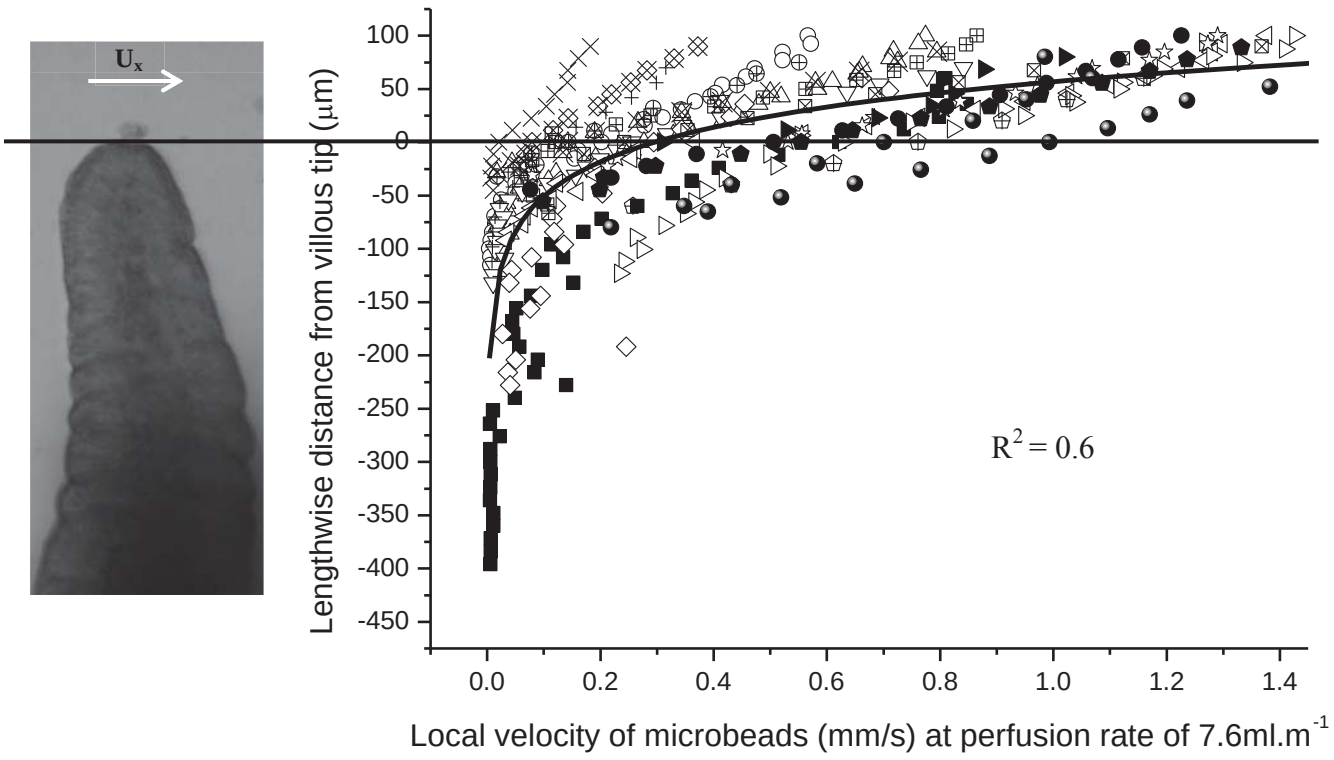
U_x
Lengthwise distance from villous tip (μm)
100
50
0
-50
-100
-150
-200
-250
-300
-350
-400
-450
0.0
0.2
0.4
0.6
0.8
1.0
1.2
1.4
$R^2 = 0.6$
Local velocity of microbeads (mm/s) at perfusion rate of 7.6ml.m^{-1}

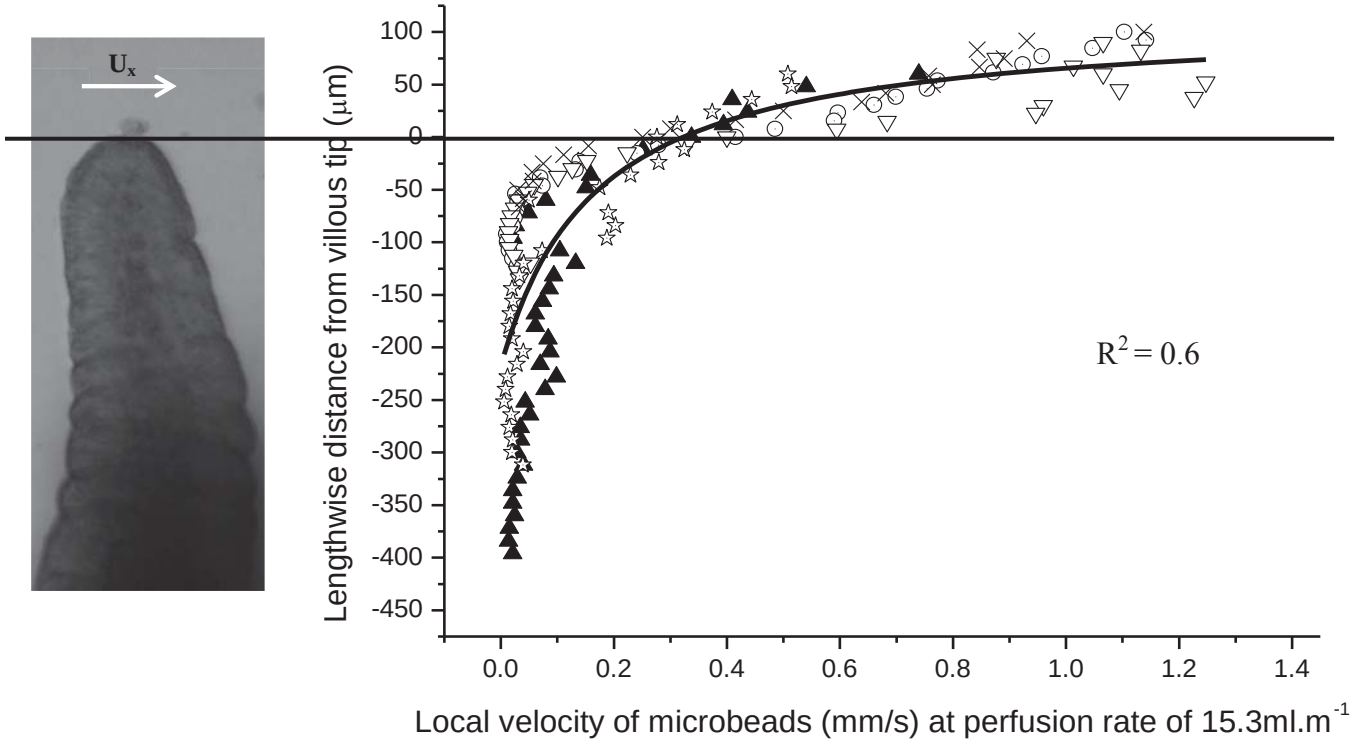
U_x
Lengthwise distance from villous tip (μm)
100
50
0
-50
-100
-150
-200
-250
-300
-350
-400
-450
0.0
0.2
0.4
0.6
0.8
1.0
1.2
1.4
$R^2 = 0.6$
Local velocity of microbeads (mm/s) at perfusion rate of 15.3ml.m^{-1}

Figure 6-15: Variation of Uy with lengthwise distance from the villous tip.

Flow velocity component parallel to the longitudinal axis of villi (U_y) were determined 5 – 15 µm from the upstream edge (left) and downstream edges (right). Hollow points indicate upflow (UF) and solid points indicate downflow (DF). There is an overall trend of upward flow on the upper upstream edge and downward flow on the upper downstream edge. Local velocities are lower at distances > 200 µm below the tip on both sides of the villus.

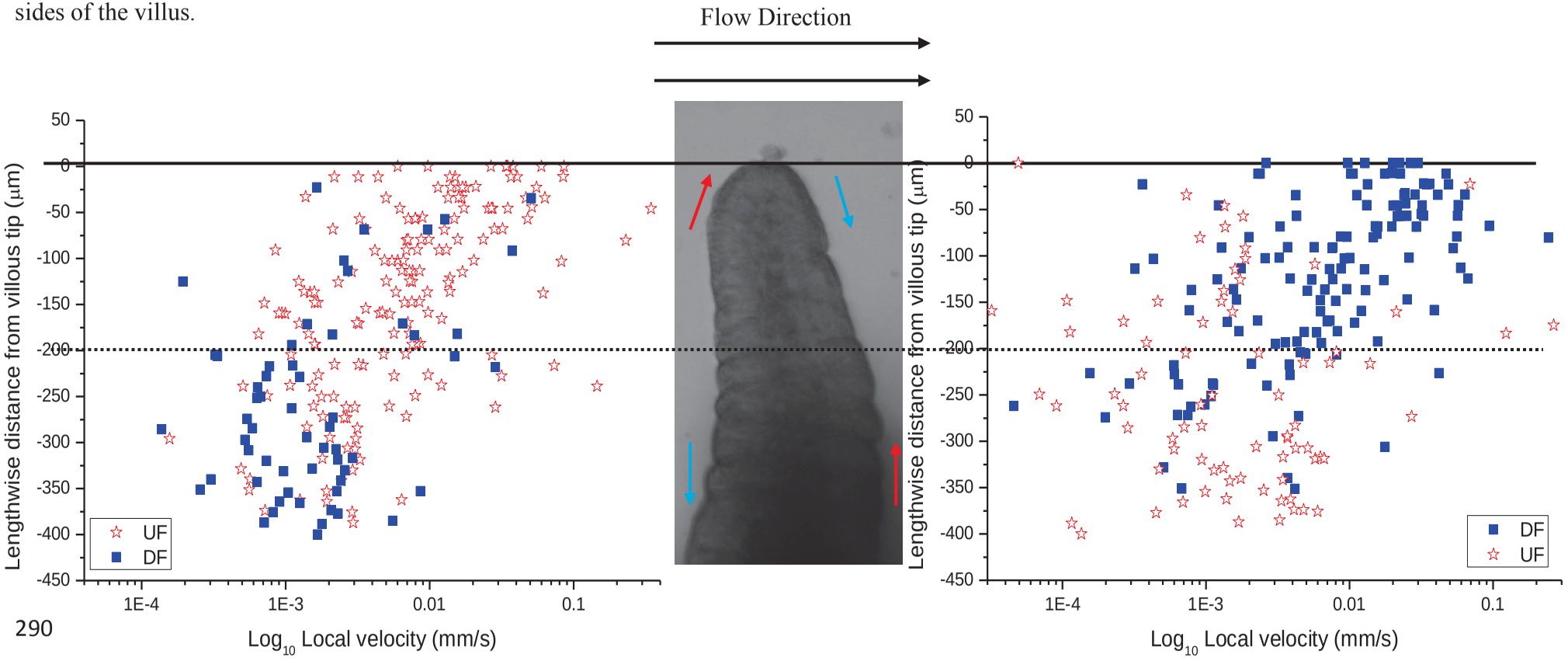

Figure 6-16: Variation of total displacement (TD) with volumetric flow rate.

A box plot showing the variation of TD with perfusion flow rate is presented. There was no significant variation of TD with flow on 'analysis of variance' (ANOVA) of logarithmically transformed data. The following are the definitions of the various symbols on the boxplots: The maximum and minimum values of the dataset are indicated by the longer horizontal lines usually found on the extreme ends of the plot, the diagonal crosses (X) indicates the 1% and 99% percentile of the dataset, the shorter horizontal lines connected to the rectangle box by a vertical line is the 5% and 95% percentile of the dataset, the longest horizontal line forming the upper and lower boundaries of the box indicates the 25% and 75% percentile (i.e. the lower and upper quartile respectively) of the dataset, the longest horizontal line within the box is the median value of the dataset whilst the square (□) indicates the mean of the dataset.

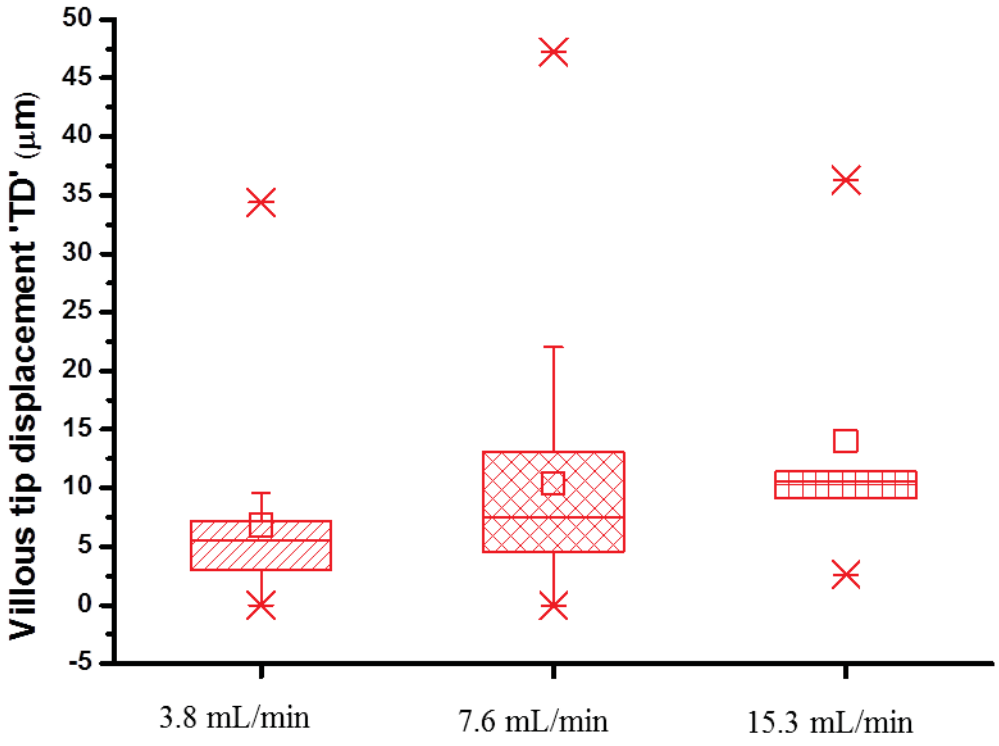

Figure 6-17: Relationship between displacement of points along the villous length with distance from the villous tip.

The plot utilized data pooled from all villi*. Displacement is expressed as a percentage of total tip displacement (TD). The regression lines that best fitted the data obtained at each perfusion rate were all linear.

* R^2 values shown are for pooled data. R^2 values for 'straight line regression' (SLR)s of individual villi were all above 0.8 at each flow rate. The dotted lines are 95% confidence intervals.

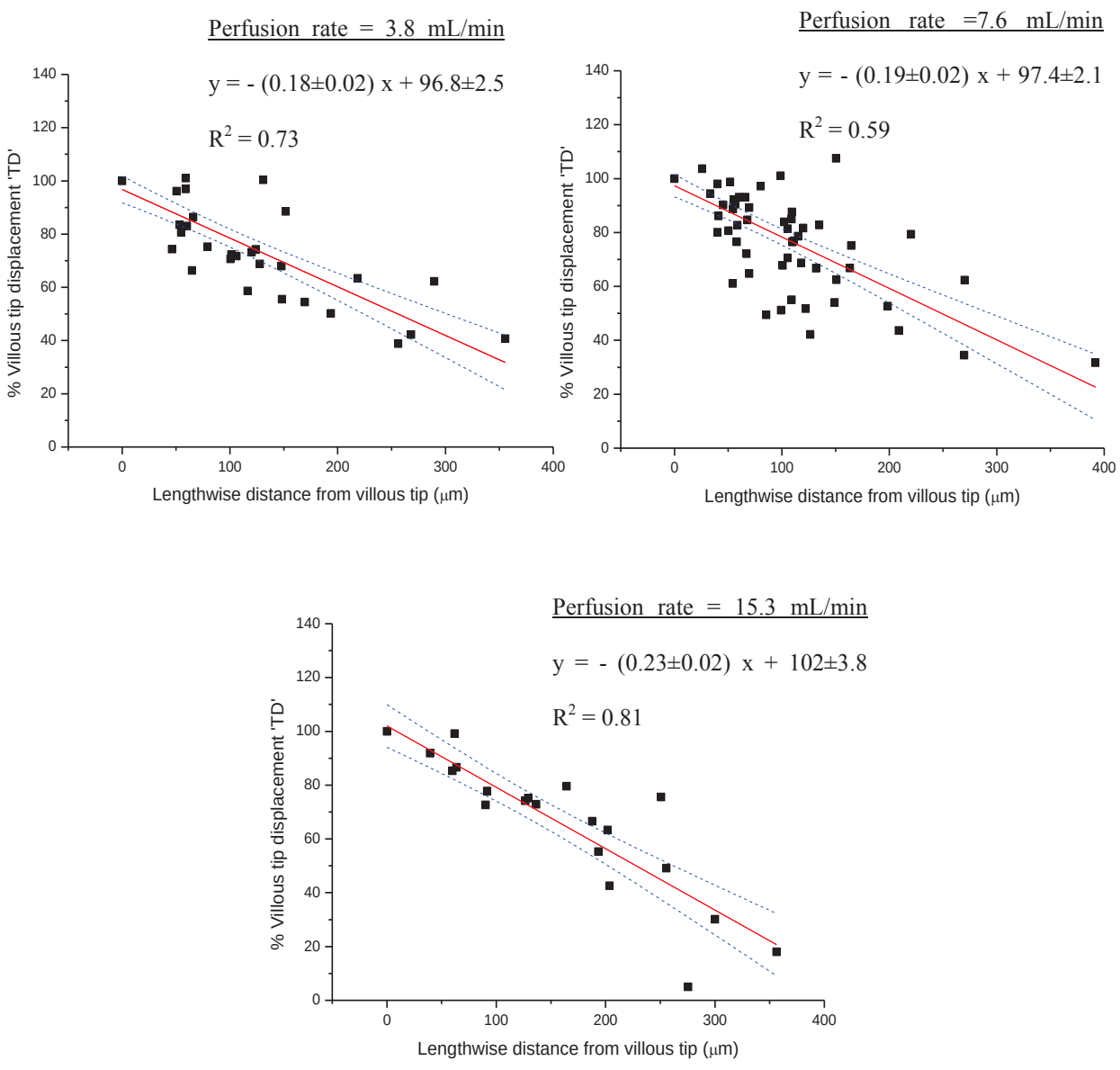

6.3.8. Additional Notes on the Published Journal

It was not possible to perform a repeated measures test on the pivoting angles of villi under all three perfusion rates as not all perfusion rates were applied to all of the villi observed. However, if we assume that all villi observed would have similar passive mechanical properties regardless of position in the ileum or between animals, this would allow a one-way ANOVA of the pivot angles with perfusion rates to be conducted with a Bonferroni post-hoc testing. The results of such an analysis showed that the pivot angles of individual villi did not vary with the perfusion rate used. Hence the pivot angles of villi at the perfusion rate of 3.8 mL/min are not significantly different ($P > 0.05$) to those at perfusion rates of 7.6 mL/min and 15.3 mL/min on Bonferroni post-hoc testing.

6.4. Additional Methods and Results

The following describes the development and the results of two Lattice Boltzmann Modelling (LBM) simulations conducted in three-dimensions (3D). Firstly, of a model of flow patterns around an isolated villus and secondly a model of the flow patterns in the intervillous space of asymmetrically arranged arrays of villi. The developed 3D computational models simulated flow patterns in the perivillous space (i.e. regions of a short distance over the apices of villi and in the intervillous space) during physiological levels of lumen flow.

6.4.1. Physical formulation

The fluid flow around an isolated villus and through an infinite array of villi was modelled by the Navier-Stokes equations in their dimensionless form. The orientation of the X, Y and Z dimensions around the villi can be viewed in Figure 6-18A (see below). The fluid phase was assumed to be Newtonian (Lim et al. 2013).

Flow was generated by the translation of the upper boundary at a constant velocity in the X-direction (perpendicular to the long axis of the villus) in order to represent the action of a propagating gut contraction that would cause lumen flow. The inlet (i.e. upper boundary) velocity U and the villi diameter $2R_{vil}$ were chosen as characteristic values for defining the Reynolds number Re:

$$Re = \frac{\rho U 2R_{vil}}{\mu} \tag{6.1}$$

where ρ is the density of the aqueous phase around villi (= 10^3 kg/m^3), μ is the viscosity of the aqueous phase as determined by microrheometry (= 1.5 mPa.s) (Lim et al. 2013) while characteristic velocities were no more than 8 mm/s derived from mPIV velocity

fields around villi, (Figure 6-13 in Lim et al. 2014). Thus flow around the villi modelled were laminar with *Re* numbers lower than 50.

The upper boundary was placed at a sufficient distance from the tips of the villi or villous tip in the case of the model 1 (see below) so that any boundary effects of pressure and velocity at the upper boundary would not artificially influence the streamlines generated in the intervillous space by lumen flow. To assess the validity of this assumption, a series of preliminary numerical simulations were performed with inlet velocities varying in the range of the velocities measured experimentally to verify that streamlines and dimensionless velocity in the intervillous space was dependent only on *U*.

6.4.1.1. Villous profile

The shape of a villous Vil_p(X, Y) was described by a polynomial to the fourth power by the following equation:

$$Vil_p = h_{vil} - \frac{l}{{R_{vil}}^4}(X^4 + Y^4) \quad (6.2)$$

where h_{vil} is the length of a villous (= 560µm), R_{vil} is half its width (= 80µm) and *X* and *Y* were the coordinates (µm). In accordance with the experimental observations (Lim et al. 2014), the villus was assumed to be static and rigid.

6.4.2. Description of models developed

6.4.2.1. Model 1: Flow profile around an isolated villus

A first 3D model of flow around an isolated villus was developed with the experimental findings of villous dimensions and flow conditions obtained from Lim et al. (2014) to reproduce the fluid flow patterns around an isolated villous as observed in Lim et al.

(2014). The inlet and outlet boundary conditions of pressure and velocity were calculated by the methods of Guo et al. (2002) as had been done in the previously described models (see chapter four and five of this thesis). The flow was assumed to be uniform and orientated in the X-direction at the inlet while the pressure field as well as the Y and Z components of the velocity field were assumed to be zero at the outlet. The velocity at the upper boundary of the model was assumed constant in the X-direction and zero in the Y- and Z-dimensions (i.e. directions).

6.4.2.2. Model 2: Flow profile around an array of diagonally staggered villi

A second model was developed in order to predict flow patterns in the intervillous space during lumen flow. In this simulation, the villi positions were staggered diagonally to form an asymmetric arrangement that persisted infinitely over the whole array. The computational domain was reduced to just 2 villi by using periodic boundary conditions in the X and Z directions. The villi were each separated by a distance equivalent to the width of a villous in both dimensions (Lentle et al. 2013).

6.4.3. Lattice Boltzmann methods

The Navier-Stokes equations were solved by lattice Boltzmann (LB) methods and has been outlined in detail in chapter four of this thesis. A similar lattice Boltzmann Bhatnagar-Gross-Krook scheme (LBGK) (Du and Shi 2010) was also used but was scaled to three-dimensions (3D). The no-slip boundary conditions on the villous were calculated by the bounce-back boundary scheme in the stair-case approximation (Sukop and Thorne 2007) in both models. The results were given in the steady state for which the criterion (Loudon and Tordesillas 1998) was:

$$\frac{\{\sum(u_i - u_{i-1})^2\}^{1/2}}{\{\sum(u_{i-1})^2\}^{1/2}} < 10^{-7} \qquad (6.3)$$

where u is the magnitude of the velocity field and *i* the number of iterations. The flow was represented by the magnitude of the velocity field as 3D and also 2D streamlines, superimposed in the plane (X, Y) intersecting the villus through its central axis.

6.4.4. Results

6.4.4.1. Fluid flow modelling around an isolated villous

The flow conditions and villous dimensions obtained from Lim et al. (2014) were incorporated into a LB model of flow around an isolated villus. A Z-dimension transect of the magnitude of flow velocity was plotted in 2D from the output of the model. The flow profile on this plot (Figure 6-18C) was similar to that obtained in the experimental work (Figure 6-14 in (Lim et al. 2014)).

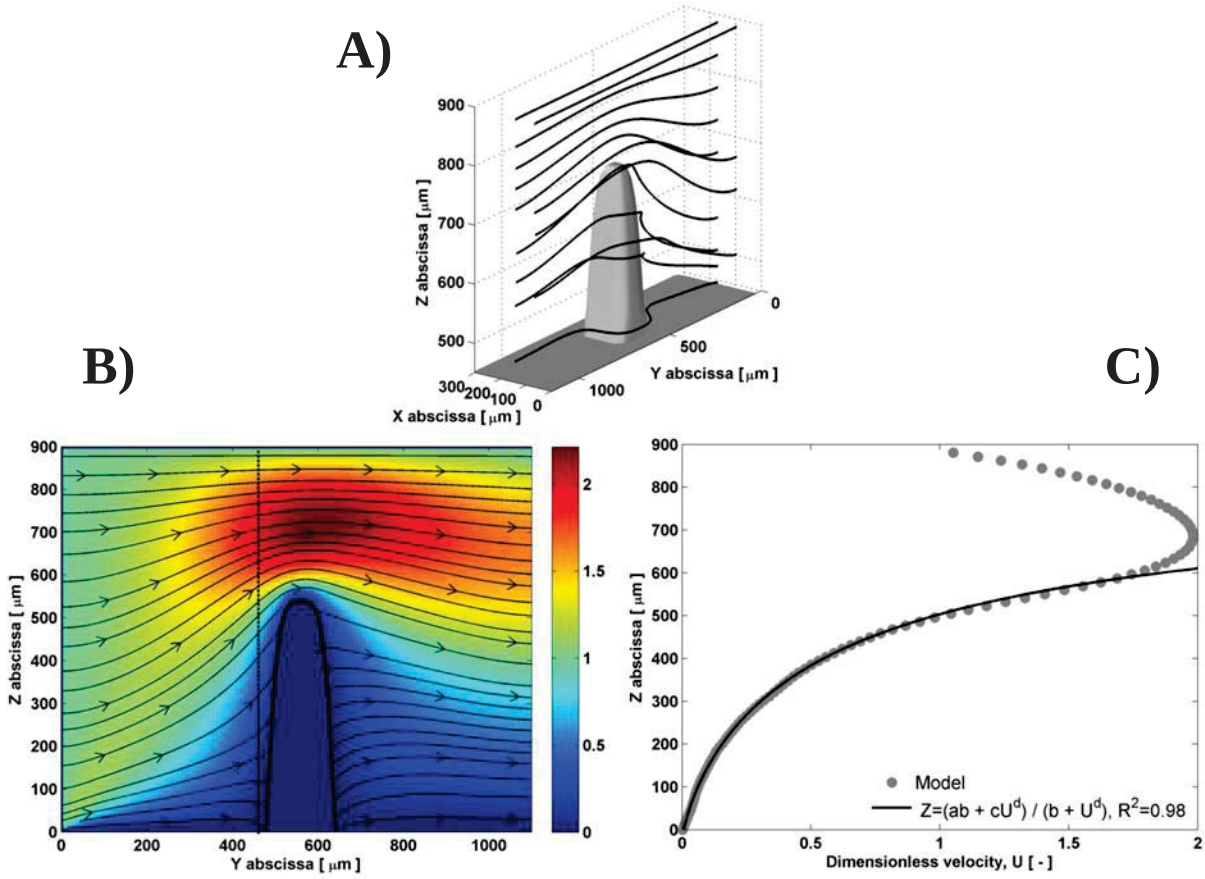

Figure 6-18: Lattice Boltzmann modelling (LBM) output based on data derived from Lim et al. (2014) simulating flows around an isolated villus. A) A 3D simulation of flow of a Newtonian fluid around an isolated villus. B) A 2D plot of flow patterns around a single villus taken of a transect near the midpoint of the villous in the Z-dimension. C) A transect plot of dimensionless flow velocity along the Y-axis 30 μm away from the villus (indicated by the location of the dotted line in B). The simulated gradation of flow along the length of the villous is similar to that observed in Lim et al. (2014) (Figure 6-14) with both fitting the same function. The flow profile above the villous tips in C) describes the Poiseuille flow profile with a 'no-slip' boundary condition at the upper boundary of the model.

In the region close to the tip of a villous, upstream and downstream streamlines were deflected upward and downward respectively. A 3D view of the flow (Figure 6-18A) showed that the streamlines travelled around the base of the villous. These phenomena were not directly visible on 2D experimental views of the flow (Figure 6-14 in Lim et al. 2014). The declining profiles of U_x with distance from the villous tip that were seen at the three perfusion rates in Lim et al. (2014) and the dimensionless velocity profile as

can be seen in Figure 6-18C (predicted by the computational model) could all be fitted by an exponential function (see equation below).

$$Y = \frac{ab+cx^d}{b+x^d} \quad (6.4)$$

This equation fitted the plot of lengthwise distance from the tip of the villus against U_x at all perfusion flow rates with an R^2 of 0.6, as well as the initial portion of the model that encompassed the length of the modelled villi (Figure 6-18C), thus validating its use.

6.4.4.2. Modelling of fluid flow around an infinite array of asymmetric villi

The accomplishment of reproducing flow profiles around an isolated villus as observed by Lim et al. (2014) using LB computational modelling as outlined in the previous sub-section allowed the model parameters to be extrapolated to allow the flow profile around an array of diagonally staggered villi to be predicted. In this second 3D model, it was observed that the streamlines deviated around the villous tips in a similar manner to that observed around isolated villi (Figure 6-19). On 2D transects, intervillous flow was characterised by a circulation (i.e. vortex) between the base and the tip generating vortices. However, the dimensionless velocity decreased by many decades along the direction parallel to the villous longitudinal axis (Y-direction).

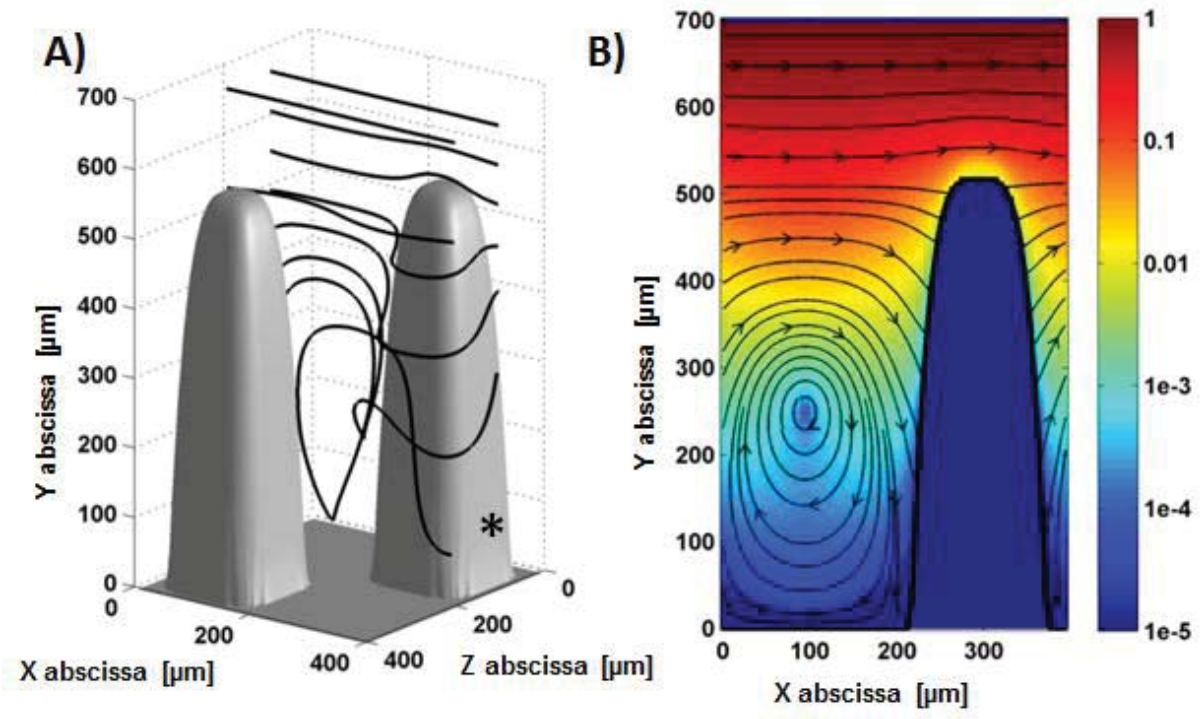

Figure 6-19: Output from model based on data derived from experimental work simulating flow in the intervillous space. Villous dimensions and flow velocities around a villus were incorporated into the model to simulate flow conditions in the intervillous space shown in three-dimensions (3D) (A) and two-dimensions (2D) (B) plots. In the latter, flow patterns are located at the plane near the mid-point of the villous marked '*' in the Z-dimension of the 3D plot. Velocity values are in units of mm/s.

6.5. Ancillary discussion – significance of chapter findings

The studies outlined in this chapter determined the rigidity of an isolated villous and the pattern of flow velocity in the perivillous region in the terminal ileum of the brushtail possum using novel experimental apparatus and techniques. Computational modeling of the perivillous fluid environment around an array of asymmetrically arranged villi that incorporated villous dimensions and fluid flow conditions observed by Lim et al. (2014) was also used to predict flow patterns in intervillous space between two adjacent villi. The following are discussions that were not included with Lim et al. (2014) in the context of additional methods and results that were presented in section 6.4.

Novel 3D computational modelling of the perivillous region around an array of villi had shown that vortices may be formed in the intervillous space. However, the velocity of flow was reduced by several orders of magnitude at the villous base. Assuming that the reported velocity of a peristaltic wave in the possum ileum (≈ 0.5 mm/s, (Lentle et al. 2007) was the characteristic velocity of the flow (U_c) and knowing that this velocity was reduced by at least two orders of magnitude in the intervillous space (Figure 6-18), it follows that the time scale that was necessary for an element of fluid to travel by advection and diffusion, a distance equivalent to the length of a villous (h_{vil}) will be around 100 s ($100*h_{vil}/U_c$). For small molecules such as glucose that have a relatively large diffusion coefficient in water ($D \approx 8.10^{-10}$ m²/s (Beaudoing et al. 1991)), the time scale of diffusion will be around 300 s (h_{vil}^2/D).

Thus it would appear that flow velocity in the intervillous region near the villous base would approach that of diffusion. As both the diffusive and advective time scales are of a similar order of magnitude, it could be expected that the intervillous vortices that were observed in the simulations highlighted in this chapter will have little effect in

augmenting mass transfer for smaller molecules. Consequently, such findings can be viewed as indicating that advective mixing by other means would be required to institute flow and augment absorption in all parts of the intervillous space (Levitt et al. 1990).

It is noteworthy that the formation of vortices during lumen flow is likely to be restricted only to the intervillous space in between the maximal cross-sectional area of rigid and static villi assuming villi were of tubular or finger-shaped in form. The vortex would likely diminish with increasing proximity to the intervillous space in between the minimum cross-sectional areas of villi hence further reducing the effect of advective mass transfer in this region. This highlights the importance of 3D modelling to delineate flow patterns around more complicated structures such as villi.

The findings of rigid villi also has further implications on potential mixing of perivillous lumen contents during lumen flow not mentioned in Lim et al. (2014). An array of rigid and static villi could approximate a static mixing device (Bertsch et al. 2001) to split, rearrange and recombine the various elements of perivillous luminal contents that flow past villi during lumen flow. However, such a mixing mechanism is reliant on minimal pivoting of the villous shaft (by laxity at the point of union of the villous base and the underlying mucosa). It was observed that villi on gut sample tautly mounted on the flow cell probe exhibited small amounts of pivoting (< 7% of the mean width of a villous) (Lim et al. 2014). Hence it is likely that villi could more readily pivot during lumen flow with lesser tension being applied to the gut sample and therefore likely to reduce the effectiveness of such mixing mechanism.

Conversely, were the rigid villi prone to pivot by a larger angle, an alternate mechanism of mixing and mass transfer in the intervillous regions could be postulated. Oscillatory

(i.e. back and forth) flow induced by *in situ* gut contractions (e.g. pendular activity) (Lentle et al. 2012) could result in the follow events: periodic contractions of such nature would cause villi to pivot to its side, an action which may diminish the intervillous volume, and straighten, an action which re-establishes the intervillous space may result in a 'pumping' action. Such a mechanism could facilitate the mass transfer of fluid containing solutes between regions above villi and the intervillous region. However, the finding of the occurrence of mucosal microfolding during non-propagating contractions that would cause villous apical crowding at least in the terminal ileum of the brushtail possum (Lentle et al. 2013) may preclude the existence of such a mechanism.

It is of note that the work outlined in this chapter did not verify the reported occurrence of spontaneous longitudinal contractions of villi on *in vivo* gut segments (King and Robinson 1945; Womack et al. 1987). However, should such activity exist, it is unlikely that the 'vigority' of such movements would be sufficient to augment mass transfer in the perivillous space (Mailman et al. 1990).

Overall, the findings of this chapter provides further support of a mechanism of mixing and mass transfer based on villous apical crowding during the formation of mucosal microfolding. The finding that villi were rigid under physiological levels of lumen flow is vital – were villi flaccid with a greater tendency of bend, this would result in a reduced capability to form villous apical crowding and effectively eject or draw luminal contents from or into the intervillous space. The finding of quasi-static fluid in the intervillous space during lumen flow and that this fluid was not fully composed of viscoelastic material (Lim et al. 2013) presents a need for mechanisms that facilitates the exchange of fluid to and from the intervillous space. Thus it is postulated that the novel mechanism of mass transfer of perivillous contents by mucosal microfolding with

rigid villi is such a process (Lentle et al. 2013). Such a mechanism is also thought to be more parsimonious as compared with a mechanism requiring coordinated neural activity and villous contractions of groups of villi (Womack et al. 1988b; Wang et al. 2010) to mix perivillous luminal contents and institute mass transfer in the perivillous region.

Finally, while villi of the terminal ileum of the brushtail possum were observed to be rigid, there is currently uncertainty whether villi in other parts of the small intestine of the brushtail possum or in other mammals would behave in a similar manner during lumen flow. Hence more work will need to be conducted to determine the rigidity of villi in other sites of the small intestine.

6.6. Chapter Conclusion

A study that was conducted to determine villous rigidity and the patterns of flow in the perivillous space around living villi of the brushtail possum has been presented in this chapter. The experimental findings show that previous assumptions (i.e. in the models described in chapter four and five) regarding the rigidity of villi is reasonable. Not only does this study add experimental results to support the literature of the passive mechanical properties of villi, it also illuminates how indeed the mucosal microfolding and physiological environment found in this work (as outlined in earlier chapters) facilitates the mixing and mass transfer of perivillous lumen contents.

Chapter Seven -

3D Models of Mucosal Microfolding

7.1. Foreword

In this chapter, a similar computational model to the one detailed in chapter five of this thesis but expanded to three-dimensions (3D) is described. To current knowledge, the computational models described in this chapter are the first ones developed to predict advective mass transfer in 3D in the perivillous region during non-propagating pendular contractions. This novel 3D model of advective mass transfer incorporated the main experimental findings of this thesis, namely:

A) The fluid environment in the perivillous space is predominantly Newtonian and of low viscosity of 1.5 mPa.s (Lim et al. 2013).

B) Villous apical crowding of villi that occurs during short-lived radially oriented mucosal microfolds during non-propagating pendular contractions ejects fluid from the intervillous spaces. Similarly, during villous apical separation of villi, fluid is drawn into the intervillous spaces (Lentle et al. 2013).

C) The rigidity of villi as well as the observed lumen flow velocities in the perivillous space during physiological levels of lumen flow result in a fluid environment characterized by a Reynolds number of less than 1 (Lim et al. 2014).

The introduction considers previous work on mass transfer in the small intestine and highlights areas where further research is needed. The methods section describes the development of 3D computational model of mucosal microfolding. This is followed by descriptions of the results obtained and discussions of their implications.

7.2. Background

Thorough mixing of enzymatic secretions and luminal contents is essential for efficient absorption of solutes at the mucosal surface of the small intestine, especially during the postprandial period. To date, the mechanics of such mixing are poorly understood. Most studies of small intestinal mixing have investigated the hydrodynamic effects of concerted circular and longitudinal contractions (i.e. peristaltic contractions) that both propel and mix the luminal content by generating radial and axial advective movement and mass transfer of digesta (Jeffrey et al. 2003; Schulze and Clark 2008; Love et al. 2013). Conversely, mass transfer generated by non-propagating circular (i.e. segmentation) (Cannon 1902; Gwynne et al. 2004) and longitudinal contractions (i.e. pendular contractions) (Melville et al. 1975; de Loubens et al. 2013) that result in minimal (if any) axial propulsion, have not been rigorously investigated, chiefly as the relative magnitudes of the component contractile activities have not been quantified until recently (Lentle et al. 2012).

The importance of the latter two patterns of motility to postprandial mixing and mass transfer should not be neglected given that peristaltic contractile activity were reported to decrease during the postprandial period (Sarna 1985; Schemann and Ehrlein 1986). Whilst segmentation may promote mixing of nutrients and secretions at the centre of the gut lumen, especially in the diets of herbivorous animals, there is currently little evidence that they also engender mixing at the wall of the gut (de Loubens et al. 2013). Hence, it is possible that mixing occurs independently at the centre and at the periphery of the lumen (Wang et al. 2010); mixing in the perivillous region being driven by pendular contraction (Melville et al. 1975; de Loubens et al. 2013) whilst at the centre,

mixing would be driven either by peristalsis (Janssen et al. 2007) or by segmentation (Gwynne et al. 2004).

It was recently shown (Lentle et al. 2013) that mixing at the periphery of the small intestinal lumen may be augmented by arrays of short-lived radially disposed mucosal microfolds that are formed during non-propagating pendular contractions. The formation of radially disposed mucosal microfolds during non-propagating pendular contractions appears to cause the tips of villi to incline and congregate in the concavities and to diverge over the crests of the underlying microfolds. In addition, computational models show that these actions cause fluid to be periodically ejected from and drawn into the intervillous regions from periodic congregation and separation of villous tips, thus augmenting peripheral mixing and mass transfer (Lentle et al. 2013).

Perivillous mixing mechanisms by villous apical crowding is also supported by recent findings that villi are relatively rigid structures (Lim et al. 2014). The finding of a degree of laxity at the point of union of the base of the villus with the underlying mucosa coupled with the relative rigidity of the shafts of villi may allow villous shafts to pivot with respect to the plane of the underlying mucosa. This mechanism and such characteristics of villi are thought to accentuate villous tip congregation within the concavity between adjacent mucosal folds during cyclical radial or longitudinal contractions (Lim et al. 2014). Mixing in this region is also facilitated by the predominantly Newtonian fluid environment of low viscosity (Lim et al. 2013).

A number of previous computational models have sought to predict the mechanisms of mixing in the small intestine. For example, Wang et al. (2010) sought to determine the interaction between the mixing pools of the lumen centre and the perivillous region, while de Loubens et al. (2013) sought to determine the fluid mechanical consequences

of pendular activity and segmentation in the absence of villi. However, all such studies, including a fluid mechanical model of the mixing capabilities of mucosal microfolds and its influence on bulk lumen mixing (Lentle et al. 2013), have been conducted only using two-dimensional models (2D).

However, it is likely that 2D flow field patterns are at best, only estimates of actual (i.e. 'real world') flow patterns (Zhou and Liu 2004). Such models assume that the predicted 2D flow field pattern will persist throughout the third dimension, a situation that is unlikely to occur in complex patterns of flow (Baetens et al. 2007; Howell et al. 2010) particularly those that may result from asymmetrically arranged villi (Wang et al. 2010).

In this chapter, novel lattice Boltzmann (LB) 3D models were developed and used to predict the flow patterns resulting from advective mass transfer in the perivillous region during the formation of short-lived radially oriented mucosal microfolds generated by non-propagating pendular contractions. Two configurations of the rows of villi were developed and compared in this study – a configuration where the rows of villi were arranged parallel (termed 'aligned configuration') to one another and a second where the rows of villi were diagonally staggered (termed 'staggered configuration') to reflect an asymmetric arrangement of villi. It is noteworthy that no experimental work has been conducted to directly determine the arrangement of villi on living gut segments of animals or humans to date.

7.3. Methods

7.3.1. Modelling strategy

The models in this chapter were developed to determine advective flow patterns at the villous scale over a group of few villi (i.e. the perivillous space) generated by the villous apical crowding (Lentle et al. 2013) of rigid villi (Lim et al. 2014) during non-propagating pendular contractions. A limited number of villi at the gut periphery were modelled to reduce the computational load and given the prediction from previous work using 2D models that villous apical crowding would predominantly augment mass transfer only in the perivillous region (Lentle et al. 2013).

In addition, the small number of villi modelled was thought to be similar to that located on the crests of a mucosal microfold during non-propagating pendular contractions (our observations). The group of villi were enclosed in an 'infinite space' (i.e. the model boundaries are far enough from the villi that they would not impact on the velocity flow fields in the perivillous region) in order to prevent any boundary effects affecting the flow near the villi. The upper boundary (lumen centre) was located at a distance above the villous tips that was equivalent to that of the scales expected in a possum ileum. As for the boundaries in the X-dimension (oral and aboral positions), this was the smallest possible so that computation time would not be increased unnecessarily but still far enough from the perivillous region preventing any impact of the boundary on the perivillous flow field. In this model, the radial dimension was in the Y-dimension, the longitudinal direction in the X-dimension and depth (e.g. villous depth) in the Z-dimension (Figure 7-1).

7.3.1.1. Villous profile, dimensions and spacing

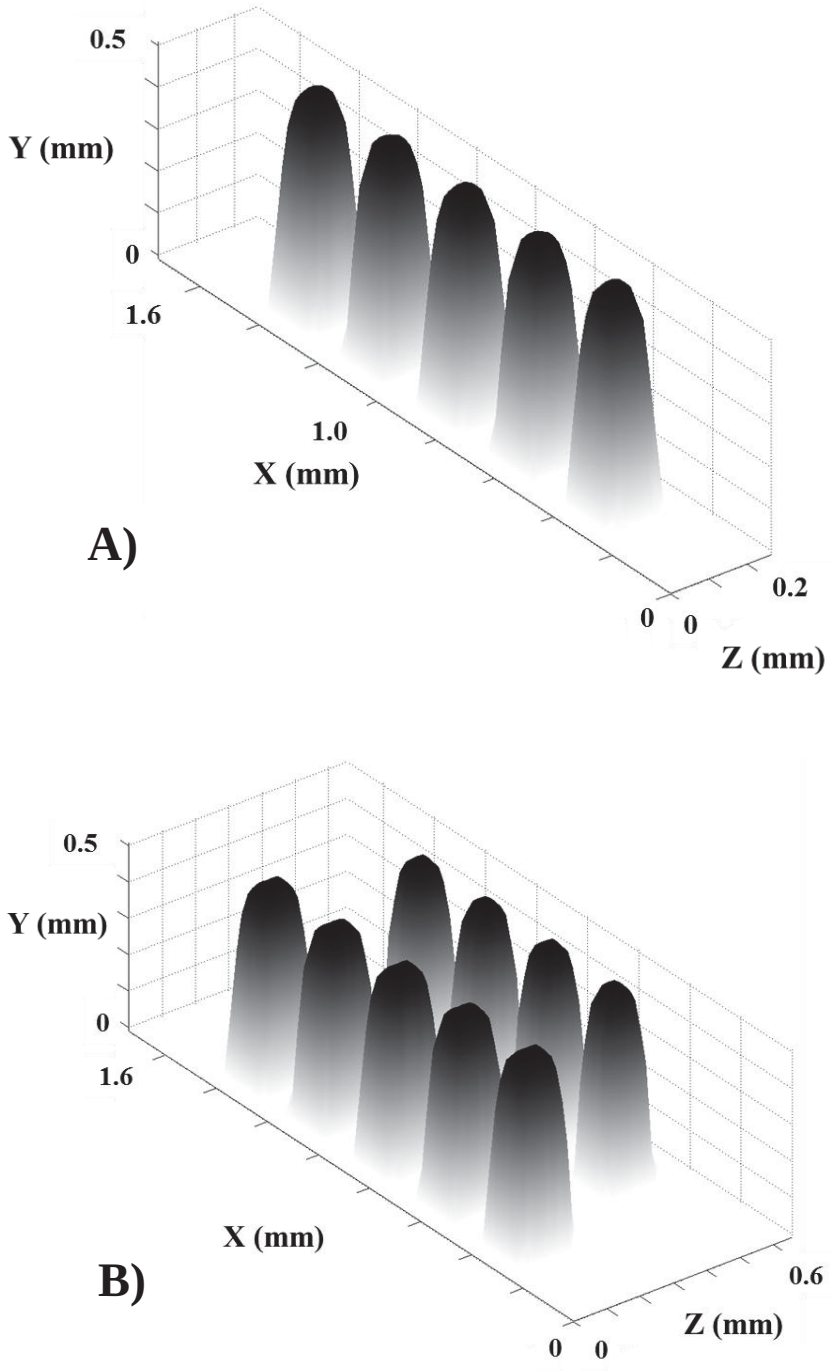

Figure 7-1: 'Three-dimensions' (3D) plots of the two villi arrangements (i.e. configuration) of villi used in the computational models described in this chapter. The A) aligned and B) staggered villi configuration.

The villous profile $Vil_p(X, Y)$ was described by a 4th order polynomial (see equation 7.1) as was done in the other models presented in this thesis:

$$Vil_p = h_{vil} - \frac{l}{{R_{vil}}^4}(X^4 + Y^4) \quad (7.1)$$

where h_{vil} is the length of a villous, R_{vil} its half width and *X* and *Y* were the coordinates on the LBM mesh.

The intervillous space (i.e. the maximal spacing between villi when the gut wall was in the relaxation phase) was the equivalent to the diameter of a villus of 160 μm (Lentle et al. 2013) in the model and was applied also to the distance between rows of villi. This intervillous space value was an estimate of the intervillous spacing measured from 2D images of a vertical view of villi of various locations along a live gut segment that was everted and assumed to be at the peak of its relaxation phase. While the measured value may not necessarily be the exact spacing generated during *in vivo* postprandial pendular contractions, it was thought to be more accurate than the value measured from histologically fixed gut wall samples.

7.3.1.2. Villous flexibility and row configuration

In accordance with the experimental findings of chapter six, the villi were initialised as rigid structures given the observation that living *ex vivo* maintained brushtail possum villi were prone to pivot and not bend during physiological levels of lumen flow. In addition, the villi were modelled as static structures as the observed villi did not exhibit spontaneous or concerted contractile activity (Lim et al. 2014).

As it is likely that the relative positions of villi in 3D space would influence mixing, the relative positions of villi were simulated in two configurations – the 'aligned configuration' (Figure 7-1A) and the 'staggered configuration' (Figure 7-1B). The intent of the latter configuration is to reflect asymmetrically arranged villi and to compare the resulting flow patterns with the flow patterns generated by the aligned

configuration. In both configurations the villi were simulated as an infinite array only in the Z-dimension and moved (see sub-section 7.3.1.3 to follow) only in the longitudinal (X) direction (see Figure 7-2).

7.3.1.3. Mucosal microfolding during pendular contractions

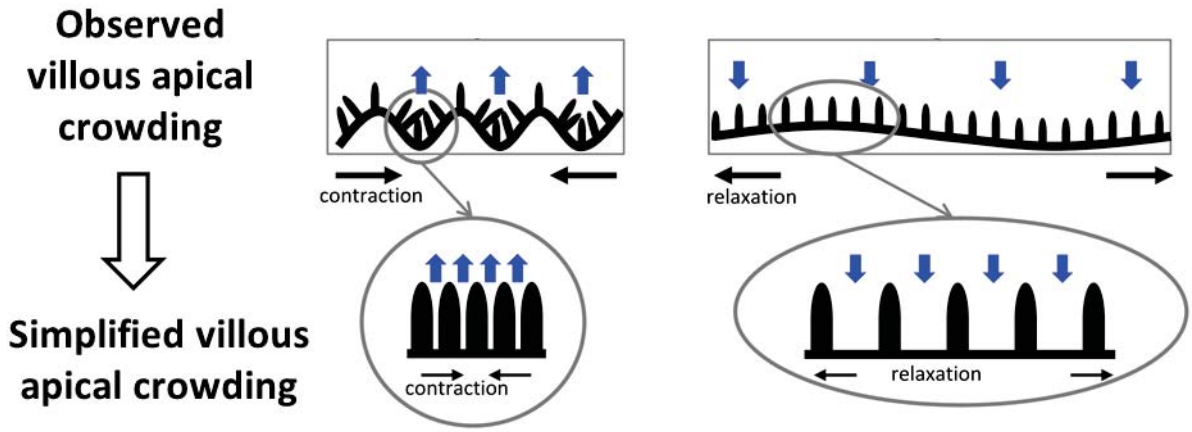

Figure 7-2: Overview of the geometry and movements used in the simulations of mixing and mass transfer in the perivillous space during non-propagating pendular contractions.

Villus apical crowding that occurs during mucosal microfolding comprises the periodic congregation (during gut longitudinal muscle contraction) and subsequent separation (during gut longitudinal muscle relaxation) of arrays of villus tips. The actual movement of the villi is complex, and hence similar strategies used in chapter five were utilized to reduce the complexity of the problem and the computational load (Figure 7-2).

As done previously, a sinusoidal function was used (see chapter five of this thesis) to represent the cyclic variation of longitudinal strain rate ($\dot{\varepsilon}$, $\%s^{-1}$) of pendular contractions of the gut wall:

$$\dot{\varepsilon}(Y,t) = \dot{\varepsilon}_{max} sin\left(\frac{2\pi}{T}t\right)(X - X_0) \qquad (7.2)$$

where $\dot{\varepsilon}_{max}$ is the amplitude of strain rate (%s^{-1}), t is the time (s) and T is the period of the longitudinal muscle (i.e. pendular) contraction (s). X (μm) is the longitudinal abscissa while X_0 (μm) is the position in the middle of the spatial domain of contraction (see chapter four, sub-section 4.4.3.1). The longitudinal velocities of the villi were calculated by integrating longitudinal strain rate $\dot{\varepsilon}$ (%s^{-1}). Relaxation and contraction of the gut wall defined by equation 7.2 occurs between the time intervals of 0 to T/2 and T/2 to T respectively.

7.3.2. Lattice Boltzmann methods

The Navier-Stokes equation (NSE) were solved via LB methods (for description and merits of this technique see chapter four), which were further developed for use on a 3D array as prescribed by Du and Shi (2010). The moving boundary conditions (imposed by the villi) were calculated by the bounce-back boundary (i.e. a particle is sent back the way it came when it encounters a solid boundary) scheme (Sukop and Thorne 2007) assuming no-slip at the boundary of the gut periphery for simplicity and to reduce computational load. As was done for the 2D model (see chapter five), the following was also implemented to the 3D model outlined in this chapter:

A) Lattice Boltzmann Bhatnagar-Gross-Krook collision operator (LBGK) developed by Guo et al. (2000).

B) Oral and aboral pressure as well as velocity conditions was modelled by the methods of Guo et al. (2002).

C) In order to simulate flow generated by villous apical crowding, with sufficient spatial resolution to predict the flow fields near the lumen centre without incurring a high computational load, grid sizes were adjusted accordingly with two sets being used (see

Figure 7-3 below). The communication and reconstruction of information at grid transitions of the two sets of different sizes (between the coarse and fine grids) were done with the coupling algorithms of Dupuis and Chopard (2003) and Stiebler et al. (2008) for the NSE.

D) The model was also developed with a bounce-back (Sukop and Thorne 2007) boundary condition at the upper boundary of the model (i.e. on the Y-dimension).

E) To simulate infinite arrays of villi in the Z-dimension, a periodic boundary condition was applied in this direction.

The final code was validated using different benchmarks (e.g. Poiseuille and Couette flow).

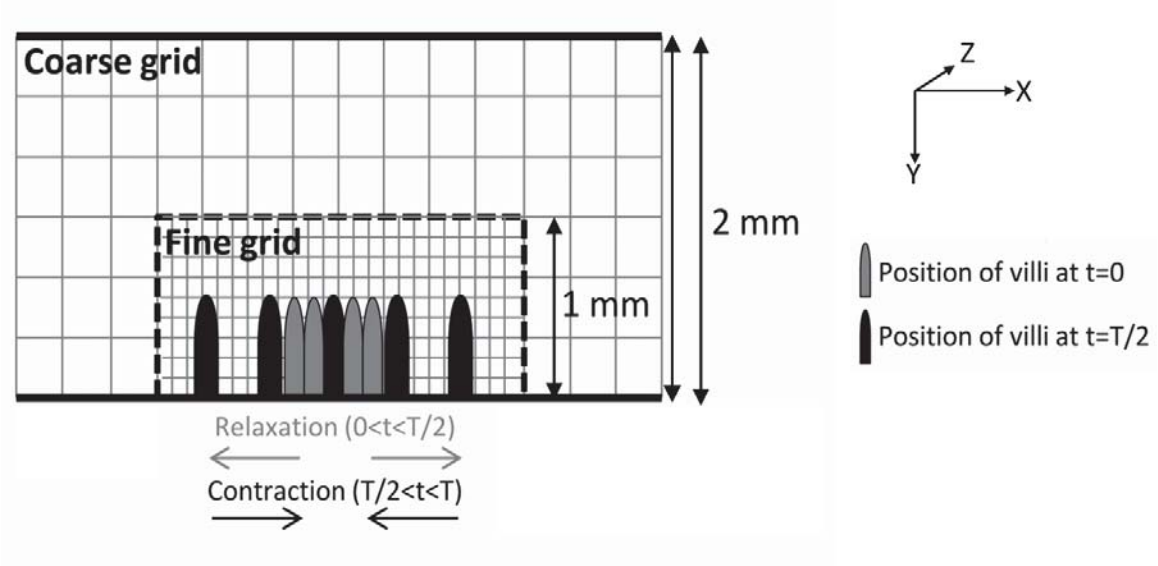

Figure 7-3: Computational simulation scheme.A two-dimensional (2D) slice of the three-dimensional (3D) modelling environment layout showing the two grid sizes used (coarse and fine). The results and discussions in the chapter will be derived only from the velocity flow fields of the fine grids (i.e. perivillous space) given that previous work using 2D models had predicted that mass transfer would predominantly only be augmented in the perivillous region (Lentle et al. 2013).

7.3.3. Use of physiological and numerical parameters

The physiological parameters used in the models described in this chapter came from previous work (Table 7-1). The ratio of the size of the fine grid to the size of the coarse grid was taken as 3 (Figure 7-3). The distance from the gut wall to the lumen centre encompassed by the fine grid (i.e. perivillous region) was two times the length of a villus (i.e. 1 mm). The comparison of the flow generated by groups of villi of different numbers during preliminary testing has shown that 5 villi for the aligned villi configuration and 9 villi (5 villi in the first row and 4 in the second) for the staggered villi configuration were suitable to obtain representative results. In addition, such villi numbers would more likely be found on the crests of the microfolds based on estimates conducted in prior work (Lentle et al. 2013). Preliminary tests were also done to choose the different numerical parameters for the models.

Parameters	Value	Reference
Strain rate amplitude ($\dot{\varepsilon}_{max}$)	20 % s^{-1}	(Lentle et al. 2007)
Period of longitudinal activity (T)	6.66 s	(Lentle et al. 2007)
Dynamic viscosity (μ)	1.5 mPa.s	(Lim et al. 2013)
Gut radius	2 mm	(our observations)
Length of villi (h_{vil})	560 μm	(Lentle et al. 2013)
Half width of villi (R_{vil})	80 μm	(Lentle et al. 2013)
Intervillous space	160 μm	(Lentle et al. 2013)

Table 7-1: Physiological parameters used for the computational models of both configurations

7.3.4. Analysis and comparison of flow fields

Qualitative and quantitative predictions of the flow fields were used to compare the predictions and model output of the two villi configurations. The simulation predictions

presented below are taken from the time when the gut wall was in its relaxation phase (i.e. between times 0 and T/2; when the villi were moving towards maximal separation from one another) unless specified otherwise. Qualitative comparisons of the magnitude of flow were achieved by plotting the magnitude of velocity as 'intensity images' with streamlines superimposed onto the images to show patterns and directions of flow. For easy comparison of such plots, the colour schemes were standardised. Quantitative comparisons of the magnitude of velocity were conducted in the following manner: the velocities in the X and Z dimensions were first averaged at all points in the Y-dimension of perivillous regions that were directly above villi. Subsequently, all of those calculated velocities were averaged into a single value that was used to compare the two models studied.

7.4. Results

The results presented below are in three main parts. In the first part, predictions of the aligned configuration of villi are presented, followed by the results of the predictions of the staggered configuration of villi. Finally, the predictions of both models are compared.

Overall, flow was predicted to be pulsatile between the intervillous spaces and the surrounding fluid as the simulation progressed through the cycle of relaxation and contraction of non-propagating pendular contractions. Hence, fluid was predicted to be drawn into the intervillous regions during time intervals between 0 and T/2 (i.e. relaxation period of the gut wall) and ejected from the intervillous space during time intervals between T/2 and T (i.e. contraction period of gut wall) as was produced by the 2D model (see chapter five). Fluid flow velocity in the perivillous region was the fastest on the outer edges of the two leading villi and slowest in the intervillous region around the middle villi (Figure 7-4 and Figure 7-6).

7.4.1. 3D model of aligned villi configuration

Figure 7-4 shows the U_{xy} magnitude and flow vector (calculated from the Pythagorean theorem) of velocity in the X and Y dimension in the perivillous region: in the plane exactly in the middle of the villi (Figure 7-4A) and the plane exactly in between the rows of villi (Figure 7-4B).

Flow velocities between 0.07 and 0.12 mm/s were predicted in between rows of villi (i.e. channels in between parallel villi) especially in the upper regions of the intervillous space (Figure 7-4B). Such a pattern of flow was predicted in all planes in the Z-dimension of the regions in between rows of villi. In addition, a vortex was also

predicted to form above the tips of the leading villi generated through the circulation of advected fluid flowing into the intervillous region around the central villi and exiting the intervillous region from the region around the two leading villi (Figure 7-4A). The magnitude of velocity of these vortexes was low and did not exceed 0.05 mm/s. Such patterns of flow persisted even in the regions in between rows of villi though they were slightly diminished in the plane exactly in the middle of the rows of villi (Figure 7-4B).

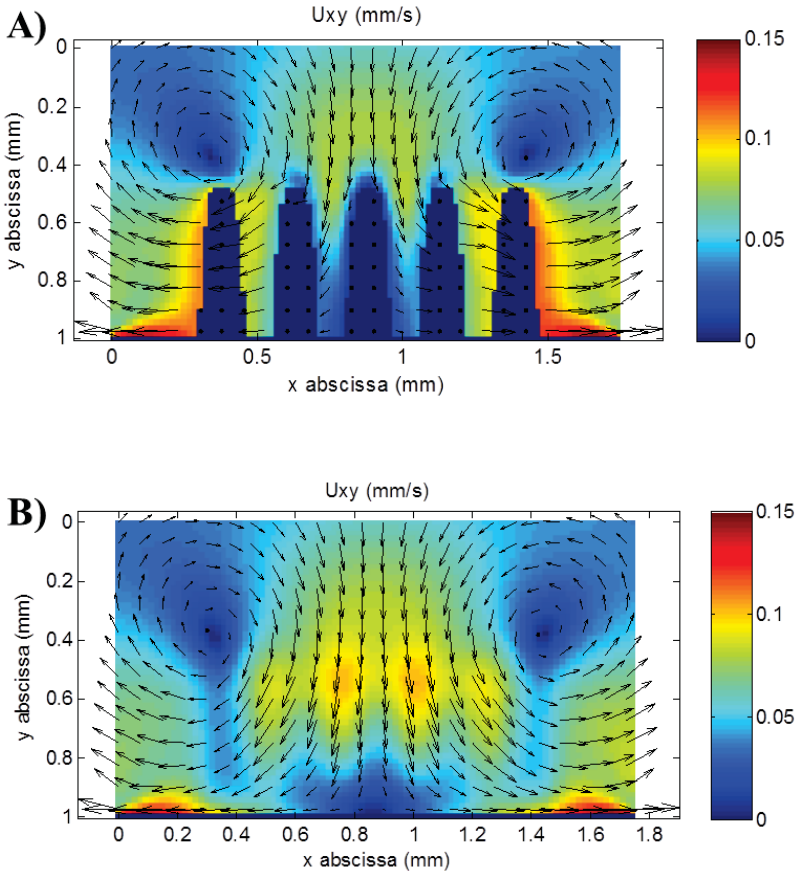

Figure 7-4: Velocity flow field of Uxy velocity intensity plots for a model of the aligned villi configuration at two different planes in the Z-dimension. The black arrows on the plots are Uxy vectors indicating the direction of flow during this period in time while the size of the arrows is a reflection of the magnitude of velocity. The flow field plot A) is of the plane in the middle of villi while B) is in the middle of the intervillous space in between rows of villi. The flow fields were taken from the time when the gut wall was in its relaxation phase (i.e. between times 0 and T/2).

Figure 7-5 shows the U_{xz} magnitude and vector of flow calculated from the velocity of the X- and Z- dimensions in the perivillous region in the upper third of villi towards the villous tips. Velocities between 0.05 and 0.1 mm/s were predicted in regions adjacent to and surrounding villi (Figure 7-5). Given the symmetry of this configuration of villi, magnitudes of velocity between 0.1 and 0.13 mm/s were predicted to be formed in the regions around the leading edge of the leading villi of all rows (Figure 7-4A and Figure 7-5).

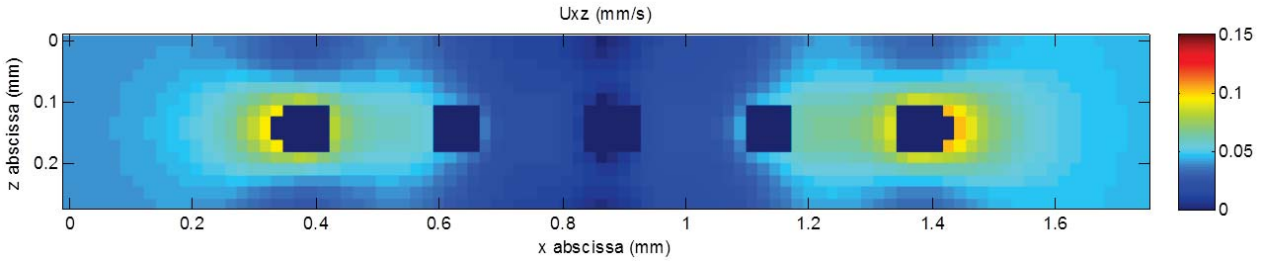

Figure 7-5: Velocity flow field of Uxz velocity intensity plots for a model of the aligned villi configuration. Flow field plot is of the plane in the upper third of villi towards the villous tips. The flow fields were taken from the time when the gut wall was in its relaxation phase (i.e. between times 0 and T/2).

In addition, during the time the gut wall was contracting (i.e. time interval between T/2 and T) and was thus ejecting fluid from the intervillous space, it was predicted that flow velocities near the villous tips were predominantly oriented in the X-dimension. This was determined by a comparison of the three components (i.e. X-, Y- and Z-dimensions) of the flow vector in that region at that time. It was predicted that the component velocity in the X-dimension was 1.5 times larger than the velocities in the Y-dimension and was two orders of magnitude larger than the velocities in the Z-dimension.

7.4.2. 3D model of staggered villi configuration

Figure 7-6 shows the U_{xy} magnitude and vector of flow calculated from the velocity of the X- and Y-dimensions in the perivillous region: in the plane exactly in the middle of the front row of five villi (Figure 7-6A), the plane exactly in the middle of the intervillous region between the row of five and four villi (Figure 7-6B) and the plane exactly in the middle over the row of 4 villi (Figure 7-6C).

Flow velocities between 0.06 and 0.09 mm/s were predicted near the villous tips in the space in between the two rows of villi especially around the central villi (Figure 7-6B). Hence, fluid entering the intervillous spaces during the relaxation phase of pendular contractions was predominantly attributed to flow to spaces in between rows of villi. Such a pattern of flow was predicted in all planes in the Z-dimension of the spaces between the two rows of villi.

In addition, a vortex was also predicted to form above the tips of the leading villi generated through the circulation of advected fluid flowing into the intervillous region around the central villi and exiting the intervillous region from the region around the two leading villi (Figure 7-6A). The vortex at the tips of the villi on the row of four villi appears to be slightly 'out of phase' with the vortex generated at the tips of villi on the row of five villi (Figure 7-6A and Figure 7-6C). The magnitudes of velocity of these vortexes were low and did not exceed 0.05 mm/s. Such patterns of flow persisted even in the spaces in between rows of villi though they were slightly diminished (Figure 7-6B).

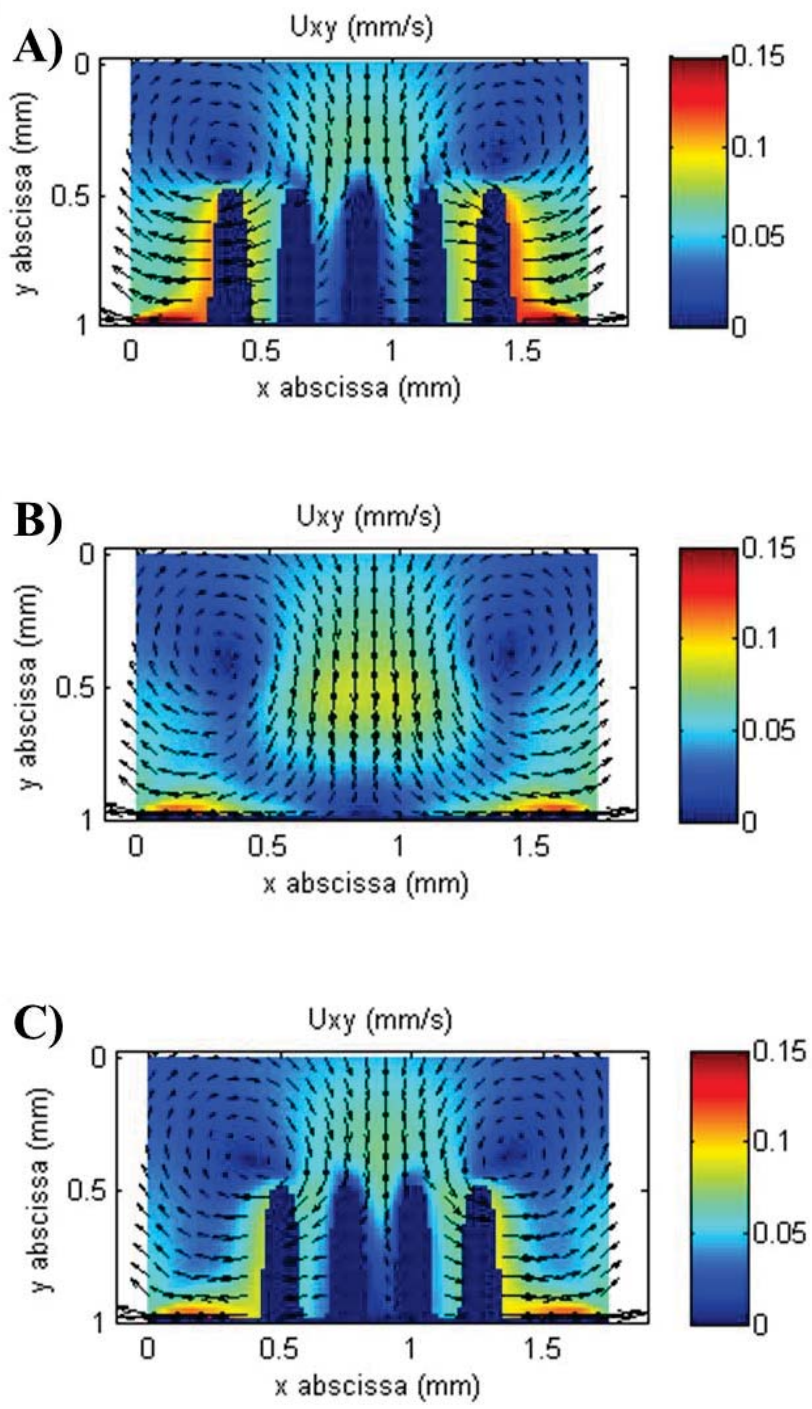

Figure 7-6: Velocity flow field of Uxy velocity intensity plots for a model of two rows of staggered villi at different planes in the Z-dimension. The black arrows on the plots are Uxy vectors indicating the direction of flow during this period in time while the size of the arrows is a reflection of the magnitude of velocity. Flow field plot in the plane of the A) middle of the row of 5 villi, B) middle of the intervillous space in between the row of 5 and the row of 4 villi and C) middle of the row of 4 villi are presented. The flow fields were taken from the time when the gut wall was in its relaxation phase (i.e. between times 0 and T/2).

Figure 7-7 shows the U_{xz} magnitude and vector of flow calculated from the velocity of the X- and Z-dimensions in the perivillous region in the plane (in the Y-dimension) from the upper third of villi near the villous tips. Flow velocities of between 0.05 and 0.1 mm/s was predicted in regions adjacent to and surrounding villi (Figure 7-7). At the row of five villi, magnitudes of velocity between 0.1 and 0.13 mm/s were predicted in the regions around the leading edge of the leading villi (Figure 7-6A and Figure 7-7). Conversely, around the leading edge of the leading villi of the row of four villi, magnitudes of velocity between 0.06 and 0.09 mm/s were predicted (Figure 7-6B and Figure 7-7).

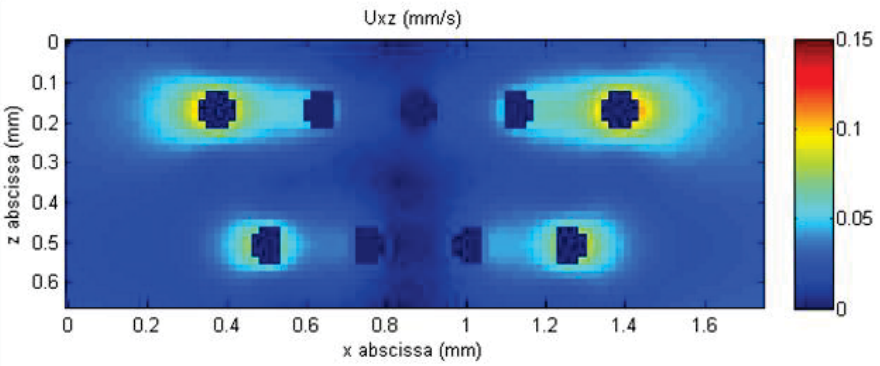

Figure 7-7: Velocity flow field of Uxz velocity intensity plots for a model of staggered villi configuration. A flow field plot of the plane in the upper third of villi towards the villous tips is presented. The flow fields were taken from the time when the gut wall was in its relaxation phase (i.e. between times 0 and T/2).

In addition, during the time the gut wall was undergoing pendular contractions (i.e. the time interval between T/2 and T) and was thus ejecting fluid from the intervillous space, it was predicted that flow velocities near the villous tips were predominantly oriented in the X-dimension. This was determined by a comparison of the three components (i.e. X-, Y- and Z-dimensions) of the flow vector in that region at that time. It was predicted that, in this scenario, the component velocity in the X-dimension was 2 times larger

than velocities in the Y-dimension and was an order of magnitude larger than velocities in the Z-dimension.

7.4.3. Comparison of the aligned and staggered villi configurations

Overall, there were several differences that could be observed when comparing the two models of different configuration of villi;

A) The velocity flow fields of the model run with the staggered villi configuration (i.e. asymmetrically arranged rows of villi) were on average 1.2 times lower than that of the model run with the aligned villi configuration.

B) The vortex predicted to form over the tips of the leading villi of the model run with an aligned villi configuration were in the same locations for all rows. Conversely, for the model run with a staggered villi configuration, the vortex of a row of villi was slightly 'out-of-phase' with the preceding and proceeding row.

C) During the time the gut wall was undergoing pendular contraction (i.e. fluid was ejected from the intervillous region), the flow around the villous tips of the aligned villi configuration model was more likely to be directed in the X-dimension (i.e. mono-directional) as compared to the model of the staggered villi configuration. This is evidenced by the prediction that the flow velocity in the X-dimension of the aligned villi configuration model is two orders of magnitude larger than flow velocity in the Z-dimension while for the model of staggered villi configuration, the flow velocity in the X-dimension is an order magnitude larger than flow in the Z-dimension.

7.5. Discussion

Novel three-dimensional (3D) fluid mechanical models of advective mass transfer in the perivillous region that result from villous apical crowding formed during non-propagating pendular contractions were developed in two villous arrangements – aligned and staggered villi configurations. Overall, new insights were gained through this work that was otherwise not obtainable when only using only two-dimensional (2D) models. There were also noted differences between the models of the two different arrangements of villi.

7.5.1. Comparison between 2D and 3D models

One of the main advantages of models developed in 3D is their ability to visualize flow patterns in all three-dimensions, especially to view flow patterns that might arise through asymmetrically arranged villi. As such, a flow pattern predicted in a given 2D plane can be verified for its actual impact by visualizing its appearance in the third dimension. For example, as discussed in the prior chapter (chapter six), the apparent formation of a vortex visualized in 2D models may have limited bearing on the augmentation of mass transfer in the intervillous space. The maximum amplitude of the vortex would only occur at the point of maximal cross-sectional area between two villi that are finger-shaped and cylindrical.

The 3D models presented, predicted that fluid interchange during non-propagating pendular contractions would occur predominantly in the regions in between rows of villi – with velocities up to 0.13 mm/s noted. In addition, the 3D model also allowed for the visualization of the actual flow distribution around individual villi. For example, as presented in Figure 7-5 and Figure 7-7, the 3D model allowed for the observation that flow velocities between 0.05 and 0.1 mm/s are distributed around all leading villi in a

given row. Such flow velocities being generated in this region would mean that advective fluid movement may significantly augment mass transfer in the perivillous space as demonstrated in the following: assuming the lower value from the range of flow velocities generated by non-propagating pendular contractions of 0.05 mm/s (V), the time scale necessary for an element of fluid to travel a distance equivalent to the length of a villous (h_{vil}; about 560 µm) will be around 11 s (h_{vil}/V). In comparison, for small molecules such as glucose, which have a relatively large diffusion coefficient in water (D ≈ 8.10^{-10} m²/s (Beaudoing et al. 1991)), the time scale of diffusion will be around 300 s (h_{vil}^2/D). Thus, advective time scales being driven by the formation of mucosal microfolding during non-propagating pendular contractions in the perivillous region is predicted to be at least 20 times faster than that of diffusion.

Besides that, 3D models also allowed the actual 'net' (i.e. predominant) flow direction to be predicted and visualized. Prior 2D models would not have predicted that fluid would be ejected primarily in the X-dimension during villous apical crowding during the contractions of longitudinal muscle at least in the terminal ileum of brushtail possums (Lentle et al. 2013). Such a finding may indicate that the exchange of fluid between the intervillous region and the regions above villi is not effective during non-propagating pendular contractions. This means that most of the luminal fluid in a given intervillous region is more likely to be advected to an adjacent intervillous region in the X-direction rather than being exchanged with 'fresh' (i.e. of higher nutrient concentration) luminal fluid from regions above the villi. Hence, it is possible that the effective exchange of luminal fluid between the intervillous region and regions above villi may instead be facilitated by the longitudinally (i.e. axially) oriented mucosal microfolds that form during segmentative contractions or peristalsis (see chapter five).

Finally, the use of 3D models also allows more accurate prediction of flow velocities that would be generated during villous apical crowding. Given that 2D models assume that model features such as villi persists in the third dimension, it is possible that such models would overestimate the amount of fluid drawn into or ejected from the intervillous region. The use of 3D models allows the modelling of advective mass transfer with villi that are shaped more alike those that would be found in the small intestine of animals (e.g. finger-shaped cylinders).

7.5.2. Comparison between aligned and staggered villi configuration

Overall, it is likely that the model run with the staggered villi configuration is better suited to augment mixing and mass transfer in the perivillous region to a larger extent than the aligned villi configuration. While fluid flow velocities in the model run with the aligned villi configuration was higher than that predicted with the staggered villi configuration, this may not translate into augmented levels of mixing and mass transfer. It is possible that fluid in the intervillous space is rapidly exchanged with the surrounding fluid or advected to another intervillous region resulting in minimal exposure of all surface of villi to luminal fluid containing nutrients and/or pharmaceuticals. Conversely, mixing and mass transfer may be relatively more augmented with a staggered villi configuration. This may be due to the reduced levels of concerted advection of fluid away from a given intervillous region (due to the asymmetrically arranged villi) causing increased levels of exposure of villi surfaces to luminal fluid.

In addition, the prediction that vortices formed above the villous tips of leading villi of a given row is slightly ‘out-of-phase’ (in the X-dimension) with the vortex formed above villous tips of leading villi of the preceding and proceeding rows of villi is likely to

mean that the augmentation of mixing and mass transfer in the perivillous region is better facilitated with the staggered configuration of villi. Given that these vortexes persisted to the region in between rows of villi, this would allow mixing between the fluids that originated from different rows of villi.

Furthermore, it was also predicted that fluid flow would be more tri-directional (i.e. tri-dimensional) in the model run with the staggered villi configuration during villous apical crowding. This indicates that variation in fluid movement is more likely to occur with such configuration resulting in more augmented levels of mixing and mass transfer as compared to the model run with the aligned villi configuration.

Finally, it should also be noted that pending more experimental observations being conducted to determine the distribution and arrangement of villi on a live gut segment, it is postulated that both configurations may exist. It is possible that some sections of small intestine may be more suited for advecting fluid while other sections more suitable for promoting mixing and mass transfer.

7.5.3. Leading villi of mucosal microfolds.

As the model was developed with the positioning of a small number of villi (i.e. not more than 5 in a row) in 'infinite space', this resulted in predictions of flow patterns around the leading villi that are different to more centrally located villi in a given row. Prior to the finding of mucosal microfolding of Lentle et al. (2013), such model setup would appear 'unphysiological'. However through the very recent work of Lentle et al. (2013) discovering that the small intestinal mucosa undergoes dynamic folding during non-propagating pendular contractions (with five villi being the estimated number of villi located on the crests of mucosal microfolds), the 3D models described in this chapter are likely one of the more 'physiological' models of advective mass transfer in

the perivillous region currently available. Hence, as was predicted, the leading edge of the leading villi would be exposed to higher levels of fluid flow velocities and more of the leading villi surface area would be exposed to fluid flow (relative to the other villi in the same row). The effect of such events would occur more readily when the small intestine undergoes non-propagating pendular contractions resulting in the maximum height of the microfold formed.

7.6. Chapter conclusion

In conclusion, this chapter presents the development of novel models that allow visualisation of flow velocity and advective mass transfer in the perivillous space in 3D. However, it should be noted that at present, the mixing and mass transfer predictions described in this chapter have not been validated by experimental work due to the extreme technological demands of such an undertaking.

Future work could attempt to confirm the predictions of the 3D model made in this chapter by simulating perivillous advective and diffusive mass transfer using a solute tracer as was done in 2D in chapter five. Additional work could further improve the model so that it is more reflective of physiological conditions; perhaps incorporating the vertical movements of villi as a result of villi moving vertically with the formation of mucosal microfolding or to explore the effect of longitudinally oriented mucosa microfolds. In addition, future models should also consider the effect of the variation of the distance in between rows of villi. Mixing and mass transfer may be further augmented should the distance between rows of villi be reduced especially in the model run with asymmetrically arranged villi.

The next chapter is an overall discussion of all of the experimental work and model predictions that has been detailed in this thesis.

It is the glory of God to conceal a matter;
to search out a matter is the glory of
kings.

Proverbs 25:2

Chapter Eight -

Overall Discussion

8.1. The perivillous fluid environment in the small intestine

The work shows the usefulness of fluorescence particle tracking techniques in the determination of the physical properties of materials whose structures are labile and difficult to access such as the fluid environment of the intestinal lumen especially those around villi *in situ*. Thus the perivillous fluid environment in the terminal ileum of a small herbivore (e.g. possum) was found to be rheologically heterogeneous rather than consisting of a homogenous 'blanket' of viscoelastic gel as had been previously assumed (Atuma et al. 2001; Cone 2009). Whilst the perivillous fluid environment consisted predominantly of a continuous Newtonian fluid phase of low viscosity, multiple non-contiguous viscoelastic bodies were dispersed within it.

Given that the work was conducted in the terminal ileum of the brushtail possum, caution is required before generalization of the results. It is likely that the disposition and chemical characteristics of mucin may differ along the small intestine and between species. Further work is necessary to validate whether mucins secreted by goblet cells commonly form discrete islands or anneal to form a contiguous layer. Such variation in mucus island disposition has great consequences for mass transfer of nutrients and protection of the intestinal mucosa *in vivo*.

In proximal intestinal sites such as the duodenum, the pH of the luminal contents may be low (Flemström and Kivilaakso 1983) enough to damage the mucosa. Thus it would be more advantageous that mucus forms a contiguous layer. Mucus islands in these regions may be more prone to undergo rapid reptative inter-diffusion (i.e. annealing).

The presence of discrete islands of mucus in the distal ileum suggests that the mass transfer of nutrients and drugs may be modulated by a process similar to 'gel filtration' rather than diffusion through a contiguous mucus layer. Such a mechanism fits in with

reports that the mass transfer of substances of smaller molecular weight is hindered to a greater extent than that of larger particles (Pohl et al. 1998). Whilst either type of disposition of mucus islands could bring about such hindrances, a suspension of mucus islands offers greater access of nutrients or drugs to the apices of enterocytes and the glycocalyx.

In this regard, the microbeads were observed to penetrate to all regions around villi. Hence microbeads may be a suitable vehicle for delivering drugs or therapeutic agents directly to the glycocalyx and the apical membrane of enterocytes. However, the finding that microbeads adhered to the viscoelastic bodies regardless of microbead surface chemistry indicates that the concentration of delivery to target sites is more important in the design of particulate drug delivery systems. The fact that quantities of different types of microbeads became trapped in viscoelastic bodies may be useful as a basis for establishing a reservoir for drug storage adjacent to the mucosa. For such drug delivery mechanisms to be effective, further studies would need to be conducted on the 'life cycle' of the viscoelastic bodies (e.g. the amount of time that a given viscoelastic body will remain within the small intestine).

It is noteworthy that the current work did not examine the glycocaleceal mucus. Further work is also needed to determine the physical properties of this type of mucus as this material forms a physical barrier on the apices of enterocytes. Similar techniques to those in this thesis could be used on a smaller scale. Alternatively, other techniques such as nano-indentation by atomic force microscopy (AFM) (Helstad et al. 2007) and fluorescence correlation spectroscopy technique (FCS) (Guigas et al. 2007) could be useful as they have previously been used to determine the physical properties of sub-micron scale environments.

As discussed in chapter three, while it is likely that the viscoelastic bodies are islands of mucus, more work is needed to verify their composition, specifically the type of mucin that predominates therein (i.e. the type of MUC gene product) using immune-histochemical techniques (Johansson et al. 2011b). An improved understanding of the mucin composition of the viscoelastic bodies will increase our knowledge of the micro-environment that surrounds encapsulated drugs. It is also possible that the Newtonian fluid in which the viscoelastic bodies were suspended also contains mucins. This seems likely given reports that soluble mucins may maintain pathogens in a 'planktonic' state preventing them from forming adherent biofilms (Caldara et al. 2012). It is also likely that these soluble entities may interact with food and drug particles.

8.2. Formation of mucosal microfolds during non-propagating contractions

The finding that the intestinal mucosa of the terminal ileum is mechanically unstable and can become 'ruckled' into short-lived radially and longitudinally oriented microfolds during non-propagating pendular and segmentative contractions presents an entirely new means of facilitating mixing in the intervillous space (Lentle et al. 2013). Hence, given that luminal contents may be drawn into and ejected from the intervillous space during the postprandial period, vehicles for drugs may be designed to target the intervillous regions or the convexities of mucosal microfolds. The careful design of micro-particle vehicles so as to promote their ability to migrate through pseudoplastic fluid toward the peripheral mucosa (Lentle et al. 2005) may promote the delivery of their contents directly to the mucosa. Together with drugs such as aspirin that may promote the 'loose-ness' of mucosal tight junctions (Sequeira et al. 2012), the encapsulated drugs, especially those of larger molecules (Bjarnason et al. 1995) could also be absorbed via the paracellular route by solute solvent drag (Pappenheimer and Reiss 1987).

It remains to be seen if the formation of mucosal microfolding exists in other sites of the small intestine and in other species of animals. It seems likely that the existence of such perivillous mixing mechanisms is not desirable in the proximal duodenum given the need to reduce stirring of the surrounding contiguous layer of mucus that protects the intestinal mucosa from acidic digesta exiting the stomach. Hence the experimental work outlined in chapter five of this thesis needs to be repeated at other sites along the small intestine and in other animals.

It is possible that the formation of mucosal microfolds could have been modulated by the eversion of the gut segment. Hence further work is needed to observe mucosal movements *in situ* and *in vivo* perhaps by 3D high resolution optical coherence tomography (OCT) (Hsiung et al. 2005). Hence when OCT is typically used in conjuction with endoscopy, it enables the mucosa to be viewed enface as opposed to the normal side on, caudad view. However, endoscopy is an invasive technique and direct contact of the endoscope with the mucosa as well as the insufflation required may affect villous movement and crowding. Further, this technique cannot be used postprandially. Alternatively, the OCT technique could be used in uneverted *ex vivo* preparations such as has been described in chapter five.

In addition, the effect of mucosal microfolding on peripheral mixing can be inferred from the residence time distribution (RTD) of intestinal perfusate as has been done during pendular contractions of the rat duodenum (de Loubens et al. 2014) and of peristalsis of the possum ileum (Janssen et al. 2007). Given that mucosal microfolding was first detected in the ileum of the brushtail possum undergoing non-propagating contractions (Lentle et al. 2013), the results of such RTD studies could be compared with those previously mentioned. Alternatively, it is possible that 3D high-definition manometry (HDM) could be used to monitor mucosal microfolding *in vivo* (Kahrilas et al. 2008; Arkwright et al. 2009). However, in spite of their name, whilst these devices can accurately record the fluid dynamics within the lumen, they cannot accurately distinguish the fluid dynamics due to longitudinal displacement from those due to radial displacement of the gut wall.

Overall, the findings of this work support a growing body of work showing that mixing and mass transfer in the small intestinal lumen differs in the central and peripheral (i.e. perivillous) lumen regions (Melville et al. 1975; Wang et al. 2010; de Loubens et al.

2013). Previous theoretical work by Wang and colleagues (2010) indicated that central lumen mixing is governed by axially oriented (i.e. 'lid-driven') propulsive flow while mixing at the gut periphery was augmented by pendular movements of villi. However, given the reduced action of peristalsis during the postprandial period (Sarna 1985) and the relative rigidity of villi (Lim et al 2014), it is more likely that mixing and mass transfer at the perivillous regions of gut lumen would be augmented by mucosal microfolding (Lentle et al. 2013).

8.3. Villous rigidity and perivillous flow conditions during lumen flow

The work showing that living ileal villi are relatively inflexible to physiological levels of shear stress from axial flow (Lim et al. 2014) indicates that endogenous contractile activity within villi would likely be insufficient to engender mixing and mass transfer. Hence these findings fit in with the discovery that mucosal microfolding (Lentle et al 2013) during radial or longitudinal contraction may generate mixing by angulation of villous shafts. In the latter case, mixing of fluid in the intervillous space is likely to be more effective with rigid than with flexible (i.e. flaccid) villi. In this respect, intervillous flow patterns that have been initially predicted from 3D computational models for an infinite array of rigid villi (Lim et al. 2014), have now also incorporated mucosal microfolding (see chapter seven). Further work is needed to validate the flow patterns predicted by the 3D computational models of the perivillous region.

The villi in our *ex vivo* preparation exhibited no visible autonomous contractile activity. However, other works have reported that such contractile activity occurs *in vivo* (Womack et al. 1987). The existence of such activity could further contribute to the peripheral effects that were observed in dye dilution (i.e. RTD) experiments that were recently conducted (de Loubens et al. 2014).

It is noted that the experimental conditions used to assess villous rigidity (i.e. tension of mucosa on the probe) were likely to limit the displacement of villous tips from pivoting and translation (villous movement as a result of the movements of the underlying mucosa). Thus it is likely that any villous tip displacement (e.g. pivoting) and associated mixing would be greater *in vivo*. More work is required to quantify this, perhaps in conjunction with the methods described hitherto. However, it is noteworthy that villi

could also be less turgid *in vivo* than was observed as there is likely to be more effective transport of absorbed water into the associated portent vascular and lymphatic systems than observed in our *ex vivo* preparations.

A further shortcoming of the work detailed is that under physiological conditions, groups of villi would be shielded from flow at times other than when they were on the crests of a mucosal microfold. Hence villi, especially only the outermost (i.e. leading) villi located on the crests of microfolds, may be displaced in such manner during the 'ruckling' of the underlying mucosal surface during non-propagating contractions. Additionally, villi may also only be displaced by villous apical crowding in the convexities of a microfold. More work is also required to quantify the production of such movements *in vivo* and during pendular and segmentative movements.

In addition, the experimental observation that the perivillous flow conditions during physiological levels of lumen flow was laminar (Lim et al. 2014), suggests that the effect of the rheology of digesta (e.g. pseudoplasticity) on mixing and mass transfer are minimized. Even with advective mass transfer of pseudoplastic digesta that was driven by mucosal microfolding, it seems unlikely that the shear rates generated would result in significant variation in their apparent viscosity of digesta postprandially. However, more work is needed in order to validate such a conjecture.

Finally, the shapes of the villi may also influence the fluid dynamics around them. Hence the broader flattened villi found in the proximal small intestine (Holmes et al. 1961; Yamauchi and Isshiki 1991; Cammarota et al. 2004) that are oriented with their flat surfaces at right angles to the direction of flow, would generate greater vortical disturbances around their downstream surfaces when on the crests of mucosal microfold (Buresti 2000). However, this would require flow rates that exceed those encountered

physiologically (Grovum and Williams 1973; Bueno et al. 1975) at the perivillous region. Were mucosal microfolding to occur, these would concurrently contribute to augment local flow to a sufficient level where advective and diffusive mass transfer would together be markedly larger than mass transfer solely by diffusion.

8.4. Computational modeling of mass transfer at the perivillous region

In the work described in this thesis, several computational models have been developed to aid the prediction and quantification of advective and diffusive mass transfer by movements of the wall of the small intestine. Such techniques have proved useful given the extreme technological challenges that are inherent in direct evaluation. However, there are a number of shortcomings to the current models largely due to several simplifications that were implemented to reduce computational load. Future work may seek to further develop more sophisticated models that better approximate the intestinal environment. Below is a list of some of the modifications and features that could be incorporated into future models. Such models would provide a useful tool for the food and pharmaceutical industry.

A) It would be of interest to examine the effect of incorporating viscoelastic bodies in the fluid phase (Lim et al. 2013) and the resulting processes of diffusive and advective mass transfer. Such models could include the effect of processes akin to gel filtration (i.e. the effects of small particles diffusing into viscoelastic regions while large particles are excluded).

B) It would also be of interest to examine the effect of incorporating paracellular 'solvent drag' (i.e. a passive process of absorption involving the transit of fluid containing nutrients via the intercellular tight junctions – a process 'triggered' by active absorption by enteroyctes). Previous work has highlighted the significance of such mechanisms for absorption when it was reported that solute solvent drag could cause a greater uptake of glucose than would occur by the active (SGLT) route (Pappenheimer and Reiss 1987).

C) The work in this thesis uses models that simplify the outcomes of villous apical crowding and provides only a rough estimate of their effects on mixing and mass transfer. More work is needed in order to more accurately model the effects of the angulation of the villous shaft that leads to villous apical crowding and the effect of the vertical displacement of villi on the crests of mucosal microfolds.

D) As discussed in chapters five and seven, it is likely that radial and longitudinally oriented mucosal microfolding may augment mass transfer in the perivillous space differently especially in the presence of axial flow through the gut lumen. Thus it is necessary to simulate the fluid mechanical consequences of both radial and longitudinal types of folding and to evaluate their relative contributions to mixing and mass transfer.

E) It would also be of interest to incorporate stochastic variation of non-propagating pendular contractions as has been observed in living *ex vivo* segments of gut (Lentle et al. 2012) to the 3D model of mucosal microfolding in the perivillous region (chapter seven).

Finally, throughout this thesis and especially in the computational models developed, the description and measure of mixing is one that is more complicated than a generalized view involving only the 'stretching' and 'folding' of lamellas of perivillous lumen contents (Ottino 1989). The presence of discontiguous viscoelastic bodies interspersed in the Newtonian fluid phase as well as villous apical crowding and separation during non-propagating pendular contractions are among the factors that could confound more simplified descriptions of mixing and mass transfer.

8.5. The overall context of the work

Overall, it should be noted that the factors that have been identified in this thesis, which could promote mixing and mass transfer in the perivillous region of the small intestine, have only been assessed in the terminal ileum of the brushtail possum. This work indicates that such sites in the small intestine could be more adapted for the processes of mixing and mass transfer for 'scavenging' in an environment of low solute concentration as compared to more distal sites. However, as has been discussed earlier, such mixing and mass transfer factors may have little influence on the breakdown of larger solids as would be found in more proximal regions of the small intestine. More work is needed to validate such a hypothesis and to better understand the processes of mixing and mass transfer in all sites of the small intestine.

Appendix

A1 Photographs of the tissue bath and experimental setup used for the determination of the Brownian motion of microbeads and mucus microrheology

Side view of tissue bath

Frontal view of tissue bath

Top view of tissue bath

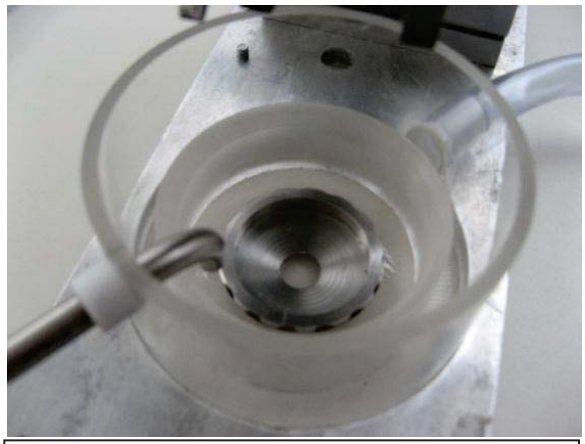

Concentric baths with attached inlet and outlet pipes

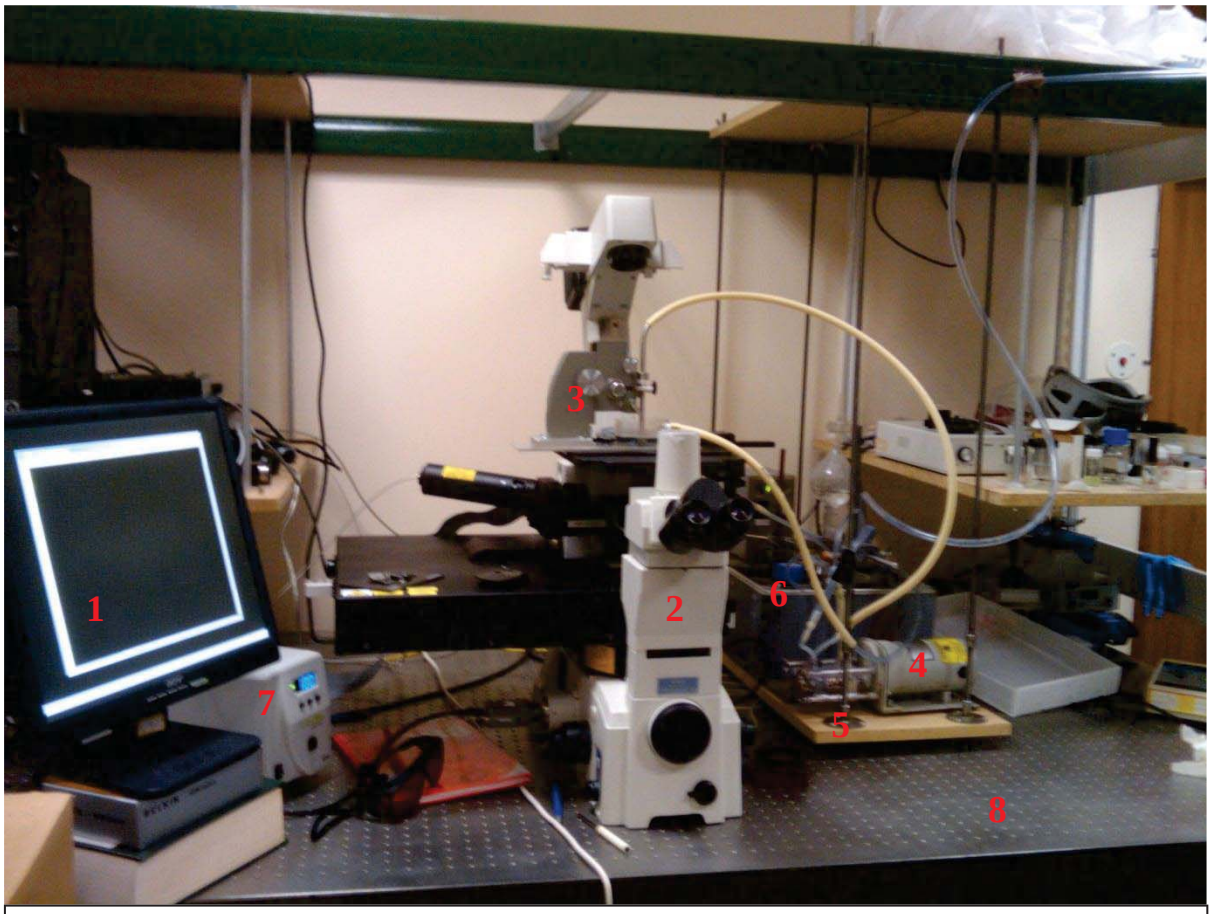

Overall view of experimental setup;

1) Computer monitor to view microbeads and the surrounding fluid environment
2) Optical micro-rheometer
3) Tissue bath positioned in the recess in the manual substage of the micro-rheometer
4) Peristaltic pump for the circulation of carboxygenated and heated Earle-Hepes solution and to facilitate a vacuum in the hollow of the tissue bath probe
5) Suspended table for the placement of heating bath and pump
6) Heating bath
7) Fluorescent lamp unit
8) Air-damped table

A2 Quantifying villous shaft bending

If it was found that villous tip displacement attributed to villous shaft bending (DB) according to the methods outlined in Lim et al. (2014)[8] was significant a second method of quantifying DB may be considered (see methods below). The premise of the following methods described is that the shafts of villi were prone to bend under physiological levels of lumen flow and the bending was in the form of an arc of a circle with a single bending modulus.

A2.1 A second method of determining the magnitude of villous shaft bending

As stated in Lim et al. (2014)[8], the total villous displacement (TD) observed may be composed of the following movements; bending of the villous shaft, villous pivoting around the point of its attachment to the mucosa, villous twisting about its long axis and translational movement of the base of the villous with respect to the microscope field of view. The method of determining the displacement of the villous shaft by bending (DB) or the lack thereof has been outlined in the published paper Lim et al. (2014) [8]. In this sub-section, another method of assessing DB was also considered. This method only utilized images in which three to five readily identifiable reference points could be identified in subsequent images over a minimum distance of 280 microns along the long axis of a villus (greater than half the mean length of a villus) in such positions that they could be joined by a straight line during the period when there was no flow. Of a total of 38 image sequences of villi used to assess TD, a total of 13 image sequences from 6 different villi over 3 animals were suitable for evaluation of DB by the second method.

[8] See attached paper to chapter six of this thesis

Similar to the first method, the first point was positioned as close as possible to the villous tip, the last at the greatest possible distance from the first and the others positioned equidistantly between the two points. The position of each point was identified on the image that was taken at the time of maximum TD, and the displacements of each of the points from their original positions were then calculated by cross-correlation (Lim et al. 2014) [8]. DB is then estimated in terms of the curvature of the villous surface about its longitudinal axis i.e. the radius of a circle based on five readily identifiable points distributed along the longitudinal axis (Figure A4.1). An arc of a circle is fitted to the five displaced points using a fitting method developed by Gabriel Taubin (1991)[9] assuming that the villous bending was homogenous with only a single bending modulus. This method was chosen as it had a higher level of accuracy in the fitting of a circle to incomplete circular arcs (Al-Sharadqah and Chernov 2009)[10] as compared with other methods. The circular perimeter fitting method was run as a MATLAB algorithm and functioned by fitting the best circular perimeter that minimized the performance function F_T in (1) below for 'n' points each with $x_{i\to n}$ and $y_{i\to n}$ coordinates (Al-Sharadqah and Chernov 2009);

$$F_T = \frac{\sum[(x_i-a)^2+(y_i-b)^2-R^2]^2}{4n^{-1}\sum[(x_i-a)^2+(y_i-b)^2]} \qquad \text{(A2.1.1)}$$

where 'R' is the radius of the generated circular perimeter with the centre point at abscissa 'a' and ordinate 'b'. Using the radius and centre point of the circle generated by the algorithm, a combined value for villous bending and twisting (BT) could then be calculated in microns from the following equations.

[9] Taubin, G. (1991). "Estimation of Planar Curves, Surfaces, and Nonplanar space curves defined by implicit equations with applications to edge and range image segmentation." IEEE Transactions on pattern analysis and machine intelligence **13**(11): 1115-1138.

[10] Al-Sharadqah, A. and N. Chernov (2009). "Error analysis for circle fitting algorithms." Electronic Journal of Statistics **3**: 886-911.

$$\theta = \frac{L_m}{R} \quad \text{(A2.1.2)}$$

$$BT = R(1 - \cos\theta) \quad \text{(A2.1.3)}$$

where L_m is the mean villus length (=560μm), θ is the angle subtended by the arc (Figure A4.1). BT has two components with the first being the bending of the villous shaft (DB) and the second being the twisting of the villous about its long axis (i.e. an artifactual value and contributor to BT). If the curvature of the circular perimeter resulting from the bending of the villus was in the direction of flow it was assigned a positive value. Correspondingly if it was in a direction contrary to that of the direction of flow it was assigned a negative value.

In order to calculate the contribution of only DB to TD, it is necessary to eliminate the effects of villous twisting. This was done by assuming that the direction of the villous twisting was randomly distributed given that it was equally likely for villi to be twisted to the left or the right during lumen flow. Therefore, the mean value of calculated BT values of a series of villi would approach DB.

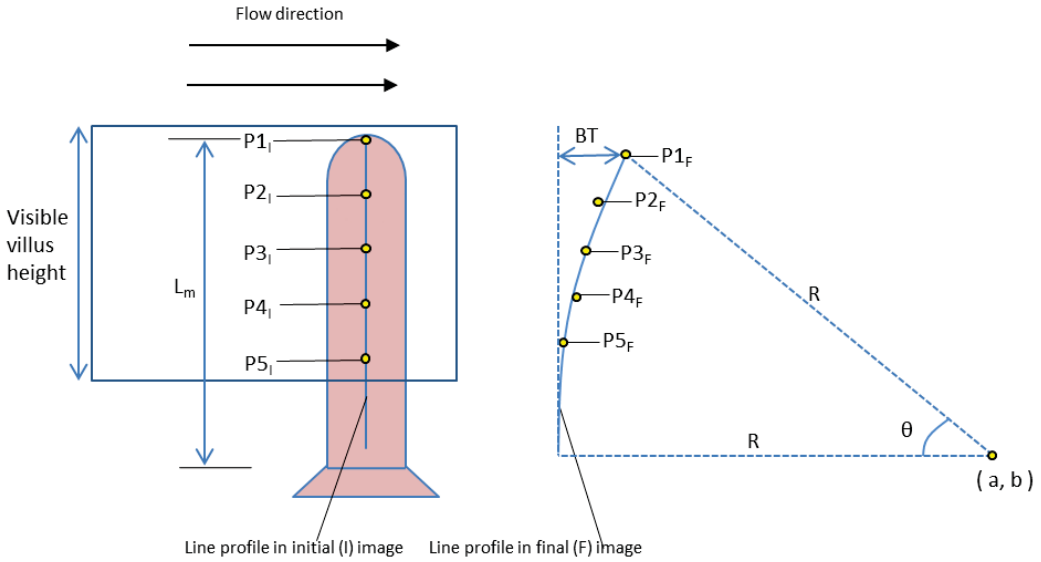

Figure A2.1: A radius 'R' and centre point coordinates are then calculated from the from the displacement and position data. BT, which is the total displacement attributed to villous bending and the twisted profile of villi, is calculated by equations 2 and 3 seen in the main text. DB is the mean value of BT from a series of villi.

A3 Miscellaneous photographs

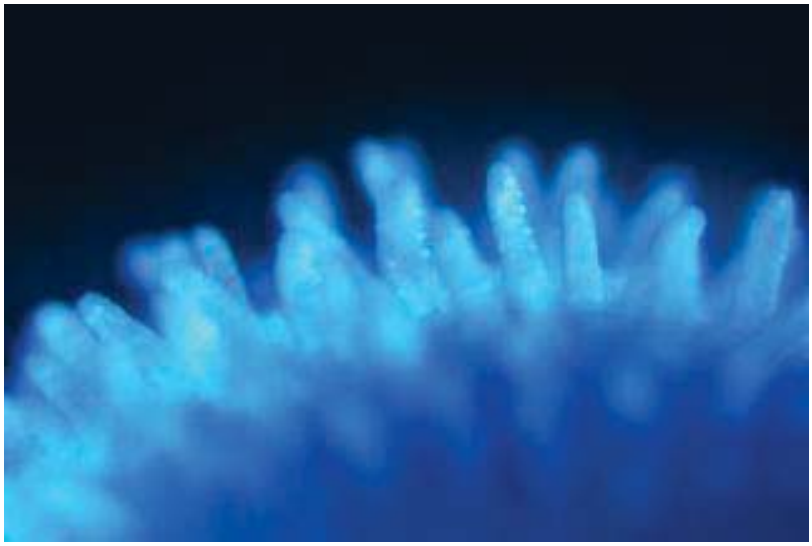

Possum ileal villi stained with Methylene Blue appears to be circular and ‘finger-shaped’.

Possum duodenal villi stained with Methylene Blue appears to be flattened and ‘paddle-shaped’.

References

Aidun, C. K. and J. R. Clausen (2010). "Lattice-Boltzmann method for complex flows." Annual Review of Fluid Mechanics **42**: 439-472.

Allen, A., A. Bell, M. Mantle and J. P. Pearson (1982). The structure and physiology of gastrointestinal mucus. Mucus in Health and Disease—II, Springer**:** 115-133.

Allen, A. and G. Flemström (2005). "Gastroduodenal mucus bicarbonate barrier: protection against acid and pepsin " American Journal of Physiology **288**: G1-G19.

Allen, A., G. Flemstrom, A. Garner and E. Kivilaakso (1993). "Gastroduodenal mucosal protection." Physiological Reviews **73**(4): 823-857.

Allen, A., D. Hutton, A. Leonard, J. Pearson and L. Sellers (1986). "The role of mucus in the protection of the gastroduodenal mucosa." Scandinavian Journal Of Gastroenterology **21**(S125): 71-78.

Ambort, D., S. van der Post, M. E. V. Johansson, J. MacKenzie, E. Thomsson, U. Krengel and G. C. Hansson (2011). "Function of the CysD domain of the gel-forming MUC2 mucin." Biochemical Journal **436**(1): 61-70.

Amidon, G., J. Kou, R. Elliott and E. Lightfoot (1980). "Analysis of models for determining intestinal wall permeabilities." Journal of Pharmaceutical Sciences **69**(12): 1369-1373.

Anderson, B. W., A. S. Levine, D. G. Levitt, J. M. Kneip and M. D. Levitt (1988). "Physiological measurement of luminal stirring in perfused rat jejunum." American Journal of Physiology **254**: G843-848.

Andrews, G. P., T. P. Laverty and D. S. Jones (2009). "Mucoadhesive polymeric platforms for controlled drug delivery." European Journal of Pharmaceutics and Biopharmaceutics **71**(3): 505-518.

Arkwright, J. W., I. D. Underhill, S. A. Maunder, N. Blenman, M. M. Szczesniak, L. Wiklendt, I. J. Cook, D. Z. Lubowski and P. G. Dinning (2009). "Design of a high-sensor count fibre optic manometry catheter for in-vivo colonic diagnostics." Optics express **17**(25): 22423-22431.

Atuma, C., V. Strugala, A. Allen and L. Holm (2001). "The adherent gastrointestinal mucus gel layer: Thickness and physical state *In Vivo*." American Journal of Physiology **280**(5): G922-G929.

Baetens, K., D. Nuyttens, P. Verboven, M. De Schampheleire, B. Nicolaï and H. Ramon (2007). "Predicting drift from field spraying by means of a 3D computational fluid dynamics model." Computers and Electronics in Agriculture **56**(2): 161-173.

Bansil, R., E. Stanley and J. T. LaMont (1995). "Mucin biophysics." Annual Reviews of Physiology **57**(635-657).

Bansil, R. and B. S. Turner (2006). "Mucin structure, aggregation, physiological functions and biomedical applications." Current Opinion in Colloid & Interface Science **11**: 164-170.

Barker, N. (2014). "Adult intestinal stem cells: critical drivers of epithelial homeostasis and regeneration." Nature Reviews Molecular Cell Biology **15**(1): 19-33.

Barker, N., M. van de Wetering and H. Clevers (2008). "The intestinal stem cell." Genes & Development **22**(14): 1856-1864.

Barnes, H. A., J. F. Hutton and K. Walters (1989). An introduction to rheology, Elsevier. **3:** 15-25.

Barry Jr, R. E. (1976). "Mucosal surface areas and villous morphology of the small intestine of small mammals: functional interpretations." Journal of Mammalogy: 273-290.

Baumgartner, H. K. and M. H. Montrose (2004). "Regulated alkali secretion acts in tandem with unstirred layers to regulate mouse gastric surface pH." Gastroenterology **126**(3): 774-783.

Bayliss, W. and E. Starling (1899). "The movements and innervation of the small intestine." The Journal of Physiology **24**(2): 99.

Beaudoing, G., B. Duding, R. Margrita, M. Launay and P. Silvestre (1991). The mass transfers of water by diffusion and permeation through a covering of wastes disposal, CEA Centre d'Etudes de Grenoble, 38 (France). Direction des Technologies Avancees.

Bell, A. E., A. Allen, E. Morris and D. A. Rees (1982). Rheological studies on native pig gastric mucus gel. Mucus in Health and Disease—II, Springer**:** 97-99.

Bell, A. E., A. Allen, E. R. Morris and S. B. Ross-Murphy (1984). "Functional interactions of gastric mucus glycoprotein." International Journal of Biological Macromolecules **6**(6): 309-315.

Bertsch, A., S. Heimgartner, P. Cousseau and P. Renaud (2001). "Static micromixers based on large-scale industrial mixer geometry." Lab on a Chip **1**(1): 56-60.

Bjarnason, I., A. Macpherson and D. Hollander (1995). "Intestinal permeability: an overview." Gastroenterology **108**(5): 1566-1581.

Bongaerts, J., D. Rossetti and J. Stokes (2007). "The lubricating properties of human whole saliva." Tribology Letters **27**(3): 277-287.

Booth, C. and C. S. Potten (2000). "Gut instincts: thoughts on intestinal epithelial stem cells." Journal of Clinical Investigation **105**(11): 1493-1499.

Borchard, G. (2009). The Absorption Barrier. Oral Delivery of Macromolecular Drugs: Barriers. Strategies and Future Trends. A. Bernkop-Schnürch, Springer**:** 49-59.

Bouzaidi, M. h., M. Firdaouss and P. Lallemand (2001). "Momentum transfer of a Boltzmann-lattice fluid with boundaries." Physics of fluids **13**(11): 3452-3259.

Bowen, R. (1995). "Absorption of water and electrolytes." Retrieved 18 March, 2014, from http://www.vivo.colostate.edu/hbooks/pathphys/digestion/smallgut/absorb_water.html.

Bueno, L., J. Fioramonti and Y. Ruckebusch (1975). "Rate of flow of digesta and electrical activity of the small intestine in dogs and sheep." Journal of Physiology **249**: 69-85.

Buresti, G. (2000). "Bluff-body aerodynamics." Lecture Notes, International Advanced School on Wind-Excited and Aeroelastic Vibrations, Genoa, Italy.

Bushby, R. J. and K. Kawata (2011). "Liquid crystals that affected the world: discotic liquid crystals." Liquid Crystals **38**(11-12): 1415-1426.

Cairns, H. (1970). "Symposium on `allergy'." The Journal of the Royal College of General Practitioners **19**(93): 242-244.

Caldara, M., R. S. Friedlander, N. L. Kavanaugh, J. Aizenberg, K. R. Foster and K. Ribbeck (2012). "Mucin biopolymers prevent bacterial aggregation by retaining cells in the free-swimming state." Current Biology **22**(24): 2325-2330.

Cammarota, G., A. Martino, G. Pirozzi, R. Cianci, F. Cremonini, G. Zuccalá, L. Cuoco, V. Ojetti, M. Montalto, F. M. Vecchio, A. Gasbarrini and G. Gasbarrini (2004). "Direct visualization of intestinal villi by high-resolution magnifying upper endoscopy: a validation study." Gastrointestinal Endoscopy **60**(5): 732-738.

Cannon, W. (1902). "The movements of the intestines studied by means of the rontgen rays." American Journal of Physiology **6**(5): 251-277.
Carleton, H. M. and H. Florey (1927). "The mammalian lacteal: Its histological structure in relation to its physiological properties." Proceedings of the Royal Society of London B **102**(714): 110-118.
Carr, K. and P. Toner (1984). Morphology of the intestinal mucosa. Pharmacology of Intestinal Permeation I, Springer**:** 1-50.
Cartwright, J. H., E. Gouillart, N. Piro, O. Piro and I. Tuval (2012). "Geometric mixing." arXiv preprint arXiv:1206.6894.
Cash, H. L., C. V. Whitham, C. L. Behrendt and L. V. Hooper (2006). "Symbiotic bacteria direct expression of an intestinal bactericidal lectin." Science **313**(5790): 1126-1130.
Celli, J., B. Gregor, B. Turner, N. H. Afdhal, R. Bansil and S. Erramilli (2005). "Viscoelastic properties and dynamics of porcine gastric mucin." Biomacromolecules **6**(3): 1329-1333.
Celli, J. P., B. S. Turner, N. H. Afdhal, R. H. Woldt, G. H. McKinley, R. Bansil and S. Erramilli (2007). "Rheology of gastric muscin exhibits a pH-dependent sol-gel transition." Biomacromolecules **8**: 1580-1586.
Chen, S. and G. D. Doolen (1998). "Lattice Boltzmann method for fluid flows." Annual Review of Fluid Mechanics **30**: 329-364.
Chretien, F., J. Cohen, V. Borg and A. Psychoyos (1975). "Human cervical mucus during the menstrual cycle and pregnancy in normal and pathological conditions." The Journal of Reproductive Medicine **14**(5): 192.
Christensen, J. (1984). Gastrointestinal motility: The regulation of nutrient delivery. The role of the gastrointestinal tract in nutrient delivery. M. Green and H. L. Greene. Orlando, Florida, Academic Press**:** 83-106.
Ciaccio, E. J., C. A. Tennyson, G. Bhagat, S. K. Lewis and P. H. Green (2012). "Quantitative estimates of motility from videocapsule endoscopy are useful to discern celiac patients from controls." Digestive Diseases and Sciences **57**(11): 2936-2943.
Cone, R. (1999). "Mucus." Mucosal Immunology **3**: 43-64.
Cone, R. (2009). "Barrier properties of mucus." Advanced Drug Delivery Reviews **61**: 75-85.
Corfield, A. P., D. Carroll, N. Myerscough and C. S. J. Probert (2001). "Mucins in the gastrointestinal tract in health and disease." Frontiers in Bioscience **6**: d1321-1357.
Corr, S. C., C. C. Gahan and C. Hill (2008). "M-cells: origin, morphology and role in mucosal immunity and microbial pathogenesis." FEMS Immunology & Medical Microbiology **52**(1): 2-12.
Crater, J. S. and R. L. Carrier (2010). "Barrier properties of gastrointestinal mucus to nanoparticle transport." Macromolecular Bioscience **10**: 1473-1483.
Daniel, H., C. Fett and A. Kratz (1989). "Demonstration and modification of intervillous pH profiles in rat small intestine in vitro." American Journal of Physiology **257**(4): G489-G495.
Daugherty, A. L. and R. J. Mrsny (1999). "Transcellular uptake mechanisms of the intestinal epithelial barrier Part one." Pharmaceutical Science and Technology Today **2**(4): 144-151.
Davidson, G., D. Gall, M. Petric, D. Butler and J. Hamilton (1977). "Human rotavirus enteritis induced in conventional piglets. Intestinal structure and transport." Journal of Clinical Investigation **60**(6): 1402.

Davis, C. W. and B. F. Dickey (2008). "Regulated airway goblet cell mucin secretion." Annual Review of Physiology **70**: 487-512.

Davis, C. W., M. L. Dowell, M. Lethem and M. Van Scott (1992). "Goblet cell degranulation in isolated canine tracheal epithelium: response to exogenous ATP, ADP, and adenosine " American Journal of Physiology **262**(5): C1313-C1323.

Dawson, M., E. Krauland, D. Wirtz and J. Hanes (2004). "Transport of polymeric nanoparticle gene carriers in gastric mucus." Biotechnology Progress **20**: 851-857.

Dawson, M., D. Wirtz and J. Hanes (2003). "Enhanced viscoelasticity of human cystic fibrotic sputum correlates with increasing microheterogeneity in particle transport." Journal of Biological Chemistry **278**(50): 50393-50401.

De Gennes, P. G. (1971). "Reptation of a polymer chain in the presence of fixed obstacles." The Journal of Chemical Physics **55**(2): 572.

De Gennes, P. G. (1979). Scalling concepts in polymer physics. USA, Cornell University Press**:** 227-235.

de Loubens, C., R. G. Lentle, C. Hulls, P. W. M. Janssen, R. J. Love and J. P. Chambers (2014). "Characterisation of mixing in the proximal duodenum of the rat during longitudinal contractions and comparison with a fluid mechanical model based on spatiotemporal motility data." Plos One **9**(4): e95000.

de Loubens, C., R. G. Lentle, R. J. Love, C. Hulls and P. W. M. Janssen (2013). "Fluid mechanical consequences of pendular activity, segmentation and pyloric outflow in the proximal duodenum of the rat and the guinea pig." Journal of the Royal Society Interface **10**(83): 20130027.

Deplancke, B. and H. R. Gaskins (2001). "Microbial modulation of innate defense: goblet cells and the intestinal mucus layer." The American Journal of Clinical Nutrition **73**: 1131S-1141S.

Desai, M. A., M. Mutlu and P. Vadgama (1992). "A study of macromolecular diffusion through native porcine mucus." Cellular and Molecular Life Sciences **48**(1): 22-26.

DeSesso, J. M. and C. F. Jacobson (2001). "Anatomical and physiological parameters affecting gastrointestinal absorption in humans and rats." Food and Chemical Toxicology **39**(3): 209-228.

Diamond, J. M. (1966). "A rapid method for determining voltage concentration relations across membranes." Journal of Physiology **183**: 83-100.

Dimotakis, P. E. (2000). "The mixing transition in turbulent flows." Journal of Fluid Mechanics **409**(1): 69-98.

Dressman, J. and K. Yamada (1991). "Animal models for oral drug absorption." Drugs and the Pharmaceutical Sciences **48**: 235-266.

Du, R. and B. Shi (2010). "Incompressible multi-relaxation-time lattice Boltzmann model in 3-D space." Journal of Hydrodynamics B **22**(6): 782-787.

Dupuis, A. and B. Chopard (2003). "Theory and application of an alternative lattice Boltzmann grid refinement algorithm." Physical Review E **67**: 066707.

Ehrlein, H. J., M. Schemann and M.-L. Siegle (1987). "Motor patterns of small intestine determined by closely spaced extraluminal transducers and videofluoroscopy." American Journal of Physiology **253**(3): G259-G267.

Elliott, H., C. Carpenter, R. Sack and J. Yardley (1970). "Small bowel morphology in experimental canine cholera. A light and electron microscopic study."

Laboratory Investigation: a Journal of Technical Methods and Pathology **22**(2): 112.

Ensign-Hodges, L., A. Henning, C. Schneider, K. Maisel, Y.-Y. Wang, M. Porosoff, R. Cone and J. Hanes (2013). "*Ex vivo* characterization of particle transport in mucus secretions coating freshly excised mucosal tissues." Molecular Pharmaceutics.

Ermund, A., A. Schütte, M. E. Johansson, J. K. Gustafsson and G. C. Hansson (2013). "Studies of mucus in mouse stomach, small intestine, and colon. I. Gastrointestinal mucus layers have different properties depending on location as well as over the Peyer's patches." American Journal of Physiology **305**(5): G341-G347.

Flemström, G. and E. Kivilaakso (1983). "Demonstration of a pH gradient at the luminal surface of rat duodenum in vivo and its dependence on mucosal alkaline secretion." Gastroenterology **84**(4): 787-794.

Florey, H. (1933). "Observations on the functions of mucus and the early stages of bacterial invasion of the intestinal mucosa." The Journal of Pathology and Bacteriology **37**(2): 283-289.

Florey, H. W. (1962). "The Secretion and function of intestinal mucus." Gastroenterology **43**(326-329).

Forstner, G. (1995). "Signal transduction, packaging and secretion of mucins." Annual Review of Physiology **57**: 585-605.

Frey, A., K. T. Giannasca, R. Weltzin, P. J. Giannasca, H. J. Reggio, W. I. Lencer and M. R. Neutra (1996). "Role of the glycocalyx in regulating access of microparticles to apical plasma membranes of intestinal epithelial cells: implications for microbial attachment and oral vaccine targeting " Journal of Experimental Medicine **184**(3): 1045-1059.

Gebhard, A. and A. Gebert (1999). "Brush cells of the mouse intestine possess a specialized glycocalyx as revealed by quantitative lectin histochemistry: Further evidence for a sensory function." Journal of Histochemistry & Cytochemistry **47**(6): 799-808.

Gibbons, R. and P. Mattner (1966). "Some aspects of the chemistry of cervical mucus." International Journal of Fertility **11**(4): 366.

Ginzburg, I. (2005). "Equilibrium-type and link-type lattice Boltzmann models for generic advection and anisotropic-dispersion equation." Advances in Water Resources **28**(11): 1171-1195.

Godl, K., M. E. Johansson, M. E. Lidell, M. Mörgelin, H. Karlsson, F. J. Olson, J. R. Gum, Y. S. Kim and G. C. Hansson (2002). "The N terminus of the MUC2 mucin forms trimers that are held together within a trypsin-resistant core fragment." Journal of Biological Chemistry **277**(49): 47248-47256.

Gordon, J. I. (1989). "Intestinal epithelial differentiation: new insights from chimeric and transgenic mice." The Journal of Cell Biology **108**(4): 1187-1194.

Gouyer, V., F. Gottrand and J.-L. Desseyn (2011). "The extraordinarily complex but highly structured organization of intestinal mucus-gel unveiled in multicolor images." Plos One **6**(4): e18761.

Grivel, M. L. and Y. Ruckebusch (1972). "The propagation of segmental contractions along the small intestine." Journal of Physiology **227**(2): 611-625.

Grovum, W. L. and V. J. Williams (1973). "Rate of passage of digesta in sheep. 1. The effect of level of food intake on marker retention times along the small intestine and on apparent water absorption in the small and large intestines." British Journal of Nutrition **29**: 13-21.

Gruby, M. and D. Delafond (1843). "Resultats des recherches faites sur l'anatomie et les fonctions des villosites intestinales, l'absorption, la preparation et la composition organique du chyle dans les animaux." Comptes Rendus Hebdomadaires des Séances de L'Académie des Sciences **16**: 1194-1197.

Guigas, G., C. Kalla and M. Weiss (2007). "Probing the nanoscale viscoelasticity of intracellular fluids in living cells." Biophysical Journal **93**(1): 316-323.

Güldner, F., J. Wolff and D. Keyserlingk (1972). "Fibroblasts as a part of the contractile system in duodenal villi of rat." Cell and Tissue Research **135**(3): 349-360.

Gum, J., J. W. Hicks, N. W. Toribara, B. Siddiki and Y. S. Kim (1994). "Molecular cloning of human intestinal mucin (MUC2) cDNA. Identification of the amino terminus and overall sequence similarity to prepro-von Willebrand factor." Journal of Biological Chemistry **269**(4): 2440-2446.

Guo, Z. L., B. C. Shi and N. C. Wang (2000). "Lattice BGK Model for Incompressible Navier–Stokes Equation." Journal of Computational Physics **165**(1): 288-306.

Guo, Z. L., C. G. Zheng and B. C. Shi (2002). "Non-equilibrium extrapolation method for velocity and pressure boundary conditions in the lattice Boltzmann method." Chinese Physics **11**(4): 366-374.

Gwynne, R. M., E. A. Thomas, S. M. Goh, H. Sjövall and J. C. Bornstein (2004). "Segmentation induced by intraluminal fatty acid in isolated guinea-pig duodenum and jejunum." Journal of Physiology **556**(2): 557-569.

Hall, J. E. and A. C. Guyton (2000). Guyton and Hall Textbook of Medical Physiology, Elsevier Health Sciences**:** 786-787.

Ham, A. W. (1969). Histology. Philadelphia, Lippincott**:** 663.

Hambleton, B. F. (1914). "Note upon the movements of the intestinal villi." American Journal of Physiology **34**(4): 446-447.

Hammer, J., M. Camilleri, S. F. Phillips, A. Aggarwal and A. M. Haddad (1993). "Does the ileocolonic junction differentiate between solids and liquids?" Gut **34**: 222--226.

Harder, J., J. Bartels, E. Christophers and J.-M. Schröder (2001). "Isolation and characterization of human β-defensin-3, a novel human inducible peptide antibiotic." Journal of Biological Chemistry **276**(8): 5707-5713.

Hecht, G. (1999). "Innate mechanisms of epithelial host defense: spotlight on intestine." American Journal of Physiology **277**(3): C351-C358.

Hellström, P., E. Husebye and K. Kraglund (1991). "Methodology for motility studies on the small intestine: a Scandinavian consensus." Acta Chirurgica: The European Journal of Surgery. Supplement(564): 51-61.

Helstad, K., M. Rayner, T. van Vliet, M. Paulsson and P. Dejmek (2007). "Liquid droplet-like behaviour of whole casein aggregates adsorbed on graphite studied by nanoindentation with AFM." Food Hydrocolloids **21**(5): 726-738.

Holdych, D. J., D. R. Noble, J. G. Georgiadis and R. O. Buckius (2004). "Truncation error analysis of lattice Boltzmann methods." Journal of Computational Physics **193**(595-619).

Holmén Larsson, J. M., K. A. Thomsson, A. M. Rodríguez-Piñeiro, H. Karlsson and G. C. Hansson (2013). "Studies of mucus in mouse stomach, small intestine, and colon. III. Gastrointestinal Muc5ac and Muc2 mucin O-glycan patterns reveal a regiospecific distribution." American Journal of Physiology **305**(5): G357-G363.

Holmes, R., D. O. B. Hourihane and C. C. Booth (1961). "The mucosa of the small intestine." Postgraduate Medical Journal **37**: 717-724.

Hooper, L. V., D. R. Littman and A. J. Macpherson (2012). "Interactions between the microbiota and the immune system." Science **336**(6086): 1268-1273.
Hosoyamada, Y. and T. Sakai (2005). "Structural and mechanical architecture of the intestinal villi and crypts in the rat intestine: integrative reevaluation from ultrastructural analysis." Anatomy and Embryology **210**(1): 1-12.
Hosoyamada, Y. and T. Sakai (2007). "Mechanical components of rat intestinal villi as revealed by ultrastructural analysis with special reference to the axial smooth muscle cells in the villi." Archives of Histology and Cytology **70**(2): 107-116.
Howell, R., N. Qin, J. Edwards and N. Durrani (2010). "Wind tunnel and numerical study of a small vertical axis wind turbine." Renewable Energy **35**(2): 412-422.
Hsiung, P.-L., L. Pantanowitz, A. D. Aguirre, Y. Chen, D. Phatak, T. H. Ko, S. Bourquin, S. J. Schnitt, S. Raza and J. L. Connolly (2005). "Ultrahigh-resolution and 3-dimensional optical coherence tomography ex vivo imaging of the large and small intestines." Gastrointestinal Endoscopy **62**(4): 561-574.
Huang, H., X. Lu and M. Sukop (2011). "Numerical study of lattice Boltzmann methods for a convection–diffusion equation coupled with Navier–Stokes equations." Journal of Physics A: Mathematical and Theoretical **44**(5): 055001.
Huizinga, J. D. and W. J. E. P. Lammers (2009). "Gut peristalsis is governed by a multitude of cooperating mechanisms." American Journal of Physiology **296**: G1-G8.
Hull, B. E. and A. Staehelin (1979). "The terminal web." The Journal of Cell Biology **81**: 67-82.
Husebye, E. (1999). "The patterns of small bowel motility: Physiology and implications in organic disease and functional disorders." Neurogastroenterology & Motility **11**: 141-161.
Janssen, P. W. M., R. G. Lentle, P. Asvarujanon, P. Chambers, K. J. Stafford and Y. Hemar (2007). "Characterization of flow and mixing regimes within the ileum of the brushtail possum using residence time distribution analysis with simultaneous spatio-temporal mapping." Journal of Physiology **582**(3): 1239-1248.
Jeffrey, B., H. S. Udaykumar and K. S. Schulze (2003). "Flow fields generated by peristaltic reflex in isolated guinea pig ileum: Impact of contraction depth and shoulders." American Journal of Physiology **285**: G907-G918.
Jin, L., L. Reynolds, D. Redmer, J. Caton and J. Crenshaw (1994). "Effects of dietary fiber on intestinal growth, cell proliferation, and morphology in growing pigs." Journal of Animal Science **72**(9): 2270-2278.
Jodal, M. and O. Lundgren (1986). "Countercurrent mechanisms in the mammalian gastrointestinal tract." Gastroenterology **91**: 225-241.
Johansson, M. E., D. Ambort, T. Pelaseyed, A. Schütte, J. K. Gustafsson, A. Ermund, D. B. Subramani, J. M. Holmén-Larsson, K. A. Thomsson and J. H. Bergström (2011a). "Composition and functional role of the mucus layers in the intestine." Cellular and Molecular Life Sciences **68**(22): 3635-3641.
Johansson, M. E., J. M. H. Larsson and G. C. Hansson (2011b). "The two mucus layers of colon are organized by the MUC2 mucin, whereas the outer layer is a legislator of host–microbial interactions." Proceedings of the National Academy of Sciences **108**(Supplement 1): 4659-4665.
Johansson, M. E. V., M. Phillipson, J. Petersson, A. Velcich, L. Holm and G. C. Hansson (2008). "The inner of the two Muc2 mucin-dependent mucus layers in colon is devoid of bacteria." Proceedings of the National Academy of Sciences **105**(39): 15064-15069.

Johansson, M. E. V., K. A. Thomsson and G. C. Hansson (2009). "Proteomic analyses of the two mucus layers of the colon barrier reveal that their main component, the Muc2 mucin, is strongly bound to the Fcgbp protein." Journal of Proteome Research **8**: 3549-3557.

Johnson, D. A. and G. L. Amidon (1988). "Determination of intrinsic membrane transport parameters from perfused intestine experiments: a boundry layer approach to estimating the aqueous and unbiased membrane permeabilities." Journal of Theoratical Biology **131**: 93-106.

Jumars, P. A. (2000). "Animal guts as ideal chemical reactors: maximizing absorption rates." The American Naturalist **155**(4): 527-543.

Kadanoff, L. P. (1986). "On two levels." Physics today **39**: 7.

Kahrilas, P. J., S. K. Ghosh and J. E. Pandolfino (2008). "Imaging and technology: challenging the limits of esophageal manometry." Gastroenterology **134**(1): 16.

Kararli, T. T. (1995). "Comparison of the gastrointestinal anatomy, physiology, and biochemistry of humans and commonly used laboratory animals." Biopharmaceutics and Drug Disposition **16**(5): 351-380.

Karlsson, N. G., A. Herrmann, H. Karlsson, M. E. Johansson, I. Carlstedt and G. C. Hansson (1997). "The glycosylation of rat intestinal Muc2 mucin varies between rat strains and the small and large intestine. A study of O-linked oligosaccharides by a mass spectrometric approach." The Journal of Biological Chemistry **272**(43): 27025-27034.

Kellow, J., T. Borody, S. Phillips, R. Tucker and A. Haddad (1986). "Human interdigestive motility: variations in patterns from esophagus to colon." Gastroenterology **91**(2): 386-395.

Kemper, A. C. and R. D. Specian (1991). "Rat small intestinal mucins: a quantitative analysis." The Anatomical Record **229**(2): 219-226.

Khosla, R., L. C. Feely and S. S. Davis (1989). "Gastrointestinal transit of non-disintegrating tablets in fed subjects." International Journal of Pharmaceutics **53**(2): 107-117.

Kim, K. C. and B. C. Lee (1991). "P2 purinoceptor regulation of mucin release by airway goblet cells in primary culture." British Journal of Pharmacology **103**(1): 1053-1056.

Kindon, H., C. Pothoulakis, L. Thim, K. Lynch-Devaney and D. K. Podolsky (1995). "Trefoil peptide protection of intestinal epithelial barrier function: cooperative interaction with mucin glycoprotein." Gastroenterology **109**(2): 516-523.

King, C. E. and L. Arnold (1922). "The activities of the intestinal mucosal motor mechanism." American Journal of Physiology **59**(1): 97-121.

King, C. E. and M. H. Robinson (1945). "The nervous mechanisms of the muscularis mucosae." American Journal of Physiology **143**(3): 325-335.

King, I. S., F. V. Sepúlveda and M. W. Smith (1981). "Cellular distribution of neutral and basic amino acid transport systems in rabbit ileal mucosa." Journal of Physiology **319**: 355-368.

Kinter, W. B. and T. H. Wilson (1965). "Autoradiographic study of sugar and amino acid absorption by everted sacs of hamster intestine " Journal of Cell Biology **25**: 19-39.

Klinger, J. D., B. Tandler, C. M. Liedtke and T. F. Boat (1989). "Proteinases of *Pseudomonas auruginosa* evoke mucin release by tracheal epithelium." Journal of Clinical Investigation **74**: 1669-1678.

Kočevar-Nared, J., J. Kristl and J. Šmid-Korbar (1997). "Comparative rheological investigation of crude gastric mucin and natural gastric mucus." Biomaterials **18**(9): 677-681.
Kokas, E. and C. L. Johnston (1965). "Influence of refined villikinin on motility of intestinal villi." American Journal of Physiology **208**(6): 1196-1202.
Koopman, J., A. Stadhouders, H. Kennis and H. De Boer (1987). "The attachment of filamentous segmented micro-organisms to the distal ileum wall of the mouse: a scanning and transmission electron microscopy study." Laboratory Animals **21**(1): 48-52.
Kopylov, U. and E. G. Seidman (2013). "Clinical applications of small bowel capsule endoscopy." Clinical and Experimental Gastroenterology **6**: 129.
Krishnan, B. (1932). "Studies on the function of the intestinal musculature: The normal movements of the small intestine and the relations between the action of the longitudinal and circular muscle fibres in those movements." Experimental Physiology **22**(1): 57-63.
Kuzmuk, K. N., K. S. Swanson, K. A. Tappenden, L. B. Schook and G. C. Fahey (2005). "Diet and age affect intestinal morphology and large bowel fermentative end-product concentrations in senior and young adult dogs." The Journal of Nutrition **135**(8): 1940-1945.
Lai, S. K., D. E. O'Hanlon, S. Harrold, S. T. Man, Y. Y. Wang, R. Cone and J. Hanes (2007). "Rapid transport of large polymeric nanoparticles in fresh undiluted human mucus." Proceedings of the National Academy of Sciences **104**(5): 1482-1487.
Lai, S. K., Y.-Y. Wang, K. Hida, R. Cone and J. Hanes (2010). "Nanoparticles reveal that human cervicovaginal mucus is riddled with pores larger than viruses." Proceedings of the National Academy of Sciences **107**(2): 598-603.
Lai, S. K., Y.-Y. Wang, D. Wirtz and J. Hanes (2009). "Micro- and macrorheology of mucus." Advanced Drug Delivery Reviews **61**: 86-100.
Lake, A. M., K. J. Bloch, K. J. Sinclair and W. A. Walker (1980). "Anaphylactic release of intestinal goblet cell mucus." Immunology **39**(2): 173-178.
Lallemand, P. and L.-S. Luo (2003). "Lattice Boltzmann method for moving boundaries." Journal of Computational Physics **184**: 406-421.
Lammers, W. J. E. P. (2005). "Spatial and temporal coupling between slow waves and pendular contractions." American Journal of Physiology **289**(5): G898-G903.
Larhed, A. W., P. Artursson, J. Grasjö and E. Björk (1997). "Diffusion of drugs in native and purified gastrointestinal mucus." Journal of Pharmaceutical Sciences **86**(6): 660-665.
Lee, J. S. (1969). "A micropuncture study of water transport by dog jejunal villi in vitro." American Journal of Physiology **217**(5): 1528-1533.
Lee, J. S. (1971). "Contractions of villi and fluid transport in dog jejunal mucosa in vitro." American Journal of Physiology **221**(2): 488-495.
Lentle, R. G., C. de Loubens, P. W. M. Janssen, P. Chambers, C. Hulls and M. D. Golding (2012). "A comparison of the organization of longitudinal and circular contractions during pendular and segmental activity in the duodenum of the rat and guinea pig." Neurogastroenterology & Motility **24**(7): 686-e298.
Lentle, R. G., Y. Hemar, C. E. Hall and K. J. Stafford (2005). "Periodic fluid extrusion and models of digesta mixing in the intestine of a herbivore, the common brushtail possum (*Trichosurus vulpecula*)." Journal of Comparative Physiology B **175**: 337-347.

Lentle, R. G. and P. W. M. Janssen (2008). "Physical characteristics of digesta and their influence on flow and mixing in the mammalian intestine: A review." Journal of Comparative Physiology B **178**: 673-690.
Lentle, R. G. and P. W. M. Janssen (2011). Flow, mixing and absorption at the mucosa. Physical Processes of Digestion, Springer.
Lentle, R. G., P. W. M. Janssen, P. Asvarujanon, P. Chambers, K. J. Stafford and Y. Hemar (2007). "High definition mapping of circular and longitudinal motility in the terminal ileum of the brushtail possum *Trichosurus vulpecula* with watery and viscous perfusates." Journal of Comparative Physiology B **177**: 543-556.
Lentle, R. G., P. W. M. Janssen, C. de Loubens, Y. F. Lim, C. Hulls and P. Chambers (2013). "Mucosal microfolds augment mixing at the wall of the distal ileum of the brushtail possum." Neurogastroenterology & Motility **25**(11): 881-e700.
Lentle, R. G., K. J. Stafford and I. M. Henderson (1997). "The effect of formalin on rumen surface area in red deer." Anatomia, Histologia, Embryologia **26**(2): 127-130.
Lentle, R. G., K. J. Stafford, M. S. Kennedy and S. J. Haslett (2002). "Rheological properties of digesta suggest little radial or axial mixing in the forestomach of the tammar (Macropus eugenii) and the parma (Macropus parma) wallaby." Physiological and Biochemical Zoology **75**(6): 572-582.
Levine, M. S., S. E. Rubesin and I. Laufer (2008). "Pattern approach for diseases of mesenteric small bowel on barium studies." Radiology **249**(2): 445.
Levitt, D. G., M. D. Levitt, C. A. Fetzer, J. M. Kneip and J. H. Bond (1987). "Quantitative assessment of luminal stirring in the perfused small intestine of the rat." American Journal of Physiology **252**: G325-G332.
Levitt, D. G., M. D. Levitt and A. Strocchi (1992). "Human jejunal unstirred layer: Evidence for extremely efficient luminal stirring." American Journal of Physiology **262**: G593-G596.
Levitt, M. D., T. Aufderheide, C. A. Fetzer, J. H. Bond and D. G. Levitt (1984). "Use of carbon monoxide to measure luminal stirring in the rat gut." The Journal of Clinical Investigation **74**: 2056-2064.
Levitt, M. D., C. Fine, J. K. Furne and D. G. Levitt (1996). "Use of Maltose Hydrolysis Measurements to Characterize the Interaction between the Aqueous Diffusion Barrier and the Epithelium in the Rat Jejunum." Journal of Clinical Investigation **97**(10): 2308-2315.
Levitt, M. D., J. K. Furne, A. Strocchi, B. W. Anderson and D. G. Levitt (1990). "Physiological measurements of luminal stirring in the dog and human small bowel." Journal of Clinical Investigation **86**: 1540-1547.
Levitt, M. D., J. M. Kneip and D. G. Levitt (1988). "Use of laminar flow and unstirred layer models to predict intestinal absorption in the rat." The Journal of Clinical Investigation **81**: 1365-1369.
Lim, Y. F., R. G. Lentle, P. W. M. Janssen, M. A. K. Williams, C. de Loubens, B. W. Mansel and P. Chambers (2014). "Determination of villous rigidity in the distal ileum of the possum (*Trichosurus vulpecula*)." Plos One **9**(6): e100140.
Lim, Y. F., M. A. K. Williams, R. G. Lentle, P. W. M. Janssen, B. W. Mansel, S. A. J. Keen and P. Chambers (2013). "An exploration of the microrheological environment around the distal ileal villi and proximal colonic mucosa of the possum (*Trichosurus vulpecula*)." Journal of the Royal Society Interface **10**(81): 20121008.

Loudon, C. and A. Tordesillas (1998). "The use of the dimensionless womersley number to characterize the unsteady nature of internal flow." Journal of Theoratical Biology **191**: 63-78.

Love, R. J., R. G. Lentle, P. Asvarujanon, Y. Hemar and K. J. Stafford (2013). "An expanded finite element model of the intestinal mixing of digesta." Food Digestion **4**(1): 26-35.

Ma, T. Y. and J. M. Anderson (2006). Tight junctions and the intestinal barrier. Physiology of the Gastrointestinal Tract. L. R. Johnson, Academic Press. **2:** 1559-1594.

Macierzanka, A., N. M. Rigby, A. P. Corfield, N. Wellner, E. N. Clare Mills, A. R. Mackie and F. Böttger (2011). "Adsorption of bile salts to particles allows penetration of intestinal mucus." Soft Matter **7**: 8077-8084.

Mack, D. R., S. Michail, S. Wei, L. McDougall and M. A. Hollingsworth (1999). "Probiotics inhibit enteropathogenic *E.coli* adherence *in vitro* by inducing intestinal mucin gene expression." American Journal of Physiology **276**: G941-G950.

Macpherson, A. J. and T. Uhr (2004). "Induction of protective IgA by intestinal dendritic cells carrying commensal bacteria." Science **303**(5664): 1662-1665.

Mailman, D., P. Tso and N. Granger (1989). "Effects of oleic acid and bile salts on canine villous motility." Life Sciences **45**: 455-461.

Mailman, D., W. A. Womack, P. R. Kvietys and N. Granger (1990). "Villous motility and unstirred water layers in canine intestine." American Journal of Physiology **258**(2): G238-G246.

Mansel, B. W., S. Keen, P. J. Patty, Y. Hemar and M. A. Williams (2013). A Practical Review of Microrheological Techniques. Rheology - New Concepts, Applications and Methods. R. Durairaj, INTECH**:** 1-21.

Markesich, D., B. Anand, G. Lew and D. Graham (1995). "*Helicobacter pylori* infection does not reduce the viscosity of human gastric mucus gel." Gut **36**(3): 327-329.

Mason, T. G., K. Ganesan, J. H. van Zanten, D. Wirtz and S. C. Kuo (1997). "Particle tracking microrheology of complex fluids." Physical Review Letters **79**(17): 3282-3285.

Matsuo, K., H. Ota, T. Akamatsu, A. Sugiyama and T. Katsuyama (1997). "Histochemistry of the surface mucous layer of the human colon." Gut **40**(6): 782-789.

Maury, J., C. Nicoletti, L. Guzzo-Chambraud and S. Maroux (1995). "The filamentous brush border glycocalyx, a mucin-like marker of enterocyte hyper-polarization." European Journal of Biochemistry **228**(2): 323-331.

McColl, K. E. (2012). "The elegance of the gastric mucosal barrier: designed by nature for nature." Gut **61**(6): 787-788.

McConnell, R. E., J. N. Higginbotham, D. A. Shifrin, D. L. Tabb, R. J. Coffey and M. J. Tyska (2009). "The enterocyte microvillus is a vesicle-generating organelle." Journal of Cell Biology **185**(7): 1285-1298.

McConnell, R. E. and M. J. Tyska (2007). "Myosin-1a powers the sliding of apical membrane along microvillar actin bundles." The Journal of Cell Biology **177**(4): 671-681.

McDonald, D., D. Pethick, B. Mullan and D. Hampson (2001). "Increasing viscosity of the intestinal contents alters small intestinal structure and intestinal growth, and stimulates proliferation of enterotoxigenic Escherichia coli in newly-weaned pigs." British Journal of Nutrition **86**(4): 487-498.

McGuckin, M. A., S. K. Lindén, P. Sutton and T. H. Florin (2011). "Mucin Dynamics and enteric pathogens." Nature Reviews Microbiology **9**: 265-278.

Melville, J., E. Macagno and J. Christensen (1975). "Longitudinal contractions in the duodenum: their fluid-mechanical function." American Journal of Physiology **228**(6): 1887-1892.

Menge, H., M. Gräfe, H. Lorenz-Meyer and E. Riecken (1975). "The influence of food intake on the development of structural and functional adaptation following ileal resection in the rat." Gut **16**(6): 468-472.

Miller, M. J., J. R. McDole and R. D. Newberry (2010). "Microanatomy of the intestinal lymphatic system." Annals of the New York Academy of Sciences **1207**(S1): E21-E28.

Miyake, K., T. Tanaka and P. McNeil (2006). "Disruption-induced mucus secretion: repair and protection." Plos Biology **4**(9): e276.

Moon, H., S. Whipp and A. Baetz (1971). "Comparative effects of enterotoxins from *Escherichia coli* and *Vibrio cholerae* on rabbit and swine small intestine." Laboratory Investigation: a Journal of Technical Methods and Pathology **25**(2): 133.

Mooseker, M. S. (1985). "Organization, Chemistry, and assembly of the cytoskeletal apparatus of the intestinal brush border." Annual Review of Cell Biology **1**: 209-241.

Mooseker, M. S. and L. S. Tilney (1975). "Organization of an actin filament-membrane complex: Filament polarity and membrane attachment in the microvilli of intestinal epithelial cells." The Journal of Cell Biology **67**: 725-743.

Nakajima, Y., N. Baudry, J. Duranteau and E. Vicaut (2001). "Microcirculation in intestinal villi." American Journal of Respiratory and Critical Care Medicine **164**(8): 1526-1530.

Nakamura, J., K. Shima, T. Kimura, S. Muranishi and H. Sezaki (1978). "Role of intestinal mucus in the absorption of quinine and water-soluble dyes from the rat small intestine." Chemical & Pharmaceutical Bulletin **26**(3): 857.

Neutra, M. (1987). Gastrointestinal mucus: synthesis, secretion, and function. Physiology of the Gastrointestinal Tract. L. R. Johnson. New York, Raven Press**:** 975-1009.

Neutra, M. R., L. J. O'Malley and R. D. Specian (1982). "Regulation of intestinal goblet cell secretion. II. A survey of potential secretagogues." American Journal of Physiology **242**(4): G380-G387.

Nicholas, C. V., M. A. Desai and P. Vadgama (1991). "pH dependence of hydrochloric acid diffusion through gastric mucus: correlation with diffusion through a water layer using a membrane-mounted glass pH electrode." Analyst **116**: 463-467.

Ogata, T. (2006). "Bicarbonate secretion by rat bile duct brush cells indicated by immunohistochemical localization of CFTR, anion exchanger AE2, Na^+/HCO_3^- cotransporter, carbonic anhydrase II, Na^+/H^+ exchangers NHE1 and NHE3, H^+/K^+-ATPase, and Na^+/K^+-ATPase." Medical Molecular Morphology **39**(1): 44-48.

Olmsted, S. S., J. L. Padgett, A. I. Yudin, K. J. Whaley, T. R. Moench and R. Cone (2001). "Diffusion of macromolecules and virus-like particles in human cervical mucus." Biophysical Journal **81**(4): 1930-1937.

Ottino, J. M. (1989). The kinematics of mixing: stretching, chaos, and transport, Cambridge University Press. **3:** 64-94.

Palay, S. L. and L. J. Karlin (1959). "An electron microscopic study of the intestinal villus I. The fasting animal." The Journal of Biophysical and Biochemical Cytology **5**(3): 363-371.

Pappenheimer, J. (2001a). "Intestinal absorption of hexoses and amino acids: from apical cytosol to villus capillaries." Journal of Membrane Biology **184**(3): 233-239.

Pappenheimer, J. R. (1998). "Scaling of dimensions of small intestines in non-ruminant eutherian mammals and its significance for absorptive mechanisms." Comparative Biochemistry and Physiology, Part A **121**(1): 45-58.

Pappenheimer, J. R. (2001b). "Role of pre-epithelial "un-stirred" layers in absorption of nutrients from the human jejunum." The Journal of Membrane Biology **179**: 185-204.

Pappenheimer, J. R. and K. Z. Reiss (1987). "Contributions of solvent drag through intercellular junctions to absorption of nutrients by the small intestine of the rat." Journal of Membrane Biology **100**: 123-136.

Parekh, N., D. Seidner and E. Steiger (2005). "Managing short bowel syndrome: Making the most of what the patient has." Cleveland Clinic Journal of Medicine **72**(9): 833-838.

Pavelka, M. and J. Roth (2010). Functional Ultrastructure: Atlas of Tissue Biology and Pathlogy, Springer Vienna**:** 158.

Penry, D. L. and P. A. Jumars (1987). "Modelling animal guts as chemical reactors." The American Naturalist **129**(1): 69-96.

Perez-Vilar, J. (2007). "Mucin granules intraluminal organization." American Journal of Respiratory Cell and Molecular Biology **36**: 183-190.

Perez-Vilar, J. (2009). Gastrointestinal mucus gel barrier. Oral Delivery of Macromolecular Drugs, Springer**:** 21-48.

Perez-Vilar, J. and R. L. Hill (1999). "The structure and assembly of secreted mucins." Journal of Biological Chemistry **274**(45): 31751-31754.

Phillipson, M., M. E. Johansson, J. Henriksnäs, J. Petersson, S. J. Gendler, S. Sandler, A. E. G. Persson, G. C. Hansson and L. Holm (2008). "The gastric mucus layers: constituents and regulation of accumulation." American Journal of Physiology **295**(4): G806-G812.

Pine, D., D. Weitz, P. Chaikin and E. Herbolzheimer (1988). "Diffusing wave spectroscopy." Physical Review Letters **60**(12): 1134.

Pohl, P., S. M. Saparov and Y. N. Antonenko (1998). "The size of the unstirred layer as a function of the solute diffusion coefficient " Biophysical Journal **75**: 1403-1409.

Potten, C. S., C. Booth and D. M. Pritchard (1997). "The intestinal epithelial stem cell: the mucosal governor." International Journal of Experimental Pathology **78**(4): 219-243.

Puchelle, E., J. Zahm and D. Quemada (1986). "Rheological properties controlling mucociliary frequency and respiratory mucus transport." Biorheology **24**(6): 557-563.

Rao, S., C. Lu and K. Schulze-Delrieu (1996). "Duodenum as a immediate brake to gastric outflow: a videofluoroscopic and manometric assessment." Gastroenterology **110**(3): 740-747.

Read, N. W., D. C. Barber, R. J. Levin and C. D. Holdsworth (1977). "Unstirred layer and kinetics of electrogenic glucose absorption in the human jejunum in situ." Gut **18**: 865-876.

Rescigno, M., M. Urbano, B. Valzasina, M. Francolini, G. Rotta, R. Bonasio, F. Granucci, J.-P. Kraehenbuhl and P. Ricciardi-Castagnoli (2001). "Dendritic cells express tight junction proteins and penetrate gut epithelial monolayers to sample bacteria." Nature Immunology **2**(4): 361-367.

Robbe, C., C. Capon, E. Maes, M. Rousset, A. Zweibaum, J.-P. Zanetta and J.-C. Michalski (2003). "Evidence of regio-specific glycosylation in human intestinal mucins " The Journal of Biological Chemistry **278**(47): 46337-46348.

Rogers, S. S., T. A. Waigh, X. Zhao and J. R. Lu (2007). "Precise particle tracking against a complicated background: polynomial fitting with Gaussian weight." Physical Biology **4**(3): 220-234.

Rose, M. C. and J. A. Voynow (2006). "Respiratory tract mucin genes and mucin glycoproteins in health and disease." Physiological Reviews **86**(1): 245-278.

Ross, I. and L. Turnberg (1983). "Studies of the 'mucus-bicarbonate' barrier on rat fundic mucosa: the effects of luminal pH and a stable prostaglandin analogue." Gut **24**(11): 1030-1033.

Roth, J. (1996). "Protein glycosylation in the endoplasmic reticulum and the Golgi apparatus and cell type-specificity of cell surface glycoconjugate expression: analysis by the protein A-gold and lectin-gold techniques." Histochemistry and Cell Biology **106**(1): 79-92.

Round, A., M. Berry, T. McMaster, S. Stoll, D. Gowers, A. Corfield and M. Miles (2002). "Heterogeneity and persistence length in human ocular mucins." Biophysical Journal **83**(3): 1661-1670.

Ryu, K. H. and E. Grim (1982). "Unstirred water layer in canine jejunum." American Journal of Physiology **242**(4): G364-G369.

Sakiadis, B. (1984). "Fluid and particle mechanics." Perry's Chemical Engineers' Handbook **5**.

Saladin, K. (2007). The Digestive System. Anatomy & Physiology: Unity of Form and Function. New York, NY, McGraw-Hill**:** 953-990.

Sander, G. R., H. Krysinska and B. C. Powell (2006). Developmental signaling networks: the notch pathway. Physiology of the Gastrointestinal Tract. L. R. Johnson, Academic Press. **1:** 287-306.

Sandoz, D., G. Nicolas and M. Laine (1985). "Two mucous cell types revisited after quick-freezing and cryosubstitution." Biology of the Cell **54**(1): 79-88.

Sarna, S. K. (1985). "Cyclic motor activity: migrating complex." Gastroenterology **89**: 894-913.

Sarna, S. K., K. H. Soergel, J. M. Harig, F. D. Loo, C. M. Wood, K. M. Donahue, R. P. Ryan and R. C. Arndorfer (1989). "Spatial and temporal patterns of human jejunal contractions." American Journal of Physiology **257**(3): G423-G432.

Sawaguchi, A., K. Ishihara, J. Kawano, T. Oinuma, K. Hotta and T. Suganuma (2002). "Fluid dynamics of the excretory flow of zymogenic and mucin contents in rat gastric processed by high-pressure freezing/freeze substitution." The Journal of Histochemistry and Cytochemistry **50**(2): 223-234.

Schemann, M. and H.-J. Ehrlein (1986). "Postprandial patterns of canine jejunal motility and transit of luminal content." Gastroenterology **90**(4): 991-1000.

Schulze-Delrieu, K. (1999). "Visual parameters define the phase and the load of contractions in isolated guinea pig ileum." American Journal of Physiology **276**(6): G1417-G1424.

Schulze, K. S. and E. Clark (2008). "Ink dispersion by sequential contractions in isolated segments of guinea pig ileum and duodenum." Neurogastroenterology & Motility **20**: 1317-1327.
Sellers, L. A., A. Allen, E. R. Morris and S. B. Ross-Murphy (1988). "Mechanical characterization and properties of gastrointestinal mucus gel." Biorheology **24**: 615-623.
Sellers, L. A., A. Allen, E. R. Morris and S. B. Ross-Murphy (1991). "The Rheology of pig small intestinal and colonic mucus: weakening of gel structure by non-mucin components." Biochimica et Biophysica Acta **1115**(2): 174-179.
Sequeira, I., R. Lentle, M. Kruger and R. Hurst (2012). "The effect of aspirin and smoking on urinary excretion profiles of lactulose and mannitol in young women: toward a dynamic, aspirin augmented, test of gut mucosal permeability." Neurogastroenterology & Motility **24**(9): e401-e411.
Sheehan, J., K. Oates and I. Carlstedt (1986). "Electron microscopy of cervical, gastric and bronchial mucus glycoproteins." Biochemical Journal **239**: 147-153.
Sheth, S. U., Q. Lu, K. Twelker, S. M. Sharpe, X. Qin, D. C. Reino, M. A. Lee, D.-Z. Xu and E. A. Deitch (2010). "Intestinal mucus layer preservation in female rats attenuates gut injury after trauma-hemorrhagic shock." The Journal of Trauma **68**(2): 279.
Shifrin, D. A., R. E. McConnell, R. Nambiar, J. N. Higginbotham, R. J. Coffey and M. J. Tyska (2012). "Enterocyte microvillus-derived vesicles detoxify bacterial products and regulate epithelial-microbial interactions." Current Biology **22**(7): 627-631.
Shiina, T., Y. Shimizu, Y. Suzuki, H. Nikami and T. Takewaki (2005). "Measurement of the propelled liquid by isolated hamster ileum as a parameter to evaluate peristalsis." European Journal of Pharmacology **517**(1): 120-126.
Singh, P. K. and M. A. Hollingsworth (2006). "Cell surface-associated mucins in signal transduction." Trends in Cell Biology **16**(9): 467-476.
Smith, M. (1985). "Expression of digestive and absorptive function in differentiating enterocytes." Annual Review of Physiology **47**(1): 247-260.
Smith, M., J. Paterson and M. Peacock (1984). "A comprehensive description of brush border membrane development applying to enterocytes taken from a wide variety of mammalian species." Comparative Biochemistry and Physiology Part A: Physiology **77**(4): 655-662.
Smithson, K. W., D. B. Millar, L. R. Jacobs and G. M. Gray (1981). "Intestinal diffusion barrier: unstirred water layer or membrane surface mucus coat?" Science **214**(4526): 1241-1244.
Snoeck, V., B. Goddeeris and E. Cox (2005). "The role of enterocytes in the intestinal barrier function and antigen uptake." Microbes and Infection **7**: 997-1004.
Sonaje, K., K.-J. Lin, M. T. Tseng, S.-P. Wey, F.-Y. Su, E.-Y. Chuang, C.-W. Hsu, C.-T. Chen and H.-W. Sung (2011). "Effects of chitosan-nanoparticle-mediated tight junction opening on the oral absorption of endotoxins." Biomaterials **32**: 8712-8721.
Southon, S., A. Wright and S. J. Fairweather-Tait (1989). "The effect of differences in dietary iron intake on 59Fe absorption and duodenal morphology in pregnant rats." British Journal of Nutrition **62**(3): 707-717.
Specian, R. D. and M. R. Neutra (1980). "Mechanism of rapid mucus secretion in goblet cells timulated by acetylcholine." Journal of Cell Biology **85**(3): 626-640.
Specian, R. D. and M. G. Oliver (1991). "Functional biology of intestinal goblet cells." American Journal of Physiology **260**(2): C183-C193.

Spiller, R. C., M. L. Brown and S. F. Phillips (1987). "Emptying of the terminal ileum in intact humans. Influence of meal residue and ileal motility." Gastroenterology **92**(3): 724-729.

Sternini, C., L. Anselmi and E. Rozengurt (2008). "Enteroendocrine cells: a site of 'taste'in gastrointestinal chemosensing." Current Opinion in Endocrinology, Diabetes, and Obesity **15**(1): 73.

Stevens, R. J., N. G. Publicover and T. K. Smith (2000). "Propagation and neural regulation of calcium waves in longitudinal and circular muscle layers of guinea pig small intestine." Gastroenterology **118**(5): 892-904.

Steyer, J. A., H. Horstmann and W. Almers (1997). "Transport, docking and exocytosis of single secretory granules in live chromaffin cells." Nature **388**: 474-478.

Stiebler, M., J. Tölke and M. Krafczyk (2008). "Advection–diffusion lattice Boltzmann scheme for hierarchical grids." Computers & Mathematics with Applications **55**(7): 1576-1584.

Strocchi, A. and M. D. Levitt (1993). "Role of villous surface area in absorption: science versus religion." Digestive Diseases and Sciences **38**(3): 385-387.

Strous, G. J. and J. Dekker (1992). "Mucin-type glycoproteins." Critical Reviews in Biochemistry and Molecular Biology **27**(1-2): 57-92.

Suh, J., K.-L. Choy, S. K. Lai, J. S. Suk, B. C. Tang, S. Prabhu and J. Hanes (2007). "PEGylation of nanoparticles improves their cytoplasmic transport." International Journal of Nanomedicine **2**(4): 735.

Suh, J., M. Dawson and J. Hanes (2005). "Real-time multiple-particle tracking: applications to drug and gene delivery." Advanced Drug Delivery Reviews **57**(1): 63-78.

Sukop, M. C. and D. T. J. Thorne (2007). Lattice Boltzmann Modeling: An Introduction for Geoscientists and Engineers. New York, Springer**:** 31-54.

Sundén, B. (2011). "Vortex shedding." Retrieved 27 March, 2014, from http://www.thermopedia.com/content/1247/.

Swidsinski, A., B. C. Sydora, Y. Doerffel, V. Loening-Baucke, M. Vaneechoutte, M. Lupicki, J. Scholze, H. Lochs and L. A. Dieleman (2007). "Viscosity Gradient within the mucus layer determines the mucosal barrier function and the spatial organization of the intestinal microbiota." Inflammatory Bowel Diseases **13**(8): 963-970.

Szentkuti, L. and K. Lorenz (1995). "The thickness of the mucus layer in different segments of the rat intestine." The Histochemical Journal **27**(6): 466-472.

Takahashi, T. (2011). "Flow behavior of digesta and the absorption of nutrients in the Gastrointestine." Journal of Nutritional Science and Vitaminology **57**: 265-273.

Takano, J. (1964). "Intestinal changes in protein-deficient rats." Experimental and Molecular Pathology **3**(3): 224-231.

Taylor, C., A. Allen, P. W. Dettmar and J. P. Pearson (2003). "The gel matrix of gastric mucus is maintained by a complex interplay of transient and non-transient associations." Biomacromolecules **4**: 922-927.

Taylor, C., A. Allen, P. W. Dettmar and J. P. Pearson (2004). "Two rheologically different gastric mucus secretions with different putative functions." Biochimica et Biophysica Acta **1674**: 131-138.

Thielicke, W. and E. Stamhuis. (2013). "PIVlab - time resolved digital particle image velocimetry tool for MATLAB." from http://pivlab.blogspot.com.

Thielicke, W. and E. J. Stamhuis (2014). "PIVlab – towards user-friendly, affordable and accurate digital particle image velocimetry in MATLAB." Journal of Open Research Software **2**(1): e30.

Thim, L., F. Madsen and S. S. Poulsen (2002). "Effect of trefoil factors on the viscoelastic properties of mucus gels." European Journal of Clinical Investigation **32**: 519-527.

Thuneberg, L. and S. Peters (2001). "Toward a concept of stretch-coupling in smooth muscle. I. Anatomy of intestinal segmentation and sleeve contractions." The Anatomical Record **262**: 110-124.

Tirosh, B. and A. Rubinstein (1998). "Migration of adhesive and nonadhesive particles in the rat intestine under altered mucus secretion conditions " Journal of Pharmaceutical Sciences **87**: 453-456.

Tooze, S. A., G. J. M. Martens and W. B. Huttner (2001). "Secretory granule biogenesis: rafting to the SNARE." Trends in Cell Biology **11**(3): 116-122.

Trier, J. S. and J. L. Madara (1994). Functional morphology of the mucosa of the small intestine. Physiology of the Gastrointestinal Tract. L. R. Johnson. New York, Raven Press. **2:** 925-961.

Troeger, H., H.-J. Epple, T. Schneider, U. Wahnschaffe, R. Ullrich, G.-D. Burchard, T. Jelinek, M. Zeitz, M. Fromm and J.-D. Schulzke (2007). "Effect of chronic *Giardia lamblia* infection on epithelial transport and barrier function in human duodenum." Gut **56**(3): 328-335.

Tümer, E., A. Bröer, S. Balkrishna, T. Jülich and S. Bröer (2013). "Enterocyte-specific regulation of the apical nutrient transporter SLC6A19 (B0AT1) by transcriptional and epigenetic networks." Journal of Biological Chemistry **288**(47): 33813-33823.

Ubelmann, F., S. Robine and D. Louvard (2011). Microvilli. Cellular Domain. I. R. Nabi. NJ, USA, John Wiley & Sons Inc.**:** 213-228.

van der Flier, L. G. and H. Clevers (2009). "Stem cells, self renewal, and differentiation in the intestinal epithelium." Annual Review of Physiology **71**: 241-260.

Van Klinken, B., J. Dekker, H. Buller and A. Einerhand (1995). "Mucin gene structure and expression: protection vs. adhesion." American Journal of Physiology **269**(5): G613-G627.

Varum, F. J., F. Veiga, J. S. Sousa and A. W. Basit (2012). "Mucus thickness in the gastrointestinal tract of laboratory animals." Journal of Pharmacy and Pharmacology **64**(2): 218-227.

Verdugo, P. (1990). "Goblet cells secretion and mucogenesis." Annual Review of Physiology **52**: 157-176.

Verdugo, P. (1991). "Mucin Exocytosis." American Review of Respiratory Disease **144**(3): S33-S37.

Verdugo, P. (2012). "Supramolecular dynamics of mucus." Cold Spring Harbor Perspectives in Medicine **2**(11): a009597.

Waigh, T., A. Papagiannopoulos, A. Voice, R. Bansil, A. Unwin, C. Dewhurst, B. Turner and N. Afdhal (2002). "Entanglement coupling in porcine stomach mucin." Langmuir **18**(19): 7188-7195.

Waigh, T. A. (2005). "Micro-rheology of complex fluids." Reports on Progress in Physics **68**: 685-742.

Wang, Y., J. G. Brasseur, G. Banco, A. G. Webb, A. C. Ailiani and T. Neuberger (2010). "A multiscale lattice Boltzmann model of macro- and micro-scale transport, with applications to gut function." Philosophical Transactions of the

Royal Society Series B; Mathematical, Physical and Engineering Sciences **368**(1921): 2863-2880.
Weinberg, S. L., E. C. Eckstein and A. H. Shapiro (1971). "An experimental study of peristaltic pumping." Journal of Fluid Mechanics **49**(3): 461-479.
Weinstein, L. D., C. P. Shoemaker, T. Hersh and H. K. Wright (1969). "Enchanced intestinal absorption after small bowel resection in man." Archives of Surgery **99**(5): 560-562.
Wen, S. and P. Huang (2012). Principles of tribology, John Wiley & Sons**:** 135-142.
Westergaard, H. and J. M. Dietschy (1974). "Delineation of the dimensions and permeability characteristics of the two major diffusion barries to passive mucosal uptake in the rabbit intestine." The Journal of Clinical Investigation **54**: 718-732.
Wilson, F. A. and J. M. Dietschy (1974). "The intestinal unstirred layer: its surface area and effect on active transport kinetics." Biochimica et Biophysica Acta **363**(112-126).
Wilson, J. P. (1967). "Surface area of the small intestine in man." Gut **8**: 618-621.
Winne, D. (1978). "Dependence of intestinal absorption *in vivo* on the unstirred layer." Naunyn-Schmiedeberg's Archives Of Pharmacology **304**(2): 175-181.
Womack, W. A., J. A. Barrowman, W. H. Graham, J. N. Benoit, P. R. Kvietys and N. Granger (1987). "Quantitative assessment of villous motility." American Journal of Physiology **252**(2): G250-G256.
Womack, W. A., D. Mailman, P. R. Kvietys and D. N. Granger (1988a). "Neurohumoral control of villous motility." American Journal of Physiology **255**(2): G162-G167.
Womack, W. A., P. K. Tygart, D. Mailman, D. N. Granger and P. R. Kvietys (1988b). "Villous motility: Relationship to lymph flow and blood flow in the dog jejunum." Gastroenterology **94**(4): 977-983.
Womersley, J. R. (1955). "Method for the calculation of velocity, rate of flow and viscous drag in arteries when the pressure gradient is known." Journal of Physiology **127**(553-563).
Yakubov, G. E., J. McColl, J. H. Bongaerts and J. J. Ramsden (2009). "Viscous boundary lubrication of hydrophobic surfaces by mucin." Langmuir **25**(4): 2313-2321.
Yamauchi, K. E. and Y. Isshiki (1991). "Scanning electron microscopic observations on the intestinal villi in growing White Leghorn and broiler chickens from 1 to 30 days of age." British Poultry Science **32**(1): 67-78.
Yudin, A., F. Hanson and D. Katz (1989). "Human cervical mucus and its interaction with sperm: a fine-structural view." Biology of Reproduction **40**(3): 661-671.
Zhou, T. and H. Liu (2004). "A 3D model for PEM fuel cells operated on reformate." Journal of Power Sources **138**(1): 101-110.